Biotribology Of The Natural Ankle Joint

Nivedah Kuganenderan (MEng, Hons)

Submitted in accordance with the requirements for the degree of

Doctor of Philosophy

The University of Leeds

Institute of Medical and Biological Engineering

School of Mechanical Engineering

July 2018

Acknowledgements

'Anything Is Possible If You Believe in Yourself'

Firstly, I would like to thank EPSRC for their funding, which allowed me to take up this PhD.

First and foremost, I'd like to express my sincere gratitude to my primary supervisor, Dr Claire Brockett. Over the last four years, Dr Claire Brockett has shown such great patience and kindness towards me and continuously encouraged me to reach my full potential. I'd like to thank my co-supervisors Professor Joanne Tipper and Professor John Fisher for their guidance throughout my PhD and for providing exceptional support.

Without the help of the technicians within iMBE, I don't think I could have achieved what I have within this PhD. They have made it possible and I'd like to thank Phil, Camille, Keith, Lee and Jane for putting my visions into reality. I'd also like to thank Irvin for putting up with my constant tissue order requests and for putting a smile on my face when I'm dissecting away. I also appreciate all the help from Abdel for the computational work and Adrian with the Talysurf machine. I'd like to thank Professor Anthony Redmond and his team who have continued to show keen interest within this project. I'm grateful for having had the opportunity to work at the Faculty of Biological Sciences (FBS) - thank you Dan, Stacy and Fiona for sharing your knowledge and taking me under your wing! Hazel – I cannot thank you enough for how much you have helped me during my desperate times!

I'd like to especially thank Nagitha who has been an incredible support in the final year when I fell pregnant and took it up on himself to carry out challenging tasks. Without him, I would not have been able to test the human tissue and he made it possible for me.

Throughout these four years, I always turn to Jenny, my disability tutor, for literally everything from presentation practice to thesis writing or just chatting away about

life! She has gone over and beyond to help me and without her support and guidance I could not have reached this day.

Everyone at the office has also been very friendly and it always felt like a family, so I thank each one of them for giving me a home away from home (I know London isn't that far!) and for making me feel comfortable and giving me an enjoyable experience in the past four years. I'd like to thank Divya - I would not have applied to this programme if it wasn't for her and Ayesha, who continues to inspire me with her uttermost dedication to both family and work. Thank you Raman, brother, for always making me laugh and for being super kind and helpful.

My family has given me great strength and constant support and without them I'd not have achieved what I have today. I'd like to take this opportunity to thank you Amma (Mum), Appa (Dad), Niro Akka (sister) and Nigarah (sister) for understanding when I had to miss birthdays/family gatherings and for continuously believing in me when I had doubted myself. Finally, words cannot express how much I appreciate my husband, who has been my pillar of strength throughout this journey and no matter how difficult it was for us living so far away from each other over these four years, he fully accepted and understood my dedication to my PhD. Last but not least, Avighnaa, my beautiful son, inspires me more and more as each day goes by and I will continue to work harder to make you proud chella kutty. Your gorgeous smile is my biggest and greatest motivation in my life.

Dedicated To Lord Ganesha

Abstract

The ankle joint is a stable and congruent joint that helps to protect the joint surfaces from high impact forces. However, possible trauma to the joint such as severe ankle sprain or fracture can cause cartilage breakdown and eventually lead to cartilage degeneration, resulting in arthritis. Ankle arthritis is considered to be a major cause of morbidity and disability. Although the ankle joint is least affected by arthritis compared to knee and hip joints, the pain and lack of mobility of end stage ankle osteoarthritis (OA) are equally debilitating and tend to be overlooked compared to hip and knee OA. Differences in the incidence rates of osteoarthritis (OA) across the joints could be partly attributed to the biomechanical properties of the articular cartilage.

The aim of the thesis was to improve the understanding of mechanical characteristics of the human ankle cartilage through developing and refining methodologies (i.e. indentation and thickness methods) on immature porcine ankle tissues. As porcine ankle joint seems to closely represent the human ankle with comparable anatomical features, cartilage deformation, cartilage thickness, coefficient of friction, surface roughness, contact mechanics and biological properties were also determined. Comparisons of mechanical characteristics between porcine and human tissues were reported.

A methodology was developed to identify the most suitable type of specimen (osteochondral samples versus whole joints) for mechanical characterisation as specimen preparation via pin extraction was hypothesised to have an effect on the tissue quality and thus on biomechanical properties. Specimen preparation of osteochondral pins had no impact on properties as cartilage deformation and thickness measurements of pins were comparable to whole joints. Therefore, for mechanical characterisation of human ankle cartilage, osteochondral pins were studied.

Porcine talar cartilage was found to be thicker, with higher surface roughness, increased water content, increased contact pressures and lower glycosaminoglycan (GAG) content compared to porcine tibial cartilage. Based on such results, the talar cartilage in the young porcine tissue (3 to 6 months) appeared more susceptible to deterioration over time when compared to tibial cartilage as these properties were considered as unfavourable potentially affecting joint function and quality of tissue during high impact forces. Overall, there were significant differences in thickness, deformation and roughness measurements (ANOVA, $p < 0.05$ for all comparators) across the porcine and human tissues. These differences between animal and human tissues can be attributed to many factors such as age, gait, lifestyle and mechanical properties. The immature porcine cartilage was considered to be a poor representative model for tribological studies.

On the human ankle joint, cartilage thicknesses, deformation and surface roughness measurements were all in a comparable range between talar and tibial joint surfaces (ANOVA, $p < 0.05$ for all comparators). Although ankle lesions were reported to be commonly found in the talar surface rather than the tibial surface, and it was assumed to result in unfavourable properties, this was not reported in the current study as no significance was observed between both joint surfaces.

.

List of Abbreviations

μCT	Micro Computed Topography
μm	Micrometre
3D	Three dimensional
AC	Articular cartilage
ACI	Autologous chondrocyte implantation
AB	Alcian Blue
ANOVA	Analysis of Variance
AOFAS	American Orthopaedic Foot & Ankle Society
ATCL	Anterior talocalcaneal ligament
ATFL	Anterior talofibular ligaments
BL	Boundary lubrication
BL	Boundary Lubrication
BW	Body Weight
CFL	Calcaneofibular ligament
CL	Confidence limits
CoCr	Cobalt Chrome
COF	Coefficient of Friction
DA	Units for molecular weight - 'dalton' (unified atomic mass unit)

DF	Dorsiflexion
ECM	Extracellular matrix
EHD	Elastohydrodynamic
EHD	Elastohydrodynamic
ESEM	Environmental scanning electron microscopy
EDTA	Ethylenediaminetetraacetic Acid (EDTA)
FE	Finite element
FFL	Fluid Film Lubrication
GAG	Glycosaminoglycan
H&E	Haematoxylin and Eosin
HA	Hyaluronan (hyaluronic acid)
hrs	Hours
ISO	International Organisation of Standarisation
ITCL	Interosseous talocalcaneal ligament
KCl	Potassium Chloride
KH2PO4	Potassium Phospahte monobasic
LAT TAL	LATERAL TALUS
LAT TIB	LATERAL TIBIA
LTCL	Lateral talocalcaneal ligament
LVDT	Linear variable differential transducer
MaxAV	Maximum average voltage

MED TAL	MEDIAL TALUS
MED TIB	MEDIAL TIBIA
min (s)	Minute or minutes
MinAV	Minimum average voltage
ML	Mixed Lubrication
mM	Molarity (milimolar = mM, 10^-3)
MRI	Magentic Resonance Imaging
MSD	Minimum significant difference
Na2HPO4	Sodium phospahte dibasic
NaCl	Sodium chloride
NBF	Neutral buffere formalin
NJR	National Joint Registry
OA	Osteoarthritis
OAT	Osteochondral autograft transplantation
OCD	Osteochondral defects
OCLs	Osteochondral lesions
PBS	Phosphate Buffered Saline
PAS	Periodic acid and Schiff's reagent
PF	Plantarflexion
PG	Proteoglycans
PMMA	Polymethyl methacrylate

PTFL	Posterior talofibular ligaments
PTOA	Post-traumatic osteoarthritis
RA	Rheumatoid arthritis
ROM	Range of motion
sec	Seconds
SEM	Scanning electron microscopy
SR	Sirius Red
TalAL	Talus Anterior lateral
TalAM	Talus anterior medial
TalCL	Talus central lateral
TalCM	Talus central medial
TalPL	Posterior lateral
TalPM	Talus Posterior medial
TAR	Total Ankle Replacement
TibAL	Tibia anterior lateral
TibC	Tibial central
TibM	Tibial medial
TibPL	Tibia posterior lateral
w/v	Weight/volume

Table of Contents

List of Figures

List of Tables

Chapter 1: Literature Review

1.1 General Introduction

In any synovial joint, such as the ankle, movement and dynamic loading are essential to maintain healthy cartilage function whilst promoting joint lubrication. The natural ankle joint is a stable joint and considered to have a high joint congruency which compliments the interaction between the talar and tibial joint surfaces (VanDijk et al., 2010). However, disruption to the cartilage function via trauma or cartilage wear over time can cause joint failure leading to diseases such as arthritis or cartilage lesions. Due to the poor repair and healing capacity of cartilage, the tissue inevitably deteriorates over time under the stresses of everyday activities (Buckwalter et al., 2005).

In the ankle joint, osteoarthritis (OA) affects 4 % of the adult population in the UK and is considered to be a major cause of morbidity and disability (Valderrabano & Horisberger, 2011). In other joints (i.e. knee and hip), osteoarthritis occurs more commonly which has been associated to fundamental anatomical differences (such as joint congruency) and/or biomechanical differences (Daniels and Thomas, 2008). A congruent joint such as the ankle was suggested to be less prevalent to OA and degeneration compared to an incongruent joint such as the knee (Kuettner and Cole, 2005). Hence, the ankle cartilage seems to protect the joint from higher compressive loading compared to the knee (Kempson, 1991; Kuettner and Cole, 2005). As with all end-stage osteoarthritic cartilages, the pain and lack of mobility impacts the quality of life and are equally debilitating.

Osteochondral defects (OCDs) are commonly found in the ankle joint which mainly affect the talar cartilage and its underlying bone causing pain, recurrent synovitis and changes the joint mechanics (Hangody et al., 2004). This condition predominately affects the younger and active population and it is currently treated surgically. Although the ankle cartilage suffers from various complications, post-traumatic OA is the most common type of cartilage damage found in the ankle joint.

Due to a lack of biomechanical studies in the ankle joint, an understanding of the pathway from injury to arthritis has not been fully understood. Such investigation will be helpful for developing successful treatment options. Hence, this thesis focuses on developing appropriate experimental methodology to evaluate the biomechanical properties of ankle cartilage. Such investigation will further add knowledge for improving treatment options in the future.

1.2 The Natural Ankle Joint

1.2.1 Ankle Anatomy

The ankle complex is made up of two main articulations; the talocalcaneal joint (subtalar joint), connecting talus and calcaneus bone and the tibiotalar (talocrural) joint (true ankle joint) connecting the lower ends of tibia and talus (Figure 1-1a). A third joint, commonly known as the inferior tibiofibular joint (Figure 1-1a) connects the lower ends of the tibia and fibula.
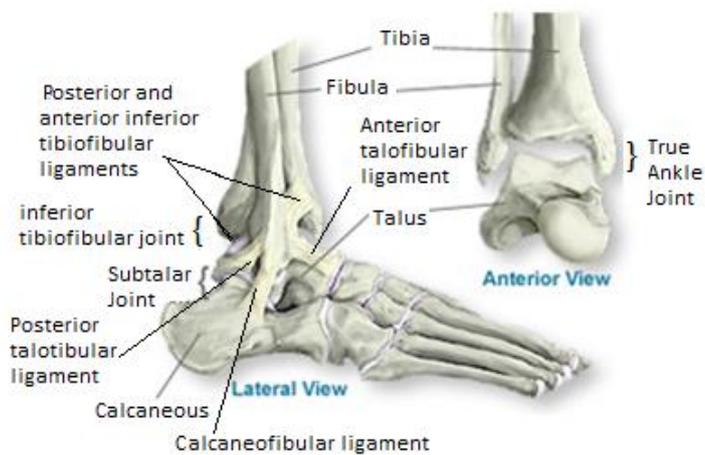
Figure 1-1: a) Bone structures within the ankle, subtalar and true ankle joints – (adapted from Southern California Orthopedic, 2012).

1.2.1.1 The Talocalcaneal (or Subtalar Joint)

The lower ankle joint or subtalar joint is situated below the talus and posteriorly connects the talus and calcaneus forming the talocalcaneal joint (Figure 1-1).

The subtalar joint permits the movements of inversion and eversion of the foot, also known as 'side to side' motion (Figure 1-2A). The total motion within this joint is approximately 20 degrees for inversion and 10 degrees for eversion (Smith, 2006). Excessive inversion could potentially sprain the lateral ligaments in the joint, and excessive eversion can damage the medial ligaments in the joint. The interosseous talocalcaneal ligament (ITCL) in the subtalar joint forms the key link between the bone structures. The lateral talocalcaneal ligament (LTCL) is a short bundle of fibres,

which attaches from the talar surface to the calcaneus and the anterior talocalcaneal ligament (ATCL) connects the lateral talar surface to the calcaneus surface (Figure 1-2B).
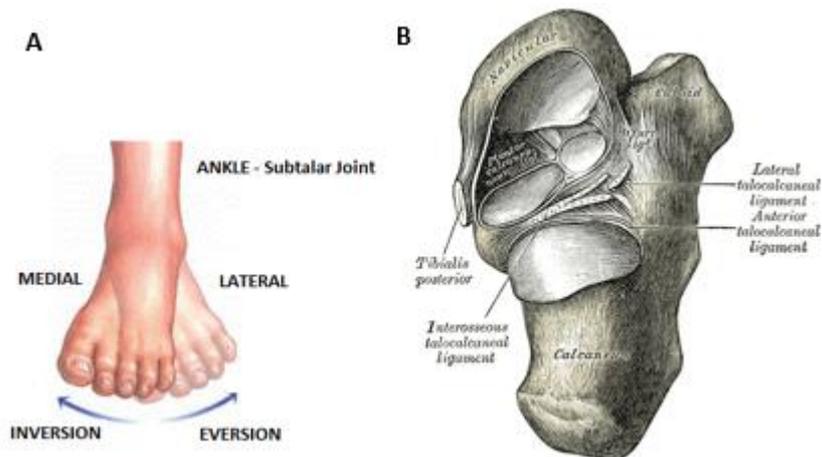
Figure 1-2: Subtalar joint motions and structure; A) Each joint in the ankle has a specific motion, with the subtalar joint being responsible for inversion-eversion motion (adapted from Olson and Pawlina, 2008); B) Illustration to indicate the ligaments in the subtalar joint – interosseous talocalcaneal ligament (ITCL), lateral and anterior talocalcaneal ligaments (Gray, 1918).

1.2.1.2 The Tibiotalar (or Talocrucal) Joint: True Ankle Joint

The tibiotalar joint is characterised as a synovial hinge joint, which consists of the tibia, fibula and talus. The tibia is known to form the inside of the true ankle joint, with the fibula forming the external section, and the talus being situated beneath the true ankle joint (Figure 1-1a). The interaction between these bones allows for movement of the joint in plantarflexion and dorsiflexion, which are downwards and upwards, respectively (Figure 1-3).
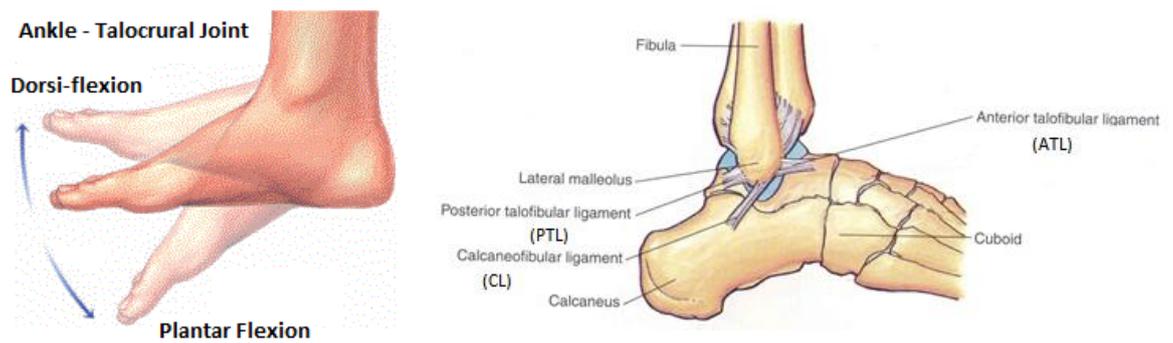
Figure 1-3: Each joint in the ankle has a specific motion, with the tibiotalar joint being responsible for dorsi-plantar flexion (adapted from Olson and Pawlina (2008)). Anterior and posterior talofibular ligaments (ATFL & PTFL) and the calcaneofibular ligament (CFL) in the ankle joint that maintain articulation are known to be 'lateral collateral ligaments' (LCL) (adapted from Martino, 2013).

The lateral aspect of the tibiotalar joint is made up of anterior and posterior talofibular ligaments (ATFL & PTFL) and the calcaneofibular ligament (CFL) (Figure 1-3B). These ligaments surrounding the lateral aspect of the ankle joint are commonly involved during an ankle sprain. The lateral collateral ligaments (LCL) (Figure 1-3B) limit 'varus' stresses on the ankle. In the varus position, the sole faces the midline and a combination of inversion and external rotation of the lower extremity takes place (i.e. supination); whereas in the valgus position, the sole faces away from the midline, with a motion of eversion, whilst the weight shifts towards the inside edge of the sole with internal rotation of the lower extremity (i.e. pronation). The lateral malleolus, which distinguishes a rounded bony segment (Figure 1-3B) is attached to the talus and calcaneus bones through ligaments, which keeps the ankle stable (Pollard et al., 2002; Ivins, 2006).

The anterior-talofibular ligament (ATFL) is known to be the weakest ligament that most frequently becomes torn during an injury (Burks and Morgan, 1994). This ligament sits on the 'dorsolateral' of the foot, pertaining to the back and side, whilst moving at an angle of approximately 45 degrees towards the talus from the frontal plane (Burks and Morgan, 1994). Its role is to limit displacement in the anterior direction of the talus and plantar flexion of the ankle (Van Den Bekerom et al., 2008).

The calcaneofibular ligament is the only ligament that connects the true ankle joint with the subtalar joint. In the varus and valgus positions of the talus joint, this ligament is tensed and relaxed respectively. Hence, it suggests a potential for ligament injury without the motion of dorsiflexion-plantar flexion in the ankle (Golanó et al., 2016).

The medial collateral ligaments (MCL) consist of three fan-shaped ligaments (Figure 1-4) also known as the deltoid ligament (Burks and Morgan, 1994). The deltoid ligament, attaching at the lateral aspect of the ankle joint, provides key stability of the medial segment of the ankle joint, whilst preventing excessive eversion movements in the joint. These ligaments limit 'valgus' stresses within the ankle. In comparison to the LCL, the MCL are known to be stronger and therefore less likely to be torn (Burks and Morgan, 1994).
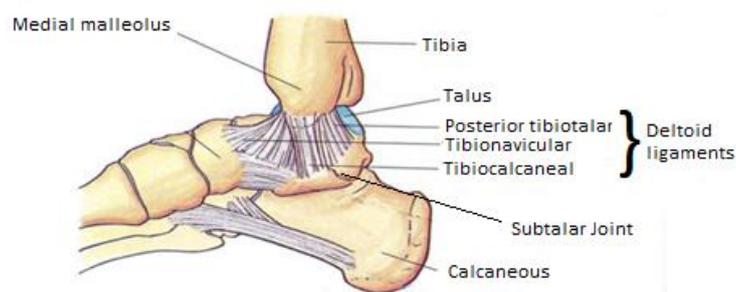
Figure 1-4: Illustration of medial collateral ligaments (MCL) in the tibiotalar joint highlighting parts of deltoid ligaments connecting the tibia to the talus. Medial malleolus is attached to the talus bone by parts of deltoid ligaments (adapted from Martino, 2013).

The primary ankle function is to enable a smooth motion and gait. The muscles, tendons and ligaments surrounding the ankle joint, detailed in this section, function alongside one another to assist in the movement of the body.

1.2.1.3 The Inferior Tibiofibular Joint

The inferior tibiofibular joint (Figure 1-1b) is positioned above the ankle joint. The articulation of the inferior tibiofibular joint is described as a 'syndesmosis' and is not a synovial joint, because the interosseous membrane, a fibrous tissue, connects the

two adjacent bones instead of the synovial capsule (Hermans et al., 2010) which is present in other synovial joints such as the talocrural joint.

The main function of this joint is to provide additional support and stability to the ankle rather than motion. The anterior and posterior tibiofibular ligaments, interosseous ligament and transverse tibiofibular ligaments are the four key ligaments (Figure 1-5) that maintain and hold the joint together whilst ensuring protection for the integrity of the joint (Hermans et al., 2010). However, such inflexibility leads to a high susceptibility of ankle sprains and ligament injuries (Sekiya and Kuhn, 2003).
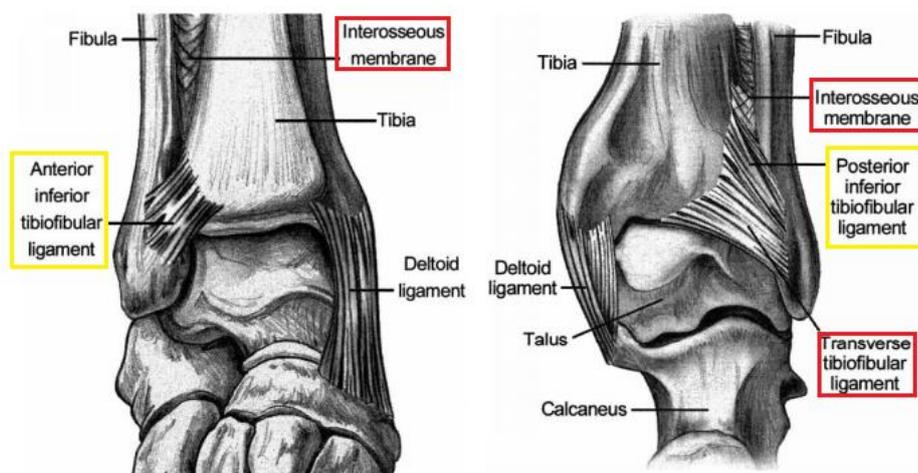
Figure 1-5: Anterior view of the inferior tibifibular joint (A) and posterior view of the same joint (B). The key ligaments are the anterior and posterior tibiofibular ligaments highlighted in yellow and the interosseous ligament and transverse tibiofibular ligaments highlighted in red (adapted from Norkus and Floyd, 2001).

The posterior talofibular ligament is relaxed in plantar flexion and in the neutral ankle position, whereas it is tensed in the dorsiflexion motion of the ankle (Golanó et al., 2016). This 'syndesmosis' joint only permits limited motion between the tibia and fibula. Any injuries to the surrounding ligaments often occur in conjunction with eversion injuries. This joint tends to be overlooked as it results in 'high ankle sprain' rather than the most commonly experienced lateral ankle sprain (Hertel, 2002).

1.2.2 Biomechanics of the Ankle

The key quantitative branches of biomechanics are kinematics, related to motion, and kinetics related to forces, torques and power.

1.2.2.1 Axis of Rotation

Studies on the axis of rotation in the ankle joint are grouped into two categories. These aim to establish the location and orientation of the axis of rotation, whilst others aim to establish kinematic and kinetic characteristics with assumptions on the location and orientation of the axis of rotation

The rotational axis of the ankle joint is known to pass through the medial and lateral malleoli (Figure 1-6).This axis moves anteriorly through the tibia to the frontal plane, yet moves posteriorly through the fibula to the same plane (Hertel, 2002).
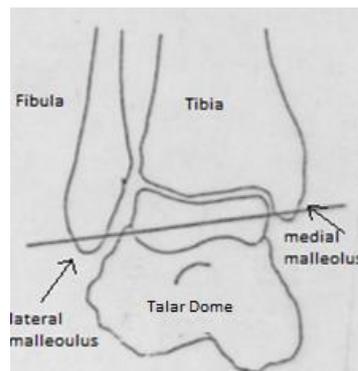
Figure 1-6: Rotational axis of ankle joint in a right leg (adapted from Hertel, 2002).

An early study by Barnett & Napier (1952) investigated the anatomy of the talus bone to determine the axis of rotation in the ankle joint. The lateral and medial curvatures were reported to be different in the talus, suggesting that the axis of rotation of the ankle joint to vary as motion changes (Barnett and Napier, 1952).

Since the 1950s, it has been recognised that the ankle joint axes differed during the movements of dorsiflexion (DF) and plantar flexion (PF) (Hicks, 1953) as shown in Figure 1-7. Hicks (1953) agreed with the findings obtained by Barnett & Napier (1952) and further defined the axes as 'PF axis' and 'DF axis'. Therefore, motion about these

axes cannot occur simultaneously (Hicks, 1953). The PF axis of rotation points upwards on the lateral side of the joint, and DF axis of rotation points downwards on the lateral aspect. Axis changeover was estimated to occur near the neutral position of the joint (Barnett and Napier, 1952).
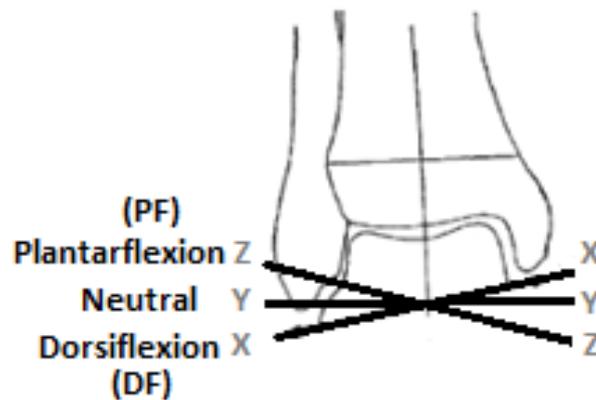
Figure 1-7: Rotational axes of ankle joint in the right leg in dorsi-plantar flexion compared to normal position (adapted from Kelikian et al., 2011)

The rear foot movements are mostly described as the following: sagittal plane movement as plantar flexion-dorsiflexion (Figure 1-8A); frontal plane motion as inversion and eversion (Figure 1-8B) and transverse plane motion as internal and external rotations (Figure 1-8C) (Huson, 1987). These motions occur as a result of coordination of the joints in the ankle to permit movement as a whole component.
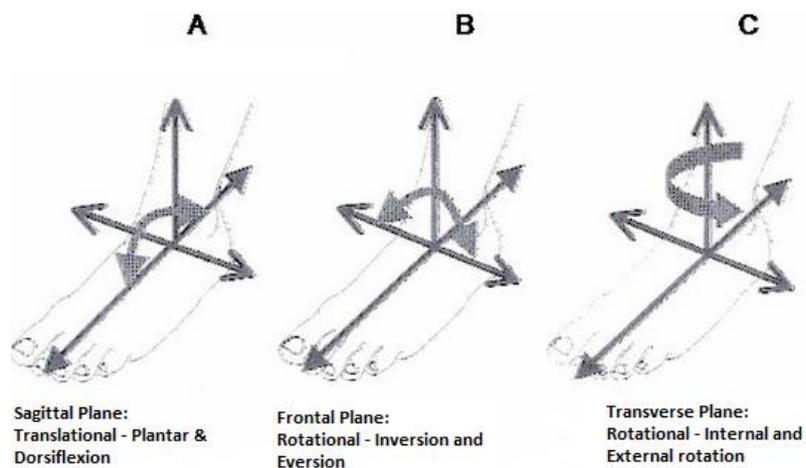
Figure 1-8: Foot movements in Sagittal (A), Frontal (B) and Transverse plane (C) (adapted from Oster, 2009).

An earlier study by Lundberg et al. (1989) used roentgen stereophotogrammetry to examine the axis of rotation, concluding that it changed continuously in the range of the sagittal plane motion, in addition to exhibiting large variations between individuals. However, the study was limited to the number of volunteers used (n=8) and by the methodology of taking 10 degrees increments between 30 degrees of plantar flexion and 30 degrees of dorsiflexion, which has not been justified (Lundberg et al., 1989).

1.2.2.2 Range Of Motion (ROM)

The ankle range of motion (ROM) has demonstrated substantial changes between individuals due to geographical and cultural differences based on their daily activities (Ahlberg et al., 1988). The ankle consists of several joints that contribute to the ranges of motion within the ankle and a key requirement of the ankle joint is to maintain stability during the full ranges of motion under certain loads. During a gait cycle, plantar flexion (PF) and dorsiflexion (DF) are expected to occur at various stages. Ankle motion mainly occurs in the sagittal plane, in which plantar- and dorsiflexion movements occur at the true ankle joint (tibiotalar). The average plantar flexion (PF) and dorsiflexion (DF) of the ankle has been recorded to be between 40 to 56 degrees and 13 to 33 degrees, respectively (Ahlberg et al., 1988; Valderrabano et al., 2003) such that the total ROM (i.e. PF and DF) is in the range between 53 to 89 degrees. In the frontal plane, the total ROM was approximately 35 degrees (Stauffer et al., 1977). These motions are considered to be major contributors to the overall function of the ankle.

During most daily activities, the total ROM in the sagittal plane is considerably reduced as shown in Table 1-1. For elderly patients, the satisfactory total ROM (i.e. PF and DF) ranges between 15 degrees to 20 degrees to complete their daily routines (Stauffer et al., 1977). Hence, the ROM for older groups are lower compared to average values obtained (Valderrabano et al., 2003), suggesting that age related changes may limit the range of motion in the ankle joint.

Table 1-1: The total range of motion (ROM) in the ankle during specific activities, PF (plantar flexion), DF (dorsiflexion) (Stauffer et al., 1977).

Activity	Total Range of Motion (ROM) (in degrees)
Walking on uneven surface	maximum 25 degrees Total ROM (10 degrees to 15 degrees PF and 10 degrees DF)
Walking upstairs	37 degrees Total ROM
Walking downstairs	56 degrees Total ROM

1.2.2.3 Load Transmission in Ankle Joint

A person's gait is as unique to that individual as a fingerprint, as it describes the subjects walking pattern and associated parameters of stride length and frequency, as well as the velocity of gait (Oberg et al., 1993). In order to understand the biomechanics of the ankle joint, load transfer characteristics need to be established. During walking, the ankle initially plantar flexes as the forefoot is lowered to the ground (Figure 1-9), whereas during running increased ankle dorsiflexion is required to achieve initial heel contact. Maximum plantar-flexion occurs during toe-off and maximum dorsiflexion occurs during heel strike during a gait cycle (Figure 1-9).
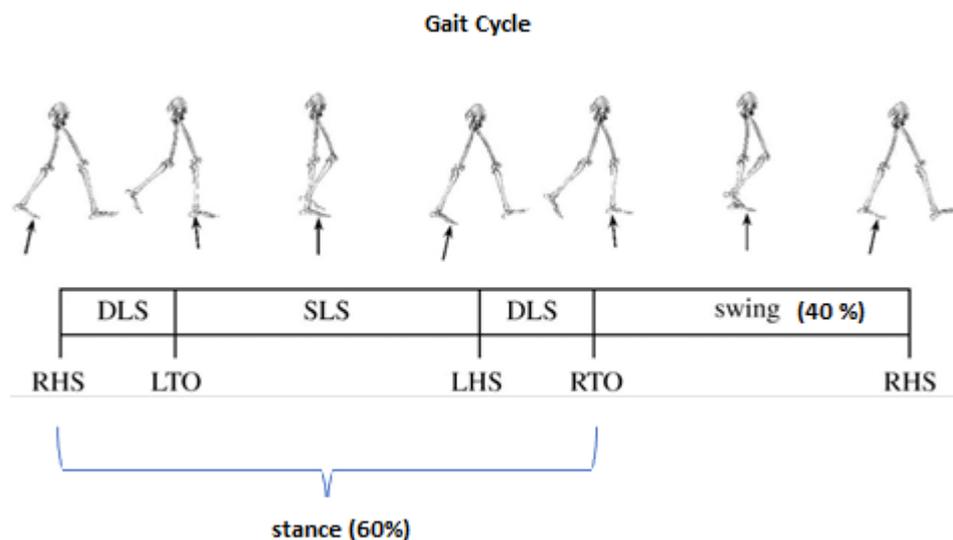
Figure 1-9: Gait Cycle - right heel strike (RHS), left-toe-off (LTO), left-heel-strike (LHS), right-toe-off (RTO), double-limb support (DLS), single-limb-support (SLS) (adapted from Umberger, 2010).

The ankle joint has to be stable in order to withstand up to five times body weight during walking and up to eight times body weight during running (Stauffer et al., 1977; Kleipool and Blankevoort, 2010). The average peak force applied onto tibiotalar joint has been recorded to be in the range of 2.9 to 4.7 times body weight during the stance phase of gait (Procter and Paul, 1982). Previous studies have reported the tibiotalar joint to experience the majority of the load transmission of 83 % compared to the remaining 17 % to be transmitted through the fibula (Calhoun et al., 1994). Around 77 % to 90 % of the load transmitted in the tibiotalar joint, is applied to the talus dome, whilst the remaining load is subjected onto the medial and lateral talar surfaces (Michael et al., 2008).

1.2.2.4 Stress in the Ankle

In the ankle joint, the contact area is only one third of that in the knee and hip joints (Kimizuka et al., 1980), which experiences nearly 64 % and 45 % higher forces compared to knee and hip joints, respectively (Michael et al., 2008). Kimizuka et al. (1980) examined *in-vitro* contact areas and pressure distribution of eight cadaveric ankle joints under compressive loading conditions of 200 N, 500 N, 1,000 N and 1,500 N using pressure sensor sheets. These authors concluded that increasing the load applied from 200 N to 1,500 N increased the average contact area by 254 mm^2 and increased average peak pressure from 4.4 MPa to 9.9 MPa.

This study suggested that in neutral position, the contact in the ankle joint was significantly in the anterior-lateral aspect, with the peak pressure reported to act either anteriorly or laterally. However, it did not consider the necessary ankle motions such as plantar-dorsiflexion.

Pressure distributions within five cadaveric ankle joints under three axial loading conditions of 490 N, 686 N and 980 N were examined using pressure-sensitive Fuji film (Calhoun et al., 1994). Plantar flexion movements lead to higher average pressures and during dorsiflexion, the pressure remained slightly lower (Calhoun et al., 1994). Pressure did not significantly increase with loading, whereas contact area did show an increase. A possible reason for a limited pressure variation with loading

could be due using a lower loading range (980 N - 490 N = 490 N), which failed to show an overall trend between load and pressure parameters. In comparison to Calhoun et al (1994), the earlier study by Kimizuka et al. (1980) represented the relationship greater with a loading range of 1300 N (1500 N – 200 N = 1300 N) in the neutral position of the joint. Limitations in pressure sensitive Fuji films including slippage, possible shearing or its thickness can alter the joint characteristics, especially in a joint as highly conforming as the ankle (Millington et al., 2007c).

Imaging techniques such as fluoroscopy or magnetic resonance imaging (MRI) have been used to study the *in-vivo* contact area and pressure distributions in the ankle joint. Fluoroscopy produces an 'X-ray movie' to obtain moving images of internal body structures to evaluate and diagnose issues related to the bones, muscles or joints. It has been used alongside computer tomography (CT) and magnetic resonance imaging (MRI) for more accurate 3D image analysis of internal body segments. A study by Wan et al. (2006) examined *in-vivo* articular cartilage contact patterns in nine ankle joints under weight-bearing conditions by simulating the stance phase during walking (Wan et al., 2006). Using a combination of magnetic resonance and a modified fluoroscopy imaging technique, the ankle joint kinematics under three different ankle positions of heel strike, mid-stance and toe-off were measured. The contact area during mid-stance was significantly greater than at heel strike and toe-off (Wan et al., 2006), which is in agreement with the derived assumption from the results obtained by Kimizuka et al. (1980). However, this study was limited by a small sample size, which may not be considered representative of the whole population (Wan et al, 2006).

A stereophotogrammetric system accurately analyses the overall ankle joint surface by assigning 3D coordinates to each pixel generating a dense point cloud. A combination of several points (typically in the order of 70,000 points for each cartilage surface) from different views generates a detailed 3D model of the specimen (Millington et al., 2007b). Millington et al. (2007b) determined the joint contact area measuring the overlap of the bone surfaces using stereophotogrammetry. The contact areas within the tibio-talar joint under various

ranges of motion with a load of 1000 N were measured (Millington et al., 2007b). During loading, the joint remains undisrupted with this method. Maximum tibio-talar contact area was recorded during dorsiflexion, whereas minimum contact area was found in plantar flexion (Millington et al., 2007b), which is in agreement with Calhoun et al. (1994). However, stereophotogrammetry generates shadows by flash that unfavourably affect 3D perception when these are merged into a 3D image (Nam and Kehtarnavaz, 2012). Furthermore, this method is expensive and extensive amount of post-processing is needed to obtain data (Millington et al., 2007b).

1.2.3 Clinical Relevance of Ankle Biomechanics

Age and gender are influencing factors that may change the ROM of the individual (Nigg et al., 1992). Nigg et al. (1992) measured ankle ROM in subjects between 20 and 80 years of age and reported younger females to have a generally greater ROM compared to younger males. However, in the oldest age group, females had 8 degrees lower dorsiflexion motion and 8 degrees greater plantar flexion motions compared to male patients (Nigg et al., 1992). In general, within the oldest age category, the ROM was in the same order of magnitude for both genders (Nigg et al., 1992). Ferrario et al (2007) examined the range of motion asymmetry of the ankle with its coupled movements in a younger population with a mean age of 22.8 years and 23.8 years for male and female subjects, respectively. This study concluded that overall 20 % of females (n=35) and 34 % of male subjects (n=30) obtained a difference of greater than 5 degrees in the total ROM. Therefore, in the younger group, asymmetries in the joint during dorsi-plantar flexion motions should be taken into consideration when using normal range of motion in the uninvolved limb as a reference in clinical practice (Ferrario et al., 2007).

Patients suffering with post-traumatic ankle OA had major kinematic differences within the foot (Valderrabano et al., 2006; Horisberger, Hintermann, et al., 2009; Kozanek et al., 2009). Joint moments and ground reaction forces, as well as ankle ROM were significantly reduced. Specifically, mean dorsi-plantar flexion was reduced to 16 degrees (Valderrabano et al., 2006).

1.3 Articular Cartilage

Articular cartilage is a connective tissue located at the ends of the bones, which supports and distributes loads across the synovial joints by delivering a nearly frictionless and smooth movement in the joint (McNary et al., 2012). Articular cartilage is subjected to mechanical stresses during day to day activities (Ando et al., 2010). Extensive research into functional articular cartilage has been undertaken, and more research is currently on-going to progress towards tissue engineering, a solution for cartilage repair and replacement. However, there are significant challenges such as reaching optimal frictional and wear properties for tissue-engineered cartilage constructs equivalent to the natural articular cartilage.

1.3.1 Structure and Composition

The articular cartilage consists of chondrocytes and hydrated extracellular matrix (ECM) which includes collagen type II, proteoglycans (PG) and water. Articular cartilage is deficient in blood supply and nerves, which give it a poor capacity for self-repair (Ando et al., 2010). The structure of the cartilage is non-linear, inhomogeneous, and anisotropic. (Woo et al., 1976; Mow et al., 1989; McNary et al., 2012).

1.3.1.1 Macrostructure

Articular cartilage is divided into three main regions (Figure 1-10) – the superficial zone, the middle zone and the deep zone (Buckwalter et al., 1994). The tide mark is the boundary layer between the non-mineralised and mineralised extracellular matrix (McNary et al., 2012). The water content decreases from the superficial zone to the deep zone (Fox et al., 2009).

Each layer provides a distinctive composition and collagen arrangement and chondrocytes vary in size, shape, location and orientation. Chondrocytes in the articular surface have a flattened shape compared to those in the calcified cartilage,

which are rounder (Figure 1-10). These also vary in size and shape throughout the zones. Collagen fibres in the superficial (tangential) zone, limit shearing forces at the cartilage surface produced by the articulating joint. These lie close together and are positioned parallel to the surface. Relatively denser collagen fibres are arranged in an oblique manner within the middle zone, while in the lower end of the deep zone, the largest diameter collagen fibres are positioned perpendicularly to the tide mark. The tide mark differentiates the deep zone and the calcified zone. The calcified zone bonds the cartilage and bone by attaching the collagen fibres of deep zone to the subchondral bone (Figure 1-10).
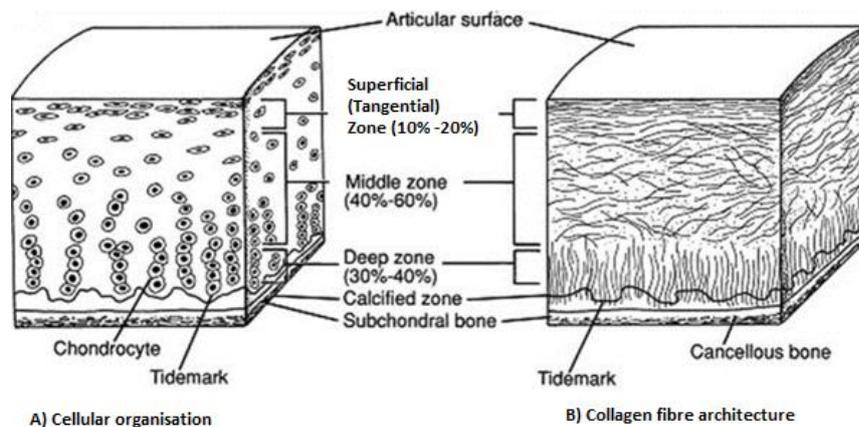
Figure 1-10: Illustration of articular cartilage classified into zones – A) Cellular organisation (left); B) Collagen fibre architecture (right) (adapted from Buckwalter et al., 1994).

The superficial zone is made up of 10 % to 20 % of the cartilage thickness (Fox et al., 2009). A moderately large number of flattened chondrocytes protect and maintain the layers beneath this level. This zone mixes with synovial fluid, which is imperative to withstand shear, tensile and compressive forces imposed by articulation. The middle zone takes up 40 to 60 % of the total cartilage volume with spherically shaped chondrocytes (Fox et al., 2009). This zone needs to resist compressive forces, whereas the deep zone is required to provide the highest resistance to such forces to minimise damage to the cartilage. The deep zone represents 30 to 40 % of the cartilage volume (Fox et al., 2009). The cell population within the deep zone is limited

and chondrocytes are larger (hypertrophy-like changes) compared to those found in superficial zones (Fox et al., 2009).

1.3.1.2 Microstructure

The extracellular matrix (ECM) consists of tissue fluid and macromolecules such as collagen, proteoglycans and non-collagenous proteins and glycoproteins (Buckwalter et al., 1994). The biomechanical characteristics of the articular cartilage are mainly governed by the ECM properties in addition to organisation and size of chondrocytes (Buckwalter and Mankin, 1997).

Chondrocytes are metabolically active cells that are important for their unique role in the development, synthesis, integration and repair of the ECM (Fox et al., 2009). Within different locations of the articular cartilage, the size, quantity and shape of the chondrocytes vary accordingly. Due to the lack of blood supply and any cell-to-cell contact, essential nutrients are obtained from the surrounding synovial fluid. In response to an injury to the cartilage, the chondrocytes provide inadequate repair capacity as they are not able to replicate.

Collagen represents roughly 60 % of the cartilage dry-weight and is in the shape of elongated fibrils, mainly located in the fibrous tissue (Figure 1-10). Collagen type II comprises of 90 to 95% of the overall collagen content in the extracellular matrix, which makes it the largest macromolecule in the matrix (Fox et al., 2009). Reduced quantities of other collagen types, such as I, IV, V, VI, IX, and XI, are also present to support the type II collagen fibril network (Figure 1-11). This network is thoroughly organised. Three polypeptide chains (alpha chains) form a triple helix structure (Figure 1-11), which provides crucial shear and tensile properties for matrix stabilisation (Fox et al., 2009).
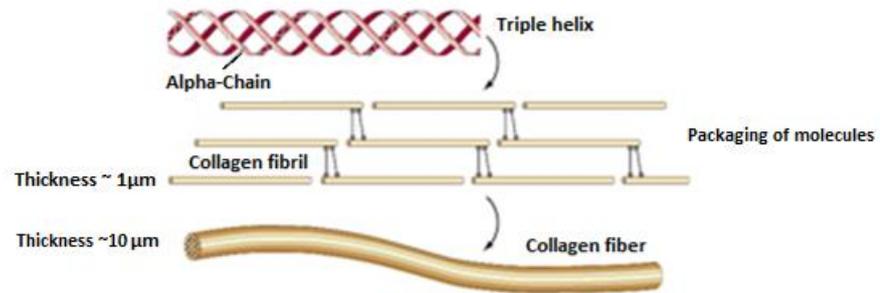
Figure 1-11: Collagen fibre structure (adapted from Rana, 2011)

Proteoglycans are composed of protein cores with covalently attached glycosaminoglycan (GAG) subunits, such as keratin sulphate and chondroitin sulphate (Figure 1-12). PG is responsible in providing cartilage with its osmotic properties that cause cartilage to swell in order to hydrate the tissue. However, this expansion of PG is limited by the collagen fibril network, thus inducing a swelling pressure, which resists compressive loads (Rosenberg et al., 1975).
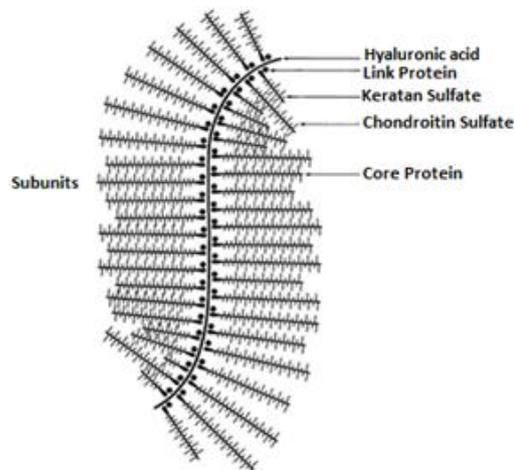
Figure 1-12: Proteoglycan Aggregate (adapted from Rosenberg et al., 1975)

Water accounts to up to 80 % of the wet-weight of the articular cartilage (Fox, et al., 2009). With the benefit of fluid flow, nutrients are transported and distributed through the cartilage and across the articular surface, permitting lubrication. Between the superficial zone to the deep zone, the water content decreases from around 80 % to 60 %, respectively (Mankin and Thrasher, 1975; Buckwalter and Mankin, 1997; Olsen and Oloyede, 2002). Throughout the matrix, the high fluid flow

resistance leads to reduced tissue permeability. Such a response helps the cartilage to withstand high loads.

Despite a small quantity of non-collagenous proteins and glycoproteins being present in the cartilage, their specific function has not been understood. Some of the protein molecules including fibronectin are important to organise and maintain the macromolecular structure of the matrix (Fox, et al., 2009).

1.3.2 Biomechanical Function and Properties of Articular Cartilage

During deformation of cartilage, fluid flow is enhanced throughout the tissue and on the surface to maintain a healthy joint lubrication (Linn and Sokoloff, 1965). Cartilage has been represented as a combination of fluid and solid phases (i.e. biphasic), since the fluid flow and deformation are dependent on each other (Mow et al., 1984). Permeability indicates resistance to fluid flow through the EC matrix (Mansour, 2009). Based on this theory, the material properties of the articular cartilage were characterised two decades ago by Mow et al. (1989), who developed a biphasic model. However, this theory only explains the flow-dependent viscoelasticity (Pawaskar, 2010) and how it contributes to time-dependent cartilage behaviour such as creep and stress-relaxation response; the 'creep mode' applies a constant load whilst measuring cartilage deformation as a function of time, whereas the 'relaxation' mode measures the internal stress using a constant displacement; as the cartilage is compressed, the stain is maintained (Mow et al., 1989). However, the flow-independent viscoelastic behaviour under a pure shear force by the collagen-proteoglycan matrix is an important aspect when cartilage damage is considered (Setton et al., 1993).

Therefore, the biological and mechanical properties of the cartilage are dependent upon the tissue structure and the interaction between the chondrocytes and the extracellular matrix. Loading conditions on the cartilage including compressive, tensile and shear stresses determine these properties and are addressed in this section.

1.3.2.1 Compressive Loads on Cartilage

Cartilage exhibits a creep and stress-relaxation response with an application of constant compressive stress (Mirzayan, 2006). As the cartilage is compressed, the deformation increases with time and it will either deform or creep until an equilibrium state has been reached (Figure 1-13).
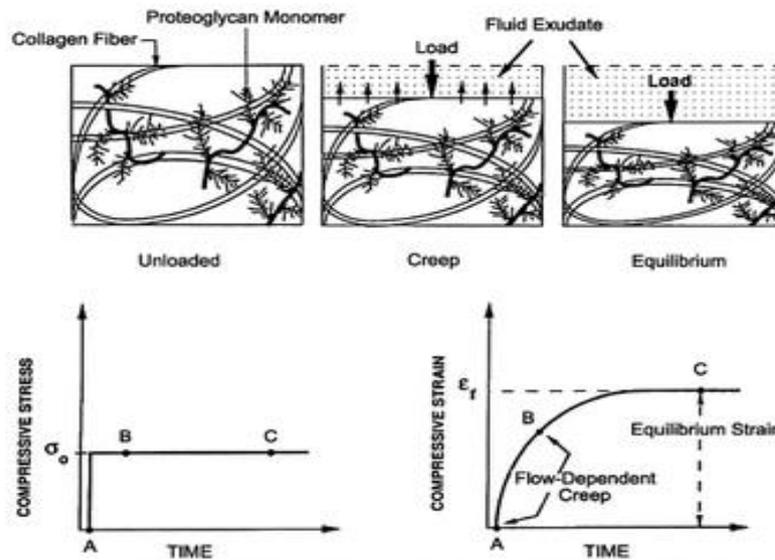
Figure 1-13: Non-linear strain dependant permeability property of articular cartilage and fluid exudation to support compressive loads – application of load causes fluid to flow out of the matrix which is balanced by a low permeability until an equilibrium strain has been reached - reprinted from Mirzayan (2006) with permission from Thieme

In addition, compression causes an increase in interstitial fluid pressure generating fluid flow out of the extracellular matrix. This creates large frictional drag on the matrix and a low permeability stops a sudden fluid flow out of the matrix due to the decreased porosity and increased negatively charged density (Mirzayan, 2006). This leads to an increase of proteoglycan concentration, which in turn increases the load-bearing capacity (Mirzayan, 2006). With the removal of compressive loads, the fluids flow back through the tissue matrix. This phenomenon is known as creep (Figure 1-13).

Stress-relaxation is the second important property exhibited by a viscoelastic material, which plays a key role in distributing loads in the cartilage. Hence, whilst

the cartilage is deforming at constant strain, it reaches a peak stress value, followed by a slow process until an equilibrium state has been reached (Figure 1-14). Therefore, the fluid is redistributed within the porous solid matrix. With an increased strain value, the cartilage becomes stiffer. The Young's modulus, which represents the slope of the stress-strain curve in the elastic region, is dependent upon the time at which the force was measured during the stress-relaxation investigation (Nordin and Frankle, 2001).
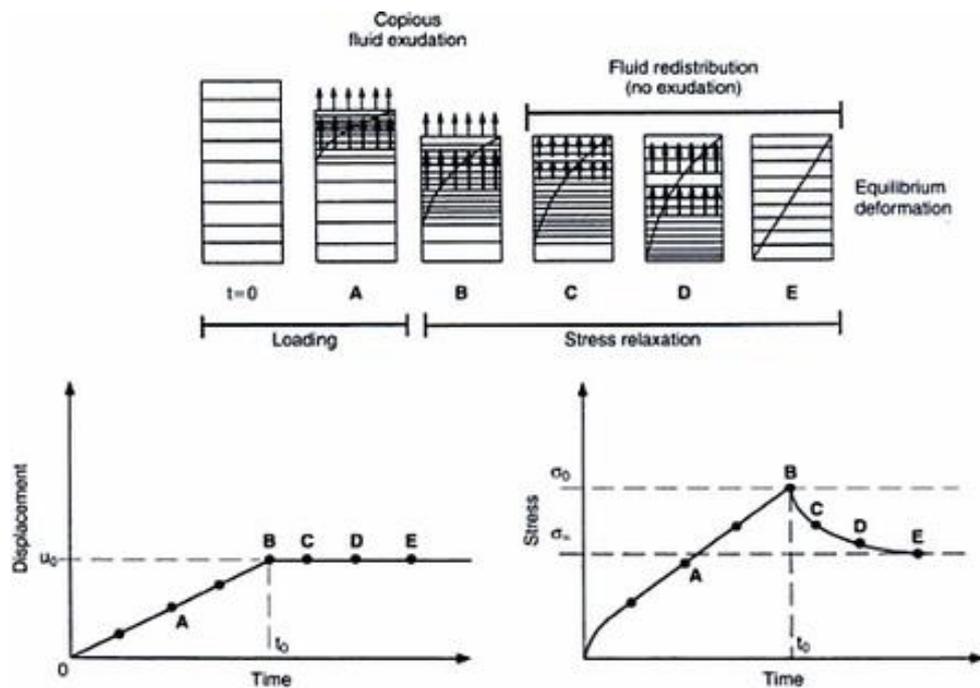
Figure 1-14: Stress-relaxation response under compression. Representation of fluid exudation and fluid re-redistribution during displacement and stress changes over time in cartilage. Initially, fluid exudates (A) and (B); then fluid is redistributed through the matrix (C), (D) and an equilibrium state is reached with reduced stress (E) - reprinted from Nordin and Frankie (2001) with permission from Wolters Kluwer Health Inc.

1.3.2.2   Tensile Stress on Cartilage

Tensile properties vary depending upon factors such as cartilage zone, orientation and location within the joint. In mature animals with fully developed skeletal structures, the tensile strength and stiffness has been suggested to decrease from the articular surface to the deep zone. While in immature animals, these parameters are suggested to increase instead (Roth and Mow, 1980).

The response of collagen matrix to tensile stress can be shown in stress-strain curve (Figure 1-15). The tensile modulus or Young's modulus (Figure 1-15) determines the stiffness of the material, which is governed by collagen-proteoglycan behaviour of the solid phase. The largest stiffness can be found at the articular surface (Mirzayan, 2006). The loading rate determines the influence of collagen network and proteoglycans on the tensile properties. During pulling at a slow loading rate, the tensile strength and the stiffness are entirely accounted for by the collagen network, whereas at increased loading rates, both the collagen network and proteoglycans determine the tensile characteristics. With rapid loading, the proteoglycans prevent rotational motion of the collagen fibres (Fox et al., 2009).
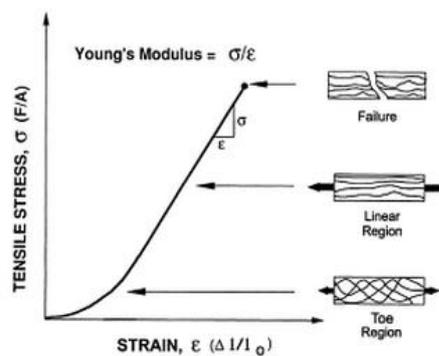
Figure 1-15: Tensile Stress-Strain curve. In the toe region, collagen fibres are aligned according to the tensile force experienced. Tensile modulus is given by the linear region, representing the cartilage stiffness. Failure occurs at maximum tensile stress - reprinted from Nordin and Frankie (2001) with permission from Wolters Kluwer Health Inc.

Cartilage under tension is the result of both flow-dependent and flow-independent viscoelastic properties (Mirzayan, 2006). Repeated tensile loading (i.e. fatigue) over time can lower the tensile strength of the cartilage. As a result of tensile fatigue failure in the collagen meshwork, cartilage may breakdown possibly showing early signs of OA (Freeman, 1962; Weightman, 1976).

1.3.2.3 Shear Stress on Cartilage

Pure shear enables a way to determine the intrinsic properties of the solid phase and consider flow-independent viscoelastic behaviours (Figure 1-16). Shear stress is applied parallel to the articular surface, unlike compressive and tensile forces which

are applied perpendicular to the surface. Therefore, with the application of shear, the volume does not change within cartilage, unlike in the other mechanical loading regimes (Mirzayan, 2006). The lack of interstitial fluid flow through the tissue, suggests that shear is caused by frictional forces between the collagen-proteoglycan matrix components (Mirzayan, 2006). Under shear stress, the considerably stretched collagen fibres are responsible for providing resistance. Therefore, cartilage under shear fails to demonstrate any viscoelastic behaviour.
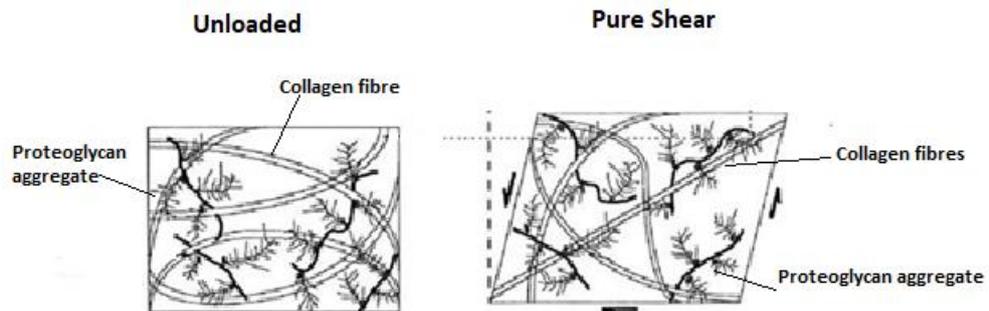
Figure 1-16: Articular cartilage in unloaded state and under pure shear stress. Collagen fibres evidently stretch under shear stress (adapted from El-Husseini, 2005).

1.3.3 Articular Cartilage in Diseased State: Osteoarthritis (OA)

In normal cartilage (Figure 1-17A), the extracellular matrix components are synthesised and catabolised by chondrocytes. The function of the matrix is to sustain the homeostasis of the environment, in which the cells operate, and cartilage structure; whereas in osteoarthritic cartilage (Figure 1-17B), matrix degradation dominates the process of chondrocyte synthesis.
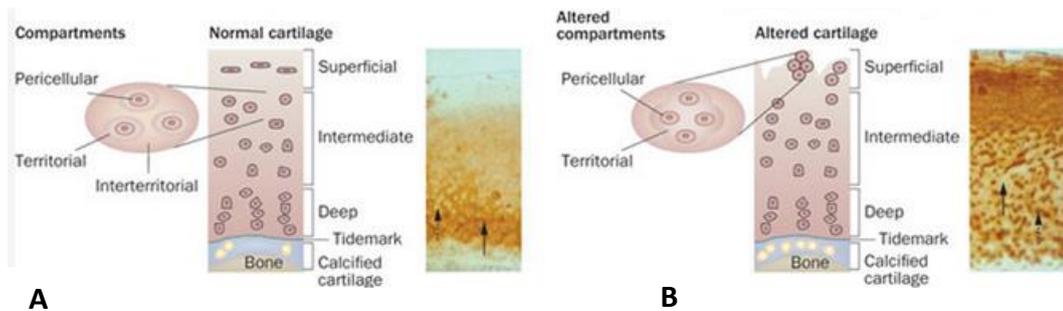
Figure 1-17: A) Compartments within the normal articular cartilage consist of three matrices – pericellular, territorial and interterritorial (left); B) Altered compartments within osteoarthritic cartilage consist of two matrices – pericellular and territorial (right). The pericellular matrix is formed around the cell and molecules within this zone interact with cell surface receptors such as fibronectin. Territorial matrix is nearby pericellular matrix and interterrotorial matrix is furthest away from the cell - reprinted from Thakker et al. (2013) with permission from Elsevier

In the early stages of the disease, a reduction of proteoglycans (PGs) and changes in their structure are evident in the superficial region. As the collagen-proteoglycan matrix and fluid support load within the matrix provide the structural support of the cartilage in the joint, repetitive loading on the cartilage creates additional stresses and strains with repeated fluid outflow and inflow throughout the matrix (Mow and Ateshian, 1997). Over time, localised fibrillation disrupts the superficial zone of the cartilage. Fibrillation is the progression of cracks on the surface and is considered to be the primary indicator of early OA in cartilage.

As the disease progresses with further repetitive cyclic stresses and strains on the cartilage, there is a rapid loss in the PG content and structural changes occur in the proteoglycan-collagen matrix, known as proteoglycan 'washout'. The collagen network is disrupted leading to lower tensile/compressive stiffness and strength leading to the softening of the cartilage (Horton et al., 2006). The load bearing capacity is also reduced (Mow and Hung, 2001). Additionally, metabolically active chondrocytes, which play an important role in the osteoarthritic changes in the cartilage, result in anabolic (matrix biosynthesis) and proliferating effects (Buckwalter and Mankin, 1997; Horton et al., 2006). However, the imbalance between anabolic and catabolic (matrix degradation) pathways suggests the progression of osteoarthritis (Horton et al., 2006).

At the final stage of OA, the progression of the disease restricts chondrocyte proliferation and matrix biosynthesis. The progression of osteoarthritis with increased catabolic activity causes an imbalance between cartilage homeostasis and matrix breakdown (Horton et al., 2006). Eventually, diminished biosynthesis with decreased proliferation causes chondrocyte death (apoptosis), and loss of cartilage. This loss is characterised as end-stage OA with excessive joint pain and lack of function (Buckwalter et al., 2005).

1.3.4 Changes in Biological and Mechanical Properties

The cartilage and subchondral bone in the joint form a functional unit, which acts as a stress distributing and load-absorbing structure (Sharma et al., 2013). Any degenerative changes within this unit needs to be recognised as being important in the study of OA because the initiation and progression of OA is promoted by further damage to the metabolism and structure of the cartilage-subchondral bone unit (Imhof et al., 2000).

As a result of cartilage degradation, the mechanical properties of the cartilage-bone unit may be altered by changing its structure and composition (Boschetti and Peretti, 2008). This further leads to biological impairment of the unit and thus forms a cycle – biological changes cause mechanical change and then changes to the biology follow again. At a stage when these changes become irreversible, the biomechanical properties vary markedly from healthy tissue and are more susceptible to degeneration. This may play a key role in the pathogenesis of osteoarthritis (Zhang et al., 2012).

It is commonly understood that cartilage degeneration leads to altered biomechanical properties preventing normal function of the cartilage (Pearle et al., 2005). In addition, the tribological and material properties are expected to be reduced with poor joint function (Pickard et al., 1998) and damaged tissue (C. Van Mow and Hung, 2001). Mow and Hung (2001) summarised tissue damage into two types – erosion of the cartilage surface and splitting of the cartilage surface. Erosion

describes the thinning of the soft surface (chondromalacia) and splitting is demonstrated by fibrillations which can proliferate into the full thickness of the cartilage. Therefore, healthy cartilage would be thicker than diseased cartilage (C. Van Mow and Hung, 2001; Horton et al., 2006). Frictional shear stress was suggested to be strongly associated with severe cartilage wear (Yamagata et al., 1987; Pawaskar et al., 2011; Taylor, 2012).

Despite the fact cartilage is known to withstand high hydrostatic pressures and compressive loads, its biphasic nature only permits slight resistance to shear stress. Hence, the frictional shear stress, which is directly related to contact stress, plays an important role in the mechanical degradation and fibrillation of the cartilage (Pawaskar et al., 2011).

1.4 Ankle Pathologies and Treatment Options for Ankle Diseases

1.4.1 Ankle Pathology

Ankle joint injuries are becoming prevalent especially in active patients. Due to the complexity of the joint, the cause and effect of the debilitating pain experienced by such patients is yet to be established (Lee and Maleski, 2002). Therefore, without appropriate diagnosis, treatment could be delayed leading to further ankle morbidity (Lee and Maleski, 2002). This section highlights complications experienced within the ankle joint.

The degenerative diseases of the ankle joint cause severe damage to the joint interface that lead to instability of the ankle. Trauma to the ankle is considered to be the main cause of degenerative joint disease (Thordarson, 2004). Following the initial trauma phase, biochemical and biomechanical changes occur, eventually leading to cartilage degeneration (Thordarson, 2004). Damage to any of the bones or supporting ligaments within the ankle may lead to instability of the joint (Nyska and Mann, 2002).

1.4.2 Ankle Osteoarthritis

Osteoarthritis is a common type of arthritis affecting the joints, particularly the hip and the knee and less frequently the ankle. This disease potentially leaves the patient disabled due to limited mobility. In severe cases this disease can lead to mortality in older persons (Buckwalter et al., 2004) due to limited physical activity, presence of comorbid conditions (i.e. cardiovascular and gastrointestinal disorders) and adverse effects of using medications to treat OA (Hochberg, 2008). Arthritis is categorised into primary, systemic and post-traumatic arthritis (Bulstrode et al., 2011). Primary OA becomes more common when advancing in age and is a chronic degenerative disorder (Cooper, 2007). Rheumatoid arthritis (RA) is a system-wide disease, which

occurs when a patient's own immune system begins to attack and destroy the cartilage in the body, known as an autoimmune inflammatory disease (Bouysset et al., 2006). Earlier trauma to the foot or ankle can often lead to the progression of post-traumatic osteoarthritis (PTOA). Therefore, PTOA is likely to occur in the longer term due to an injury to ligament, severe ankle sprain or a simple fracture (Valderrabano et al., 2007; Horisberger, Valderrabano, et al., 2009). Therefore, previous trauma should be explored thoroughly, since it is the most frequent cause of degenerative joint disease within the ankle (Thordarson, 2004).

Valderrabano et al. (2009) investigated the end-stage osteoarthritis in a total of 406 ankles. This study concluded that 78 % of these ankles were suffering from post-traumatic osteoarthritis (such as fractures and ligament lesions in the ankle joint), and the remaining 22 % were primary osteoarthritis and secondary arthritis (such as clubfoot, infections, rheumatoid arthritis). It was further suggested that 62 % out of the 78 % were due to fractures and the remaining 16 % due to ligament injuries (Valderrabano et al., 2009).

The literature has suggested that the progression of post-traumatic OA in the ankle is associated with the extent of the ankle injury, in addition to poor maintenance after the initial trauma (Lindsjö, 1985; Horisberger, Hintermann, et al., 2009). Whilst a study by Stufkens et al. (2010) suggested that post-traumatic OA starts to develop once the ankle has suffered damage to the cartilage (Stufkens et al., 2010). Other studies have supported this finding and revealed that the major cause of post-traumatic OA is due to ligamentous injury (Hirose et al., 2004; Valderrabano et al., 2006).

Using gait analysis, injuries to the lateral ligaments in the ankle was found to lead to abnormal pronation and external rotation during heel strike and abnormal supination and internal rotation during acceleration phase (Hashimoto and Inokuchi, 1997). Such variation in ankle mechanics with specific dysfunctional muscles may be the cause of repetitive damage to the cartilage surface in the medial ankle. Hence,

these characteristics may lead to ankle OA causing varus alignment in the joint (Valderrabano et al., 2009). Therefore, treating osteoarthritis has been a frequent challenge over the years, to manage the disease as well as to prevent it from affecting the patients' mental and physical state. Hence, appropriate treatment methods to ensure long-lasting outcomes are essential to restore ankle function and improve the patients' quality of life (Glazebrook et al., 2008).

1.4.2.1 Osteochondral Lesions in the Ankle

Osteochondral lesions (OCLs) is also known as 'osteochondritis dissecans' and are commonly found in the active population mainly affected by talar lesions. Nearly 70 % of all sprains and fractures in the ankle had reported to result in OCLs (Hannon et al., 2014). However, the cause for this disease is still unclear, although it has been assumed to be due to trauma to the joint (Barnes and Ferkel, 2003). Talar lesions were commonly evident on posterior medial aspect and/or anterior lateral aspect. Anterior lateral lesions result from inversion and dorsiflexion injuries, where this region comes in contact with the fibula, whereas posterior medial lesion result from inversion, plantar flexion and external rotation injuries, where this region impacts the tibial surface. Both lesions present differences in their appearances as the direction of impact (i.e. tangentially or perpendicularly) varies between these. The anterior lateral lesion is shallow and wafer-shaped (Berndt and Harty, 1959), and posterior medial lesions are deeper and cup-shaped (Berndt and Harty, 1959). Osteochondral lesions in the talus also cause weakness, stiffness, locking, and pain is experienced at specific locations of lesions (Chew et al., 2008).

1.4.3 Current Treatment Options for Diseased Ankle

A better understanding of articular cartilage in the ankle joint will benefit early interventions to treat ankle diseases (section 1.4.1). Improved treatment options will help to restore natural joint function and may prevent the need for amputation after primary surgery (Kugan et al., 2013). Depending on the severity of the cartilage damage (or lesions) such condition can also be treated non-operatively. A common

treatment option for cartilage damage involves arthroscopic procedures (i.e. keyhole surgeries). Arthroscopic methods performed to initially treat cartilage damage include debridement, microfracture, drilling, mosaicplasty and autologous chondrocyte implantation (ACI). Other surgical interventions such as joint replacements are commonly required at end stage cartilage damage (arthritis) to repair and restore joint function.

1.4.3.1 Arthroscopic Debridement, Microfracture and Drilling

Typically, one of the three methods or a combination of two from arthroscopic debridement, microfracture (or bone marrow stimulation, BMS) and drilling techniques are predominately used to treat mild to moderate cartilage damage in the ankle joint. An arthroscopic method was regarded to be insufficient for lesions greater than 1.5 cm in diameter as greater risk in healing complication and poor response to treatment with microfracture alone was reported (Alexander and Lichtman, 1980).

Primary treatment methods for talar lesions are arthroscopic debridement or BMS as these have a success rate of 85 % (Zengerink et al., 2010). Arthroscopic debridement is a minimally invasive procedure that involves the removal of areas with loose/redundant cartilage and inflamed tissue (synovitis) from the ankle joint. Bone marrow stimulation (BMS), also known as microfracture, involves creating small holes on the bone surface to cause bleeding from the underlying bone. This forms a blood clot helping to achieve an optimal environment for the tissue to regenerate within the lesion. As a result of microfracture, fibrocartilage (type 1 collagen) is formed. Fibrocartilage is less durable compared to hyaline cartilage found in the joint (Hattori et al., 2004) and hence this method does not replicate mechanical function of healthy articular cartilage found in the ankle.

Previous studies have reported microfracture to show improved patient satisfaction at the start that was poorer in the long-term follow up. A study by Hunt and Sherman (2003) found only 56 % of patients had fair or poor outcomes after arthroscopy or

microfracture at 66 weeks (Hunt and Sherman, 2003). However, another study by Ferkel et al. (2008) reported good to excellent outcomes in 72 % of patients that underwent microfracture after an average of 71 months (Ferkel et al., 2008).

Another method to treat small cartilage lesions is the drilling technique, which includes three types: transmalleolar, antegrade or retrograde. The retrograde drilling technique triggers an inflammatory response such that new bone formation is stimulated in the lesion area whilst not impacting on the healthy cartilage. Retrograde drilling has shown a 100 % success rate in smaller lesions (Kono et al., 2006) when compared against other drilling methods such as transmalleolar or antegrade that involves drilling through the malleolus into the cartilage and the subchondral bone. The latter drilling techniques reported a lower success rate of 60 % as the native cartilage was noted to be damaged post drilling (Robinson et al., 2003).

1.4.3.2 Osteochondral Autograft Transplantation (OAT or Mosaicplasty)

Osteochondral autograft transplantation or mosaicplasty has been used since 1996 in synovial joints to treat large osteochondral lesions (Hangody et al., 1997). Small cylindrical pins are harvested from the donor healthy hyaline cartilage on non-weight bearing joint surface such as ipsilateral medial or lateral articular facet of talus. The pins or grafts are then delivered, compressed and fitted into the talar defect. Hangody et al. (2001) reported this method in talar lesions to have resulted in good to excellent outcome in 94 % of patients with large and unstable lesions of greater than 10 mm in diameter over a 2 to 7 year follow up period (Hangody et al., 2001). No donor site morbidity in long term follow up (7 years) was reported using OAT method for treating talar lesions (Hangody et al., 2001; Georgiannos et al., 2016). Hence, for larger lesions, OAT is a preferred treatment option compared to debridement, microfracture and drilling (Hangody et al., 2001). Furthermore, OAT has a main advantage of preserving hyaline cartilage rather than fibrocartilage, as fibrocartilage does not handle wear as hyaline cartilage and it is more likely to result in early graft failure (Badekas et al., 2013). However, OAT has been used as a

secondary treatment option after failure was observed with microfracture, debridement and/or drilling.

1.4.3.3 Autologous Chondrocyte Implantation (ACI)

Autologous chondrocyte implantation is widely used to treat osteochondral defects in the knee joint (Brittberg et al., 1994; Peterson et al., 2003). This method involves the insertion of concentrated solution of chondrocytes. Advantages of this method include donor site availability and its suitability for any size of defect. However, other studies reported ACI to be suitable for superficial defects rather than cystic lesions and involve a two-stage surgery in the ankle (Baums et al., 2006; Reddy et al., 2007). In a study by Giannini et al. (2014) on the human ankle joint in 46 patients, post-operative outcomes using a scoring system (American Orthopaedic Foot & Ankle Society, AOFAS) have shown greater patient satisfaction compared to pre-operative outcomes. In failed implants (3 out of 46), several aspects of fibrocartilage was also present (Giannini et al., 2014).

1.4.3.4 New Treatment Methods for Diseased Ankle Cartilage

Focal metal resurfacing implants is a new treatment option for talar lesions (van Bergen et al., 2014). A metal resurfacing inlay implant, HemiCAP (Arthosurface Inc, Franklin, MA) with a diameter of 15 mm, was developed to treat osteochondral lesions in the talus in 20 patients with 2 to 5 year follow up period (van Bergen et al., 2014). The implant consists of a cobalt-chrome (CoCr) articular component and a titanium screw. However, longer-term study with more number of patients is required to determine the quality and longevity of the implant.

1.4.3.5 Ankle Fusion (Ankle Arthrodesis)

Since 1879, ankle fusion (or ankle arthrodesis) has been frequently applied as a method for treating ankle arthritis (Bentley, 2009). The surgical technique involves the removal of bone from the tibia and talus and connecting them together with screws (Figure 1-18) which offers compression whilst preventing rotational movement (Caron et al., 1999). Tibio-talar arthrodesis is a traditional operative

procedure and considered a gold-standard treatment designed to deal with the problems of end-stage osteoarthritis (Chow, 2001; DiGiovanni and Greisberg, 2007). However, it is becoming increasingly preferred as an option for treating any stage of arthritis (Bentley, 2009). Ankle fusion aims to alleviate pain, whilst improving overall ankle functionality. Despite this approach being perceived as a salvage option, it permanently modifies gait with the possibility for further degeneration due to the onset of arthritis in adjacent joints, such as the ipsilateral hind-foot (Thomas et al., 2006).

Hendrickx et al. (2011) analysed 121 ankle arthrodeses between 1990 and 2005. The technique of using two incisions with three screws was considered to be a reliable and safe method to treat end-stage OA. Overall, 91 % of patients after undergoing primary surgery were satisfied with the outcome. Ankle fusion resulted in the onset of arthritis in adjacent joints (Hendrickx et al., 2011), which was in agreement with Thomas et al. (2006).

Figure 1-18: Radiographic image of a patient that underwent ankle fusion surgery to treat arthritis - reprinted from Gougoulias et al. (2009) with permission from Oxford University Press.

1.4.3.6 Total Ankle Replacement (TAR)

Total ankle replacement replaces the areas in the ankle affected by arthritis using a prosthesis made up of two or three components (Figure 1-19) (Doets et al., 2006;

Gougoulias et al., 2009). The main advantage is that this method relieves pain, whilst restoring the movement of the ankle to the patients' pre-operative condition.
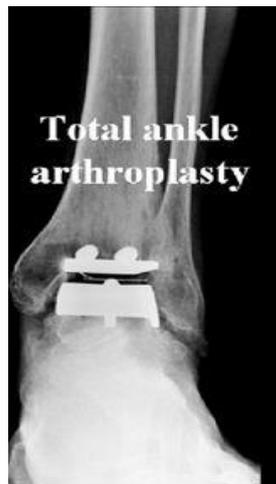
Figure 1-19: TAR performed in patient with arthritis - reprinted from Gougoulias et al. (2009) with permission from Oxford University Press.

In the 1970s, the introduction of TAR resulted in poor results (Lord and Marotte, 1973) and ankle fusion was favoured until the late 1980s and early 1990s. With improved designs that were closer to mimicking the natural anatomy of the ankle, an improvement in clinical outcome for TAR was evident in the late 1990s (Stauffer and Segal, 1981; Saltzman, 1999; Bonasia et al., 2010).

TAR in younger patients (<50 years) has been contra-indicated due to a higher level of activity after surgery compared to older patients (>50 years). A more vigorous and active life can lead to prosthesis loosening and therefore TAR may not be a suitable treatment option for younger osteoarthritic patients compared to older patients. Therefore, TAR was considered to be more suited for patients with lower physical demands (DiDomenico and Anania, 2011).

Total ankle replacement is performed for patients suffering from osteoarthritis, rheumatoid arthritis or post-traumatic arthritis. Total ankle replacement for post-traumatic arthritic ankles resulted in higher complications, revision surgeries and lower patient satisfaction due to high physical demands from younger sufferers compared to other arthritic ankles (Hintermann, 1999).

1.4.3.7 Summary of Current Treatment Options for Damaged Ankle Cartilage

Despite ankle having a low prevalence to OA compared to knee and hip joints (Schumacher et al., 2002), other diseases such as osteochondral defects in the ankle are a major cause for leading to joint damage and was considered as equally as painful to ankle osteoarthritis (VanDijk et al., 2010). Differences in biomechanical and biochemical properties across all three joints may be reasons for how each joint varies in sensitivity to cartilage damage and therefore to the prevalence of osteoarthritis. The characterisation of biomechanical properties of cartilage tissue is important such that effective treatment options for cartilage damage presented at an earlier stage can be identified in the future rather than resulting in end-stage OA which requires surgical intervention such as TAR.

1.5 Current Approaches to Determine Biomechanical Biotribological Properties of Cartilage

Biomechanical properties along with tribological performance of joints need to be thoroughly investigated. Biomechanical testing is used to identify properties such as thickness and structure of the cartilage. These properties are unique due to the complex structure and environment of the joint. Such properties are studied on macroscopic and microscopic levels to reveal the principle of metabolism in cartilage tissue and potential treatment options for cartilage diseases and repair for cartilage defects. Biotribological investigation focus on understanding friction, wear and lubrication which play an important role in the characterisation of natural and artificial joints. Such investigation can help to determine the lubrication mechanisms in articular cartilage as a low coefficient of friction is expected in healthy cartilage to minimise wear. Therefore, these aspects require further investigation to understand the principles underpinning the natural ankle joint.

1.5.1 Biomechanical Testing of Cartilage

1.5.1.1 Cartilage Thickness in Synovial Joints

Several methods for evaluating cartilage thickness have been reported. Non-destructive and destructive methods in both *in-vitro* and *in-vivo* have been studied. *In vivo* imaging methods to obtain cartilage thickness measurements are clinically relevant in understanding the pathogenesis of OA; however are challenging as it requires a high soft tissue contrast to detect the cartilage layer. Previous studies have focused on using CT imaging based method (Siebelt et al., 2011) and needle probe method technique (Shepherd and Seedhom, 1999) to determine cartilage thickness in the ankle joint, whereas in other joints, MRI and shadowgraph have been utilised.

An *in-vivo* CT method has been used to characterise ankle morphometry using 3-D images on 21 patients (average age 40 ± 10 years). This method was concluded to be useful for clinical application such as for designing ankle replacement implants by assessing the geometry of the ankle joint (Hayes et al., 2006). However, due to the

'wedged' shape of the talus, sections on images in the sagittal plane were often taken in an oblique manner, which obscured its contour and had an impact on the overall reliability (Hayes et al., 2006). Hayes et al. (2006) had not quantified ankle cartilage thickness; however another study by Siebelt et al. (2011) used MicroCT *in-vivo* method to quantify cartilage structural properties such as the thickness in the knee joint in a rat. This method was reported to accurately determine cartilage thickness as small changes were able to be detected (Siebelt et al., 2011). Although CT techniques proved to be challenging to characterise whole ankle geometry due to curved samples, cartilage thickness of ankle osteochondral pins using CT techniques was assumed to eliminate high surface curvature factor as pins are considerably smaller in size.

Destructive *in-vitro* methods such as needle probe techniques to quantify cartilage thickness have been previously reported in the ankle joint (Athanasiou et al., 1996; Shepherd and Seedhom, 1999) and other joints such as the knee (Fermor et al., 2015) and hip (Taylor et al., 2011). Shepherd & Seedhom (1999) recorded the thickness of human ankle cartilage of tibial and talar surfaces to range between 1.06 mm to 1.63 mm and 0.94 mm to 1.62 mm respectively using a needle probe technique (Shepherd and Seedhom, 1999). This method involves a sharp needle piercing through the cartilage surface before it reaches the subchondral bone by measuring displacement and load against time (Figure 1-20). It was concluded that thinner cartilage exhibits a higher modulus. The weight and height of individuals also had an influence on the data obtained and showed that the cartilage was thicker in heavier and larger donors. However, an average of 11 cadaveric donor ankle joints in this study, with a mean age of 65.1, may not be an accurate representation of the thickness within the natural ankle joint, as the body mass index (BMI) varied largely between the donors, (13.7 to 24.2). Therefore an updated measurement needs to be established (Shepherd and Seedhom, 1999).
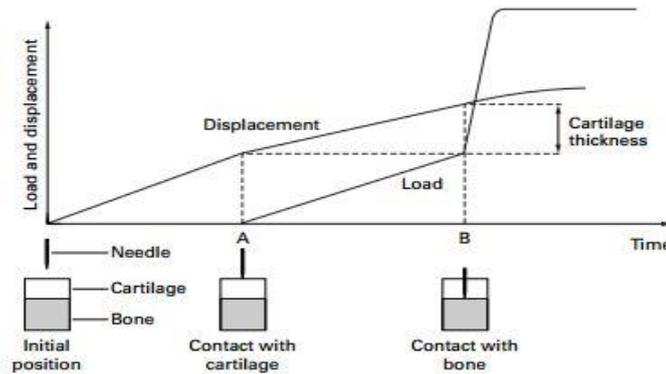
Figure 1-20: Load and displacement over time to determine cartilage thickness using needle probe method - reprinted from Shepherd and Seedhom (1999) with permission from BMJ

Shadowgraph is another imaging technique that has been used to characterise cartilage thickness *in vitro* in the hip (Pawaskar, 2010; Taylor, 2012) and knee (McLure, 2012), but is considered to be a destructive method as there is a risk of dehydration of cartilage tissue from beam of light (Taylor, 2012). Shadowgraphs were concluded to be inaccurate due to significant differences in thickness values compared to needle probe and μCT methods (Taylor, 2012; McLure, 2012).

Magnetic resonance imaging (MRI) is considered to be non-destructive as it operates without radiation. Kladny et al. (1996) measured cartilage thicknesses *in-vitro* in 14 proximal tibial surfaces (knee joints) that were dissected from human tissue. The accuracy of MRI method in thin cartilage layers such as the ankle has been reported to be challenging due to sharp surface curvatures, whereas a greater reliability in cartilage thickness in cartilage layers thicker than 2 mm such as the knee was reported (Kladny et al., 1996). Unlike Kladny et al. (1996), Koo et al. (2005) used *in-vivo* MRI methods in the knee to study segmented MR 3D images on six regions of porcine femur, where contact was established on the cartilage surface during walking to determine cartilage thickness on weight-bearing regions. Both studies were in agreement, cartilage thickness thinner than 2 mm produced less accurate measurements as maintaining acceptable scan time and the signal to noise ratio whilst obtaining sufficient resolution was challenging in a clinical scenario (Kladny et al., 1996; Koo et al., 2005). *In-vitro* testing was considered to be less complex compared to *in-vivo* methods, in which patients would be required to remain still in

a specific position (i.e. sitting or lying) for extended period of time to obtain results. A specific ankle based *in-vitro* MRI study on ten cadaveric ankles was in agreement with the previous studies on the knee joint, suggesting the resolution to be insufficient to precisely determine ankle cartilage thickness resulting in errors ± 100 % in measurements due to the higher congruency and thinner cartilage (Tan et al., 1996).

Articular cartilage thickness varies depending on the species, type of joint, position in the joint and age. The variation of thickness within different synovial joints may be related to joint congruency. A more congruent joint such as the ankle consists of a thinner cartilage than in knee joint, an incongruent joint (Table 1-2). In the thinner talar cartilage, the superficial zone compromises of an increased depth of cartilage thickness, which creates a protective layer to be resistant to damage (Treppo et al., 2000). Furthermore, a congruent joint is more able to distribute loads across the joint surface than an incongruent joint. Therefore, thinner cartilage in a congruent joint such as the ankle is less sensitive to cartilage damage compared to an incongruent joint with thicker cartilage such as the knee (Athanasiou et al., 1995). Cartilage thickness characterisation is a key geometric parameter to understand how it relates to joint congruency.

Table 1-2: Human and porcine cartilage thickness variation among different synovial joints – knee, hip and ankle are presented.

Synovial joint	Cartilage Thickness (mm)	In-vitro Technique	Studies
Human Knee	1.54 to 2.98	Needle Probe	Shepherd & Seedhom (1999)
Human Knee	1.57 to 2.43	MRI	Eckstein et al. (2000)
Porcine Knee	0.82 to 2.23	Needle Probe	Fermor (2013)
Human Hip	1.82 ± 0.18	Needle Probe	Taylor et al. (2012)
Human Hip	1.20 to 2.25	Needle Probe	Shepherd & Seedhom (1999)
Human Hip	0.32 to 3.13	CT	Wyler et al. (2007)
Porcine Hip	1.22 ± 0.05	Needle Probe	Taylor et al. (2012)
Human Ankle	0.94 to 1.63	Needle Probe	Shepherd & Seedhom (1999)
Human Ankle	1.01 to 1.45	Needle Probe	Athanasiou et al. (1995)
Porcine Ankle	unknown	-	-

1.5.1.2 Mechanical Testing of Cartilage

Compression and indentation tests have been used to derive material properties such as aggregate modulus (H_A), permeability (k), Poisson's ratio, and Young's modulus (E) of articular cartilage (Mow et al., 1984; Athanasiou et al., 1995; Taylor et al., 2011). Aggregate modulus (H_A) is the compressive stiffness at equilibrium without any fluid flow. For human cartilage this is in the range between 0.5 to 0.9 MPa. Permeability (k) is an indication to resist fluid flow through its matrix (Mansour, 2009). This is in the range of 10^{-15} and 10^{-16} m^4/Ns (Athanasiou et al., 1991). Poisson's ratio measures the amount of cartilage expansion in plane perpendicular to the applied compressive force. Therefore, a material with zero value will expand along this plane. However, as articular cartilage is attached to the subchondral bone, it cannot swell in this direction (Mirzayan, 2006). Young's modulus (E), which defines the elastic stiffness (modulus) of the material, is in the range between 0.45 MPa and 0.8 MPa for the cartilage. Therefore, cartilage exhibits a significantly lower stiffness value in comparison to steel (200 GPa) (Mansour, 2009).

Confined compression determines two material properties known as aggregate (compression) modulus (H_A) and permeability (k) using the linear biphasic theory (Mow and Huiskes, 2005). Generally, the linear biphasic theory, however, contain three material parameters in a set such as H_A, v, k or E, v, k – by considering Young's modulus (E) or Poisson ratio (v) as a third property. Using unconfined compression tests, Young's modulus can be easily evaluated to indicate the tendency of the cartilage to elastically deform (Boschetti et al., 2004) and Poisson ratio can be evaluated by an optical method to measure the lateral expansion in equilibrium (Lu and Mow, 2008). Confined and unconfined compression tests can either be in a creep mode (Figure 1-21) or relaxation mode whereby a constant load or constant displacement is applied, respectively (Mansour, 2009). Creep has been a more favourable mode to determine deformational behaviour compared to 'relaxation', as 'creep 'is mainly attributed to the fluid exudation (Athanasiou et al., 1991; Athanasiou et al., 1995; Taylor et al., 2011).
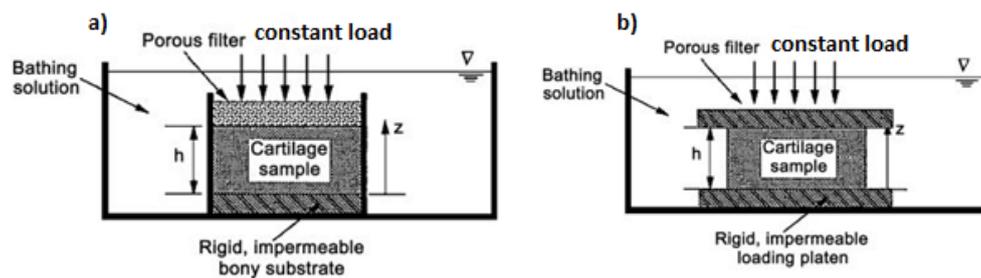
Figure 1-21: Creep test in a) confined compression b) unconfined compression - reprinted from Lu and Mow (2008) with permission from Wolters Kluwer Health, Inc.

Indentation testing replicates the biphasic model of the cartilage more closely due to the evaluation of three parameters, compared with the confined compression studies (Mow and Huiskes, 2005). Indentation tests are mainly in creep mode to determine cartilage deformation as a function of time. During 'creep' indentation testing on cartilage, the underlying bone remains attached to provide a natural environment for testing. A porous indenter allows fluid flow to escape the cartilage through which a constant load is applied onto a small region on the cartilage surface. Depending on the surface curvature the diameter and the shape of the indenter (i.e. flat or hemispherical) can vary. The rate of deformation is related to the permeability

– a high permeability causes fluid to flow out of the tissue easily, which in turn leads to a quicker equilibrium state. A low permeability causes a slow transition from rapid initial displacement to the equilibrium state (Mansour, 2009). These properties were suggested to be helpful in identifying changes in quality of cartilage state – normal and osteoarthritic cartilage (Mansour, 2009). Hence, if the fluid flowed easily out of the tissue matrix, the solid matrix bears the full contract stress, which under high stresses can lead to failure.

Between 1991 to 1995, Athanasiou and his team studied the material properties in the human ankle joint, and in the human and bovine knee joints using creep indentation methods. A 1.5 mm diameter, flat-ended, cylindrical rigid and porous indenter tip was used to perform the tests with a load of 0.03 N to 0.05 N (Athanasiou et al., 1991; Athanasiou et al., 1995). Taylor et al. (2011) reported the mechanical properties of the hip joint in animal and human tissues using creep indentation technique. Taylor et al. (2011) used a rigid hemispherical instead of a flat-ended indenter tip that was twice the size (i.e. 3 mm diameter), and also used a higher load of 0.8 N compared to Athanasiou et al. (1991). The human ankle cartilage had a lower modulus (0.92 to 1.34 MPa) compared to human hip joint (4.89 MPa) and was the least permeable tissue (0.80 to 1.79 x 10^{-15} m^4/Ns) when compared to hip and knee joints across human and animal tissues (Table 1-3). A lower permeability indicates how well the ankle cartilage retains water content which helps to lubricate the joint for healthy function. Hence, any differences in biomechanical properties between the ankle joint and other joints need to be better understood to establish a link to prevalence to OA.

Table 1-3: A summary of aggregate modulus (H$_A$) (compressive stiffness) and permeability (k) of ankle, hip and knee joints in human, bovine and porcine tissues are presented.

Synovial Joints/Studies	Aggregate modulus H$_A$ (MPa)	Permeability (k x 10^{-15} m^4/Ns)
Human Ankle (Athanasiou et al., 1995)	0.92 to 1.34	0.80 to 1.79
Human Knee (Athanasiou et al., 1991)	-	2.17
Bovine Knee (Athanasiou et al., 1991)	-	1.42
Porcine Hip (Taylor et al., 2011)	1.15	5.53
Human Hip (Taylor et al., 2011)	4.89	1.40
Bovine Hip (Taylor et al., 2011)	1.84	3.03

1.5.1.3 In Silico Derivation of Cartilage Mechanical Properties

In-silica simulations have been performed after indentation tests to derive material parameters such as elastic modulus and permeability of the cartilage tissue samples using finite element (FE) models (Pawaskar, 2006; Taylor, 2012; McLure et al., 2012). This can be used to make comparisons between the theoretical and experimental deformation graphs as shown in Figure 1-22 with curve fitting function using Matlab (version 7.4, MathWorks Inc., Boston, MA, USA) (Pawaskar, 2006; Taylor, 2012; McLure et al., 2012).

McLure et al. (2012) investigated the knee cartilage and prior to simulations the cartilage was modelled as a poroelastic material with 900 elements, 80 % of water content with a void ratio of 4. To attain maximum compression, the Poisson's ratio was assumed to be zero. The material properties of the indenter and subchondral bone were also modelled as a rigid incompressible solid and elastic solid, respectively, to replicate the experimental method as closely as possible. The curve fitting function was used to display the theoretical curve onto the experimental curve, highlighting the final 30 % of deformation only. The properties obtained

through in-silica simulations were assumed to represent the intrinsic mechanical properties of the cartilage samples (McLure et al., 2012)
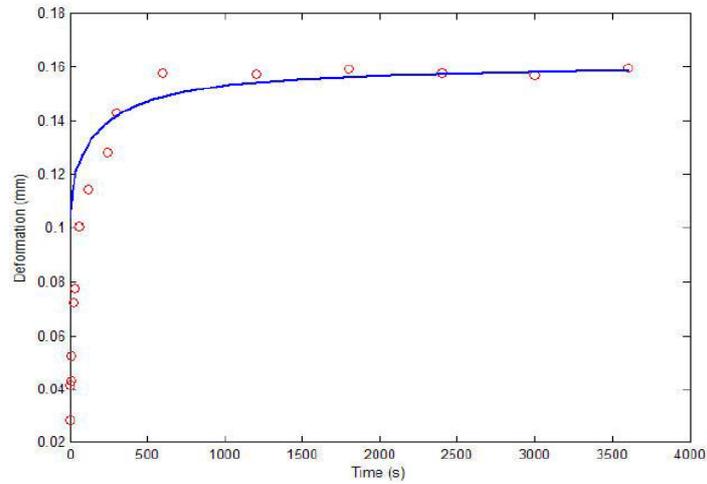
Figure 1-22: An example of curve fitted graph, red circles represent the indentation results (experimental); blue line represent the theoretical model derived by finite element model (Taylor, 2012).

A study by Taylor et al. (2012) applied the same methodology to derive such properties of hip cartilage samples instead. For the hip cartilage sample, a 3 mm in diameter hemispherical indenter and subchondral bone were modelled using ABAQUS (Version 6.9-1) (Figure 1-23) similarly to McLure et al. (2012). McLure et al. (2012) and Taylor et al. (2012) have applied a ramp load from 0 to 0.8 N through the hemispherical indenter onto the cartilage surface for a period of two seconds only; it was then held constant for a further 60 mins.
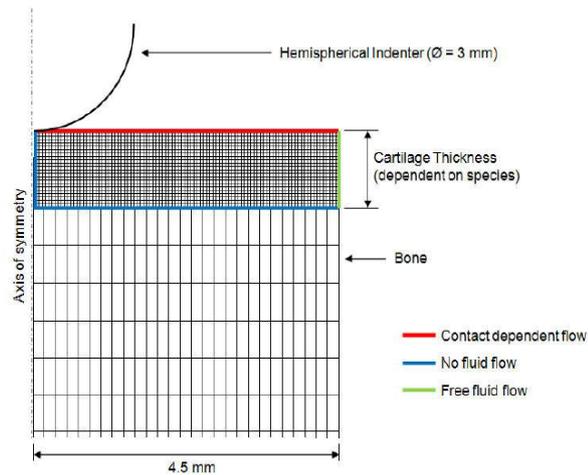
Figure 1-23: Axisymmetric poroelastic biphasic finite element (FE) model replicating the indentation method performed on the cartilage surface using a hemispherical indenter of 3 mm in diameter (Taylor, 2012).

Computational modelling is an important tool for evaluation of tribology and biomechanics. A three-dimensional (3D) finite element (FE) model can be used to predict load distribution and biomechanical behaviour. Therefore, it can be adopted to study the tribological properties and develop close to natural mechanisms of the joint. The models are limited by the accuracy of the geometrical measurements and material properties used to develop accurate representations of the joints.

1.5.2 Biotribological Characterisation of Cartilage

Friction, wear and lubrication studies play an important role in the biotribological characterisation of natural and artificial joints. Such investigation can help to determine the lubrication mechanisms in articular cartilage as a low coefficient of friction is expected in healthy cartilage to minimise wear. Therefore, these aspects require further investigation to understand the principles underpinning the natural ankle joint.

1.5.2.1 Introduction to Tribology

Tribology is a multidisciplinary science that contributes to every aspect of our daily lives, starting from live cell friction to engine lubrication (Myant, 2013). Tribological characterisation of materials has been associated with physical, mechanical and

chemical properties as well as with the conditions under which the relative motion takes place (Arnell et al., 1991). For a given structure, the tribological characteristics are influenced by factors including sliding velocity, temperature, geometry, change in load and other physical and environmental conditions (Furey, 1995).

1.5.2.2 Introduction to Biotribology

The term *biotribology* was introduced in 1970s and aims to specifically address the same principles in biological systems. These include joints, the spine, eyes and jaw which are considered to encounter tribological characteristics of biological tissues (Dowson and Wright, 1973).

1.5.2.3 Biotribology in Synovial Joints

The conditions the natural joint works under, such as range of motion, load, contact pressure, number of joint cycles and velocity are individualistic (Dumbleton, 1981). These parameters can be used to evaluate the performance of the joint. Information on both, a macroscopic level, highlighting articulation between the joint surfaces, and on a microscopic scale, examining friction and wear through the interaction between the surface materials and the fluid, may be beneficial for comparison with a diseased joint (Dumbleton, 1981).

Numerous lubrication regimes in the joint have been established over the years which focus on friction only (Medley, 1981; Furey, 1995). Wear has not been taken into account (Furey and Burkhardt, 1997). Hence, understanding cartilage wear, damage and the process of degeneration in the natural joint is still limited.

1.5.2.4 Basic Theories of Friction

Friction is described as a resistive motion that occurs when two solid objects move relative to each other (Freeman, 1962). Interaction between these surfaces at the point of contact can lead to frictional resistance. In most cases, friction leads to failures in mechanical systems, such as natural joints as well as artificial joints.

Two theories of frictional interaction between surfaces were introduced in the 1930s, one is adhesion and the other is interlocking or displacement (Bowden and Tabor, 2001). In the adhesion theory, the tips of the asperities on surfaces come into contact with each other during loading. As the real contact area (apparent area) is small, the pressure is presumed to be higher to cause deformation over the asperities (Bowden and Tabor, 2001). The other type of friction arises from ploughing out a grove by a hard asperity that has penetrated into softer counterface. At the microscopic level, the surface is known to be rough. Bowden & Tabor also proposed a combined friction theory of adhesion and ploughing, known as the composite theory (Bowden and Tabor, 2001).

The frictional laws state that frictional force is directly proportional to the applied load, and independent of the apparent area in addition to the sliding velocity (Freeman, 1962). The coefficient of friction (COF) (μ) quantifies the frictional resistance and is the ratio between the frictional force (F) and the applied load (N) on the surfaces as shown below in Equation 1-1.

$$\mu \text{ (Coefficient of Friction or COF)} = \frac{\textbf{Frictional Force (F)}}{\textbf{Applied Load (W)}}$$

Equation 1-1: First law of friction

An increase in applied load leads to a decrease in the value of coefficient of friction (COF) (Callaghan, 2003).

Coefficient of Friction in Cartilage

Cartilage provides a bearing surface with low friction by distributing loads between opposing bones in the natural joint. Smooth cartilage surfaces provide an area for sliding, reducing friction and enabling bone movement. Therefore, the coefficient of friction in natural joints is low, roughly 0.001 (McCutchen, 1962; Unsworth et al., 1975). In the ankle, the frictional coefficient is relatively lower compared to other natural joints (Table 1-4). The mechanisms responsible for such low values in synovial joints have been an ongoing area of research over many years. Reduced levels of friction lead to lower energy losses and increase the efficiency of operation. Hence,

low friction keeps the joint healthy and lubricated maintaining smooth and effortless movement.

Table 1-4: Coefficient of friction values of articular cartilage in synovial joints (adapted using Callaghan, 2003).

Study	Coefficient of Friction	Type of Joint
Charnley (1959)	0.005 – 0.020	Human Ankle
McCutchen (1959)	0.02-0.35	Porcine shoulder
Linn (1967)	0.005 – 0.010	Canine ankle
Unsworth et al. (1975)	0.01 – 0.04	Human hip
Malcom (1976)	0.002 – 0.030	Bovine shoulder

Over a century, several frictional methods have been employed to study the outstanding properties of the articular cartilage and the lubrication modes it operates within. Several studies investigated frictional behaviour of cartilage under various lubrication modes with different lubricants, or with mechanically or chemically changed tissue engineered cartilage specimens. Cartilage on cartilage configurations represents a more realistic model with synovial fluid acting as the lubricant. Instead, many studies have used glass or metal contacts with non-physiological loading conditions which are not representative of tribological condition found *in vivo* (Freeman et al., 2000; Katta et al., 2008; Gleghorn and Bonassar, 2008). A possible reason for studying cartilage on glass or metal contacts is to improve function of current implant designs. Hence, natural interaction between two cartilage joint surfaces is often not fully understood and mostly dated in need for further investigation.

As cartilage friction is assumed to be influenced by variables such as contact stress, contact area, lubricant, sliding velocity and distance and loading time, it is important to vary these accordingly to obtain the necessary data. Typically, the stroke length ranges between 4 mm to 10 mm, contact stress between 0.2 to 16 MPa, sliding velocity of 4 mm/s and loading time between 1 to 24 hours (Katta, 2007; Northwood and Fisher, 2007; Katta et al., 2008; Lizhang et al., 2011). A low sliding speed of 4

mm/s promotes the configurations to remain within mixed or boundary lubrication modes during sliding (Forster and Fisher, 1999). Contact stresses greater than 8 MPa cause severe damage to the cartilage during friction tests (Lizhang et al., 2011). When cartilage was tested against cartilage and metal plates using bovine knee tissue, the COF was reported to have reached up to 0.3 for using synovial fluid and Ringer's solution as lubricant (Forster and Fisher, 1996). Although no significance was reported for using different lubricants for cartilage on metal contacts, cartilage on cartilage showed significantly lower COF using synovial fluid compared to Ringer's solution. Northwood and Fisher (2007) also studied friction output for both configurations, suggesting a significantly higher COF of 0.70 ± 0.02 for cartilage on metal contacts compared to cartilage on cartilage with 0.05 ± 0.015 in bovine knee samples (Northwood and Fisher, 2007).

Friction studies on articular cartilage mainly focus on knee or hip samples during testing. However, ankle cartilage can also be employed in such friction testing to derive frictional properties of the joint. Based on the available literature, the variables and inputs will be adopted accordingly, in order to test cartilage properties of the ankle.

1.5.2.5 Wear Theory

Wear usually occurs due to direct contact between rough surfaces at sliding interfaces, which is typically known to be the onset of wearing (Stachowiak and Batchelor, 2011). Wear involves the removal of material from a surface, which can be detectable as mass (weight) loss and/or volume loss. Indications of wear include changes to the surface roughness, waviness and form. However, it is important to distinguish whether these changes are due to wear or result from plastic deformation, which occurs without any material loss.

The basic mechanisms of wear include adhesive wear, abrasive wear, fatigue wear, corrosive and erosive wear.

Adhesive wear has been identified for nearly 40 years and is the most common type of wear mechanism which involves transferring the material from one surface to another due to cold welding at asperity junctions (Berthier et al., 1989). This type of wear can be minimised by selecting materials with low adhesion tendency and promoting effective lubrication. Abrasive wear results from ploughing out grooves by hard asperities into a softer counterface. When hard particles are entrained in the interface and abrade the softer surfaces, this is commonly known as third-body abrasion. Fatigue wear results in the removal of material due to cyclic stress variations over a period of time. Unlike adhesive and abrasive wear, fatigue wear can occur without direct contact between the surfaces (Berthier et al., 1989; Stachowiak and Batchelor, 2014). Corrosive wear occurs when tribological components are operating in corrosive environments resulting in reaction products that do not effectively adhere to the surfaces. With further sliding, the reaction product is easily displaced and further chemical reactions occur at a higher rate. Erosive wear causes damage to the surfaces due to the impact of solid particles within a fluid. This form of wear does not require two solid surfaces in relative motion. Therefore, it is not often addressed in the subject of tribology.

Cartilage Wear Studies

Early studies evaluated cartilage wear using several *in-vitro, in-vivo* and *ex-vivo* methods on the whole joint. *In vitro* studies included changing loading conditions, lubricants, sliding speed and type of biomaterials used for joint replacement purposes. However, *in-vitro* and *ex-vivo* cartilage wear is not directly comparable to *in-vivo* tests and does not accurately mimic the physiological environment. Changes to the loading conditions and motions are not comparable between tests and therefore alter the lubrication mode in which the cartilage operates. Hence, the outcomes of in-vitro wear studies were largely dependent upon the experimental setup.

Wear rate estimates the thickness of the worn layer from the cartilage surface (Neu et al., 2008). This is an important parameter to evaluate wear patterns. However, a

consistent method for measuring wear rates for cartilage is yet to be determined and has been a challenge as the cartilage tends to swell due to hydrophilic nature of proteoglycans (Thomas et al., 2009).

From 1974 to 1979, Glimcher, Lipshitz and Etheredge investigated the wear on the femoral knee cartilage in an *in-vitro* study using bovine tissue. With the application of a cyclic sliding motion on a cartilage-metal system, the authors concluded that wear rates increased with an increase of normal load, considering the surfaces were moving at a relative speed (Lipshitz and Glimcher, 1974; Lipshitz et al., 1975; Lipshitz and Glimcher, 1979). The change in weight, roughness, and surface damage help to determine overall wear of cartilage specimens. A recent study evaluated several *in-vitro* wear methods in knee specimens including using a modified wear factor, Indian ink to identify surface damage and changes in surface roughness (McGann et al., 2012). This study concluded that surface damage technique on cartilage as an effective approach to evaluate wear.

With the use of imaging techniques such as environmental scanning electron microscopy (ESEM) and scanning electron microscopy (SEM) of the articular cartilage, the extent of damage can be qualitatively evaluated. Using ESEM, the natural state of the cartilage can be imaged. Above the collagen matrix, a surface layer has been identified with this technique. During the onset of wear, this layer becomes disrupted (Graindorge and Stachowiak, 2000).

An *in-vivo* study by Seireg and Gerath (1975) investigated the wear of the whole patella joint in the mouse with the evaluation of histology and X-ray methods. These authors concluded that below the damaged cartilage surface, the collagen fibril arrangements change from being an open mesh to more closely packed, which is also evident in an arthritic joint. The limitations of using an *in-vivo* whole joint model include difficulties comparing joints due to variation in geometry which changes the contact area and contact stresses applied onto the joint (Seireg and Gerath, 1975).

The presence of water in the cartilage also proves certain difficulties in SEM analysis, as the cartilage dehydrates and changes result.

An earlier *ex-vivo* whole joint study by Radin et al. (1982) on the bovine knee joint used an arthrotripsometer to examine the influence of loading conditions on the wear properties of the cartilage. The arthrotripsometer was designed to measure frictional behaviour and cartilage deformations. Based on histological analysis from strained cartilage sections, a reduction in thickness was identified as wear which did not change with the presence of lubricant (Radin et al., 1982). However, the applied loads onto the whole joint did not replicate natural joint motion. Furthermore, the molecular component of the synovial fluid and its lubricating ability is likely to have changed with the addition of other fluids or additives.

Wear tests on the cartilage cannot easily be compared due to differences in loading and motion regimes used, in addition to the changes in the mode of lubrication due to altered biological components of the lubricant. Combinations such as cartilage-on-material or material-on-material do not mimic the physiological conditions of a natural joint and its surface interactions. Cartilage wear testing techniques do not vary much between different synovial joints despite the change in surface geometry. Therefore, despite the fact that whole-joint models may provide close to natural joint motion, analysing data has been a challenge due to complex surface geometries. A standard wear test between two cartilage surfaces, with given geometry, applied stresses and sliding distances could be an option to investigate the wear mechanisms involved in the process of cartilage degeneration.

Cartilage Wear in the Ankle Joint

A vast majority of studies on ankle joints focus on prostheses and their performance rather than the natural synovial joint (Lord and Marotte, 1973; Conti and Wong, 2002; Valderrabano et al., 2003; Glazebrook et al., 2008; Flavin et al., 2013). Wear mechanisms in the natural ankle joints are poorly understood. Overall, the surface geometries of the ankle compared to other joints, such as the knee joint, are

different; therefore wear properties and lubrication abilities of the synovial fluid cannot be assumed from studies of other load-bearing joints. The articulating surfaces are markedly curved compared to the knee specimens, which are relatively flat. Therefore, wear tests specific to the ankle joint need to be designed in order to evaluate the process of wear during cartilage degeneration.

1.5.2.6 Lubrication Regimes

The form of lubrication acting within a tribological system such as synovial joint is a function of the materials used, surface conformity and texture, lubricant properties and operating conditions such as speed, temperature, load and environment. There are four regimes known as boundary lubrication, mixed lubrication, elastohydrodynamic lubrication and hydrodynamic lubrication. Although these lubrication regimes are commonly found in a tribological system, the most important form of lubrication in the cartilage is the biphasic lubrication.

Biphasic lubrication combines the solid and fluid phases in the cartilage and adapts the biphasic theory that both phases are not compressible, separate and immiscible (Mow and Hung, 2001). Biphasic and load-bearing properties of the cartilage suggests that the load carried by the fluid phase plays a key role in determining friction and the mode of lubrication operating in the cartilage. Boundary lubrication (BL) is not ideal, as the asperities of these surfaces are in constant contact. Therefore, it is expected to occur in 'rough bearing surfaces, or as a result of third body formation or protein deposition' (Hamrock et al., 1994). The properties of surface materials and lubricant films at their common interfaces are used to evaluate friction and wear behaviour. Mixed lubrication (ML), known as a transition stage, combines two regimes which are fluid film lubrication (FFL) and boundary lubrication (BL) (Hamrock et al., 1994). Until fluid-film lubrication is reached, the coefficient of friction (COF) will continue to decrease. Within this regime, the lubricant separates the surfaces in contact. This regime is also referred to as hydrodynamic lubrication and depending on conformity of the articulating surfaces, it can be separated into two categories – conforming and not conforming (Hamrock et al., 1994). When a

considerable increase in fluid-film pressure is capable of deforming the asperities of the articulating surfaces, elastohydrodynamic (EHD) lubrication occurs. The shape of the surfaces is considerably modified and physical properties of the lubricant are enhanced within this regime.

Joint Lubrication: Synovial Fluid

Natural joints seem to perform within better lubrication modes due to the presence of a natural joint fluid (i.e. synovial fluid) when compared to artificial joints. Therefore, low friction and wear in natural joints is associated with the existence of a natural lubricant, which produces an efficient lubrication system. Synovial fluid is a nourishing material within the joints and is a clear, pale yellow, viscous solution that is not prone to clotting (Cooke et al., 1978). Unlike other fluids in the body derived from plasma, synovial fluid contains a large amount of hyaluronic acid (HA) (mucin). The normal viscosity of synovial fluid is achieved with the presence of HA, which determines the lubrication ability (McCutchen, 1983).

The normal volume of the fluid is variable between different joints, with healthy knee joint containing up to 4 ml of synovial fluid (Mundt and Shanahan, 2010) (Mundt & Shanahan, 2010). The role of the fluid is to transport nutritional substances, such as glucose in addition to supporting the mechanical function of the joint by lubricating the articular surfaces (Dumbleton, 1981). In the presence of a degenerative disorder in the joint, lubrication regime in which the joint operates within will be altered. However, research is limited on understanding the impact of synovial fluid and changes to the lubrication regimes within the joint during the process degeneration.

Cartilage Lubrication

Despite the on-going research on the lubrication modes acting within the natural joints, studies aim to establish fluid film and mixed modes to enhance the cartilage lubrication (McCutchen, 1983; Berthier et al., 1989). Boundary lubrication may possibly lead to cartilage wear due to higher friction and low to zero sliding velocity.

Therefore, as sliding velocity decreases, the load is subsequently increased leading to boundary lubrication mode.

Intra-articular injections of lubricants have been implemented to treat osteoarthritis in addition to cartilage tissue engineering approaches (McNary et al., 2012). However, these have limitations such as the lubricant not being strongly bonded or absorbed to the cartilage surface (McNary et al., 2012). During implant testing on the simulators, bovine serum has been used as a substitute for natural synovial fluid (Affatato et al., 2008). Ringer's solution and Phosphate Buffered Saline (PBS) have also been used (Katta et al., 2008).

In the human ankle joint, boundary lubrication seems to be operating under steady sliding speed during gait, once the cartilage zones are damaged (Hlavácek, 1999; Hlaváček, 2000). However, a continuous synovial fluid film thickness of approximately 1 µm is evident during gait under steady motion (Hlavácek, 1999).

However, lubrication studies on the ankle still seem fairly limited and require further research to provide up to date understanding of how the ankle operates. The main focus seems to be on wear and friction on artificial joints rather than natural joints. Hence, this project highlights the necessary areas to study this aspect of biotribology.

1.5.3 Biological Properties of Cartilage

The purpose of biological characterisation will be to identify differences in structure and biological constituents of the cartilage between the animal and human tissues.

Histological analysis can be used to qualitatively characterise cartilage thickness, chondrocytes distribution, GAG distribution and collagen orientation using staining methods such as H&E, Alcian blue and Sirius red/Miller's elastin. Quantitative assay analysis is used to calculate the collagen and proteoglycan content. Collagen and proteoglycan content in the cartilage are important constituents and contribute to the mechanical properties, such as stiffness and strength of the cartilage.

In a healthy cartilage, the water content, which makes up of up to 80 % of the fluid phase in the cartilage, is lower with higher PG content and collagen fibrils are larger in diameter compared to a diseased cartilage (Fox et al., 2009). As the frictional resistance against the water flow through the matrix is very high in the healthy cartilage, the permeability is expected to be low (Fox et al., 2009). A study by Kuettner and Cole (2005b) reported that the ankle cartilage in its healthy state compared to the knee cartilage to have significantly higher chondrocytes synthesis rate (28,799 cpm/mg DNA in the ankle vs 15,510 cpm/mg DNA in the knee) and significantly lower water content (i.e. decreased permeability) with an increased PG synthesis rate and turnover (22.68 days in knee vs 16.58 days in the ankle). These properties were suggested to reduce permeability and increase stiffness of the ankle cartilage (Kuettner and Cole, 2005). This was in agreement with previous studies (Callaghan, 2003; Fox et al., 2009), suggesting a low water content, low permeability, high PG synthesis and high collagen and PG content are all favourable cartilage properties which maintain normal joint function.

1.6 Rationale

The current project will determine the biomechanical properties of natural ankle cartilage using mechanical, tribological and biological testing approaches. Such investigation will help to comment on its sensitivity to damage. For the human ankle study, immature porcine model will be used and its methods will be refined and further developed in preparation for investigating mechanical characteristics such as cartilage thickness, deformation and surface roughness of the human ankle cartilage. Porcine ankle joints were chosen as their anatomical features were comparable to human ankle joint (i.e. single tibiotalar joint).

Currently, all ankle treatments and any early interventions for osteoarthritis (OA) and other diseases such as osteochondral defects are based on knee and hip joints technologies. Human knee cartilage has been previously used (Whittaker et al., 2005) to treat ankle osteochondral defects and this could potentially result in mismatch as both joints vary in overall joint congruency (Simon, 1970; Hangody et al., 2001), thickness (Shepherd and Seedhom, 1999) and other biomechanical characteristics such as increased stiffness and reduced permeability (Treppo et al., 2000; Kuettner and Cole, 2005). Due to poor surgical interventions and limited information on the natural ankle joint, studying the mechanical characteristics of the ankle joint could potentially contribute to the field, and be useful in developing methods to interventions. The current project may also feed into other research opportunities to identify a closer link to possibly finding targeted treatment options for cartilage damage in the ankle joint. Presently, existing clinical interventions for ankle OA are considered to be unsuccessful compared to the other joints due to limited research. Ankle osteoarthritis (OA) is less prevalent compared to other joints, although pain and lack of mobility in the ankle is comparable to that in knee and hip joints. Ankle cartilage damage progressing into end stage OA requires surgical intervention such as total ankle replacement to treat the damage. However, this surgical method of treatment often results in revision surgeries and in the ankle this was reported to have been higher than that in the knee (National Joint Registry, 2013). Current treatment options for ankle cartilage damage at an early stage needs to be more

effective to prevent its progression into end stage OA without the need to surgically replace the joint; therefore an understanding of the mechanical characteristics could be helpful to address this.

The current project is the first of its kind to compare mechanical characteristics between porcine and human ankle joints which could potentially help in future for the replacement of cartilage. Furthermore, such investigation will help to predict ankle cartilage function in its natural state ('healthy model'), understand tribological behaviour and identify how cartilage composition may contribute to mechanical and tribological properties observed.

1.7 Aims and Objectives

The main aim of this thesis will be to develop and adapt experimental methods to investigate the biomechanical properties of the porcine and human ankle joints. New knowledge on the ankle cartilage can help to understand its function and its tribological behavior in its natural state. This can be helpful to predict how sensitive the ankle is to cartilage damage.

The primary objectives for this thesis will be as follows:

- Modifying existing experimental methods to determine cartilage thickness of porcine tissue

- Establishing a method for evaluating human ankle cartilage thickness

- Determining cartilage deformation of talar and tibial cartilages in the ankle joint of porcine and human ankle joints

- Developing a method to compare pin study and whole joint study using porcine tissue to study the influence of specimen preparation for osteochondral pins compared to whole joint surfaces

- Investigating and comparing mechanical characterisation of porcine ankle and human ankle cartilages

- Developing an understanding of tribological behaviour of ankle cartilage in porcine tissue

- Quantifying and characterising biological constituents such as GAG and visualising cell structure in porcine ankle cartilage using histological techniques

Chapter 2: General Materials and Methods

2.1   Introduction

Experimental studies of cartilage are an important tool in understanding the properties of cartilage and predicting function of the natural joint. This chapter outlines the materials and methods for joint dissection, extraction and storage of porcine and human ankle tissues.

2.2   General Materials

2.2.1 Phosphate Buffered Saline

Phosphate buffered Saline (PBS) was used throughout all studies documented in this thesis to maintain cartilage hydration. PBS was sprayed onto cartilage samples during specimen preparation and during storages the cartilage samples were covered in PBS-soaked tissue. For preparing the saline solution, tablets obtained from MP Biomedicals (OH, United States) were used according to the manufacturers' instructions – dissolving one tablet per every 100 ml of sterile, distilled water. PBS contains several other components as highlighted in Table 2-1.

Table 2-1: Components found in Phosphate Buffered Saline provided by MP Biomedicals (OH, United States).

Components	Concentration (mg/litre)	Molecular Weight (DA)	Molarity (mM)
Potassium chloride [KCl]	200.00	74.55	2.68
Potassium phosphate monobasic [KH2PO4]	200.00	136.09	1.47
Sodium chloride [NaCl]	8000.00	58.44	136.89
Sodium phosphate dibasic [Na2HPO4]	1150.00	141.96	8.10

2.3 Specimen Preparation: Porcine Tissue and Human Tissue

The porcine tissue was studied as the the ankle joint has a comparable anatomical feature to the human tibio-talar joint in which the tibial surface articulates over the talar surface making up a 'single' tibio-talar joint. The skeletal structures of porcine ankle joint are highlighted in Figure 2-1. However, the surface curvature in the porcine ankle joint was considerably higher compared to the human ankle joint. The porcine ankle tissue has not been studied before and as the tissue was readily available, the initial tests were conducted on the animal tissue in preparation for the human tissue testing.

2.3.1 Porcine Ankle Joint

The characteristics of the animal tissue used in this study are summarised in Table 2-2. The tissue was juvenile (3-6 months) and received within three days of slaughter.

Table 2-2: Porcine ankle joints dissected in the current study and their characteristics.

Species	Received Post Slaughter	Age	Left or Right Leg	Condition	Source
Porcine	24 - 72 hrs	3 to 6 months	Right-sided	Full leg with tissue	Penny's Abbattoir, Rawdon, Leeds, UK (meat used for human food chain)
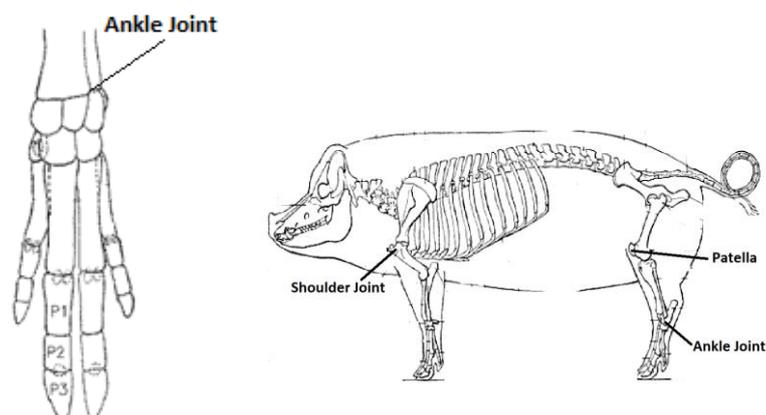
Figure 2-1: Skeletal structure and anatomy of porcine ankle joint (adapted from Cuyer (2011))

2.3.1.1   Dissection of Porcine Ankle Joints

The talar and tibial cartilage surfaces were dissected from the porcine ankle joint (Figure 2-2A). The porcine tissue was delivered as a whole leg and it was cut off below the knee in the labs using a blade (Figure 2-2A) and a hand-held saw tool to isolate the ankle joint (Figure 2-2B). This was done by removing the external skin including muscles, ligaments and joint tissue (Figure 2-2C; Figure 2-2D) leaving the ankle surface exposed (Figure 2-2E; Figure 2-2F). The cartilage was visually inspected to ensure undamaged cartilage was sampled.
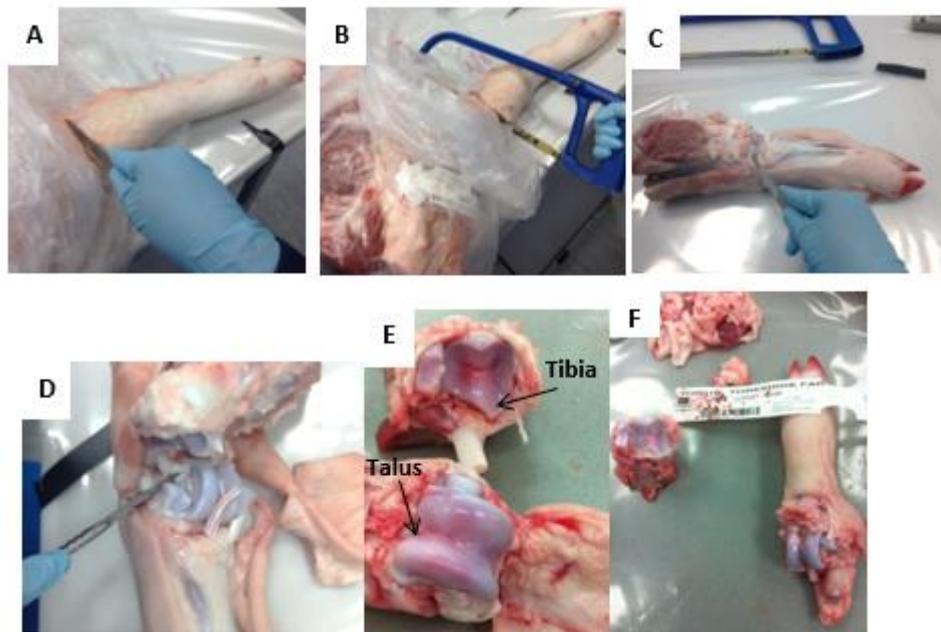
Figure 2-2: The talar and tibial surfaces were dissected from porcine tissue; A) to D) dissection of porcine ankle joint; E) and F) dissected joint surfaces of talus and tibia.

2.3.1.2   Preparation of Porcine Intact Talus for Testing

Mechanical testing and cartilage thickness mapping were performed on the porcine intact talus joint (whole joint study, n=6) (Chapter 3, section 3.5.6 and section 3.5.2). The talus (Figure 2-3) was dissected from the tissue using a scalpel and saw to remove additional bony structures (Figure 2-2). Care was taken to ensure the cartilage surface remained undamaged during dissection.

PBS-soaked tissue paper was placed over the talar surface and the bone inserted into a sealable bag and frozen at - 20ºC. The samples were then thawed in the fridge overnight before testing. The specific details of the experimental setup will be discussed in Chapter 3 (section 3.6).

Figure 2-3: Porcine talus surfaces. A) Talus attached to the rest of the feet; B) Further dissection had to be completed to isolate talus from porcine tissue by removing joint tissue.

2.3.1.3 Extraction of Osteochondral Pins: Porcine Tissue

An 8.5 mm diameter corer tool (Figure 2-4A), Smith & Nephew, Andover, MA) used for mosaicplasty procedures to repair cartilage defects in the knee joint, was used for extracting osteochondral pins from lateral and medial aspects of the talar and tibial surfaces, n=6 for each region. The marking on the side of the corer tool identified the depth once the tool was placed though the joint surface. Each pin was extracted to a depth of at least 5 mm by hammering through the cartilage surface (Figure 2-5E).

Figure 2-4: Pin removal tools included three separate instruments; A) 8.5mm diameter corer tool; B) Summary of all tools used during pin extraction, from bottom up – hammer, 4 mm diameter rod, corer tool, 8 mm diameter stainless steel rod, ruler and small saw for removing excess bones attached.

The tibial and talar surfaces were secured into the vice such that movement during extraction was limited (Figure 2-5). To ensure tissue hydration inbetween pin extraction, the joint surfaces were covered in PBS soaked tissue. Using the corer tool (Figure 2-4A) a circular groove of 8.5 mm diameter was created on the cartilage surface (Figure 2-5B) such that a precise extraction from the chosen location was possible. The corer tool was placed over the marked region and carefully hammered in to a depth of at least 5 mm using the markings on the corer tool (Figure 2-5C). Using a metal rod (Figure 2-4B) inserted at the top end of the corer tool, with a few twists and swift sharp motion, the pin became detached from the joint surface (Figure 2-5D). To carefully remove the extracted pin from within the corer tool, a metal rod (Figure 2-4B) was inserted into the corer from the bone end (Figure 2-5F). The same technique was used to extract the tibial pins.
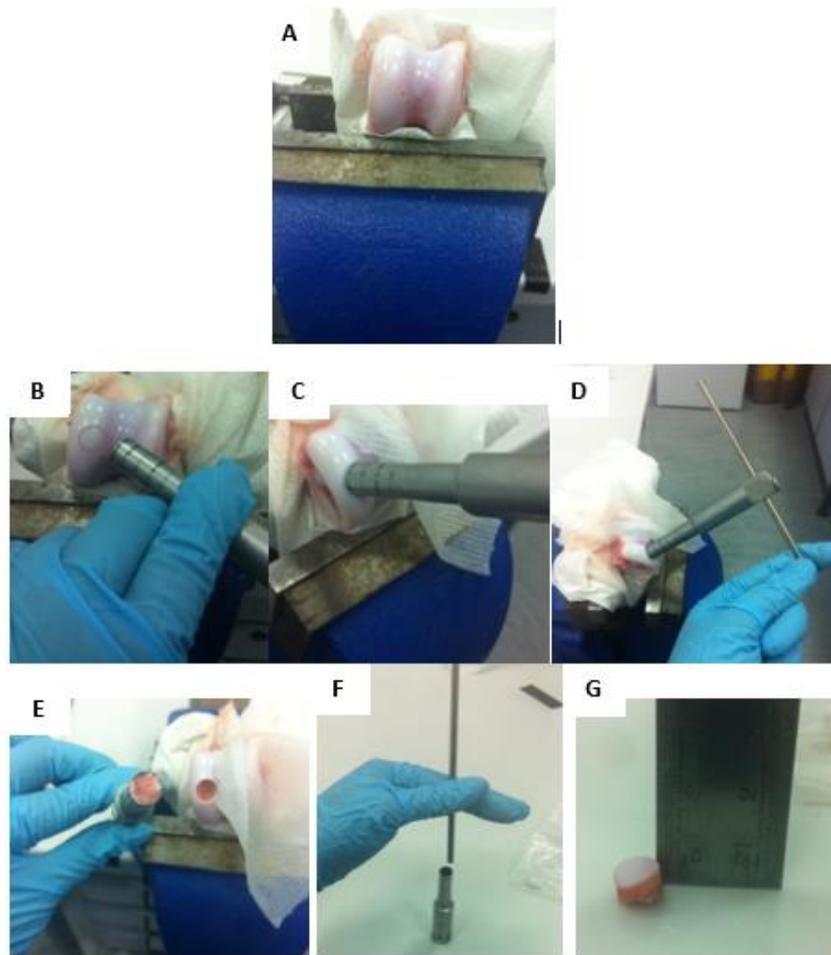
Figure 2-5: Porcine talar pins were extracted using Smith & Nephew 8.5 mm corer tool using a hammering technique by securing the joint surface onto a vice.

2.3.2 Bovine Ankle Joint

Previous studies reported comparable cartilage thicknesses and high levels of proteoglycans between the bovine and human cartilage despite differences in anatomical structures in the knee joint (Rieppo et al., 2003; McLure, 2012; Fermor, 2013). Therefore, the bovine ankle joint was also dissected (Figure 2-6) to further investigate the ankle joint properties such that comparisons were made between different species.
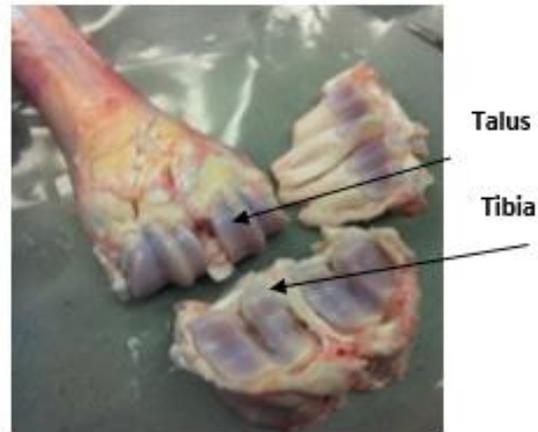
Figure 2-6: The talus and tibial surfaces were dissected from bovine tissue exposing talar and tibial surfaces.

Significant differences in cartilage thickness and mechanical properties were reported across different species in the hip joint suggesting any variations in the animal tissue would need to be considered prior to choosing an animal tissue to represent the human tissue (Taylor et al., 2011). Although the bovine and human ankle joints appeared to be comparable in anatomical size, a difference in joint articulation between both species was noted. The bovine ankle joint is made up of a 'double' *talar-tibial* joint (Figure 2-6), whereby the talar joint surfaces articulate over the tibial joint surfaces, whereas the porcine (Figure 2-2) and human ankle joints (Figure 2-9) are made up of a 'single' *tibial-talar* joint. As the bovine ankle tissue consists of variable joint surface geometry and articulation to the human ankle tissue, it was considered to be insufficiently matched to the anatomy of the human ankle. Hence, this animal tissue was discounted for further research.

2.3.2.1 Dissection of Bovine Patella Femoral Plates

Cartilage plates were extracted from bovine patella femoral joints (Figure 2-8) for the cartilage on cartilage pin on plate study. The cartilage plates were of approximate dimensions: length of 45 mm, width of 17 mm and depth of 7 mm (Figure 2-8). Prior to dissection, the cartilage surface was inspected for any signs of damage or disease.

The patella-femoral joint (Figure 2-7A) was clamped carefully into vice (Figure 2-7B). Sections of the cartilage tissue were marked using a scalpel blade such that the region of interest was identified before sawing through the joint surface. Using a handheld saw, the medial and lateral edges of the patella groove were removed (Figure 2-7C to Figure 2-7F). Horizontal lines were sawn through on the joint surface that measured a distance of 45 mm apart (Figure 2-7F). On the medial and lateral edges of the patella groove, 17 mm was measured from the edge to the centre of the joint and vertically sawn through the joint surface (Figure 2-7G and Figure 2-7H).
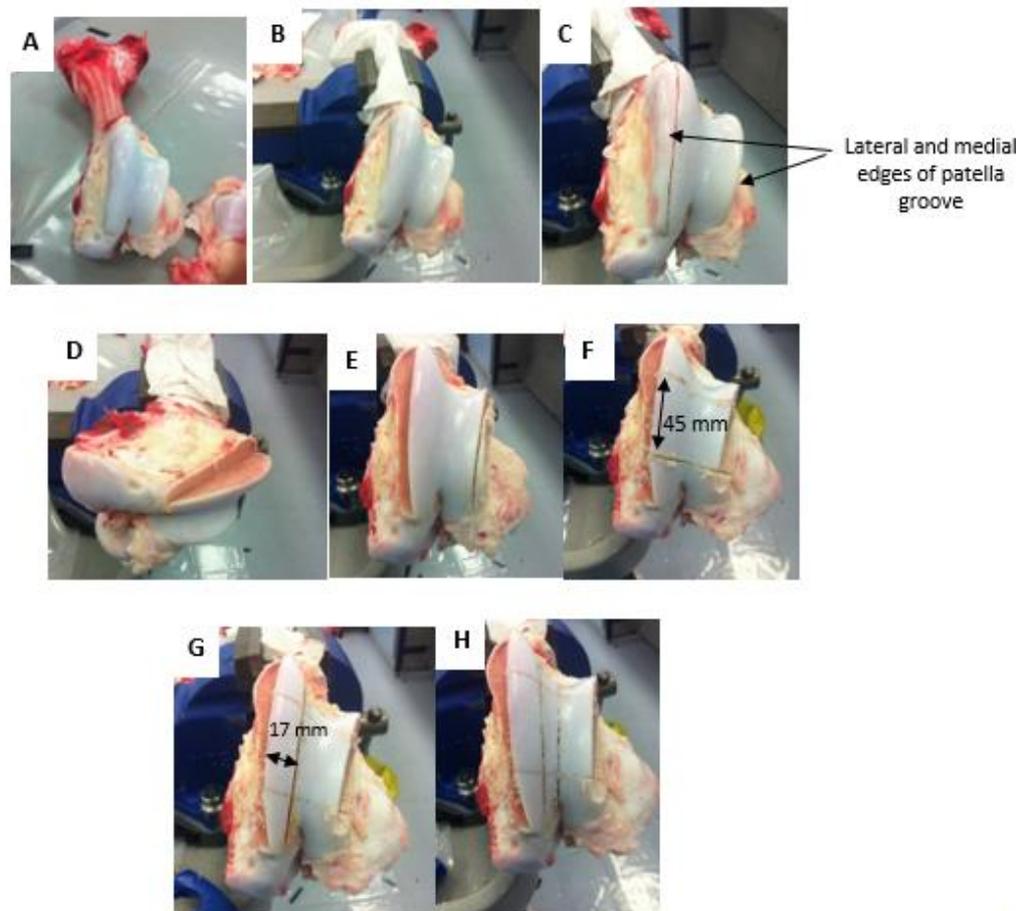
Figure 2-7: Dissection and extraction of bovine patella femoral plates.

Bovine patella plates were extracted by sawing through the depth on lateral and medial edges of the joint until the plate completely detached itself. Finally, each plate was clamped into a pre-made rig to saw through to obtain depth of 7 mm (Figure 2-8).
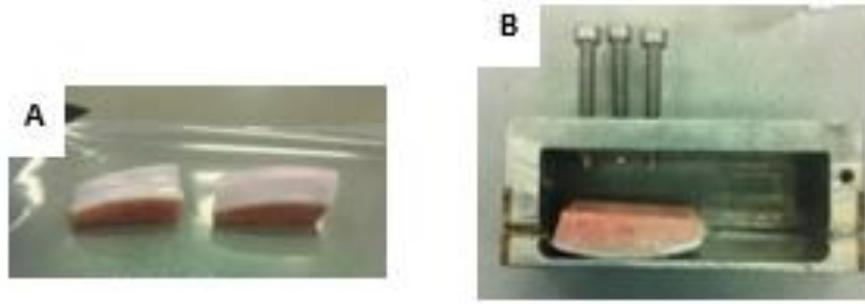
Figure 2-8: Dissection and extraction of bovine patella femoral plates. These plates measured approximately by a length of 45 mm, width of 17 mm and depth of 7 mm.

2.3.3 Human Ankle Joint

The human ankle joints were obtained from MedCure, USA and also were all right-sided as porcine ankle joints studied (Appendix B).

2.3.3.1 Dissection of Human Ankle Joint

Human tissue studies were carried out within the Human Tissue Act framework (outside NHS framework, as non-NHS Tissue) at the University of Leeds, under local ethics granted by MEEC FREC (MaPS and Engineering joint Faculty Research Ethics Committee). The tissue was collected and stored by MedCure, USA, with consent obtained from the donor prior to death for use of tissue in research and for imaging purposes. It was imported to the University of Leeds under a tissue transfer agreement, which ensured that the tissue was stored, used, tracked and, as appropriate, disposed of in accordance with the University of Leeds/Leeds Teaching Hospitals Trust Human Tissue Act research governance framework. The cadaveric tissue was delivered as a whole foot, removed mid-tibia. Mr Ioannis Ktistakis, a clinical ankle fellow at Leeds Teaching Hospital NHS Trust performed expert dissection of the ankle joint, removing excess skin, muscles, tendons and ligaments, until the ankle was made visible (Figure 2-9A). The remaining excess tissue was dissected to expose the tibial and talar surfaces for pin extraction (Figure 2-9B to Figure 2-9D).
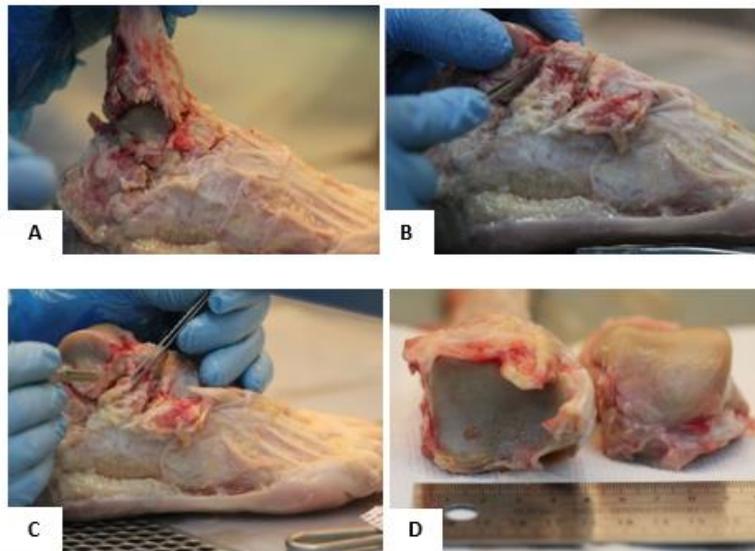
Figure 2-9: Dissection of human ankle joint. A) Removed external tissue, muscles, ligaments and tendons to expose the ankle joint; B) Dissecting talus separately; C) Removing excess tissue surrounding the talus using scalpel and forceps; D) Tibia (left) and talus (right) have been extracted.

2.3.3.2   Extraction of Osteochondral Pins: Human Tissue

For the human tissue work, new fixtures and tools were made or procured such that no cross-over of animal and human tissue was allowed. Osteochondral pins (8.5 mm diameter) were extracted from lateral and medial and aspects of the talus and tibia. A Smith and Nephew corer tool of 8.5 mm diameter (Figure 2-4A, Figure 2-10) was used to extract the pins as used for the porcine tissue (section 2.3.1.3). However, the clamping method differed between both species. Several fixtures and tools were needed to extract pins from human talar and tibial surfaces as highlighted in Figure 2-10.
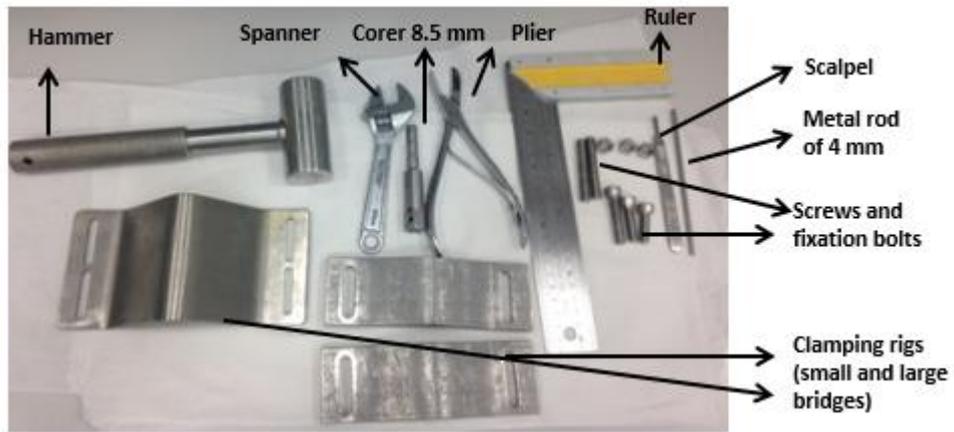
Figure 2-10: Fixtures and tools needed to extract pins from human talus and tibia.

Clamping rigs were used to secure the talar and tibial joint surfaces during extraction. To limit movement during extraction, fixation bolts and screws were used to tighten the tissue samples in the clamping rigs. For the talus, the two smaller clamping bridges were used to secure the tissue (Figure 2-11).
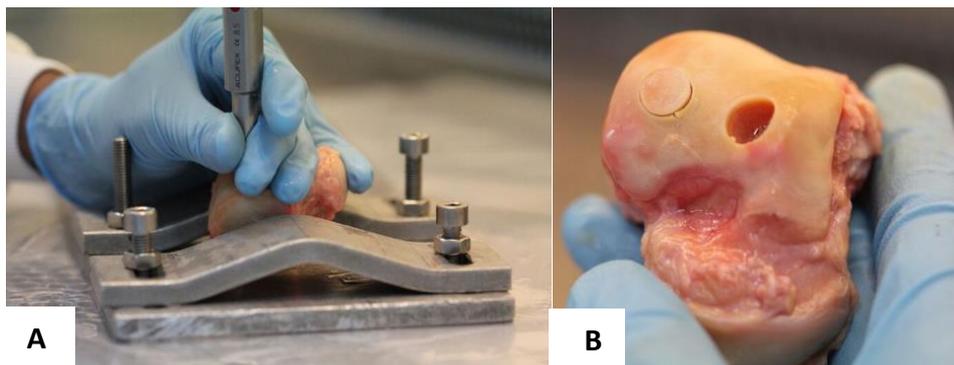
Figure 2-11: Extraction method of talus. A) Using tubular chisel, pins from the talus were extracted; B) On the talus, one pin was extracted and another region was marked for extraction.

For the tibia, a different set up was developed by securing the long bone end in-between two C-clamps to stabilise the joint surface prior to extraction (Figure 2-12).

A   **B**
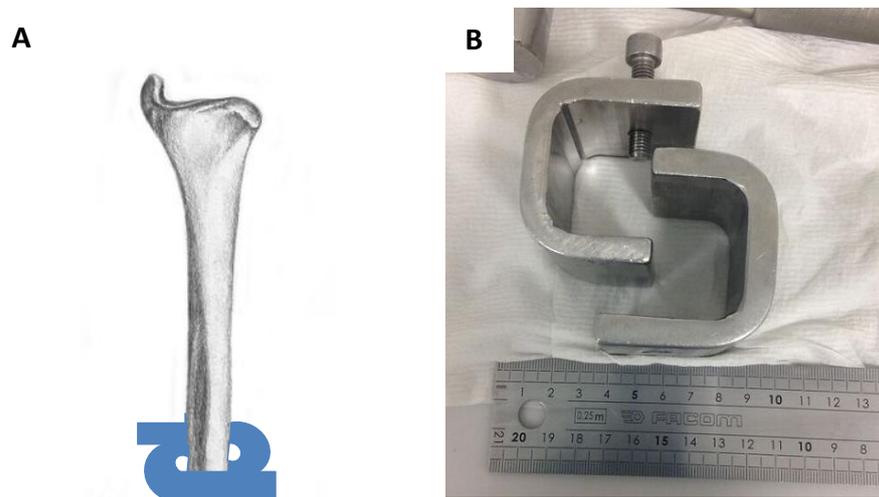
Figure 2-12: Two C clamps were used to hold the tibial surface in place during pin extraction A) Modified human tibia illustration (Gray, 1918), in-between two clamps; B) Two clamps used to secure the tibia.

The metal rod was used to gently push out the pins from the corer tool of 8.5 mm diameter as performed on porcine tissue (section 2.3.1.3).

2.3.4 Specific Locations on Porcine and Human Ankle Joints

Previous authors have investigated properties of cartilage at different joint locations (Athanasiou, Rosenwasser, & Buckwalter, 1991). To determine such differences in the ankle joint, specific regions, medial and lateral aspect of the cartilage surface, were studied on the talar and tibial cartilage of the porcine and human tissue (Figure 2-13; Figure 2-14). For the porcine tissue, lateral and medial pins, close to mid-point of the joint surfaces were obtained from the talus and tibia (Figure 2-13). For the human tissue, pins were extracted anteriorly (anterior-lateral), centrally (CM – central medial and CL - central-lateral) and posteriorly (posterior-medial) from the talus (Figure 2-14). Posterior-medial and anterior-lateral locations were chosen as these were commonly found to be involved in osteochondral defects (VanDijk et al., 2010). On the tibial joint surface, pins from medial (M), central (C) and lateral regions (PL – posterior lateral and AL – anterior lateral) were extracted (Figure 2-14).

2.3.4.1   Labelling Porcine Osteochondral Pins

In all species, the lateral and medial aspects of the tibial surface were referred to as 'LAT TIB and 'MED TIB', respectively, and the lateral and medial aspects of the talar surface were referred to as 'LAT TAL and 'MED TAL', respectively. The porcine tissue is labelled as 'P' followed by a number, i.e. P1, to describe the number of repeats. The locations for pin extractions are highlighted in Figure 2-13.
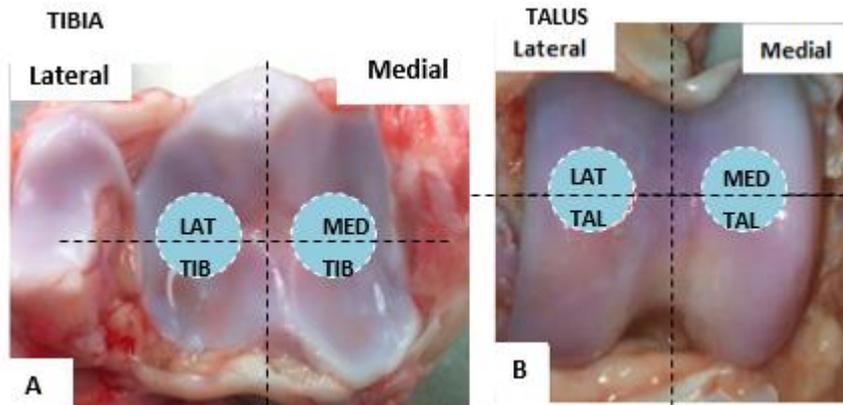
Figure 2-13: Central areas highlighted show lateral and medial aspects on the tibial (A) and talar surfaces (B) of the porcine tissue.

2.3.4.2   Labelling Human Osteochondral Pins

In the current study, three human ankle joints were studied (n=3). The locations of pin extractions are highlighted in Figure 2-14. From the talus, two lateral pins (TalCL and TalAL) and two medial pins (TalCM and TalPM) were extracted and from the tibia, one medial (TibM), one central (TibC) and two lateral pins (TibAL and TibPL) were extracted, whereby P-posterior and A-anterior.
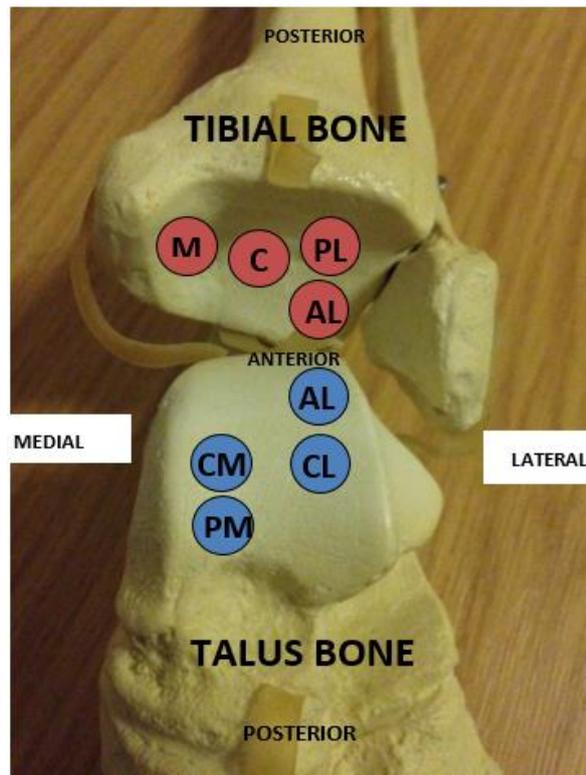
Figure 2-14: Regions were labelled where pins were extracted from the human ankle joint; A) Talus (adapted from Gray, 1918) and SawBone materials used to highlight extraction location on tibial and talar surfaces; M – Medial site; L – Lateral site. A – Anterior, C – Central, P – Posterior.

2.3.5 Storage of Osteochondral Pins

After pin removal, all osteochondral pins underwent visual inspection to assess for potential damage caused by the extraction process before freezing at -20˚C covered with PBS-soaked tissue within bijou tubes until ready for testing. The pins were then thawed in the fridge overnight before testing. Based on literature, the mechanical properties of the cartilage pins were not expected to alter during the freezing process (Forster & Fisher, 1996).

2.4 Statistical Methods

Numerical data was analysed using Microsoft Excel (version 2010, Microsoft) and presented as the mean (n≥3) ± 95 % confidence limits (CL). The data analysis package within Microsoft Excel under descriptive statistics was used to calculate 95 % confidence intervals (α = 0.05). Further detail on statistical analysis carried out for data presented in Chapter 3, 4, 5 and 6 have been highlighted within their respective chapters.

One-way analysis (ANOVA) was used to compare the means of two groups and more. Tukey method (Sokal and Rohlf, 1995) was used to calculate the minimum significant differences (MSD) at p = 0.05 for identifying individual differences between the group means (Equation 2-1). The critical value (Q) compares a point on test distribution to the test statistic to determine whether the null hypothesis will be rejected or not. If the test statistic is more extreme than critical value, null hypothesis will not be rejected.

Q = Critical Value

α = p = 0.05

k = number of groups

ν = degrees of freedom (n-1)

SE = standard error

$$MSD = Q_{(\alpha[k,\nu])} \; x \, SE$$

Equation 2-1: Calculation of Minimum Significant Difference (MSD).

2.4.1 Arcsine Transformation

Arcsine transformation is also known as inverse transformation and this method is commonly used in the analysis of percentage data that tends to be skewed when the distribution is not normal (Sokal and Rohlf, 1995). This approach helps to normalise percentage data and has the ability to eliminate the function that ties the variance to the mean (i.e. stabilises variances). The minimum and maximum are in the range

between 0 to 100 %, respectively (Quinn and Keough, 2002; Taylor, 2012; Fermor, 2013).

In the present study, data presented in percentages (such as for deformation studies in Chapter 3 and Chapter 6 and water content in Chapter 5) were transformed to arcsine to accurately calculate 95 % CL and statistical analysis. The averages of transformed values were calculated, and then standard deviation was obtained. Following analysis, the mean arcsine values were transformed back for graphical presentation.

2.4.2 Linear Regression Analysis

In Chapter 5 (section 5.5.5 and 5.5.6) linear regression analysis was performed on standard curves to interpolate the results for GAG (glycosaminoglycan) and hydroxyproline assays.

In Chapter 5 for determining the GAG and hydroxyproline content, a relationship between absorbance against the standard concentrations was plotted and linear regression analysis of the standard curve was used to interpolate unknown values (Equation 2-2). A linear regression attempts to plot a relationship between these two variables (absorbance and standard concentrations) by fitting a linear equation to the observed data.

$$\text{unknown x} = \frac{mean\ measured\ y\ variables}{y\ value\ of\ linear\ regression\ line\ equation}$$

Equation 2-2: Calculation to interpolate unknown values using linear regression analysis

Chapter 3: Mechanical Characterisation of Porcine Ankle Cartilage

3.1 Introduction

This chapter investigates the mechanical characterisation of porcine ankle cartilage. Mechanical characterisation of ankle cartilage may help to build a fundamental understanding of cartilage properties such as thickness and how the tissue responds to loading. The function of articular cartilage is to provide a bearing surface whilst helping to distribute loads between opposing surfaces which is important to understand the mechanical properties and cartilage mechanics.

Several methods that are non-destructive and destructive have been used to measure cartilage thickness in various joints (Chapter 1, section 1.5.1.1). Imaging methods such as MRI (Kladny et al., 1996; Tan et al., 1996; Koo et al., 2005) or CT (El-Khoury et al., 2004) are considered as 'non-destructive' compared to 'destructive' methods such as needle probe method which can damage the cartilage through piercing into the surface and limiting any further tests on the sample (Shepherd and Seedhom, 1999). When two non-destructive methods (MRI vs CT) were compared against direct calliper measurements using osteochondral pins extracted from talus and tibial surfaces, CT images were within 0.1 mm of overall cartilage thickness of 1.70 mm (El-Khoury et al., 2004). MRI had a greater scatter of readings, whereas this was minimal using CT (El-Khoury et al., 2004). However, the 'destructive' needle probe method may result in more accurate measurements as thickness location is specific and the needle pierces through the full thickness, compared to CT method which provides an estimate of the thickness in the selected region on the image. Based on this, the current study has compared CT and needle probe methods and criteria for selection is based on ensuring the tissue quality (i.e. hydration).

Mechanical characterisation of cartilage such as indentation testing helps demonstrate cartilage response to loading and to determine material time dependent characteristics (Chapter 1, section 1.3.2). Cartilage deformation under

loading is important for maintaining healthy joint function as fluid flow in cartilage ensures tissue is hydrated during movement (Linn and Sokoloff, 1965; Maroudas and Bullough, 1968) to ensure friction and wear is kept to a minimum. Higher cartilage deformation due to trauma/injury to the joint is hypothesised to cause further damage to the subchondral bone plate possibly leading to osteochondral defects (OD) clinically (VanDijk et al., 2010), and may contribute to degeneration of the joint surfaces. In the ankle this is most frequently a talar lesion involving the talar cartilage and the subchondral bone (Van Dijk, Reilingh, Zengerink, & Van Bergen, 2010).

Previous studies have used cartilage specimens to study biomechanical properties of cartilage with the assumption specimens reflect the whole joint surface (Treppo et al., 2000; Boschetti et al., 2004; Northwood and Fisher, 2007; Russell, 2010; Taylor et al., 2011; McLure et al., 2012; Fermor et al., 2015). However, pin extraction may impact the quality of the tissue and potentially alter the biomechanical properties due to disruption to the cartilage surface. This may change the biphasic properties of the cartilage (i.e. interaction between solid and fluid phases during loading) such that the load is carried by the solid phase (extracellular matrix) instead of fluid phase, potentially leading to cartilage damage over time. Therefore, part of this chapter will focus on studying the impact of specimen preparation through pin extraction by comparing cartilage properties in osteochondral specimens and whole joint surfaces.

3.2 Aims and Objectives

3.2.1 Aims

The overall aim of the study was to determine the biphasic deformation and cartilage thickness of porcine ankle cartilage. This study will provide key information and enhance understanding of the natural ankle joint in its healthy state, as well as developing the methods for human cartilage characterisation (Chapter 6).

3.2.2 Objectives

- To determine the cartilage thickness of the porcine ankle osteochondral tissues from the tibial and talar joint surfaces (pin study) and intact talus surface (whole joint study)

- To compare two thickness measurement techniques: CT (non-destructive) and needle probe method (destructive), using porcine ankle osteochondral tissues to find a method that ensures tissue hydration and optimisation of human tissue usage

- To characterise the deformational behaviour of the porcine ankle osteochondral tissues from the tibial and talar joint surfaces

- To determine whether specimen preparation has an impact on the measured biomechanical properties (i.e. thickness and percentage deformation) of porcine cartilage through a comparative study of the intact talus (whole joint study) and osteochondral talar pins (pin study)

3.3 Materials

For the thickness and indentation studies, osteochondral pins of 8.5 mm diameter were extracted from the lateral and medial aspects of the talar and tibial joint surfaces as outlined in Chapter 2, section 2.3.1.3 (n=6 for each aspect, unless otherwise stated). For the whole joint study, talar joint surfaces (n=6) were extracted from the porcine ankle tissue (Chapter 2, section 2.3.1.2).

For the whole joint study, polymethyl methacrylate (PMMA) bone cement was used to fix the intact talus bones during both indentation and needle probe testing. The solid powder (Cold Cure) and liquid monomer (Rapid Repair Liquid) were mixed together according to the manufacturer's instructions (WHW Plastics, Hull, UK). The ratio between the solid powder and liquid was 2:1. During the curing period, the cement slowly heats up to fully set. The likelihood of thermal damage was thought to be low as the cement line was well offset from cartilage tissue (Figure 3-1).
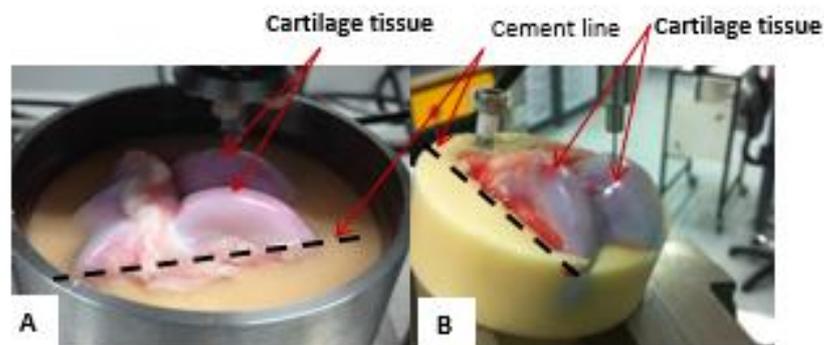
Figure 3-1: The cement line was well offset from cartilage tissue; A) Cemented intact talus surface using PMMA; B) intact talus surface during needle probe testing

3.4 Methods

Needle probe testing and indentation testing were performed on pins (8.5 mm in diameter) extracted from two regions (LAT TIB - lateral tibia and MED TIB - medial tibia) on porcine tibial surface and two regions (LAT TAL - lateral talus and MED TAL - medial talus) on porcine talar surface (Figure 3-2) and on four regions (LA - lateral anterior, LP - lateral posterior, MA - medial anterior and MP - medial posterior), on the porcine intact talus surfaces (Chapter 2, section **2.3.1.2**) to obtain cartilage thickness and deformation measurements, respectively.
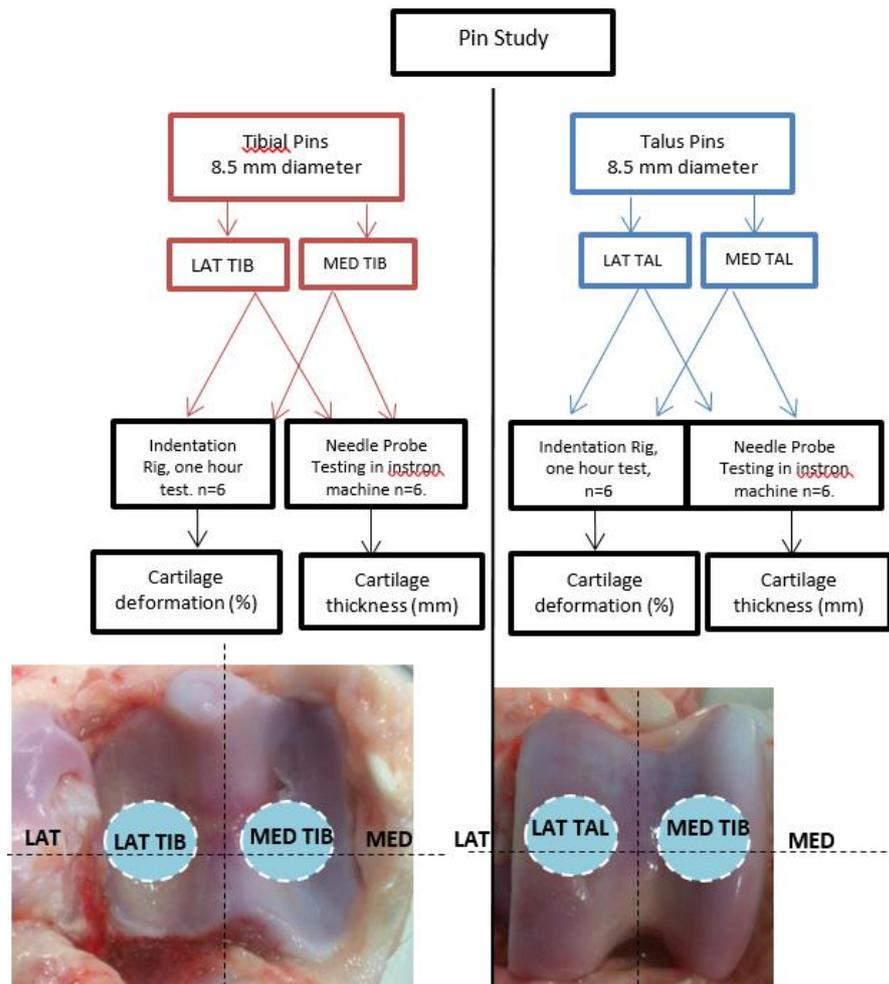
Figure 3-2: Flow diagram of mechanical testing on porcine tibial and talar pins of 8.5 mm diameter (pin study) using indentation testing on indentation rig and needle probe testing on Instron machine to determine cartilage deformation (%) and thickness measurements (mm), respectively; For each sample (i.e. LAT TIB), n=6 was conducted for each test. Lateral talus (LAT TAL), medial talus (MED TAL), lateral tibia (LAT TIB), medial tibia (MED TIB).
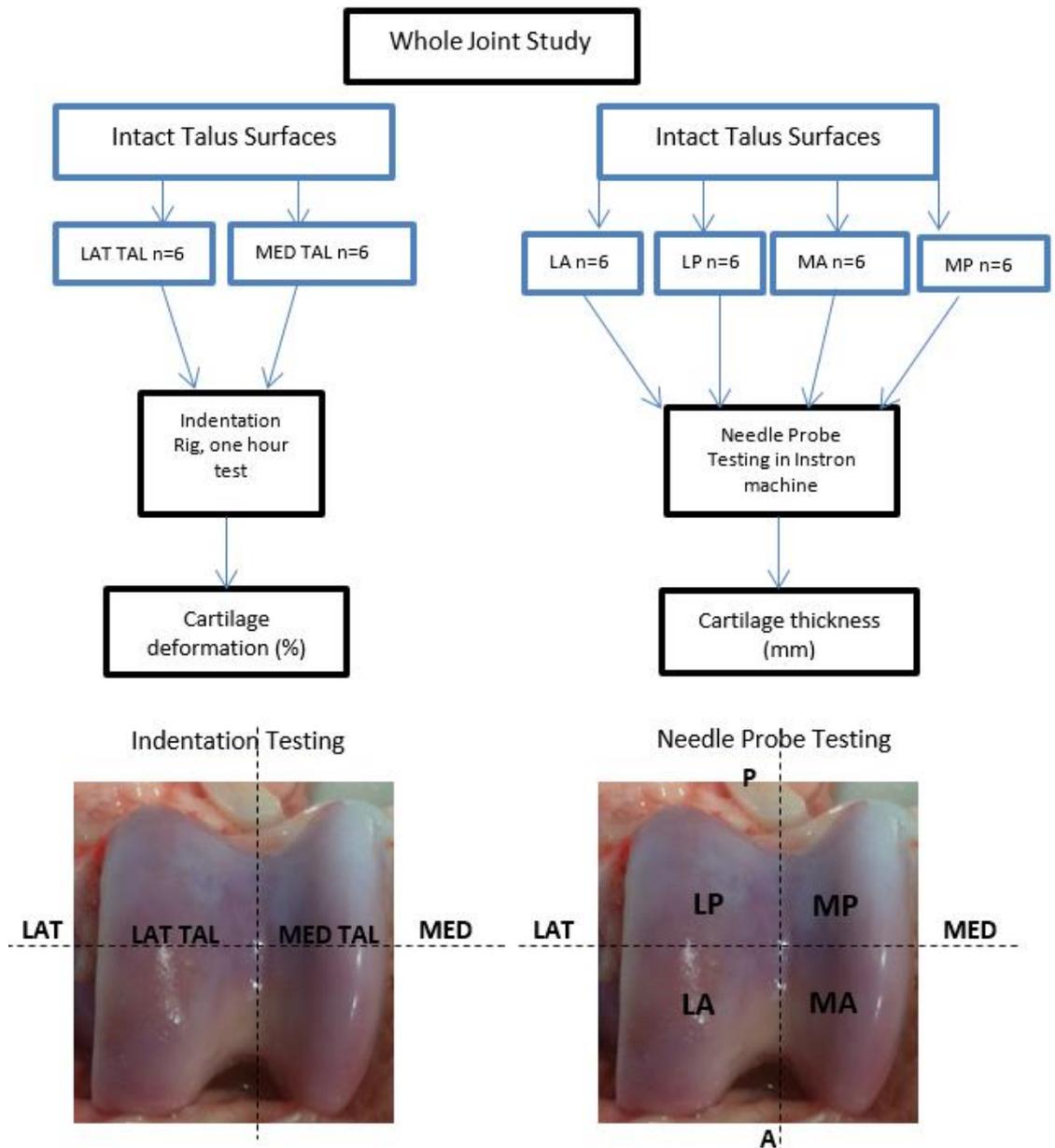
Figure 3-3: Flow diagram of mechanical testing on porcine intact talus surfaces (whole joint study) using indentation testing on indentation rig and needle probe testing on Instron machine to determine cartilage deformation (%) and thickness measurements (mm), respectively; For each sample (i.e. LAT TAL), n=6 was conducted for each test; A – anterior, P – Posterior, LA – lateral anterior, LP – lateral posterior, MA – medial anterior, MP – medial posterior.

A comparative study was performed to identify potential differences in cartilage deformation and cartilage thickness measurements using talus osteochondral pins (pin study) (Figure 3-2) and intact talus surfaces (whole joint study) (Figure 3-3)

Cartilage thickness measurements were assessed using two different methods (3.5.1) – a destructive needle probe test and a non-destructive CT imaging technique, on cartilage pins obtained from four regions in the porcine ankle joint (LAT TIB, MED TIB, LAT TAL and MED TAL) (Figure 3-4). The puncture mark locations on the cartilage pin using needle probe are visible on the CT images. Hence, needle probe testing was conducted first followed by MicroCT such that the thicknesses in the same regions on the pin were determined by both methods.
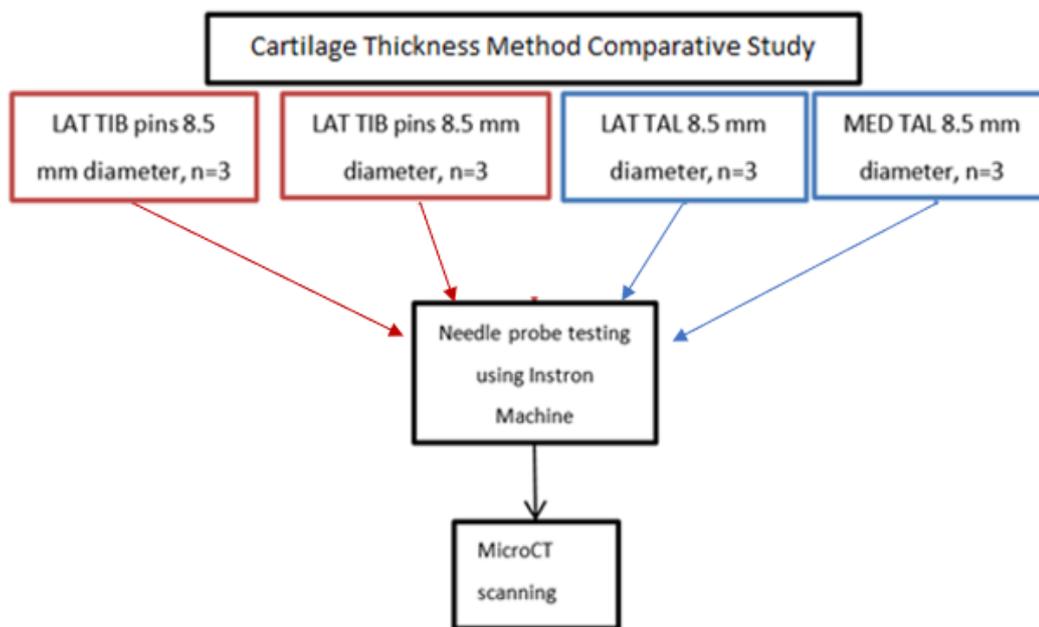
Figure 3-4: Flow diagram showing the comparative study using two cartilage thickness methods – needle probe testing using Instron testing machine followed CT imaging technique on porcine lateral talus (LAT TAL, n=3), medial talus (MED TAL, n=3), lateral tibial (LAT TIB, n=3) and medial tibial (MED TIB, n=3) pins (8.5 mm in diameter).

3.4.1 Cartilage Thickness Measurement Methods using Porcine Ankle Tissue

3.4.1.1 Needle Probe Testing using Instron Testing machine

An Instron material testing machine (Instron 3365, Bucks, UK) (Figure 3-5A) was used to determine porcine cartilage thickness using a needle probe of 0.5 mm diameter attached to the Instron arm (Figure 3-5A). A universal three-way angle machine vice

(Mitchell, Fox & Co. Ltd, UK) was used in the Instron material testing machine (Figure 3-5A) to enable positioning of the sample such that the needle entry into cartilage surface was perpendicular to the cartilage surface.
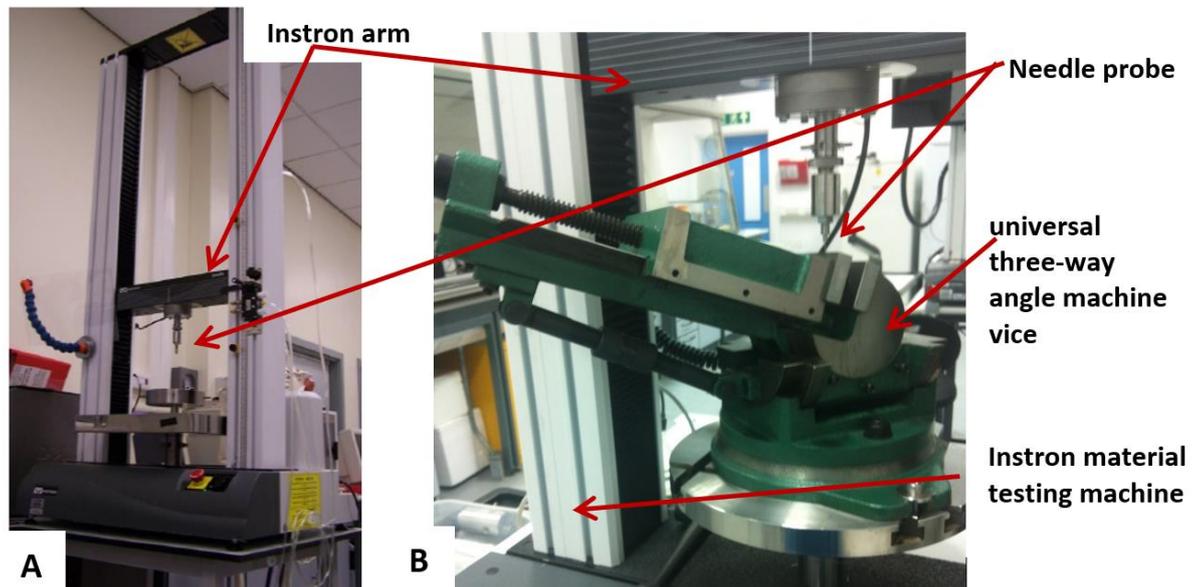
Figure 3-5: A) Instron material testing machine; B) A machine vice was placed onto the Instron machine and used for cartilage thickness measurements.

Before contact was established between the needle and the surface of the sample to be tested (Figure 3-9A), the needle probe was visually assessed to be positioned approximately 1 mm above the sample surface. At a speed of 4.5 mm per minute, the needle was driven into and through the surface of the cartilage to measure the thickness.

3.4.1.2   Determination of Cartilage Thickness using Needle Probe Technique on Porcine Ankle Osteochondral Tissue

Osteochondral pins were placed in a collet to restrict movement and tightened onto the vice (Figure 3-5B) prior to adjusting the positioning of the vice. On each pin, five thickness locations were recorded and the mean was calculated (Figure 3-6B).
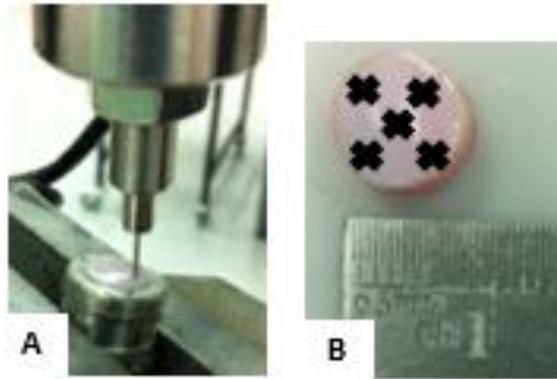
Figure 3-6: Pin cartilage thickness testing using the needle methods and an Instron material testing machine. A) Each pin was fitted into a collect and tightened to vice; B) Regions from which cartilage thickness measurements were taken on each pin.

3.4.1.3 Determination of Cartilage Thickness using Needle Probe Technique on Porcine Intact Talus Surface

A custom-made Delrin fixture was used to cement the intact talar surfaces using PMMA (section 3.3). Over the ventilation bench, PMMA was poured into the base of the fixture (Figure 3-7A) to initially create a surface of dried cement to cover the internal squared base of the fixture (approximately 30 mm in height) prior to securing the intact talus surface with further PMMA. As the purpose of the Delrin fixture was to create a solid base for the intact talus surface such that it was possible to be secured onto machine vice (Figure 3-5B) for testing, the height of the PMMA added to secure the intact talus surface did not need to be consistent between samples, as long as it was below the internal wall cavity height of 20 mm such that PMMA did not overflow out of the fixture. The cartilage surface was left exposed for testing. PBS-soaked tissue was replaced every 5 mins over the exposed cartilage surface during the cementing process to keep the tissue hydrated. Once the cement had fully cured, within 30 mins, the cemented intact talus was gently pushed out of the Delrin fixture using the tapered base (Figure 3-7B) and attached onto the vice (Figure 3-8B).

The squared base of the cemented fixture (Figure 3-8) was securely attached onto the machine vice (Figure 3-8) and the orientation of the cemented fixture was adjusted, such that perpendicular needle entry into the cartilage surface was

obtained (Figure 3-8C). To ensure tissue hydration throughout the test, the intact talus surface was covered with PBS-soaked tissue between each measurement.

The intact talus was divided into four regions – Lateral Anterior (LA); Lateral Posterior (LP); Medial Anterior (MA); Medial Posterior (MP) (Figure 3-7D) and five cartilage thickness measurements were recorded within each region (Figure 3-7B) and an average determined.
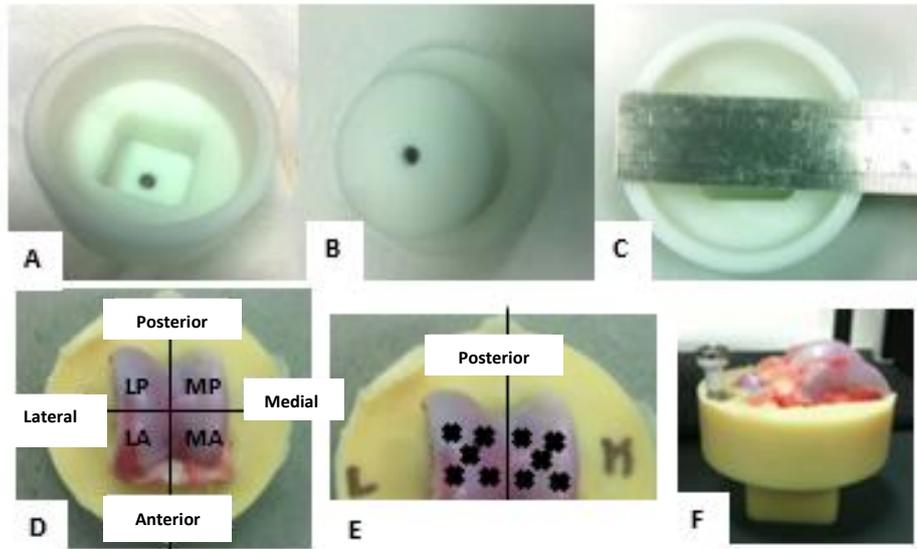
Figure 3-7: A) Custom designed Delrin fixture for cementing porcine intact talus surface with square base to be fixed to a vice for rotational movement; B) Base view of the fixture, tapered to remove cemented fixture using allen key; C) The fixture was made with an internal diameter of 60 mm and 30 mm by 30 mm squared base; D) The intact talus was divided into four sections - Lateral Anterior (LA); Lateral Posterior (LP); Medial Anterior (MA); Medial Posterior (MP); E) Regions from which cartilage thickness measurements were taken from on LA and MA talus using an Instron testing machine; F) Potted intact talus surface.
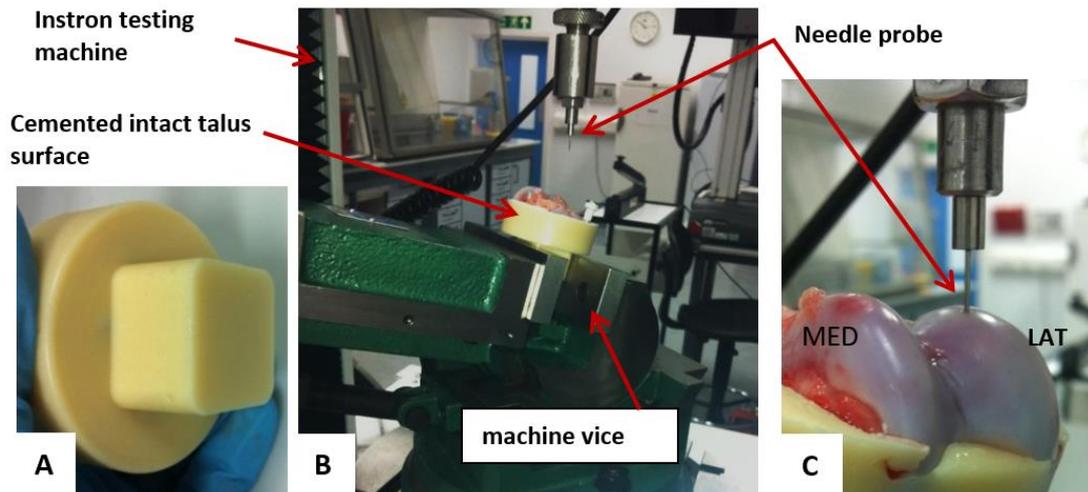
Figure 3-8: Attaching the cemented intact talus surface onto the Instron machine; A) The squared base of the cemented fixture to be attached to the machine vice; B) The cemented intact talus surface fixture was tightened to the machine vice and orientation of machine vice was changed for each measurement to allow perpendicular needle entry into the cartilage surface prior to testing; C) Close up of the needle entry into the lateral (LAT) aspect of the joint surface, MED – medial.

3.4.1.4 Analysis of Needle Probe Data

The study was completed when a sudden change in resistive force with displacement was observed once the needle penetrated from cartilage (soft tissue) into subchondral bone (stiffer material). During the thickness measurement, the load-displacement response exhibits differing behaviour depending on the stage of testing. During the initial stage (Figure 3-9B) a gradual change in load with displacement is observed due to needle entering the cartilage surface, a soft tissue. As the needle penetrated into the stiffer bone material, the load shown as a function of displacement rapidly increased. Cartilage thickness was evaluated by plotting the needle displacement (mm) against the resistive load (N) for each test.

There was an apparent difference in the gradients of the load-displacement graph corresponding with passage of the needle through the cartilage and the bone material. The corresponding linear equations for these gradients were equated and solved to derive the cartilage thickness.
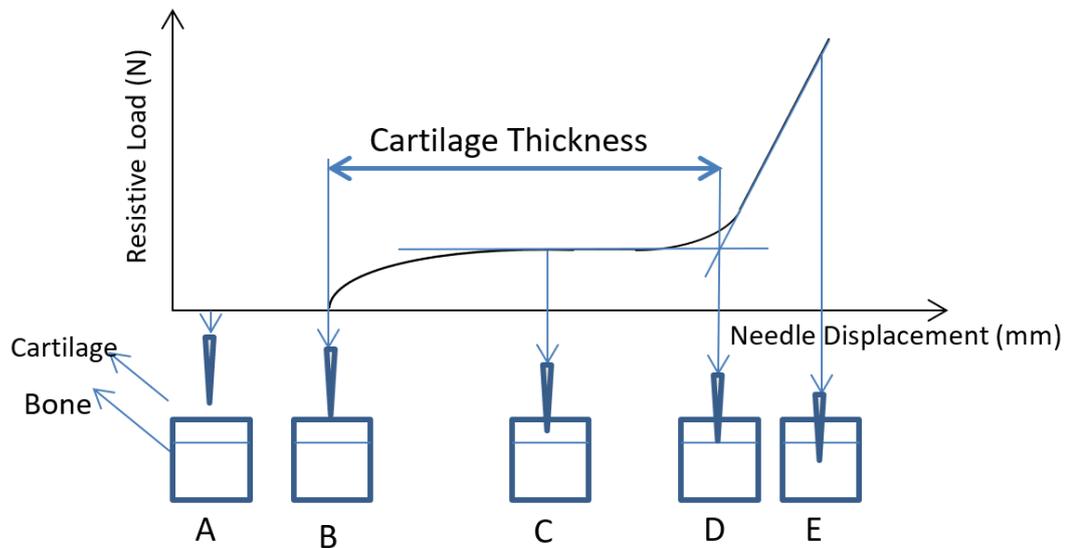
Figure 3-9: An example of output obtained from using the needle probe on the Instron testing machine to calculate the cartilage thickness.

3.4.1.5 Comparative Study: Needle Probe Technique and CT Imaging Technique to Determine Cartilage Thickness Measurements using Porcine Ankle Osteochondral Tissues for the Use of Human Tissue

Cartilage thickness readings were measured using two methods to permit a comparison between needle probe testing (destructive) and a CT imaging technique (non-destructive). The purpose of comparison between both methods was to determine a method that would be considered suitable for the human tissue. As limited human tissue was available, unlike the porcine tissue, the human samples needed to be further retested to optimise. Therefore, the chosen method will need to ensure the quality of the tissue during testing such that further tests were possible on the same samples.

To ensure comparison of methods was conducted over the same cartilage regions, the orientation of the pins were kept the same in both methods. A custom-made perspex holder (Figure 3-10) was used which ensured the pins were held in a fixed orientation throughout testing with both methods. On the perspex holder, there

were three holes in the cap (Figure 3-10). The needle probe method was used through each hole to record three thickness readings on each pin.
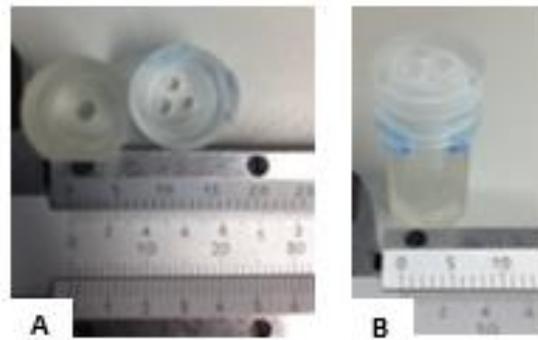
Figure 3-10: A custom-made perspex holder was used to secure porcine ankle cartilage pins in the Instron testing machine and MicroCT to obtain cartilage thickness readings; A) Top view of the perspex holder; B) Side view of the perspex holder. The cap had three holes drilled to allow needle entry when using the Instron machine.

The testing on Instron machine was manually stopped when a change in load was obtained for cartilage and bone material (section 3.4.1.1, Figure 3-9) as the needle penetrated further into the tissue reaching the subchondral bone. The needle probe method left puncture marks on the cartilage pins that were visible in the CT images (Figure 3-11), this was used to determine the thicknesses in the same regions on the pin by both methods. Each cartilage pin was tested using needle probe testing followed by CT imaging technique.
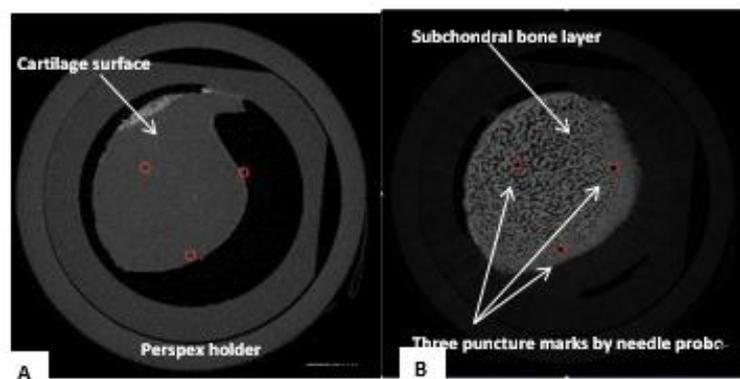
Figure 3-11: CT images illustrating the three puncture marks from needle probe testing using Instron testing machine on ankle osteochondral pin sitting within perspex holder; A) A cross section image of the cartilage surface of the osteochondral pin; B) A cross section image of the subchondral bone layer showing more distinctively the three puncture marks.

Comparative Study: Needle Probe Testing using Porcine Osteochondral Ankle Tissue

For the purpose of the comparative study, the needle probe method previously outlined (section 3.4.1.1) was performed with some modification, whereby the machine vice (Figure 3-5B) was not attached and instead a stainless steel rig (Figure 3-12) was used to provide a flat base for the perspex holder.

Figure 3-12: Stainless steel rig used on the Instron machine to create a flat platform for the perspex holder to be secured to.

MicroCT Imaging Technique using Porcine Osteochondral Ankle Tissue

A MicroCT imaging technique (µCT100, Scano Medial AG, Basserdorf, Switzerland) was used to assess ankle cartilage thickness using porcine osteochondral tissues as part of the comparative study (Figure 3-4). The scanner consists of a cone-beam X-ray source and a 0.5 mm Aluminum filter. A customised matrix size of 3522 by 3522 and a beam hardening correction algorithm based on a HA-phantom (1200 mg HA/cm^3) was provided by the CT manufacturer. This method is considered to be a non-damaging method, as it uses X-rays to display grey scale images of the sample. The scanner accomodates up to 12 sample holders and maintains maximum imaging resolution of 4 µm. In the current study, the pins were placed vertically into the scanner using a CT specimen holder (14 mm by 92 mm) and PBS aded to ensure hydration of the cartilage throughout the scan (approximately 20 minutes duration). The scanner was set to a voltage of 70 kV, current of 114 mA with an integration time of 300 ms as provided by the CT manufacturer. The direction of scans were taken parallel to the cartilage surface (Figure 3-13). As the cartilage thickness was expected to be of the order of 1 mm, the slice resolution of 5 µm was considered to be

acceptable to measure thickness accurately. Although this generated a large number of pixels, and a high quantity of data, a lower resolution, was not adopted due to the potential impact on thickness measurement.
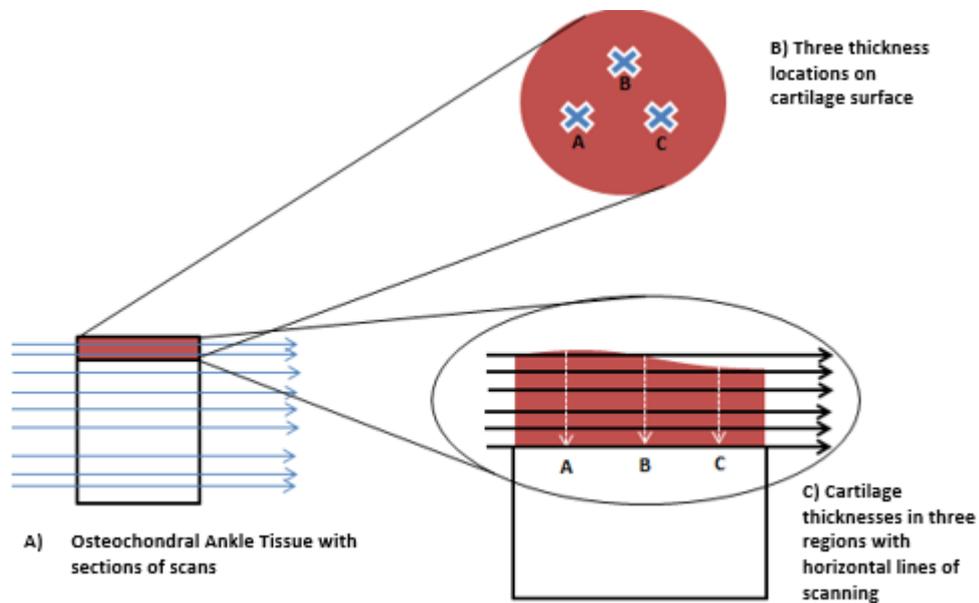
Figure 3-13: Pin samples were placed vertically into the scanner and sections were taken horizontally. Each section was taken a resolution of 5 μm and three cartilage thickness measurements were obtained on each sample.

Subsequently morphological analysis of scans were conducted by horizontally selecting the region of interest such that full cartilage layers were included. These layers were above and below the cartilage (Figure 3-14).
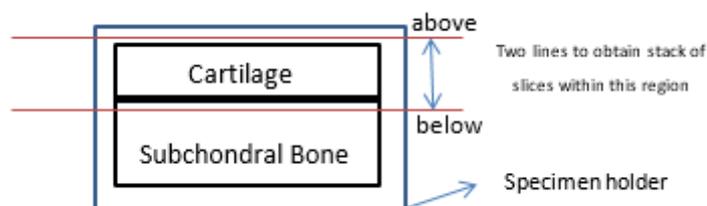
Figure 3-14: Schematic of cartilage pin within CT specimen holder by selecting two lines (one above and one below the cartilage) from which slices will be selected to best represent the whole cartilage thickness.

To calculate the thickness, the cross-section of the pin in which the cartilage first appeared Figure 3-15A) and the image in which bone first appeared (Figure 3-15B)

were identified and the number of slices between them multiplied by the spatial resolution.
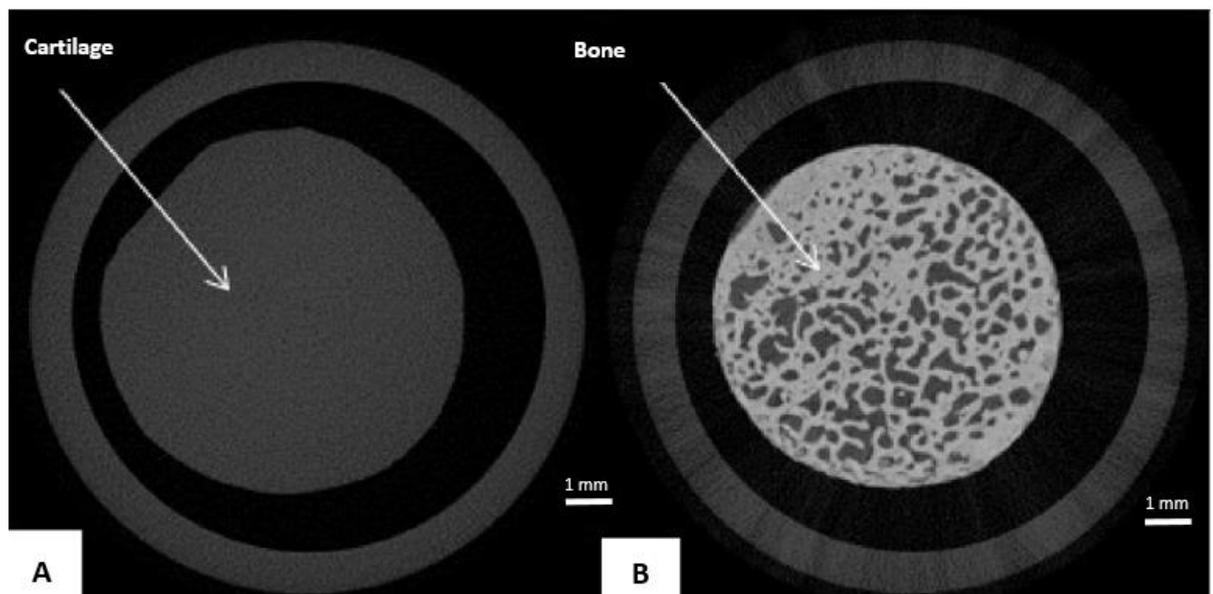
Figure 3-15: Cross-sections of osteochondral tissue using MicroCT to calculate cartilage thickness; A) Cartilage appearance, B) Subchondral appearance or cartilage disappearance.

3.4.2 Indentation Testing of Porcine Ankle Tissue

All percentage data were arcsine transformed as needed by analysis of variance (ANOVA), to fulfil a normal distribution that was assumed. Mean cartilage deformation values in percentages obtained on porcine osteochondral tissue (n=6) and intact talus surfaces (n=6) were arcsine transformed prior calculation of the 95% confidence limits and back transformed for graphical presentation (Chapter 2, section **2.4**).

3.4.2.1 Indentation Testing Apparatus

The indentation apparatus (Figure 3-16) was used to perform mechanical tests on the cartilage surface to derive cartilage deformation. The apparatus applied a constant load of 0.24 N in a perpendicular direction to the cartilage surface through a rigid hemispherical indenter of 2.5 mm diameter over a one-hour period; such load ensured the cartilage surface was minimally deformed. For the indentation data to

be accurate, the surface tested upon was assumed to be flat (Pawaskar, 2006). In the current study, as pins were highly curved, an appropriate shape of indenter was considered, as otherwise an increase in contact area will result in continuous deformation without reaching equilibrium (Delaine-Smith et al., 2016). A hemispherical indenter was chosen based on the surface curvature of the porcine ankle tissue. A linear variable differential transducer (LVDT, RDP D5-200H; Electrosence, PA, USA) located on top of the shaft, monitored the displacement of the shaft and the piezoelectric force transducer (Part No. 060-1896-02, Electrosence, PA, USA) measured the force. The data from LVDT and force transducer was displayed on an analogue-digital converter connected to a PC. LabView 8 software (National Instruments, TX, US) was used to display and record the force and displacement outputs.
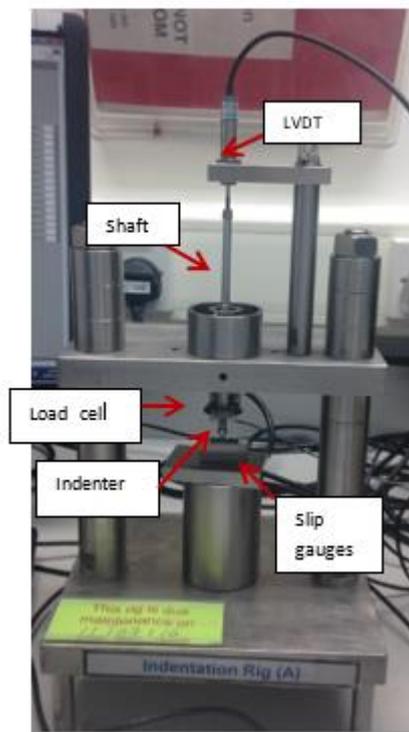
Figure 3-16: The apparatus of Indentation rig during calibration procedure.

3.4.2.2   Calibration

The calibration procedure used was developed by previous researcher at the University of Leeds (Latif, 2011). Calibration procedures were carried out for the LVDT and the force transducer prior to testing to determine appropriate calibration factors. This factor is used to convert the voltage outputs of the LVDT and the transducer into millimetres and Newtons, respectively.

With the use of standard stainless steel slip gauges, the LVDT was calibrated in mm by measuring the voltage at zero displacement followed by ten further readings using slip gauges to deliver incremental changes between 0.005 mm and 2 mm. The output voltage was plotted against the cumulative height and a linear trend line determined. The equation derived from the graph was used to determine the calibration factor for the apparatus for the LVDT to convert the units into mm (Figure 3-17).
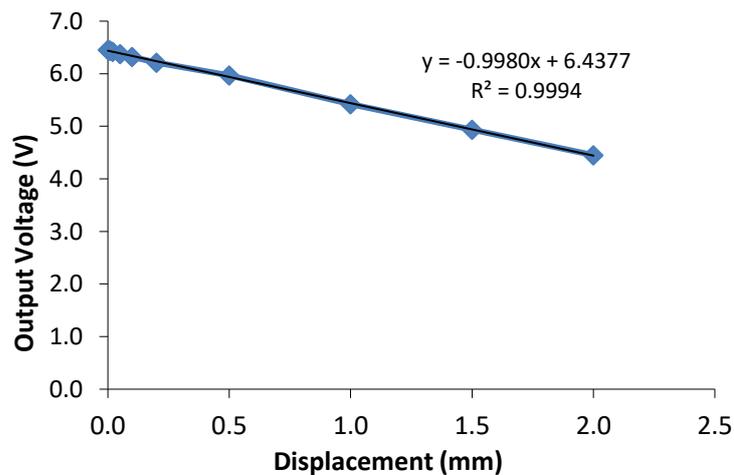
Figure 3-17: Example trace of calibration of LVDT using indentation rig with slip gauges to determine calibration factor for LVDT to convert the output voltage (V) to displacement (mm).

Similarly for the force transducer, masses of up to 40 g were incrementally added to the indenter shaft using weights of 4 x 10 g, and the voltage output on the load cell was measured. A linear trend line was plotted from the voltage outputs and the corresponding masses (Figure 3-18). The equation of the line of best fit was applied

as the calibration factor for the force trandsucer to convert the units into Newtons (Figure 3-18).

$$y = 0.0091x + 0.2051$$
$$R^2 = 0.9994$$
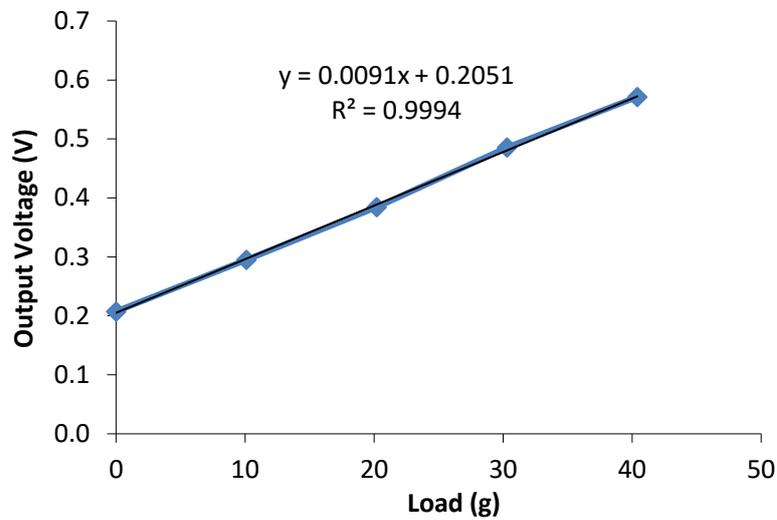
Figure 3-18: Example trace for the calibration curve of load cell measured using indentation rig by incrementally adding known masses of up to 40 g to determine calibration factor for the force transducer to convert output voltage (V) into Newtons (N).

3.4.2.3   Biphasic Indentation Method on Porcine Ankle Osteochondral Pins

Each porcine cartilage pin was placed in a collet (Figure 3-19B), secured in a small specimen holder (Figure 3-19B) and housed in a large stainless steel specimen holder which was then screwed into the indentation apparatus (Figure 3-16). The indenter was attached to the load cell (Figure 3-19C). The specimen holder was filled with PBS covering the cartilage surface to ensure the tissue was hydrated throughout the tests. The indenter was positioned approximately 1 mm below the cartilage surface. This height was chosen such that a minimum impact was created between the indenter and the cartilage surface to minimise any possible damage to the surface.
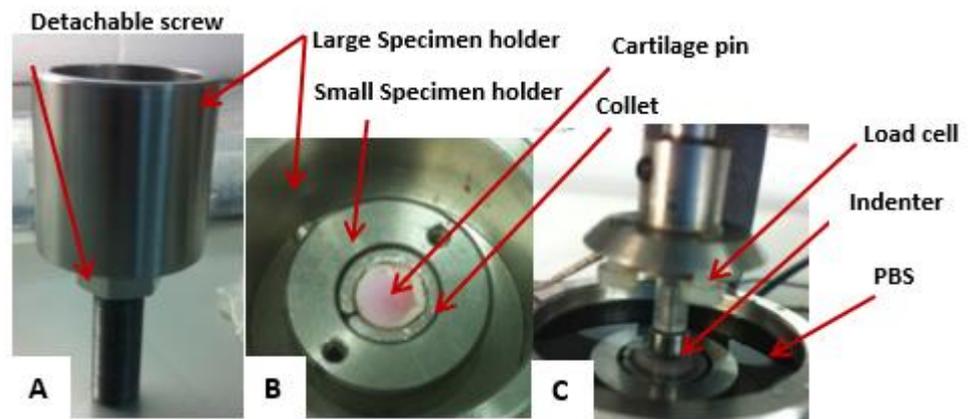
Figure 3-19: Setting up of the indentation rig for porcine cartilage pins (8.5 mm diameter); A) The specimen holder with detachable screw at the base; B) An example of porcine cartilage pin held within a collet; C) The hemisperical indenter of 2.5 mm diameter was attached to the load cell whilst the porcine pin was immersed in PBS during testing.

During the test, constant load with change in displacement as function of time was measured over a period of one hour.

3.4.2.4 Biphasic Indentation Method on Porcine Intact Talus Surface

The test conditions for the whole joint study (Figure 3-3), including indenter diameter and applied load, were identical to the pin study (section 3.4.2.3), but the set-up procedures varied between experiments. For whole joint study (Figure 3-3), a custom-made stainless steel fixture (Figure 3-20) was designed and manufactured in-house to secure the intact talus surfaces. Using PMMA (section 3.3), the intact talar surfaces (approximately 40 x 32 mm) were cemented in the metal fixture and transferred onto the indentation apparatus (Figure 3-20C). As pins were extracted from the central regions of the lateral and medial aspects of the talus (Chapter 2, section 2.3.1.3), these tests were set up to measure corresponding locations. The cartilage deformation of the medial and lateral aspects of the intact talus were studied and compared with the results from the talar osteochondral pin study (section 3.4.2.3).
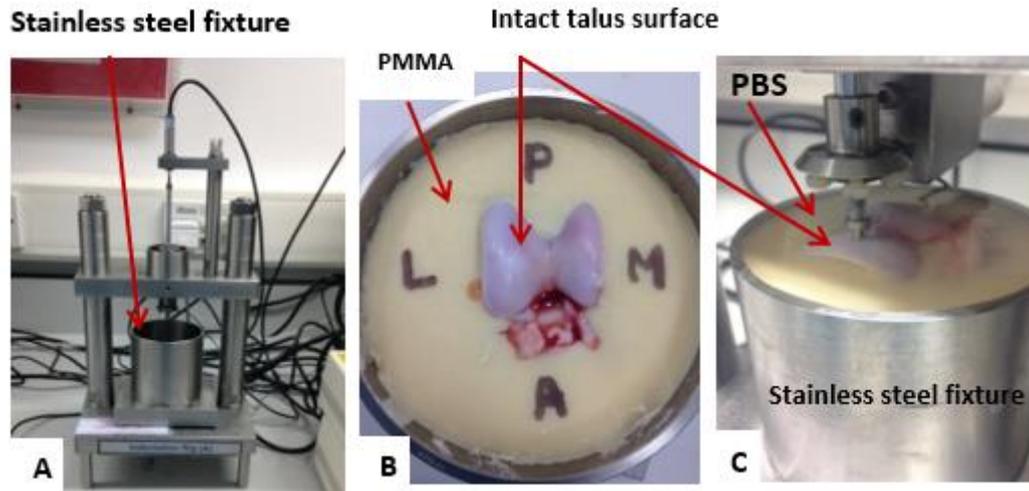
Figure 3-20: Indentation testing set up on a cemented intact talus surface using stainless steel fixture; A) Fixture securely placed within the indentation rig; B) Intact talus surface has been secured within the fixture using PMMA to limit movement during testing; C) Testing on lateral talus (LAT TAL), whereby tissue was immersed in PBS throughout testing.

3.4.2.5 Biphasic Indentation Testing: Determination of the Rate of Deformation

As part of creep indentation study, the rate of deformation was studied for the porcine osteochondral pins tested under constant load. The rate of deformation was identified from the gradient of the deformation curve (deformation versus time). This gradient can be used as an indicator of mechanical properties whilst providing a relative comparison amongst samples. At the initial phase of loading, a rapid exudation of fluid and nutrients is expected and as the fluid is fully diminished out of the cartilage, equilibrium deformation is reached such that the solid phase bears the load. (Figure 3-21).
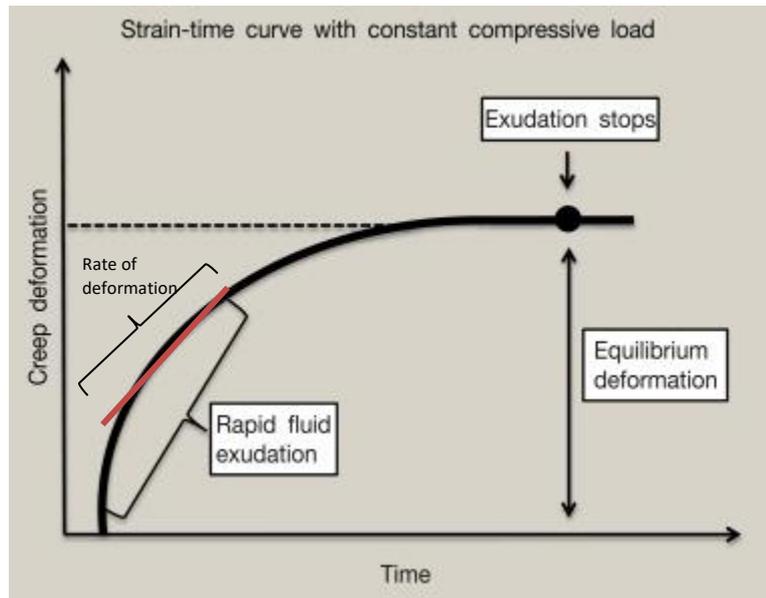
Figure 3-21: A diagram showing the fluid exudation process during creep deformation test over time adapted from Lees and Partington (2016). The 'orange' straight line represents the rate of deformation (gradient) in the initial phase of testing.

A steeper (i.e. higher) gradient indicates that the tissue deforms at a faster rate (Figure 3-22). As Figure 3-21 shows, with a steeper gradient, a higher rate of fluid exudation (i.e. higher permeability) is assumed at the initial phase of testing. Once the fluid is exuded out of the tissue, the steady state indicates the aggregate modulus (i.e. stiffness) of the solid content. A material with a higher modulus is reported to deform less under a given load. Overall, studying the rate of deformation and equilibrium deformation can be used as an indicator to predict mechanical properties (permeability and stiffness) of the tissue under a given load.
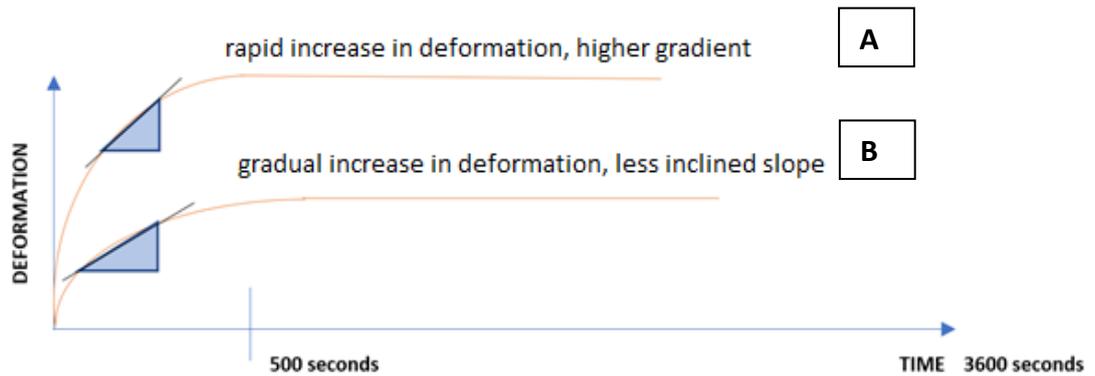
Figure 3-22: A diagram showing the fluid exudation process during creep deformation test over time for two examples.; A) rapid increase in defromation over time, whereby a higher gradient is observed; B) a gradual increase in deformation is observed, with a less inclined slope.

Furthermore, using the rate of deformation obtained from each gradient, the strain rate was calculated by taking the average thickness measurement into account for each sample in the ankle joint.

3.4.3 Statistical Method

For statistical analysis, ANOVA (one-way analysis of variance) was used to find the overall p-value to determine significance across the means. Further analysis was required when significant differences were reported across the means; in such instances, Tukey-method was used to determine individual significant differences across the means (Chapter 2, section 2.4).

3.5 Results

3.5.1 Determination of Cartilage Thickness using Needle Probe Technique on Porcine Ankle Osteochondral Tissue

Cartilage thickness readings across four regions in the porcine ankle joint were determined using needle probe technique, whereby comparisons were made across talar and tibial pins (Figure 3-23).
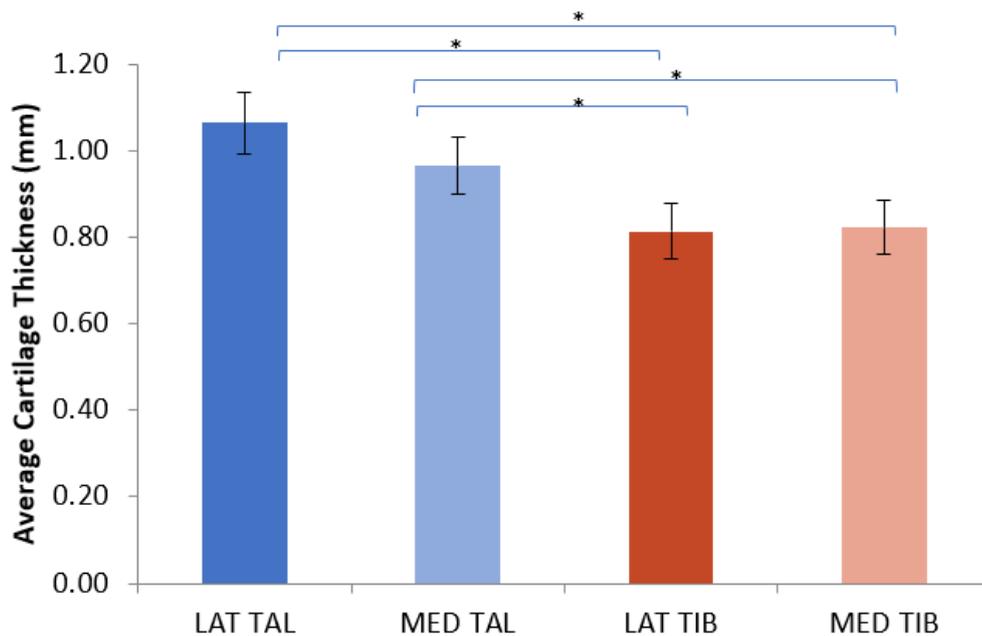
Figure 3-23: Comparison of average cartilage thicknesses (mm) in all four regions of the porcine ankle joint using needle probe technique on Instron testing machine. Data is expressed as mean (n=6) ± 95% confidence limits, * indicates significant difference (ANOVA, $p<0.05$); lateral talus (LAT TAL), medial talus (MED TAL), lateral tibia (LAT TIB) and medial tibia (MED TIB).

Statistical analysis (ANOVA, $p<0.05$) revealed that the cartilage of the lateral tibial (LAT TIB) pins was significantly thinner than the cartilage of the lateral talus (LAT TAL) and the medial talus (MED TAL) regions. In addition, the average cartilage thickness measurement of the medial tibial (MED TIB) region was significantly lower (ANOVA, $p<0.05$) than both the lateral talus (LAT TAL) and the medial talus (MED TAL) regions. These results indicated that the tibial cartilage was significantly thinner than the tibial cartilage.

3.5.2 Determination of Cartilage Thickness using Needle Probe Technique on Porcine Intact Talus Surface

The mean cartilage thickness was below 1 mm across the intact talar surface (Figure 3-24). The thickness was comparable (ANOVA, $p > 0.05$, $p = 0.54$) across all four different regions on the talar surface (LA=0.93 mm, LP=0.84 mm, MA=0.96 mm, MP=0.95 mm; (Figure 3-24A), and comparable with the cartilage thickness measurements obtained in the talar pin study (Figure 3-24B).
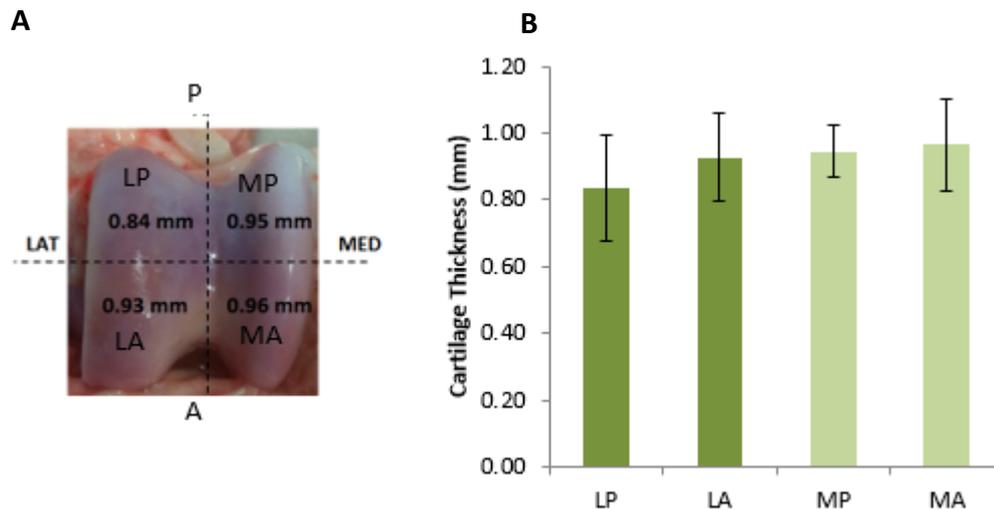
Figure 3-24: Comparison of mean cartilage thicknesses (mm) in four regions of the intact talus using the needle probe technique in the Instron testing machine. Data was analysed by ANOVA which revealed no significant differences across four regions in the intact talus ($p > 0.05$). Data is expressed as mean (n=6) ± 95% confidence limit; LAT- lateral, MED – medial, LA – lateral anterior, LP – lateral posterior, MA – medial anterior, MP – medial posterior.

After statistical analysis revealed no significant difference in cartilage thicknesses across the four regions of the talus (ANOVA, $p > 0.05$) (Figure 3-24) lateral regions were combined (i.e. LA and LP, n=6 for each region) to give an a mean value for lateral talus (LAT TAL, n=12) and the medial regions were combined (i.e. MA and MP, n=6 for each region) to give and mean value for medial talus (MED TAL, n=12). The data was combined such that comparisons could be made with the talar pin study.

3.5.3 Comparison of Cartilage Thickness using Needle Probe Technique on Porcine Talar Pins and Porcine Intact Talus Surface

Comparison of the pin and whole joint surface measurement demonstrated no significant difference in cartilage thickness for either lateral or medial aspects (ANOVA, p>0.05; p=0.11, Figure 3-25).
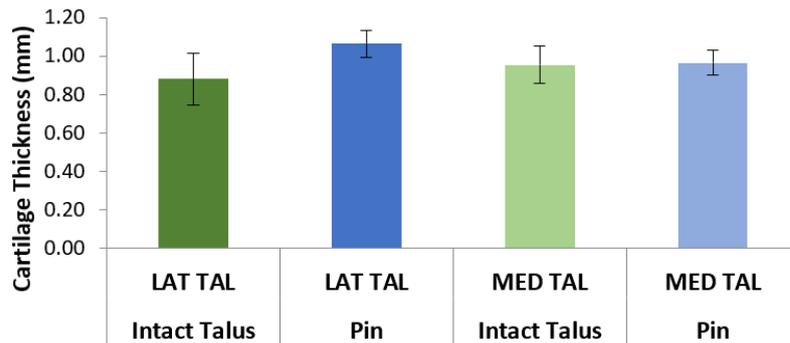
Figure 3-25: Comparison of mean cartilage thicknesses (mm) obtained using needle probe testing on Instron machine in lateral and medial aspects of intact talus (n=12) and talar pins (n=6). Data was analysed by ANOVA which revealed no significant differences between lateral and medial aspects of talar pins and intact talus (ANOVA, p>0.05). Data was expressed as mean ± 95% confidence limits; lateral talus (LAT TAL), medial talus (MED TAL).

3.5.4 Comparison of Cartilage Thickness Methods using Porcine Ankle Osteochondral Tissues: Needle Probe Technique vs CT Imaging Technique

Measurements of cartilage thickness were achieved through CT and needle probe methods, and mean values for each joint surface (i.e. talus and tibia) were calculated (Figure 3-26).
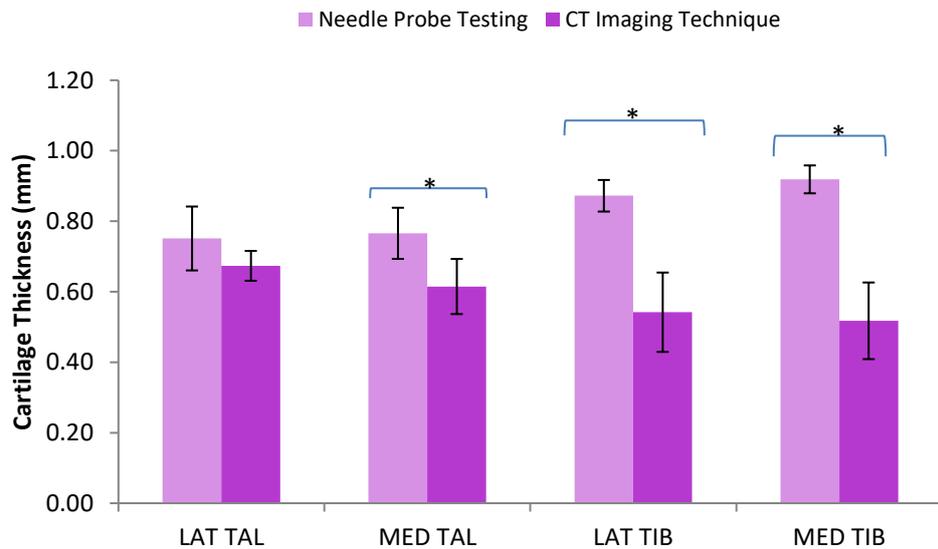
Figure 3-26: Comparison of porcine mean cartilage thicknesses (mm) using needle probe testing on Instron machine and CT imaging techniques using a CT scanner. Data was expressed as mean (n=3) ± 95% confidence limits. * indicates significantly different (ANOVA, p<0.05); lateral talus (LAT TAL), medial talus (MED TAL), lateral tibia (LAT TIB) and medial tibia (MED TIB).

Overall, thicknesses obtained using the CT imaging technique were lower in all regions in the porcine ankle compared to needle probe method, whereby these were significant in the medial talus (MED TAL), the lateral tibial (LAT TIB) and medial tibial (MED TIB) regions (ANOVA, p<0.05, Figure 3-26). Using the needle probe technique, medial tibial (MED TIB) was thickest (0.92 ± 0.11 mm) in four regions of the porcine ankle joint, whereas in the CT method it was the thinnest (0.52 ± 0.04 mm). The thinnest cartilage using needle probe technique was found in the lateral aspect of talus (LAT TAL) (0.75 ± 0.04 mm), which was the reported to be the thickest cartilage using CT method (0.67 ± 0.09 mm). Therefore, a vice versa relationship in cartilage thickness in porcine ankle cartilage pins between both methods was apparent.

A Bland and Altman graph was plotted showing the difference between method 1 (needle probe) and method 2 (CT) plotted against the mean of the two measurements (Figure 3-27). Such graph allows to determine the relationship between measurement error and the true value. The true value is represented as the mean of the two measurements.
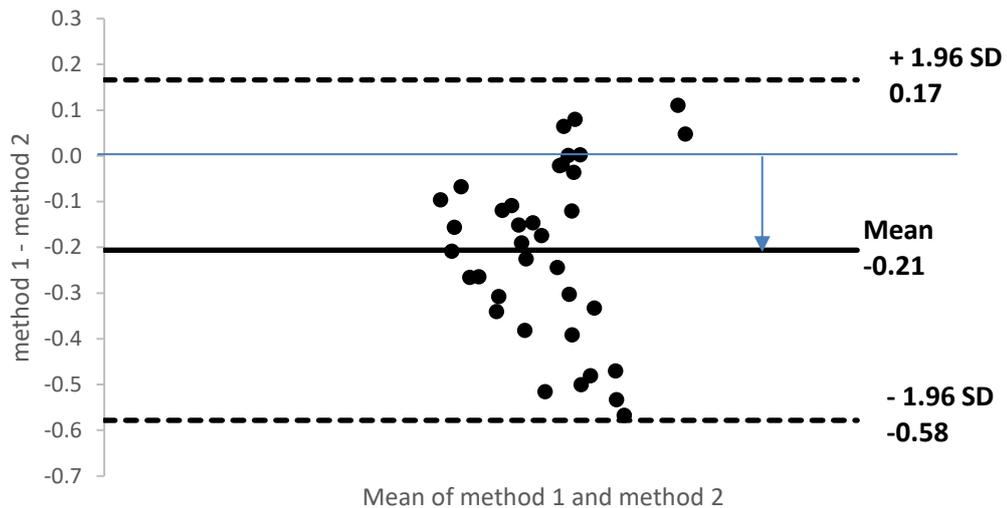
Figure 3-27: A Bland Altman graph is plotted to compare two thickness methods: CT method and needle probe method. SD – standard deviation and mean represents the average difference between both methods. The bias of -0.21 is represented by the gap between X -axis, corresponding to a zero difference, and the parallel line to the X-axis at -0.21 units.

For this study, a negative bias of -0.21 was reported (Figure 3-27). There is an expectation that 95% of the differences should lie between mean difference of +/- 1.96, also known as the limits of agreement. The limits of agreement of +0.17 mm and -0.58 mm was obtained (Figure 3-27). Overall, there seems to be a poor correlation between both methods as the data points are mostly located closely together (Figure 3-27). The measurements were within the limit of agreement and therefore both methods were considered to be in agreement and could be used interchangeably. For the purposes of human tissue study, the chosen method will be discussed later in this chapter.

3.5.5 Biphasic Indentation Method on Porcine Ankle Osteochondral Pins

This study compared the cartilage deformation results obtained using porcine osteochondral tissue extracted from the talar and tibial joint surfaces – lateral talus (LAT TAL, n=6), medial talus (MED TAL, n=6), lateral tibia (LAT TIB, n=6) and medial tibia (MED TIB, n=6) using indentation testing (Figure 3-28). Cartilage deformation in four regions of the porcine ankle joint had all reached an equilibrium state at 3600th second (Figure 3-28). A comparable mean cumulative deformation was reported in

all regions of the porcine ankle joint (Figure 3-28). As the displacement and load were recorded at every 0.1 second during indentation tests, a slight amount of vibration due to background noise levels was noted in the output.
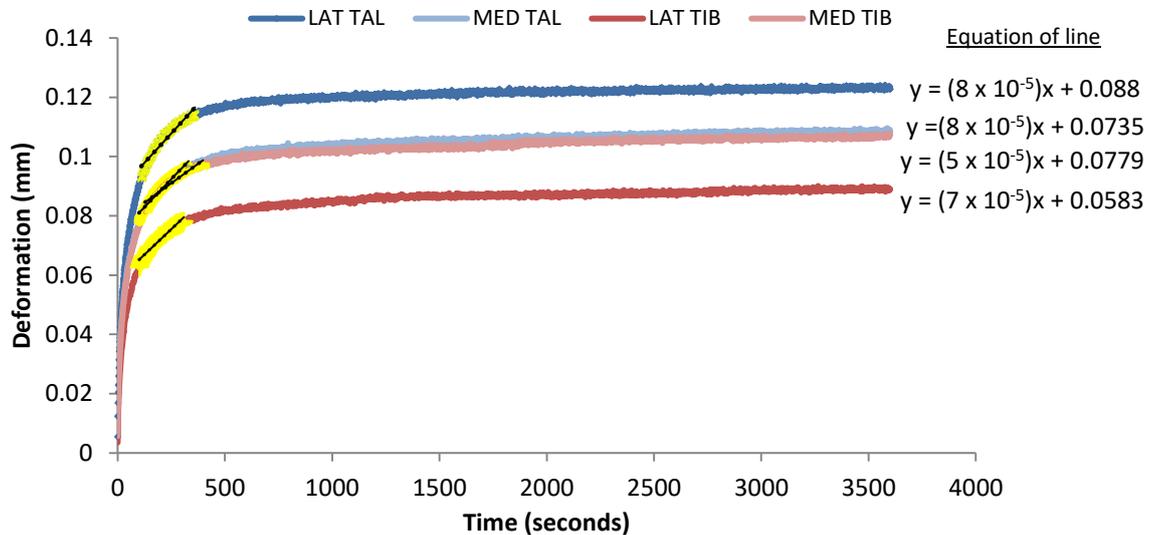
Figure 3-28: Porcine mean cartilage deformation (mm) over 3600 seconds during indentation in the four regions of the porcine talus and tibial bone surfaces (n=6 for each region); lateral talus (LAT TAL), medial talus (MED TAL), lateral tibia (LAT TIB) and medial tibia (MED TIB). The rate of deformation in the initial phase was determined for each region using the equation of line (right) represented in black dotted line over yellow region.

Based on the deformation gradients in the ankle joint, the highest rate of deformation was found in the lateral talar cartilage (8×10^{-5} mm/s), and the lowest was found in lateral tibial cartilage (5×10^{-5} mm/s) (Figure 3-28). Overall, the talar joint surfaces underwent higher deformation. The strain rates for LAT TAL, MED TAL, LAT TIB and MED TIB were 7.55×10^{-5} s^{-1}, 8.23×10^{-5} s^{-1}, 6.17×10^{-5} s^{-1} and 8.55×10^{-5} s^{-1}, respectively, suggesting the lowest and highest rates were found in the LAT TIB and MED TIB samples, respectively (Table 3-1).

Table 3-1: Summary of all gradients determined for porcine ankle cartilage based on curves presented in Figure 3-28.

Location	Talus		Tibia	
	LAT	MED	LAT	MED
Equation of line	y = 8E-05x + 0.088	y = 8E-05x + 0.0735	y = 5E-05x + 0.0779	y = 7E-05x + 0.0583
Rate of deformation mm/s (x 10⁻⁵)	8	8	5	7
Strain rates (per second) (x 10⁻⁵)	7.55	8.23	6.17	8.55

The percentage deformation of the ankle cartilage ranged between 8.79 ± 2.44 % and 12.23 ± 1.60 % in lateral talar (LAT TAL) region and lateral tibial (LAT TIB) region, respectively, at 3600th second of indentation testing (Figure 3-29).
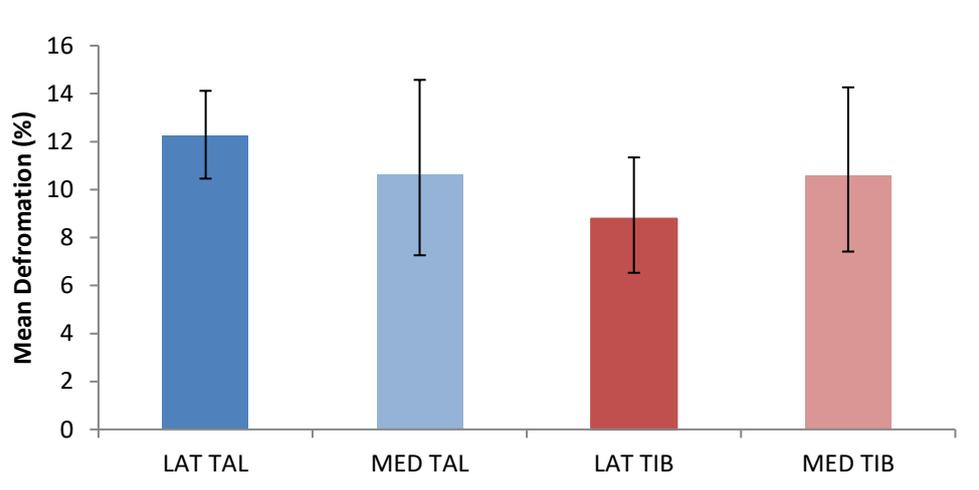
Figure 3-29: Porcine mean cartilage deformation (%) at 3600th second during indentation testing on 8.5mm diameter talar and tibial pins (n=6 for lateral and medial, respectively). Data was subject to arcsine transformation prior to calculation of the 95 % confidence limits. Error bars represent mean (n=6) ± 95% confidence level; no significant difference reported across the regions (ANOVA, p>0.05); lateral talus (LAT TAL), medial talus (MED TAL), lateral tibia (LAT TIB) and medial tibia (MED TIB).

There was no significant difference between all four regions of the porcine ankle joint (ANOVA, p>0.05, p=0.24). Cartilage deformation in the talar and tibial pins were comparable.

3.5.6 Comparison of Cartilage Deformation using Biphasic Indentation Method on Porcine Talar and Pins Intact Talus Surface

The deformation results for the intact talus (Figure 3-30) and talar pins (Figure 3-30), indicate both specimen types to have reached an equilibrium (steady) state by 3600 seconds at a comparable rate; the intact talus reached a steady state between 341 seconds to 464 seconds (for lateral and medial, respectively) and talar pins reached a steady state between 320 seconds to 420 seconds (for lateral and medial, respectively).
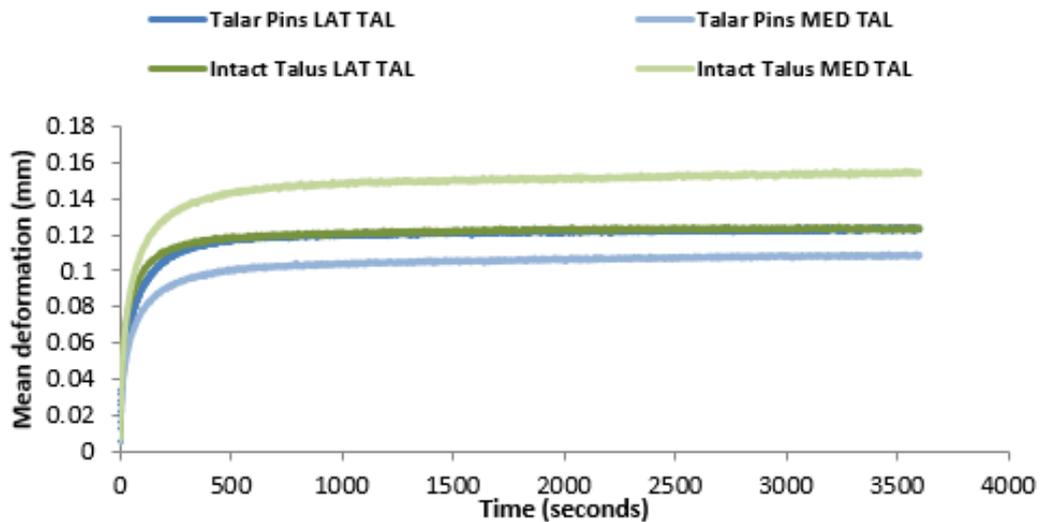
Figure 3-30: Porcine mean cartilage deformation (mm) over 3600 seconds during indentation on lateral and medial aspects of intact talus (n=6 for each region) and osteochondral pins of talus surfaces (n=6 for each region); LAT TAL – lateral talus; MED TAL – medial talus.

A comparison of the four data sets (pins v intact joint surface; medial v lateral) demonstrated there were no statistically significant differences in deformation between the different regions or between the different specimen types (ANOVA, p>0.05) (Figure 3-31).

In the pin study, the mean deformation was comparable between LAT TAL (12.23 ± 1.22 %) and MED TAL (10.64 ± 2.60 %). In the intact talus study, the mean deformation was also comparable between LAT TAL (12.15 ± 2.92 %) and MED TAL

(15.32 $\pm$ 1.86 %). Hence, no significant differences were reported when comparisons were made between lateral and medial aspects within pin study (ANOVA, p>0.05) and intact talus study (ANOVA, p>0.05, Figure 3-31).
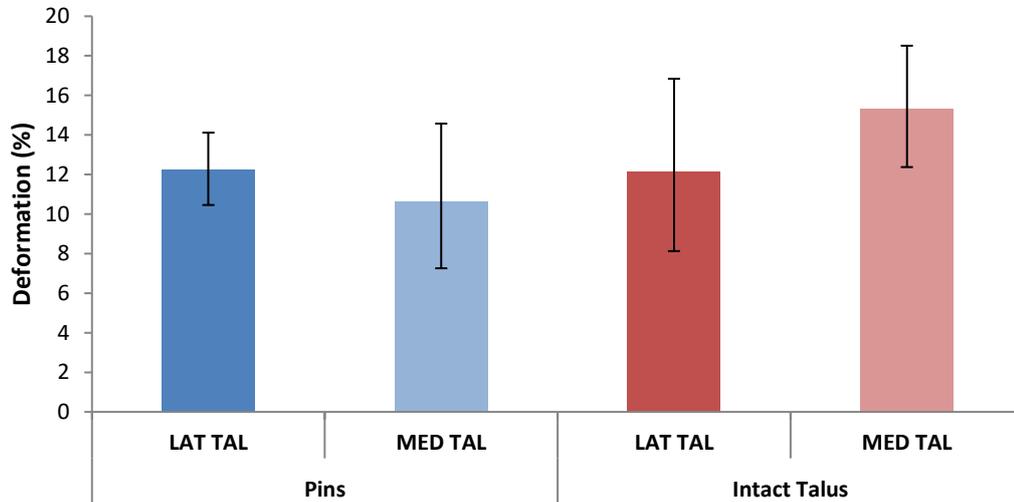
Figure 3-31: Porcine mean cartilage deformation (%) at 3600th second during indentation on lateral and medial aspects of the intact talus bone (n=6 for each region) and osteochondral pins of talus bone surfaces (n=6 for each region). Data was subject to arcsine transformation prior to calculation of the 95 % confidence limits. Data is expressed as mean (n=6) ± 95% confidence limits; no significant difference was reported across the samples (ANOVA, p>0.05); lateral talus (LAT TAL), medial talus (MED TAL).

3.6 Discussion

Overall, this chapter determined the biphasic deformation and thickness of porcine ankle cartilage to provide an understanding of mechanical characteristics of the 'healthy' ankle tissue in its natural state. In the current study, porcine study was investigated as this animal tissue closely represents the human tissue with its comparable geometrical feature of a 'single' tibiotalar joint and methods were developed and refined for the purposes of human tissue investigation later in this thesis (Chapter 6). Based the comparable features in the ankle joint of both species, it was assumed that the talar cartilage in the porcine tissue may present with unfavourable characteristics as also reported in the human tissue, whereby defects are commonly found in the talus (van Dijk et al., 2010). In the current study, such outcome was evident in the talus, whereby this joint surface was significantly thicker and deformed more than the tibial cartilage. As part of this study, using porcine ankle cartilage, two thickness methods were compared to identify a suitable method for the human ankle tissue going forwards (Chapter 6). As the human tissue was limited, the chosen method using porcine tissue had to ensure the quality of the specimens such that it was possible to retest the same samples to optimise the usage of the tissue. Based on the outcome, CT method was chosen as tissue hydration allowed pins to be remain intact, unlike the needle probe method which damaged the cartilage surface and no longer allowed retesting of such samples. Furthermore, a study using porcine pins determined that specimen preparation did not have any impact on the thickness and deformational behaviour using porcine tissue. This study helped to identify the tissue type to be taken forward for the human tissue (Chapter 6). Therefore, as both tissue types (osteochondral pins study versus intact talar study) presented with no significant difference, pins were taken forward for the human study (Chapter 6). Each of these outcomes in this Chapter will be discussed in greater detail.

3.6.1 Cartilage Thickness of Porcine Ankle Cartilage Pins and Porcine Intact Talus

In the porcine tissue (pin study), cartilage thicknesses of the tibial surfaces were significantly thinner than talar surfaces using needle probe method. Porcine ankle cartilage thickness has not been studied previously, whereas human ankle joint has been studied using a needle probe method; tibial cartilage was reported to be significantly thicker in 7 out of 10 samples than talar cartilage (Shepherd and Seedhom, 1999). Although porcine and human ankle joint had a single tibio-talar joint, the assumption that both species may present with possible similarities in their properties had not been investigated.

A study by Koo et al. (2005) (Chapter 1, section 1.5.1.1) reported cartilage thickness in the lateral aspect of porcine distal tibial knee cartilage to be generally thicker than that on the medial aspect using an imaging method. This was in agreement with the current study on porcine ankle cartilage on the pin study using needle probe method; however the intact joint had shown thinner cartilage in the lateral regions compared to the medial regions instead. Such differences between pin and intact joint study in the present study may be attributed to the specific location tested on the joint surfaces, as pins were extracted from the central regions on the joint, whereas in the intact joint study, four regions and their inter-specimen variability were studied (LA – lateral anterior, LP – lateral posterior, MA – medial anterior, MP- medial posterior) (Chapter 2, section 2.3.4.1). Although the current study on the intact joint and Koo et al. (2005) studied thickness across the whole joint surface, variation in thickness relationship between lateral and medial aspects could be due to possible differences in the methodology studied and the average thicknesses obtained from different pin locations on the joint (i.e. needle vs imaging; central regions were not considered in the present study). Furthermore, since load distribution varied between the knee and ankle joints in the human tissue (Stauffer et al., 1977; Kleipool and Blankevoort, 2010; Kutzner et al., 2010a; Sanford et al., 2014a), such variation may be present between both joints in the porcine tissue which may have resulted in differences within medial-lateral distribution. For accurate representation of thickness variation across

the joint surface, the location of interest should be comparable. As the current study focused on porcine ankle and Koo et al. (2005) studied porcine knee, differences may exist across joints as each joint operates within an environment to ensure joint stability with varied mechanical loading (Simon et al., 1973). However, load transmission in the porcine model remains unknown and further research may reveal such differences, if any, between knee and ankle joints as reported in the human tissue (Stauffer et al., 1977; Kleipool and Blankevoort, 2010; Kutzner et al., 2010b; Sanford et al., 2014b).

3.6.2 Comparison of Cartilage Thicknesses with Other Porcine Joints

Based on the findings reported in the current study on the ankle joint, porcine tibial cartilage was generally thinnest when compared to previously reported studies on other joints such as the porcine hip (Taylor, 2012) and the porcine tibial and femoral knee cartilages (McLure et al., 2012) using needle probe methods on osteochondral tissues. Furthermore, a large variation in thickness was reported in the porcine knee joint (McLure et al., 2012) (Table 3-2).

Table 3-2: Summary of cartilage thickness values within porcine joints – knee, hip and ankle.

	Thickness (mm)	Joint
Knee (McLure, 2012)	0.86 ± 0.10[+] 2.10 ± 0.30[++]	[+]tibial knee cartilage, n=6 [++]femoral knee cartilage, n=6
Hip (Taylor, 2012)	1.22 ± 0.05	femoral head cartilage, n=6
Ankle (current study)	0.82 ± 0.07[+++] 1.02 ± 0.08[++++]	[+++]tibial ankle cartilage (med & lat), n=12 [++++]talar ankle cartilage (med & lat), n=12

3.6.3 Comparison of Cartilage Thickness Methods: CT Imaging vs Needle Probe Technique

Overall, based on the Bland-Altman graph (Figure 3-27), CT and needle thickness methods can be used interchangeably as no correlation was reported. A statistical

comparison was also conducted to identify any differences in thickness data across both methods. Based on such statistical comparison of thickness data (Figure 3-26), differences were reported, whereby CT method resulted in lower measurements in all regions in the porcine ankle compared to needle probe method. A possible reason for lower thickness readings with CT method compared to needle technique could be due to inaccuracies in establishing the two slices in which the full cartilage layers were displayed and the slice in which the subchondral bone became visible. These two slices need to be accurately determined to avoid misjudgement for thickness measurement; each scan consists of approximately 900 slices in total in which a stack of slices will need to be selected to determine thickness and if for instance 50 less slices (0.25 mm) were not considered as part of the cartilage, it would result in considerably large error if the cartilage tissue was in the region of 1 mm. Although the needle probe method was suggested to provide consistent thickness results as the scatter between measurements were small (Jurvelin et al. 1995), there is a potential to induce errors, as the needle in most instances pierced through the bone resulting in higher thickness readings. This could present with a sudden exponential increase in resistive load as the needle penetrates through a harder material, which changes the load-displacement gradient thus affecting the cartilage thickness value. Furthermore, surface curvature could influence the accuracy of cartilage thickness measurements, as a perpendicular needle entry may not be achieved with a poorly adjusted orientation of the sample. In the present study, as samples were held in a custom-made Perspex holder, surface orientation in respect to the needle was not considered, thus potential changes in local thickness measurements on the pin sample may exist. There may be limitations with both methods, however thickness measurements were in agreement for both methods in the current study as also reported by Taylor (2012) on porcine hip osteochondral tissues.

Although either method could be chosen to measure cartilage thickness in the human tissue, CT method was preferred in the current study as this method ensured tissue hydration and allowed the possibility to re-test samples which was essential with limited human tissue availability.

3.6.4 Percentage deformation of Porcine Cartilage Pins and Porcine Intact Talus

For all specimens, as the load was applied, a rapid rate of fluid exudation was evident with an initial linear increase in displacement over time. This was in agreement with previously published deformation curves (Mow et al., 1989), whereby the initial phase represents the decrease in water content until the load is supported by the solid phase at which point a steady state (i.e. equilibrium deformation) is reached within one hour of testing. As the strain rate was suggested to influence the load distribution between the solid matrix, fluid pressurisation and thereby the stiffness of the cartilage tested (Li et al., 2003), an increase in strain rates was associated with increased collagen damage (Quiroga et al., 2017). In the current study, a higher rate of deformation (and strain rates) in the initial phase of testing and higher equilibrium deformation was found in the talar joint surface compared to tibial joint surface, although the creep response was comparable for porcine talar and tibial joint surfaces. This suggests that the talar cartilage could deform more under the same load due to a faster loss of the fluid content compared to the tibial cartilage as there is an inferior ability to trap fluid or increased permeability. As the ability of the solid component to withstand the load (i.e. stiffness) is measured once the tissue reaches a steady state, stiffness may be lower in the talar cartilage as the tissue deforms more easily than tibial cartilage. A combination of high permeability and low stiffness are considered to be unfavourable properties in cartilage as a low frictional resistance against fluid flow and poor ability to withstand high stresses are associated with cartilage deterioration over time (Mansour, 2009). These could be potential reasons as to why perhaps defects are found in the talus more commonly than tibia; however defects in the porcine ankle joint have not been previously reported and literature is mainly based on human joints (Hangody et al., 1998; VanDijk et al., 2010; van Bergen et al., 2013).

In the current study, cartilage deformation in the porcine talar and tibial cartilages (8.79 ± 2.44 % and 12.23 ± 1.60 %), were considerably lower compared to porcine hip

(22 to 34 %, Taylor 2012) and porcine knee (21 to up to 49 %, Fermor, 2012). A possible reason for the differences in deformational cartilage behaviour in the porcine tissue could be due to the additional loads added onto the indentation rig applied through the indenter on hip (Taylor, 2012) and knee joints (Fermor, 2013). Taylor (2012) and Fermor (2013) used a higher weight of 82 g (0.8 N). In the current study, no additional weights were added, and the applied load was kept to an absolute minimum (0.24 N) which only included the weights of displacement shaft, load cell and indenter shaft (total of 23 g) to mimic low physiological behaviour. Under a constant load (i.e. creep test), the deformation is not instantaneous (Mansour, 2009), whereby varying loading conditions could affect the initial fluid exudation phase and result in varied final displacement.

In the current study, a hemispherical indenter was used on cartilage pins and on intact talus surfaces. A hemispherical indenter can reduce soft tissue damage, stress concentrations and plastic deformation compared to conical or pyramidal indenters (Delaine-Smith et al., 2016). Although as with conical and pyramidal indenters, a hemispherical indenter on a flat surface increases in contact area during loading, which presents non-linear load-displacement response (i.e. not reaching equilibrium state) (Delaine-Smith et al., 2016), this was not the case in the present study, as porcine samples were largely curved resulting in a linear response. In the present study, the contact area was assumed to be only minimally increased throughout the period of loading as the hemispherical indenter resulted in improved conformity with 'curved' porcine pins as the opposing material.

A study by Eckstein et al. (2005) used *in-vivo* method to determine the deformational behaviour in the femorotibial cartilage (knee joint) using MRI imaging method. This study suggested that an increased loading did not seem to have any impact on *in-vivo* cartilage deformation (Eckstein et al. 2005). The current study used an *in-vitro* indentation test set-up to determine deformational behaviour of cartilage under constant load. As the forces in the joint during physiological activities are not known and load transmission is considered to be variable, *in-vitro* indentation set up on soft tissues are more challenging to incorporate these. Despite the determination of

cartilage deformation using *in-vivo* method may be clinically more relevant to understand pathogenesis of osteoarthrosis, the *in-vitro* set up using indentation testing is a helpful tool to understand how cartilage responds to physiological loading and can be compared to other existing *in-vitro* studies to build an understanding of joint biomechanics.

3.6.5 Impact of Specimen Preparation on Talus: Pin Study vs Whole Joint Study

Based on the assumption that both pin study and whole joint study would result in comparable measurements as the tissue type and location of measurements were kept consistent, the current study supported this hypothesis and resulted in comparable cartilage thicknesses using needle probe testing and deformational behaviour using indentation tests between pin and whole joint study. Although the test set up varied for both tissue states, this did not have any effect on their mechanical characteristics.

Studying whole joints to determine mechanical characteristics was suggested to closely replicate *in-vivo* state of the joint. However, direct comparisons amongst other whole joints may present difficulties due to different geometries. To eliminate any discrepancies, osteochondral tissue specimens are generally studied instead to ensure comparison is kept consistent across different species (Berrien, 1999; Taylor, 2012; Fermor, 2013). Therefore, the method of pin extraction should be consistent for accurate comparison. The current study used a hammering technique, whereby other researchers have used a drilling technique (Berrien, 1999; Taylor, 2012; Fermor et al., 2015). With the latter approach, a possibility of frictional heating around the edges of the cartilage cannot be ruled out. Taylor (2012) measured the cartilage edges for thickness readings and reported these edges to have become damaged through extraction using an imaging technique (shadowgraph) as a significant change in thickness was reported. In the current study a hammering technique with Smith & Nephew's corer for clinical applications was used instead to prevent any such damage. In clinical settings, these corer tools are used to treat osteochondral defects in knee and ankle joints using autogenous osteochondral transplantation method

(Chapter 1, section 1.4.3.2). During pin extraction, the cartilage surface needs to remain intact, since any disruption to the tissue can affect the fluid flow behaviour of the tissue leading to possible changes in cartilage properties such as deformational behaviour and/or cartilage thickness. In the current study, the disruption of cartilage edges through pin extraction appears to have no effect on the overall results obtained in the present study. Based on these results, the pin study was chosen as a reliable tissue state to accurately characterise the properties for human studies (Chapter 6).

3.7 Conclusion

- In the pin study, talar cartilage was significantly thicker (ANOVA, $p<0.05$) and deformed generally more than tibial cartilage (ANOVA, $p>0.05$).

- Based on the Bland Altman plot, overall no correlation was observed between CT imaging and needle probe method.

- In this case, CT method was considered as a preferred choice as tissue hydration was maintained throughout test period and was a non-destructive method, hence the specimens remained intact throughout testing and could be used for further studies.

- Specimen preparation did not have an impact on the measured biomechanical properties of porcine ankle cartilage, as whole joint study and talar pins resulted in comparable thicknesses (ANOVA, $p>0.05$) and deformational behaviour (ANOVA, $p>0.05$).

- For the human tissue (Chapter 6), osteochondral pins will be studied, and CT thickness method will be taken forward based on the results obtained in this chapter.

Chapter 4: Friction and Surface Roughness Characterisation of Porcine Ankle Cartilage

4.1 Introduction

Articular cartilage enables low friction movement under high loads in the joint through one primary lubrication mechanism - biphasic lubrication (Park et al., 2004). Biphasic lubrication is defined by the load induced pressurisation of the interstitial fluid to support the load (Park et al., 2004). The high fluid-load support can be maintained as long as contact migrates on the cartilage surface and the previously loaded tissue sufficiently recovers through rehydration (Forster and Fisher, 1999). Any disruption to this lubrication mechanism has the potential to result in the degeneration of the cartilage due to changes in the biphasic nature of the cartilage (Milner et al., 2018). Therefore, frictional properties such as coefficient of friction can help to understand lubrication mechanisms and is one of the key elements in defining the overall tribological behaviour of cartilage. In this chapter, experiments were conducted to determine the coefficient of friction (COF) of porcine ankle cartilage through pin on plate studies. A low coefficient of friction between 0.002 to 0.3 is expected in articular cartilage depending on the configuration (Forster and Fisher, 1996). Typically, the coefficient of friction values in cartilage on cartilage configuration has been considerably lower (Northwood and Fisher, 2007; Caligaris and Ateshian, 2008; Katta et al., 2009) compared to cartilage against metal plates (Forster and Fisher, 1996; Pickard et al., 1998; Lizhang et al., 2011), as the biphasic nature of the cartilage helps with high fluid-load support in ensuring low friction. Testing against the metal plates results in a high frictional interaction between solid phases in the contacting surfaces, which ultimately increases the coefficient of friction (Krishnan et al., 2004; Katta et al., 2009; Ateshian, 2009). In the current study, cartilage on cartilage configuration was assumed to represent the interaction observed within the natural joint, whereas cartilage on metal was used as a control study, whereby higher friction was expected. Furthermore, several factors such as contact stress, sliding speed, counterface material, stroke length, environment,

lubricant, length of test, and contact area may play an important role in determining coefficient of friction. Due to limited studies on the porcine tissue, conditions such as contact stress of 1 MPa, sliding speed of 4 mm/s over 4 mm sliding distance with a testing period of 1 hour were chosen to closely represent physiological conditions reported in the human ankle (Conti and Wong, 2002).

Surface roughness characterisation can help to identify the quality of the cartilage surface and comment on sensitivity to damage and possible wear. Previous studies have measured the surface roughness of cartilage using contacting methods such contact stylus profilometry (Sayles et al., 1979; Kobayashiv and Kurogouchf, 1995; Kobayashi et al., 1996; Forster and Fisher, 1999). Contact stylus profilometry uses a stylus tip by tracing along the sample to measure surface texture and roughness values. This method has been widely used to measure surface roughness of cartilage surfaces (Udofia et al., 2009; McCann et al., 2009; Katta et al., 2009; Russell, 2010; Patrick A. Smyth et al., 2012; Taylor, 2013). A disavantage is that the tip contacts the material surface which could result in surface deformation, however this method is easy to use compared to non-contacting methods (Whitehouse, 2000). To avoid direct contact with the cartilage sample, the surface of tissue may be replicated using silicon moulds (Kimizuka et al., 1980) such that the tests are repeatable and the cartilage sample can remain intact and used to perform further tests. Furthermore, large areas are scanned relatively quickly (Patrick A. Smyth et al., 2012).

Contact mechanics such as contact area and pressure in synovial joints have been analysed using pressure sensor sheets such as Fuji films (Bruns and Rosenbach, 1990; Calhoun et al., 1994; Pereira et al., 1996; Lizhang et al., 2011) or using a Tekscan system (Bachus et al., 2006; Padalecki et al., 2014). Some of the advantages of using Tekscan system over Fuji film include the capability to perform dynamic tests, capability to produce real time data, reusability of sensors (Demarco et al., 2000) and to evaluate a wider loading range with enhanced accuracy and reliability (Bachus et al., 2006). However, in both methods, pressure sheets are prone to wrinkling, slippage and shearing (Patterson et al., 1997; Herregodts et al., 2015) that can affect the accuracy of the results. A study by Bachus et al. (2006) compared the accuracy of

both pressure sensor sheets (i.e. Tekscan vs Fujifilm) by placing these sheets between a cylindrical Delrin peg and a flat aluminium plate on Instron testing machine (Instron 8500, Canton, MA). Bachus et al. (2006) reported the measured errors between measurements to be within 5 % using Tekscan system, whereas Fuji film significantly underestimated the true area by 8 to 14 %. However, the accuracy of Tekscan depends on surface geometries studied. Static loading on curved surfaces or small contact areas may influence the accuracy of the system (Wilson et al., 2003; Brimacombe et al., 2009). Therefore, conformity between two interacting surfaces plays an important role in understanding contact mechanics as poor conformity could lead to an increase in friction and/or wear as contact area is decreased and stresses increased (Udofia et al., 2009).

This chapter will determine coefficient of friction values, surface roughness measurements and contact mechanics (area and pressure) on the porcine ankle tissue. Coefficient of friction of porcine ankle cartilage will be determined using pin on plate studies tested against cartilage plates and metal plates. Surface roughness measurements will be taken on pre-tested and post-tested cartilage pins and plates using pin on plate rig to study potential differences in test conditions and the influence this may have on the cartilage quality. Contact area and contact pressure will be determined with the pin on plate test set-up using Tekscan system with cartilage against metallic and cartilage counterfaces.

4.2 Aims & Objectives

4.2.1 Aims

The overall aim of this study was to investigate coefficient of friction, surface roughness and contact mechanics of porcine ankle cartilage to determine the fundamental tribological characteristics of the cartilage. This will help to comment on its sensitivity to damage.

4.2.2 Objectives

- To determine coefficient of friction for porcine cartilage pins against cartilage plates (bovine patella femoral) using pin on plate rig

- To determine coefficient of friction for porcine cartilage pins against CoCr metal plates (control study) using pin on plate rig

- To characterise changes to the surface roughness of cartilage pins and plates using Talysurf (contact stylus profilometry) following the friction studies

- To determine the contact area and pressure between pins and plates in both test configurations (cartilage on CoCr, and cartilage-on-cartilage) using TekScan system

4.3 Materials

For each study, porcine osteochondral pins of 8.5 mm diameter were extracted from the lateral and medial aspects of the talus (n=6 for each aspect) and tibial joint surfaces (n=6 for each aspect) as previously described (Chapter 2, section 0)

For the cartilage on cartilage configuration, cartilage plates were extracted from the bovine patella femoral joint (Chapter 2, section 2.3.2) as this tissue provided a flatter and larger surface compared to porcine ankle joint. For cartilage on metal configurations, the cobalt chrome (CoCr) plates were used (Figure 4-1).

Figure 4-1: A photograph of A) Cobalt Chrome (CoCr) plate after testing as cartilage residue is present,

4.4 Methods

4.4.1 Friction Characterisation of Porcine Ankle Cartilage using Pin on Plate Friction Rig

4.4.1.1 Pin on Plate Friction Rig

A single station multidirectional pin on plate friction rig (Forster and Fisher, 1999), was used for the friction study (Figure 4-2).
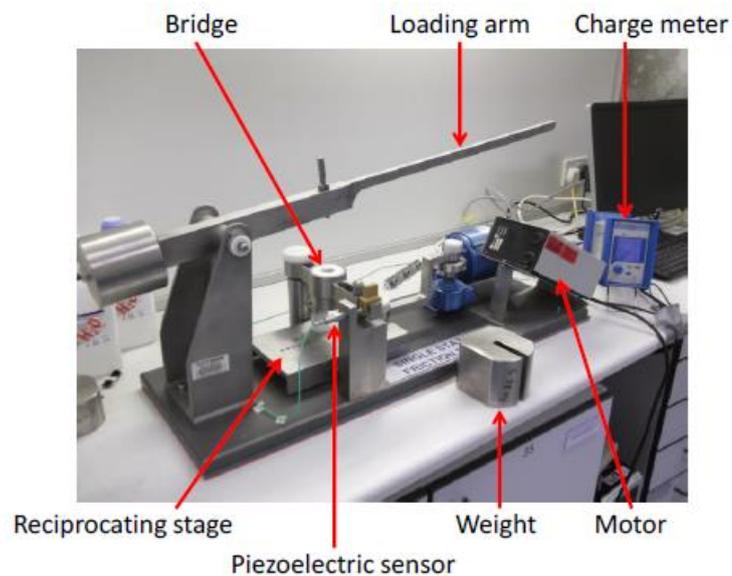
Figure 4-2: The in-house single station multidirectional pin on plate friction rig (Taylor, 2013).

A piezoelectric sensor (Kistler, Germany, Figure 4-2) attached to the bridge of the rig detected the frictional force between the cartilage pin and plate. The motor was used to reciprocate the stage through a specific distance and speed, determined by the experimental conditions. The loading arm that pivoted on one end was above the bath and perpendicular to the direction of motion.

4.4.1.2 Calibration of Pin on Plate Friction Rig

Calibration of the single station pin on plate rig was performed prior testing, using the following method. The pin holder was placed through the bridge of the rig and a cotton thread was looped to the end of the holder, placed horizontally over the

wheel and hung vertically with the weight holder/hanger attached to the end of the thread with specific weights (Figure 4-3).
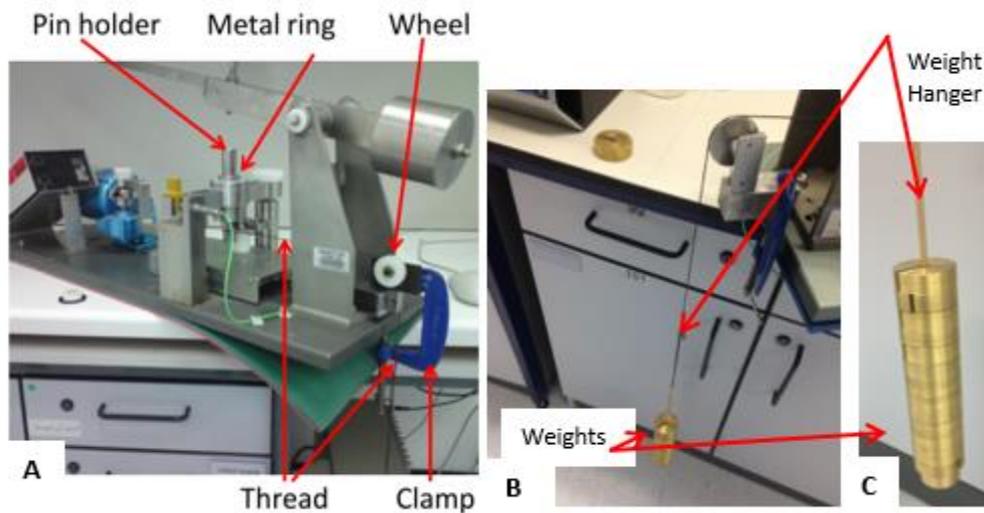
Figure 4-3: Calibration set up of the single station multidirectional pin on plate friction rig. A) The thread is attached to the base of the pin holder and stretched over the wheel/pulley which is secured to the rig using a G-clamp; B) A hanger is attached to the end of the thread with masses attached C) weights are added to the hanger/weight holder.

Once the test was started in the LabView programme, each 200 g weight was added to the hanger and a measurement was taken every 20 seconds, such that three readings for each mass were noted over a 60 second period. This was performed for a total of 14 weights (30 N), and the whole process was repeated three times sequentially. Whilst adding or removing weights, care was taken to keep the swinging of the thread and hanger to a minimum to prevent any inaccuracies in the output. The force applied to the pin holder was calculated from the total mass added and plotted against the average voltage of each reading to determine the calibration co-efficient (Figure 4-4). The linear relationship between the average voltage (V) and mass (N) enabled calculation of the friction co-efficient (Equation 4-1) from the voltage output.

$$Friction\ coefficient = (\frac{MaxAV - MinAV/_2 - Y\ intercept}{gradient\ of\ calibration})/Load$$

Equation 4-1: The calculation to determine coefficient of friction using calibration curve; MaxAV – maximum average output voltage, MinAV – minimum average output voltage.
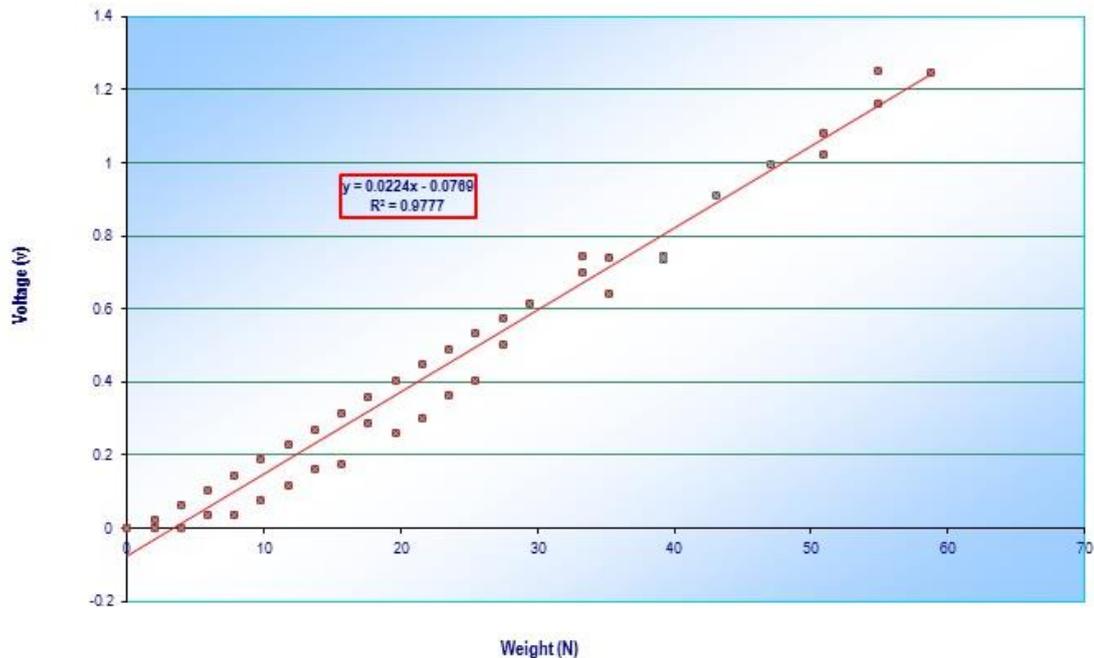
Figure 4-4: Example graph demonstrating the derivation of the calibration constant. The equation of the line is also presented with R^2 value (1).

The coefficient of friction was calculated as the ratio of frictional force outputs to the applied normal load on the cartilage pin (Equation 4-1). The frictional force was calculated using the corresponding output voltage with a known calibration factor obtained from the linear equation . As a strong linear response with an R^2 value of close to 1 was obtained between the average voltage (V) and load (N) reaching 60 N (Figure 4-4). The MaxAV and MinAV (maximum average voltage and minimum average voltage, respectively) were obtained from the charge meter and an overall average voltage output was calculated. From the equation on the graph (y=mx + c), the y-intercept value is c-value which is 0.0769, the gradient of calibration is the m-value in the equation which is 0.0224 and the load in the current study is 60 N.

4.4.1.3 Pin on Plate Friction Rig Set-Up

For the pin on plate set up, the following fixtures were needed as shown in Figure 4-5. The assembly of the ball bearing (Figure 4-5B; Figure 4-5C) was intended to reduce friction to a low value as possible such that the friction of the test interface was assumed negligible.
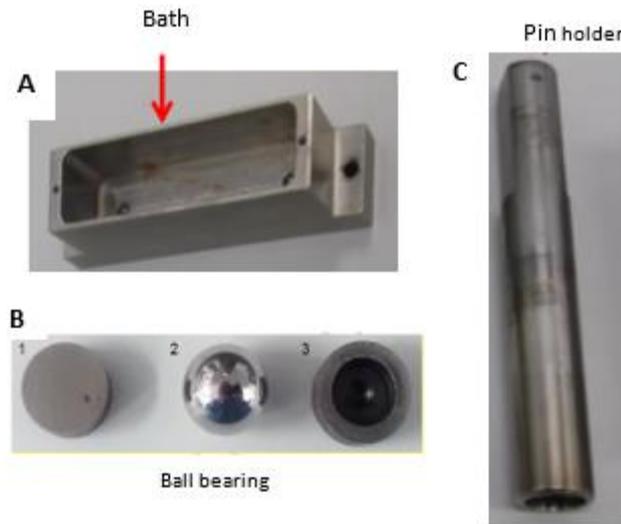
Figure 4-5: Fixtures needed for setting up pin on plate friction rig; A) Bath used for plate studies such as cartilage and metal plates; B) ball bearings -1) solid disk 2) ball bearing 3) shallow disk; C) pin holder to mount cartilage pins for testing against plates

The osteochondral pin was secured within the pin holder using a small stainless steel holder (Figure 4-6). This pin holder (Figure 4-5C) was used to secure the pins such that cartilage surface was exposed in order to make contact with the counterface (Figure 4-6A).
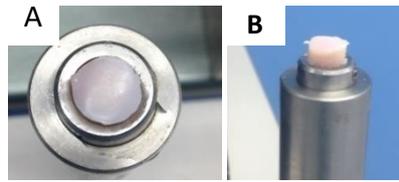
Figure 4-6: Small stainless steel holder required to secure pin samples within and the placed within the pin holder; A) top view of the pin fixture placed within the pin holder, B) side view of pin set up for testing.

Once the pins were secured in the pin holder, this was placed through the bridge of the friction rig such that the cartilage surface was contacting the counterface. To apply load on the contacting surfaces, the loading arm was lowered to make contact with the bearings (Figure 4-7).
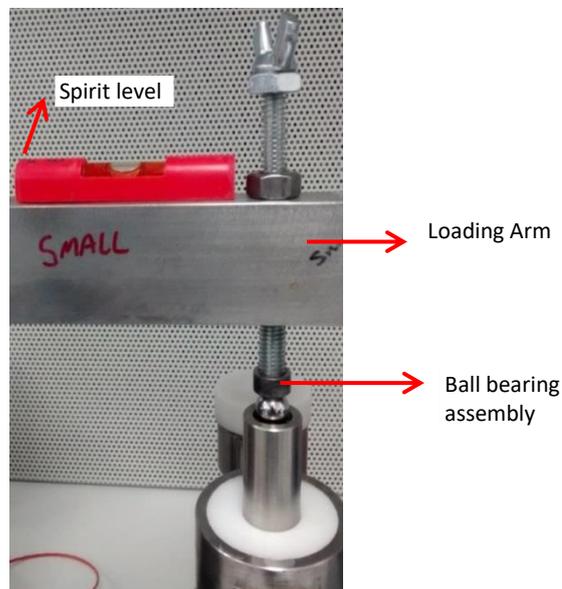
Figure 4-7: The ball bearing assembly of the friction rig whilst the loading arm is lowered such that contact is established between the pin and plate.

The cartilage pins were submerged in PBS within lubricant bath to ensure tissue hydration during testing (Figure 4-8).
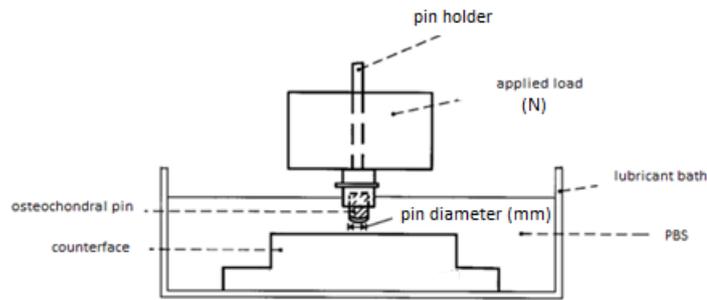
Figure 4-8: A schematic diagram illustrating the friction rig set up with cartilage pin against counterface in PBS (adapted from Forster and Fisher (1999))

For both cartilage-on-cartilage and cartilage-on-metal studies, a counter weight of 2 kg was added to the arm, to apply a load of 60 N on cartilage pins of 8.5 mm diameter to obtain a minimum contact stress of 1 MPa. A selected of speed of 4 mm/s with a stroke length of 4 mm such that a total cycle was 8 mm for a total of one hour (Table 4-1). As studies on porcine tissue is limited, these conditions were chosen based on the translations reported human ankle during movement (Conti and Wong, 2002).

Table 4-1: Summary of two studies performed on the friction rig.

Condition	Type of Plate	Pin diameter (mm)	Load (N)	Contact Stress (MPa)	Lubricant	Sliding velocity	Stroke length	Duration
Negative Control	CoCr	8.5	60	1	PBS	4 mm/s	4 mm	1 hr
Positive Control	Cartilage	8.5	60	1	PBS	4 mm/s	4 mm	1 hr

The data was collected every 30 seconds over a period of 60 minutes. The data acquisition unit recording, and the charge meter were connected to a PC and data was recorded using Labview 15 software (National Instruments, USA).

4.4.1.4 Cartilage Pins against Cobalt Chrome Plates using Pin on Plate Rig

The cobalt chrome (CoCr) plate (90 mm x 30 mm) was fixed into the bath (Figure 4-9), and the bath was attached to the reciprocating stage of the friction rig using clamp screws. Approximately 14 ml of PBS (Chapter 2, section 2.2.1) was added to the bath

to cover the CoCr plate. The osteochondral pin was placed within a stainless steel fixture (approximately 12 mm in height, Figure 4-6) and then tightened within the pin holder.

Figure 4-9: A photograph of CoCr plate and bath (Russell, 2010) used for cartilage on metal configurations.

4.4.1.5 Cartilage Pins against Cartilage Plates using Pin on Plate Rig

A bespoke fixture was used to retain the cartilage plate within the experimental rig. The cartilage plate (Chapter 2, section 2.3.2.1) was clamped between the two opposing stainless steel fixtures, one of which had a window to expose the cartilage surface (Figure 4-10). This ensured the plate did not move during testing but would not cause deformation to the cartilage surface through the fixture.
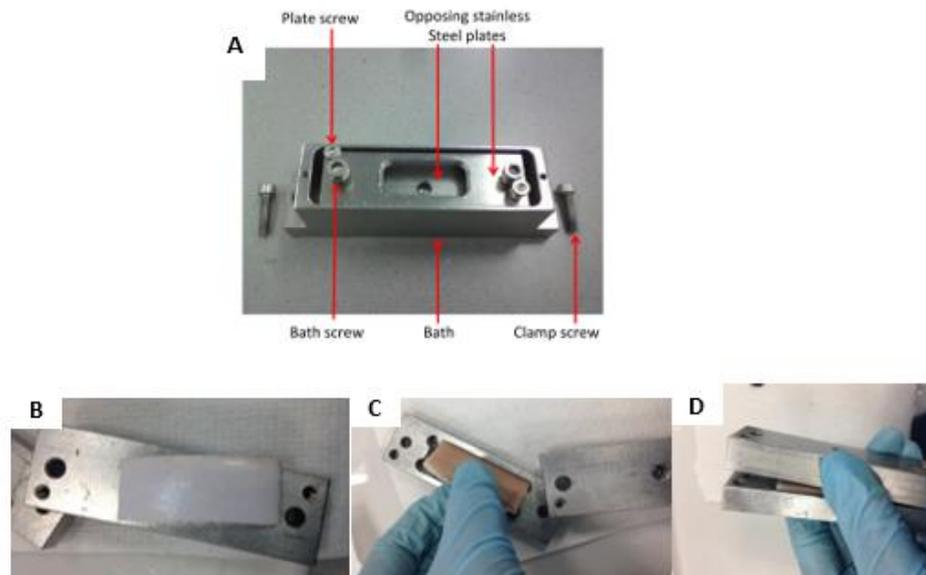
Figure 4-10: The setup of cartilage plate using two opposing stainless steel plates, one which has a cut open window to expose the cartilage surface during testing; A) The components needed to secure the cartilage plate into the bath; B) extracted bovine cartilage plate; C) The cartilage surface is placed onto the cut open window side; D) The base stainless steel plate is closed to ensure the plate sits within the two plates.

4.4.1.6 Standard validation

A standard validation test was performed using a GUR 1120 polyethylene (PE) pin (Figure 4-11) against metal plate to ensure the coefficient of friction values were within a similar range (0.06 to 0.07) before running a series of studies. A test of three repeats, studied for a 10 min period each was performed. Previous users obtained a friction range between 0.06 to 0.08 on an 8 to 9 mm PE pin with an applied load of 25 to 30 N over a sliding distance of 20 mm at a speed of 4 mm/s (Forster and Fisher, 1996; Northwood and Fisher, 2007; Katta et al., 2009). Although, in the current study, an applied load of 60 N was used on 8.5 mm PE pin against CoCr plate with 4 mm/s sliding speed over a sliding distance of 4 mm, similar friction range was observed to those reported in literature.

8.5 mm

12 mm

12 mm

8.5 mm
diameter face

Lateral view of PE pin

Aerial view of PE pin
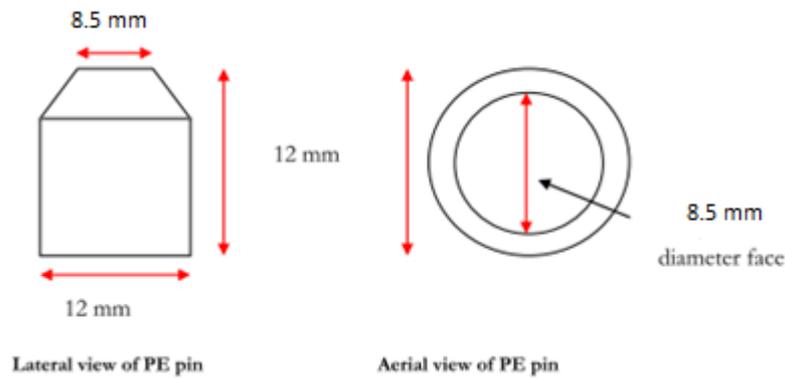
Figure 4-11: A modified schematic diagram illustrating dimensions of polyethylene pins used for standard validation tests (Russell, 2010).

4.4.2 Surface Roughness Characterisation of Porcine Ankle Cartilage

4.4.2.1 Using Silicon Rubber to Determine Cartilage Surface Roughness

The surface structure of the cartilage specimens was replicated using the silicon rubber replicating compound (Silicon mould kit, 50 ml system, Microset) (Figure 4-12A). The cartridge (Figure 4-12A) was attached onto a silicon gun and the nozzle (Figure 4-12A) was placed over the cartridge before pouring the liquid over the cartilage surface. Prior to covering the cartilage surface with the silicon rubber liquid over the ventilation bench, the sample was allowed to air dry for two minutes.

Silicone Gun   Cartridge   Pin Mould

A   B

Nozzle   Plate Mould
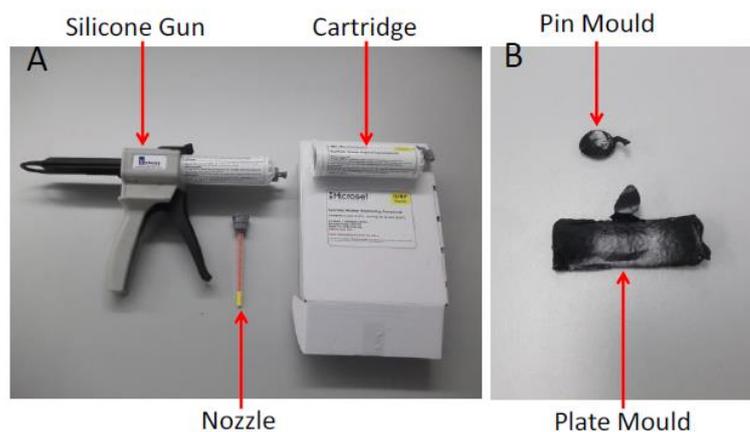
Figure 4-12: Images of Microset components and replicas. A) Cartridge was attached onto the silicon gun and the nozzle was attached to the cartridge (Taylor, 2013); B) pin and plate rubber replicas (Taylor, 2013).

Once the liquid had hardened, within 10 to 15 mins, the moulds were removed from the cartilage samples (Figure 4-12B) and stored in a separate plastic pot at room temperature.

Surface profilometry was used to determine the surface roughness (Ra) of the silicon rubber moulds. The replicas were permanent records of the specimens' features, and therefore surface roughness measurements were able to be determined at a later date. Silicon moulding has been used to replicate the cartilage surface (Kimizuka et al., 1980) rather than directly testing on the tissue specimens as extreme drying would have limited any further analysis.

Silicon moulds were taken from porcine cartilage specimens before testing on the friction rig (control study), and after testing against the cartilage plate (section 4.4.1.5).

4.4.2.2 Surface profilometry

A Talysurf Ultra PGI800 Profilometer (Taylor & Hobson Ltd, Leicester, UK) was used to measure the surface roughness of all samples (Figure 4-13).

Figure 4-13: Talysurf PGI800 used to measure surface roughness of silicon replicas of cartilage specimens (Russell, 2010).

4.4.2.3 Calibration of Talysurf PGI800 Profilometer

A roughness standard (Figure 4-14) was used to calibrate the machine. This consisted of a specific trace length sample with a surface roughness of approximately 0.8 µm.

0.8 µm Ra measurement line
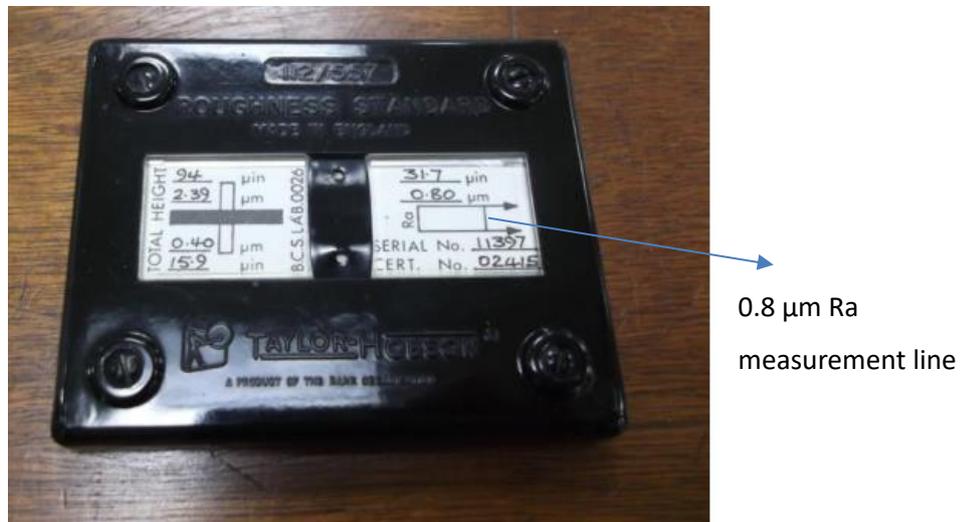
Figure 4-14: Roughness Standard used to calibrate Talysurf PGI800

The stylus was set to measure the trace indicated in Figure 4-14 to obtain a surface roughness of approximately 0.8 µm with a typical calibration trace shown in trace (Figure 4-15).
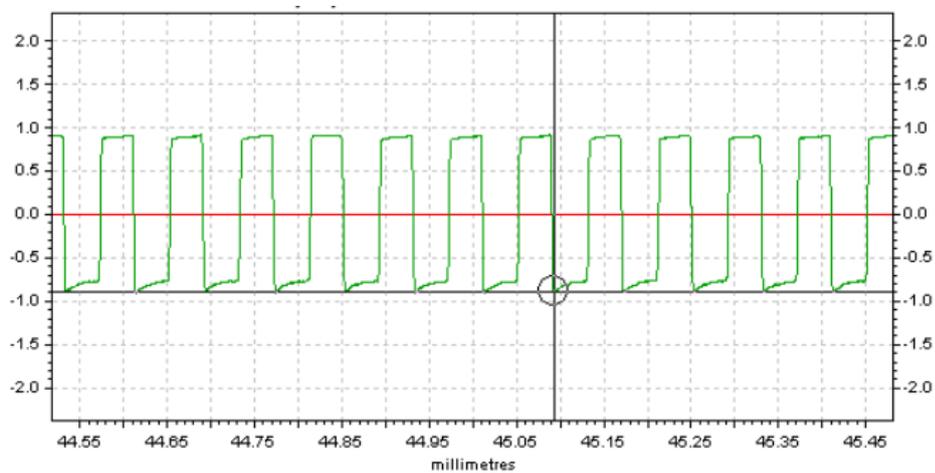
Figure 4-15: An example of a typical calibration curve produced from 0.8 µm trace on the roughness standard.

Surface roughness measurements were taken on the CoCr plates, cartilage plates and osteochondral pins, either directly or with the moulds (outlined in 4.4.2.1) (Table 4-2) prior to the friction study and at completion of the test.

Table 4-2: Summary of two studies (control study and post friction study) performed on the Talysurf PGI800 Profilometry to measure surface roughness measurements of samples considered.

Condition	Details of Specimens tested on Talysurf			
Control Study (No testing)	CoCr plate	Cartilage plate	Ankle Cartilage Pins	
Post Friction Study	CoCr plate	Cartilage plate	Pins (against CoCr plate)	Pins (against cartilage plate)

In the current chapter, for both types of plates (cartilage and metal), the region on which contact was established between pin and plate, was labelled as the 'wear region', whereas the region with no contact established was defined as the 'non-wear region'. For the cartilage and metal plates, all trace lengths were 14 mm in length. To represent the 'wear region', a mean surface roughness was calculated by taking two traces perpendicularly and two traces in parallel to the experimental sliding track (positions 1 to 4, P1-P4 in Figure 4-16A). A mean surface roughness in a 'non-wear region' was calculated from two traces taken at positions 5 (P5) and 6 (P6) as indicated in Figure 4-16A. Two perpendicular traces were taken across the surface mould of each pin (Figure 4-16B) and a mean roughness measurement was calculated for each pin. Due to the nature of the pin geometry, the trace lengths varied between pin samples, but were generally between 7 to 8 mm.
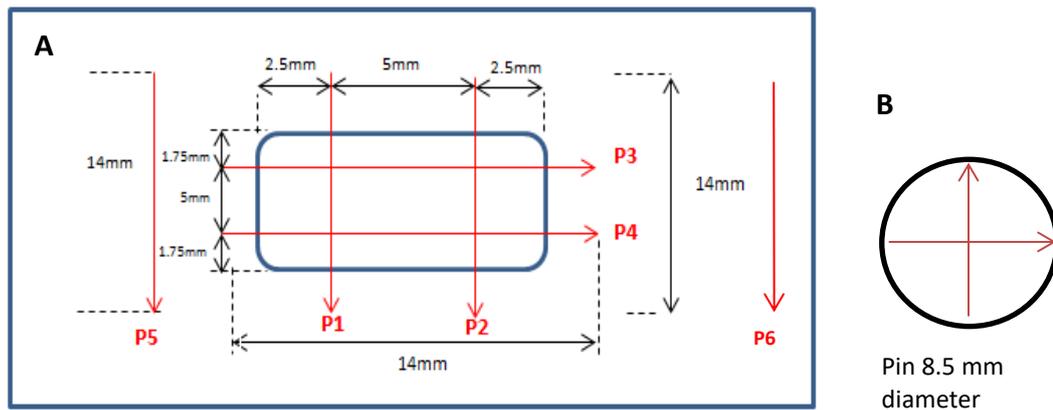
Figure 4-16: Trace patterns (trace length =mm) for pin and plate specimens. Red arrows indicate the traces measured on the A) plate, whereby 'P' stands for 'position' and B) on the pin.

All measurements were taken with a diamond-tip stylus with a radius of 2.5 µm and traces were measured at scanning speed of 0.5 mm/s for all specimens. Once the samples were placed on the stage, the stylus was manually lowered towards the centre of the sample surface. To prepare for testing, the stylus was set up to initiate an automatic contact with the surface and a trace was taken along the pre-defined length upon starting the test. As the stylus moved across the surface of the specimen along the Z-axis, electronic signals were converted to digital measurements to construct a roughness profile from the trace.

Using Taylor Hobson Ultra software (Taylor Hobson, Leicester, UK), each trace was analysed. A form-removal function was performed to account for the form of each sample surface. Depending on the sample, either a least-square arc or line removal was performed, effectively 'levelling' the sample. A Gaussian filter with an upper cut-off of 0.25 mm and lower cut-off of 2.5 µm (100:1 bandwidth) was applied, in accordance with ISO 4287:1997 (International Organisation for Standardisation, 2015). This filter was used to suppress the waviness such that only surface roughness was measured.

4.4.3 Characterisation of Contact Area & Pressure of Porcine Ankle Cartilage Using The Tekscan System

4.4.3.1 The Tekscan System

The Tekscan I-Scan pressure measurement system (Tekscan, Inc, Boston, MA) is made up of pressure sensors, a handle and Tekscan software installed onto a laptop. The pressure mapping sensor '6900' with a resolution of 121 (number of sensels), a density of 62 sensels/cm^2 and a matrix dimension of 14 mm (width) by 14 mm (height) (Figure 4-17) was used for measuring the contact area and pressure between pins and plates when assembled in the pin on plate rig.
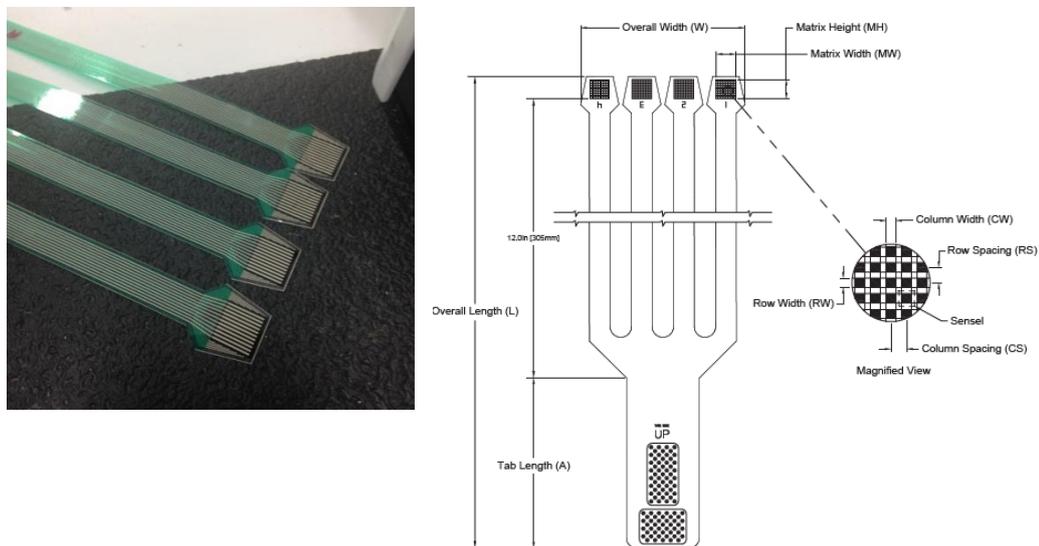
Figure 4-17: Pressure sensors '6900'. These are 14 mm by 14 mm in dimension and ensure coverage of an 8.5 mm diameter pin against a plate; A) pressure sensors used during testing; B) detailed drawing of pressure sensor '6900' (Tekscan Inc., 2015).

4.4.3.2 Equilibration

To ensure the sensitivity level of sensing elements is equal an equilibration method is used to normalise all sensing elements on the sheet with the application of pressure across the sensor sheet (Figure 4-19). This method is used as a quality assurance check and to ensure the sensor is not damaged. During equilibration, the sensors were first inserted into the thin gap (Figure 4-18A). Through the pressure source entrance at the top, air was used to inflate the bladder membrane such that

uniform pressure was applied onto the active area of the sensor. The pressures applied on the sensors were at a medium range at four stages from 25 psi, 50 psi, 75 psi and to 100 psi. This range was a standard equilibrator for the sensor '6900' used in the current study (Tekscan, 2013).
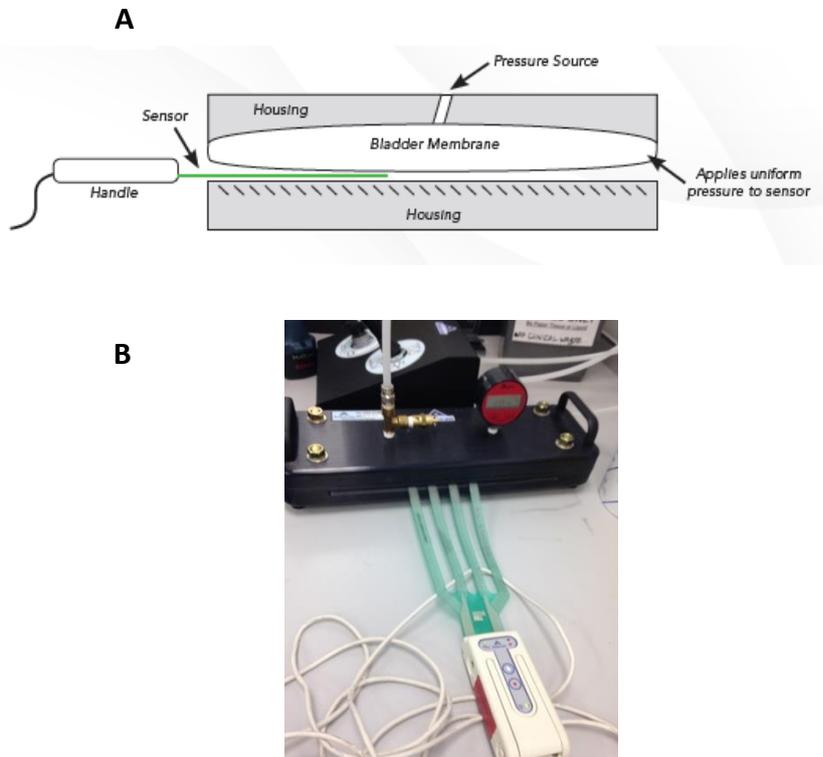
Figure 4-18: Equilibration testing set up. A) Illustration of the set up showing the view within the pressure applicator (Tekscan Inc., 2015); B) Equilibration of sensor '6900' attached to handle and connected to the equilibration machine.
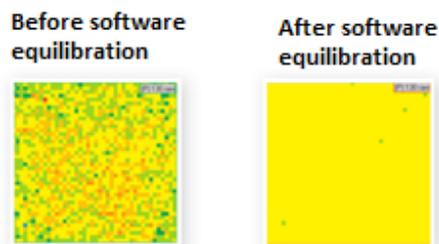
Figure 4-19: Equilibration method illustrating the normalising of sensing elements on the pressure sensors sheets before and after testing (adapted from Tekscan (2013)).

4.4.3.3 Calibration

The sensor 6900 (14 mm by 14 mm) was calibrated up to a maximum applied load of 60 N on the friction rig using flat-faced polyethylene pin, with a diameter of 8.5 mm against a CoCr plate. This set up was also used for standard validation tests on the friction rig (section 4.4.1.6).

In the calibration dialog box, the horizontal axis illustrates the digital output (pressure legend) that ranges from 0 to 255 (Figure 4-20), which shows that the sensels saturation point is 255 to a load. The calibration converts the raw 8-bit digital output (0 to 255 per sensel) into engineering units such as pounds (force) and PSI (pressure) (Figure 4-20). The expected peak load should fall at approximately 75 % of the sensor range as recommended by the manufacturers.
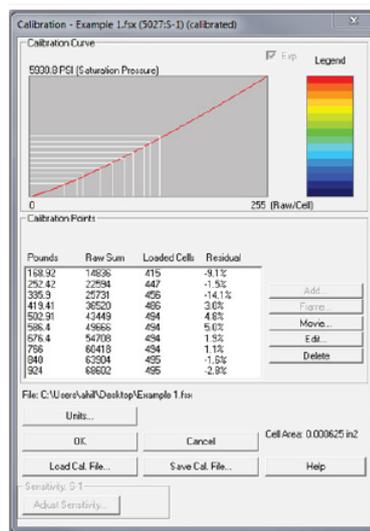
Figure 4-20: An example of linear calibration method followed illustrating 10 calibration points on the calibration curve.

A force of 60 N was entered to replicate tests in the current study on cartilage samples. The calibration point lasted between 5 to 10 seconds between contacting surfaces on a linear calibration curve. This single point recorded is displayed on a linear graph and a linear calibration is determined from this calibrated point and its origin. This is a linear calibration method which is used when only a small range of pressure value is to be measured (Brimacombe et al., 2009).

4.4.3.4 Measuring Contact Area and Pressure using Tekscan

The friction rig was set up using cartilage pin against CoCr plate (section 4.4.1.4) and also cartilage pin against cartilage plate (section 4.4.1.5). The sensor sheet was carefully placed as flat as possible between the two opposing surfaces prior to lowering the loading arm and applying a load of 60 N. Any bending of the sensor may cause an inaccurate reading, as those regions will not be contacting against the sensor. PBS was also added to ensure the test was replicated as followed in the friction testing and to keep the cartilage surface hydrated during testing. Each test was conducted for a period of 10 seconds and the contact area and pressure were obtained for each test. Tests were repeated three times for each specimen, and a mean calculated. For each test, the mean pressure distribution was recorded at 10 seconds, once pressure had stabilised.

4.4.4 Statistical Method

For statistical analysis, ANOVA (one-way analysis of variance) was used to find the overall p-value to determine significance across the means. Further analysis was required when significant differences were reported across the means; in such instances, Tukey-method was used to determine individual significant differences across the means (Chapter 2, section 2.4).

To compare means across two or more data sets such as between different test conditions/configurations (i.e. cartilage on cartilage vs cartilage on metal), ANOVA (two-way analysis) was used to find overall p-value.

4.5 Results

4.5.1 Determination of Coefficient of Friction of Porcine Osteochondral Pins

4.5.1.1 Cartilage on Metal Configuration

Porcine ankle cartilage pins of 8.5 mm in diameter were reciprocated against CoCr plates in phosphate buffered solution (PBS), for one hour with a load of 60 N resulting in an approximate contact pressure of 1 MPa, based on the assumption of a flat pin counterface and a nominal pin diameter of 8.5 mm. For all four regions, an equilibrium state had been reached by 3600 seconds. The tibial pins appeared to reach equilibrium more quickly than the talar pins. The lateral tibia (LAT TIB) pins reached equilibrium at approximately 810 seconds and the medial tibial (MED TIB) pins at approximately 840 seconds. The mean time to reach equilibrium for the lateral talus (LAT TAL) was 1680 seconds, and 1560 seconds for the medial talus (MED TAL) pins (Figure 4-21).
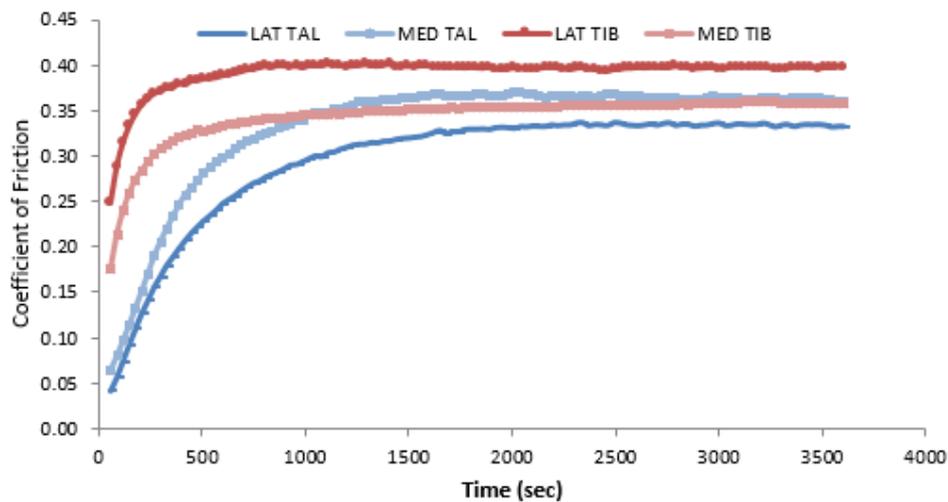
Figure 4-21: Coefficient of friction (COF) values obtained of porcine cartilage pins against CoCr plates using pin on plate rig over a period of 3600 seconds within four regions in the ankle joint of lateral talus (LAT TAL), medial talus (MED TAL), lateral tibia (LAT TIB) and medial tibia (MED TIB). Data is expressed as mean (n=6).

The mean coefficient of friction for each region was 0.33 ± 0.04, 0.36 ± 0.04, 0.40 ± 0.05 and 0.36 ± 0.04 for lateral talus (LAT TAL), medial talus (MED TAL), lateral tibia (LAT TIB) and medial tibia (MED TIB), respectively (Figure 4-22). Overall, no significant differences were found between the coefficient of friction values across all four regions in the ankle joint (ANOVA, $p > 0.05$). A comparison of friction across the medial and lateral aspects also did not show any significant difference. The confidence limits were reasonably low and consistent across the four regions in the ankle, showing little variation between the data sets.
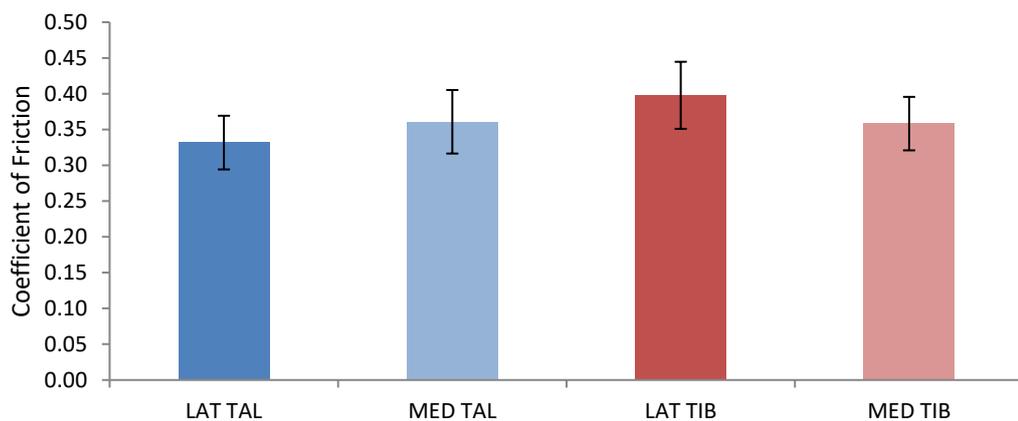
Figure 4-22: Coefficient of friction (COF) values obtained of porcine cartilage pins against CoCr plates using pin on plate rig at 3600th seconds within four regions in the ankle joint of lateral talus (LAT TAL), medial talus (MED TAL), lateral tibia (LAT TIB) and medial tibia (MED TIB). No significant difference reported across four regions in the porcine ankle joint (ANOVA, $p > 0.05$). Data is expressed as mean (n=6) ± 95% confidence limits.

4.5.1.2 Cartilage on Cartilage Configuration

Cartilage pins were reciprocated against cartilage plates in phosphate buffered solution (PBS) for one hour with an applied load of 60 N. The friction measured over the test duration was comparable for lateral talus (LAT TAL), medial talus (MED TAL) and medial tibia (MED TIB), whereby an equilibrium state was reached by approximately 1000 seconds for each of these conditions. The frictional output for lateral tibia (LAT TIB) was generally higher than the other regions in the ankle joint and appeared to reach equilibrium at approximately 2500 seconds (Figure 4-23).
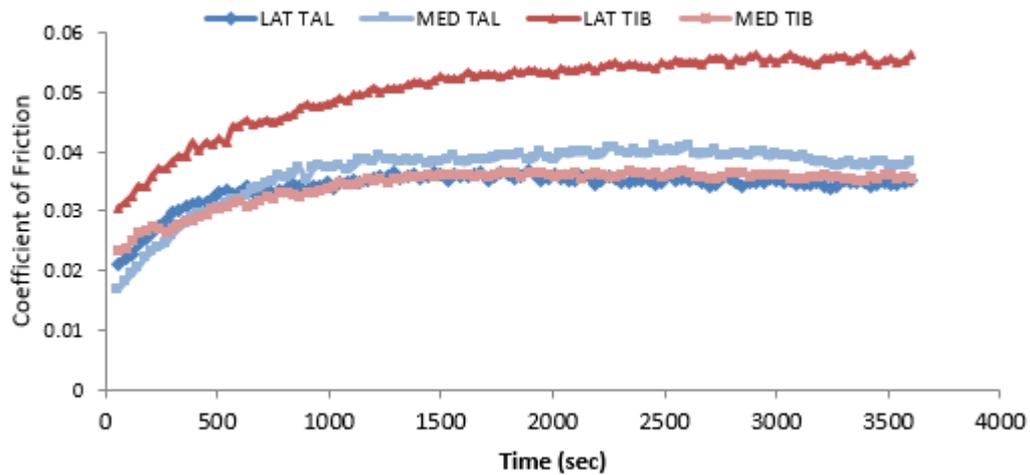
Figure 4-23: Coefficient of friction (COF) values obtained of porcine cartilage pins against cartilage plates using pin on plate rig over a period of 3600 seconds within four regions in the ankle joint of lateral talus (LAT TAL), medial talus (MED TAL), lateral tibia (LAT TIB) and medial tibia (MED TIB). Data is expressed as mean (n=6).

The mean coefficient of friction for each region was 0.03 ± 0.01, 0.04 ± 0.01, 0.06 ± 0.02 and 0.04 ± 0.01 for lateral talus (LAT TAL), medial talus (MED TAL), lateral tibia (LAT TIB) and medial tibia (MED TIB), respectively (Figure 4-24). Similarly, to the configuration of cartilage pins against metal plates, no significant differences were found between the coefficient of friction across all four regions in the ankle joint (ANOVA, $p > 0.05$). There were observed differences in friction between the regions, but these were not statistically significant. The variability for lateral tibia (LAT TIB) was higher than the other regions, as indicated by the larger confidence limits, (Figure 4-23). Overall, coefficient of friction within talar and tibial cartilage pins were comparable. Friction values within medial and lateral aspects also have not shown any significant difference.
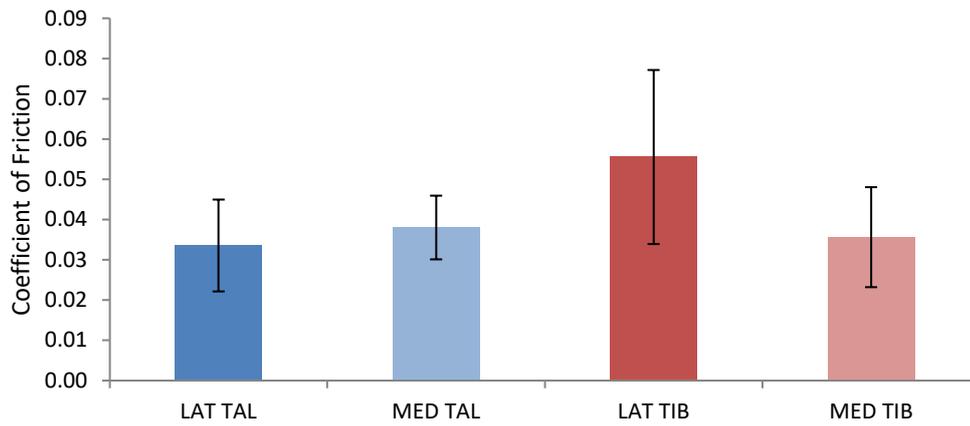
Figure 4-24: Coefficient of friction (COF) values obtained of porcine cartilage pins against cartilage plates using pin on plate rig at 3600th seconds within four regions in the ankle joint of lateral talus (LAT TAL), medial talus (MED TAL), lateral tibia (LAT TIB) and medial tibia (MED TIB). No significant difference reported across four regions in the porcine ankle joint (ANOVA, p>0.05). Data is expressed as mean (n=6) ± 95% confidence limits.

4.5.1.3 Comparison of Coefficient of Friction of Porcine Ankle Osteochondral Tissues using Cartilage Plate and Metal Plate

The coefficient of friction values for cartilage pins against metal plates were significantly higher in all regions in the ankle in comparison to cartilage pins against cartilage plates (ANOVA, p<0.05, Figure 4-25). In all four regions within cartilage against CoCr (metal), the coefficient of friction was nearly ten-fold higher compared to the friction output for cartilage against cartilage configuration.
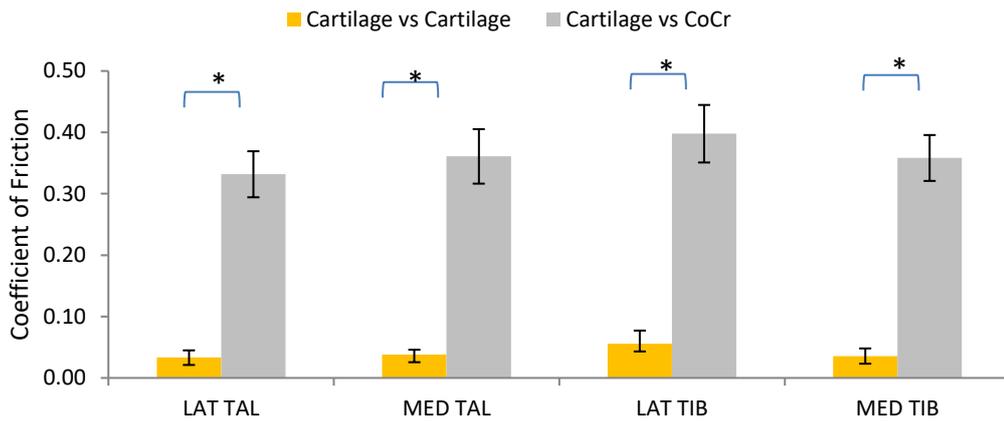
Figure 4-25: Comparison of coefficient of friction values for porcine ankle cartilage pins against cartilage and metal (CoCr) plates using pin on plate rig over a period of 3600 seconds within four regions in the ankle joint - lateral talus (LAT TAL), medial talus (MED TAL), lateral tibia (LAT TIB) and medial tibia (MED TIB). A significant difference was reported between cartilage plate and metal plate configuration across four regions in the porcine ankle joint (ANOVA, p<0.05). Data is expressed as mean (n=6) ± 95% confidence limits, * indicates a significant difference reported.

4.5.2 Determination of Surface Roughness of Ankle Cartilage

4.5.2.1 Surface Roughness of Porcine Ankle Osteochondral Pins

The surface roughness values (Ra) of porcine ankle cartilage pins (8.5 mm in diameter) were measured with contact profilometry using cartilage and metal plates in pre- and post-friction tests (Figure 4-26).

In most cases, the surface roughness of the cartilage pins was highest in those samples that had been tested against CoCr plates. In the untested samples, the highest roughness was measured in the medial tibia (MED TIB, 0.71 ± 0.22 μm), with the lowest measured in medial talus (MED TAL, 0.41 ± 0.12 μm). The surface roughness values observed in post pin against CoCr, ranging from 0.52 ± 0.14 μm (MED TIB) to 1.13 ± 0.40 μm (MED TAL), had a minimum and maximum difference of 0.07 μm and 1.15 μm, respectively. The surface roughness values observed in post pin against cartilage, ranging from 0.45 ± 0.07 μm (MED TIB) to 0.69 ± 0.20 μm (LAT TAL) had a minimum and maximum difference of 0.11 μm and 0.51 μm, respectively.
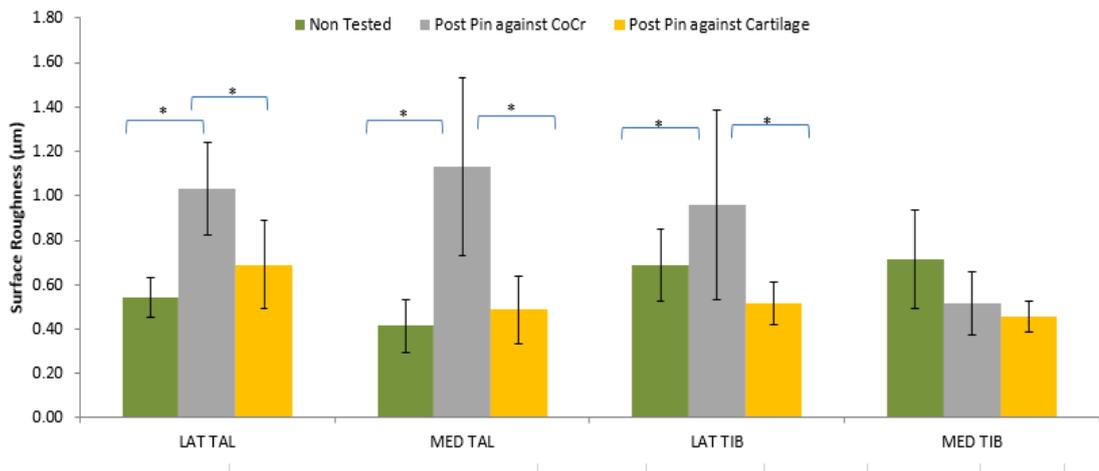
Figure 4-26: Comparison of surface roughness values (µm) of porcine ankle cartilage pins in non-tested state, post pin against metal (CoCr) and cartilage plates using contact profilometry within four regions in the ankle joint - lateral talus (LAT TAL), medial talus (MED TAL), lateral tibia (LAT TIB) and medial tibia (MED TIB). A significant difference was reported between cartilage plate and metal plate configuration across three regions in the porcine ankle joint (ANOVA, $p<0.05$), apart from MED TIB. Data is expressed as mean (n=6) ± 95% confidence limits, * indicates a significant difference reported.

Overall, no significant difference was noted between the four regions within each of the test conditions (ANOVA, $p>0.05$). The surface roughness of porcine ankle cartilage in four regions following testing against cartilage plates was not significantly different to the untested samples (ANOVA, $p>0.05$). However, the surface roughness of porcine ankle cartilage in most regions were significantly increased following testing on CoCr plates (ANOVA, $p<0.05$). After testing on the medial tibia (MED TIB) samples using both plates, the surface roughness was reduced. The porcine ankle cartilage in all regions apart from MED TIB of the joint were significantly rougher after testing against metal plates when compared to those tested against cartilage plates (ANOVA, $p<0.05$).

4.5.2.2 Surface Roughness of Cartilage Plates and Metal Plates

For the cartilage plates, as the pre-test condition (eight plates in total, n=8, non-tested) was separately studied compared to post-test (24 plates in total, n=24, tested) Thus, a relative change could not be reported. For porcine cartilage pins against the cartilage plates (Figure 4-27), no significant differences were noted

comparing 'wear and non-wear regions' within the pre-test and post-test conditions (ANOVA, p>0.05; ANOVA, p>0.05, respectively). However, there were significant differences in surface roughness between pre-tested and post-test conditions in 'wear region' (ANOVA, p=0.007) and 'non-wear region' (ANOVA, p=0.03).
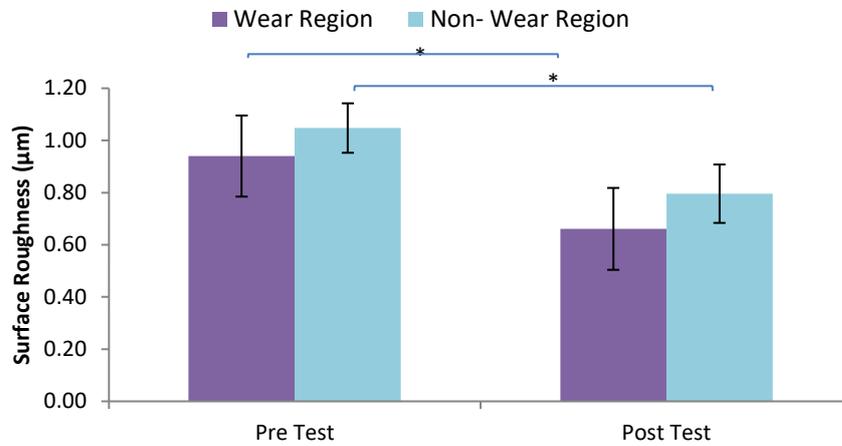
Figure 4-27: Surface roughness values (µm) of cartilage plates in two test conditions – pre-test (n=8) and post-test (n=24) on pin on plate rig. A significant difference was reported between pre-test and post-test in the 'wear region' (ANOVA, p<0.05) and in the 'non-wear region' (ANOVA, p<0.05). No significant difference was reported within each test condition comparing 'wear' and non-wear region (ANOVA, p>0.05). Data is expressed as mean ± 95% confidence limits; * indicates a significant difference reported.

For the metal plates (Figure 4-27), no significant difference was noted comparing the regions of the pre- and post-test conditions (ANOVA, p>0.05; ANOVA, p>0.05, respectively). Although a slight increase in surface roughness was observed in the 'wear region' following testing, this was not statistically significant (ANOVA, p>0.05).
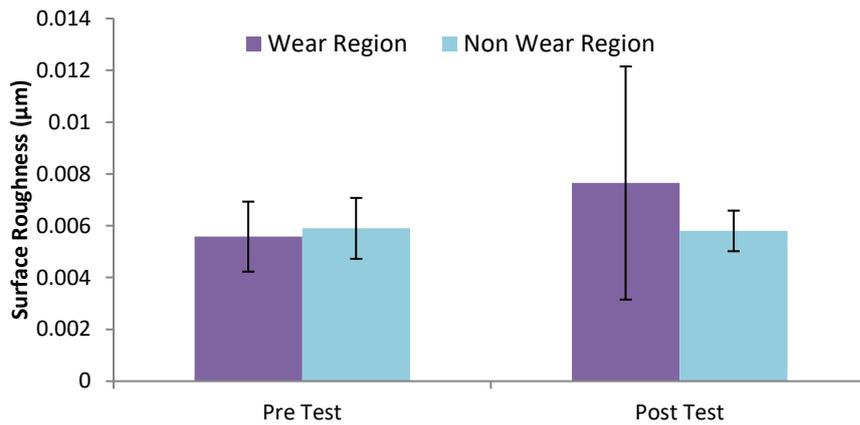
Figure 4-28: Surface roughness values (μm) of metal plates in two test conditions – pre-test and post-test on pin on plate rig. No significant difference was reported between pre-test and post-test in the 'wear region' (ANOVA, $p < 0.05$) and in the 'non-wear region' (ANOVA, $p < 0.05$) and within each test condition comparing 'wear' and 'non-wear region' (ANOVA, $p > 0.05$). Data is expressed as mean ± 95% confidence limits.

The large variation observed in post-test condition of the 'wear region' may be attributed to material transfer (Figure 4-29).

Figure 4-29: Material transfer onto metal plates in post testing condition.

4.5.2.3 Visual Observation of Cartilage Pins and Plates Pre- and Post Testing

After friction testing, the cartilage surfaces of the plates from bovine patella-femoral joint (Chapter 2, section 2.3.2.1) and pins from porcine ankle joint of lateral talus (LAT TAL), medial talus (MED TAL), lateral tibia (LAT TIB) and medial tibia (MED TIB) were generally observed. The pins across four regions in the porcine ankle joint appeared comparable between pre- and post-testing conditions. No visible damage was noted

(Figure 4-30). However, after testing (post-test) an hour on the pin on plate rig, all cartilage plates (LAT TAL, MED TIB, LAT TIB and MED TIB) had a small 'wear region' clearly marked on the surface; two examples are shown in Figure 4-30.
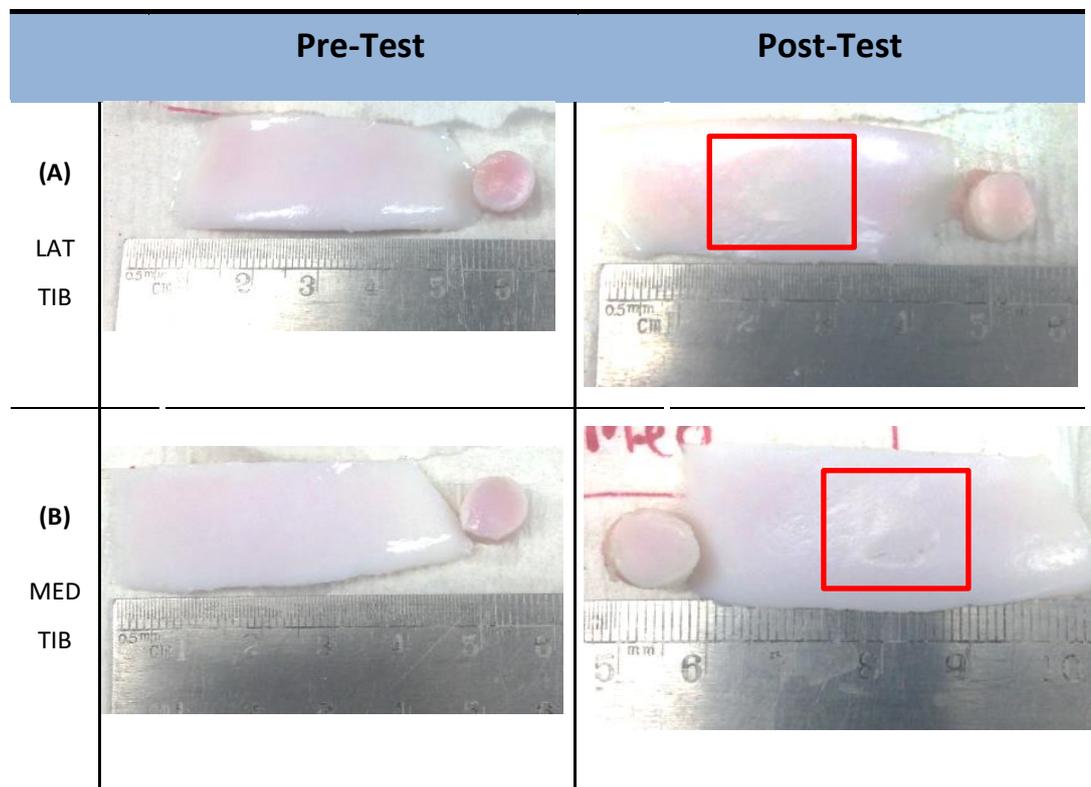
Figure 4-30: Visual observation pre- and post-friction testing of porcine pins against cartilage plates; A) lateral tibia (LAT TIB) and B) medial tibia (MED TIB). In post-test condition, red regions mark 'wear region' where contact was established between the pin and plate.

4.5.3 Determination of Contact Area and Pressure of Porcine Ankle Cartilage Pins against Plates using Pin on Plate Rig

4.5.3.1 Contact Area of Cartilage Pins against CoCr or Cartilage plates using TekScan System on Pin on Plate Rig

The contact area was determined using TekScan system (section 4.4.3.1) on pin on plate rig (section 4.4.1.1) for each configuration – cartilage on cartilage and cartilage on metal through the use of pressure sensors (section 4.4.3.1). The largest contact

area was found for the lateral tibia (LAT TIB) for both pins against cartilage plate (77.6 mm^2) and metal plate (63.2 mm^2) and the smallest was found in lateral talus (LAT TAL) for both pins against cartilage plate (55.4 mm^2) and metal plate (42.5 mm^2) (Figure 4-31). This equated to maximum differences of 22.2 mm^2 and 20.6 mm^2 for cartilage and metal plates, respectively. Overall, the contact areas of cartilage pins against a cartilage plate in all four regions of the ankle joint were comparable (ANOVA, p>0.05). However, the contact area was significantly larger when a cartilage plate was used compared to a CoCr plate for the medial talus (MED TAL) (ANOVA, p<0.05) and medial tibia (MED TIB) pins (ANOVA, p<0.05). The contact area of lateral tibia (LAT TIB) pins against a CoCr plate was significantly higher compared to lateral talus (LAT TAL) pins (ANOVA, p<0.05).
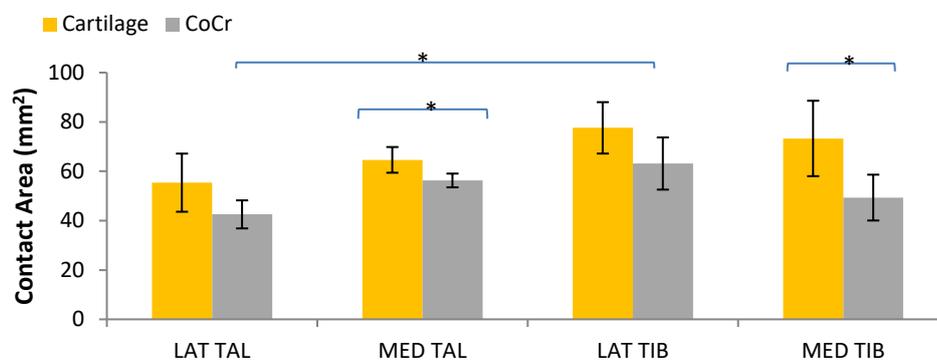
Figure 4-31: Comparison of contact area (mm^2) values for cartilage pins against cartilage plate and metal plate within four regions in the ankle joint - lateral talus (LAT TAL), medial talus (MED TAL), lateral tibia (LAT TIB) and medial tibia (MED TIB). Significant differences were reported between lateral aspects of talus and tibia in pin against metal configuration (ANOVA, p<0.05) and comparing cartilage and metal plates in medial aspects of talus (ANOVA, p<0.05) and tibia (ANOVA, p<0.05). Data is expressed as mean (n=6) ± 95% confidence limits; * indicates significant difference reported.

4.5.3.2 Contact Pressure of Porcine Ankle Cartilage Pins against Plates

The contact pressure was determined using the TekScan system (section 4.4.3.1) using the pin-on-plate test configuration (section 4.4.1.1) for each configuration through the use of pressure sensors (section 4.4.3.1). The highest contact pressure was found in lateral talus (LAT TAL) for both pins against cartilage plate (1.14 ± 0.07 MPa) and metal plate (1.05 ± 0.10 MPa) and the lowest was found in medial tibia

(MED TIB) for both pins against a cartilage plate (0.92 ± 0.11 MPa) and against a metal plate (0.83 ± 0.09 MPa) (Figure 4-32).

The contact pressure was significantly higher in medial talus (MED TAL) pins tested against a cartilage plate compared to a metal plate (ANOVA, $p<0.05$). The mean contact pressure of medial tibia (MED TIB) pins tested against cartilage plate was significantly lower than lateral talus (LAT TAL) and medial talus (MED TAL) pins (ANOVA, $p<0.05$). The mean contact pressure of lateral talus (LAT TAL) pins tested against a metal plate was significantly higher than lateral tibia (LAT TIB) and medial tibia (MED TIB) pins (ANOVA, $p<0.05$).
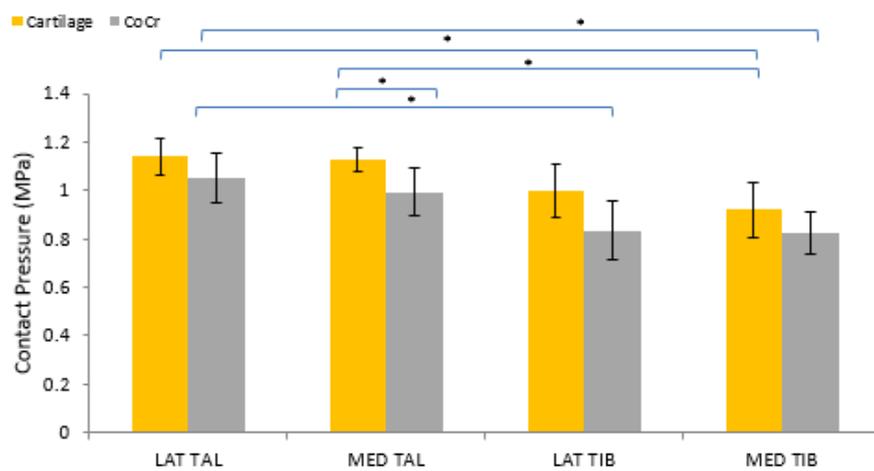
Figure 4-32: Comparison of contact pressure (MPa) values for cartilage pins against cartilage plate and metal plate within four regions in the ankle joint - lateral talus (LAT TAL), medial talus (MED TAL), lateral tibia (LAT TIB) and medial tibia (MED TIB). Data is expressed as mean (n=6) ± 95% confidence limits; * indicates significant difference reported (ANOVA, $p<0.05$).

The pressure distribution across the pin surface, when comparing cartilage and metal plates has shown slight variability (Figure 4-33). Overall, the pressure distribution in talar cartilage was almost round in shape whereas pressure distributions in the tibial pins were more varied and smaller by comparison, which reflects the contact pressure values obtained (Figure 4-32).
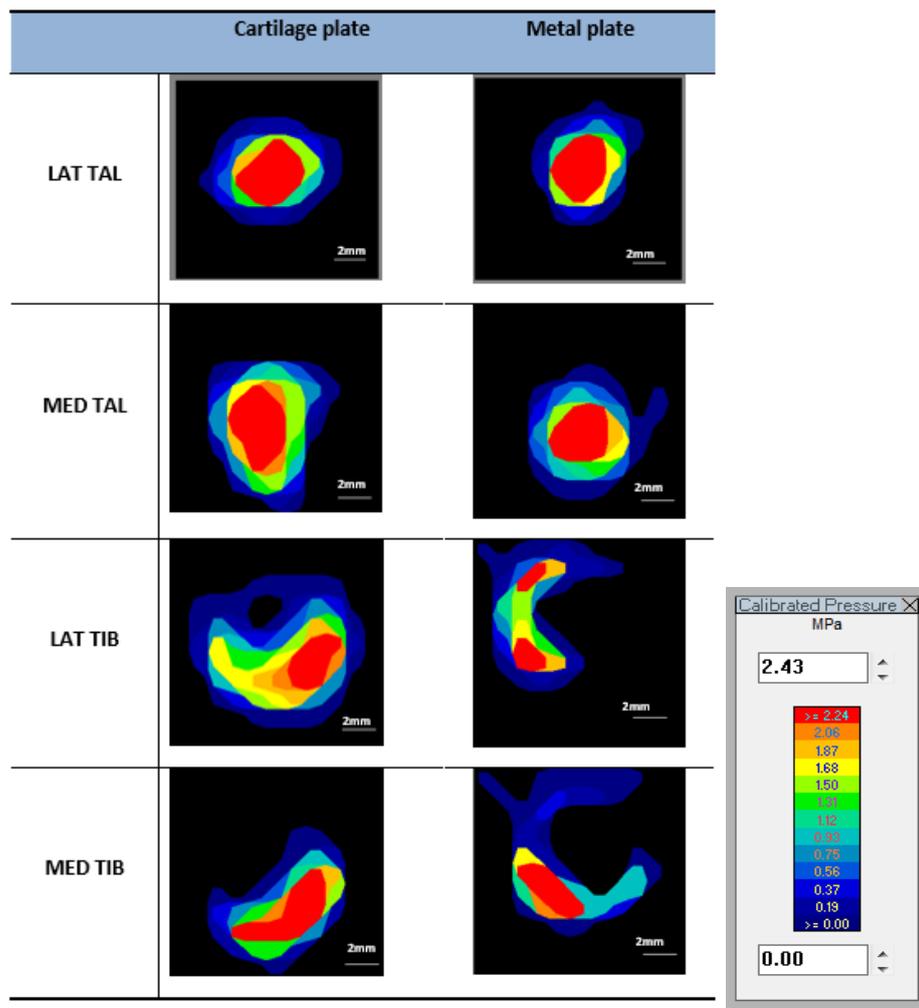
Figure 4-33: Summary of pressure distribution across four regions in the porcine ankle joint - lateral talus (LAT TAL), medial talus (MED TAL), lateral tibia (LAT TIB) and medial tibia (MED TIB) comparing cartilage and metal plates obtained from Tekscan System on pin on plate rig with an applied load of 60 N. Scale bar presented on each image. The pressure scale ranges from 0 to 2.43 MPa.

4.6 Discussion

This chapter identified the tribological performance of porcine ankle joint by determining the coefficient of friction, surface roughness and contact mechanics. These findings will help to understand how sensitive ankle cartilage is to damage. Due to biphasic nature of the cartilage, lubrication and friction play an important role in hydrating the contacting surfaces and maintaining a low friction. However, in the current study, the coefficient of friction and surface roughness were both significantly higher when cartilage was tested against metal plates compared to cartilage plates. This was in agreement with other friction studies using metal plates (Forster and Fisher, 1996; Pickard et al., 1998; Lizhang et al., 2011), suggesting the counterface material chosen to replace the natural joint will need to ensure friction and wear is kept to a minimum during joint articulation (Krishnan et al., 2004; Katta et al., 2009; Ateshian, 2009). Furthermore, contact mechanics such as contact pressure and contact area can help to evaluate how the load is distributed over the cartilage surface and determine the region in which contact is made, respectively. Contact mechanics can be useful to understand any differences in conformity between contacting surfaces. An improved conformity was suggested to reduce friction and wear with increased contact area and reduced stresses (Udofia et al., 2009). In the current study, cartilage on cartilage configurations had generally higher contact area and pressure when compared to cartilage on metal configurations. Each of these outcomes in this Chapter will be discussed in greater detail.

4.6.1 Friction Characterisation of Porcine Ankle Cartilage using Pin on Plate Friction Rig

In the present study, a reciprocating pin on plate model was used to determine the coefficient of friction in porcine ankle cartilage, which has been previously used to investigate the tribological nature of articular cartilage (Forster and Fisher, 1996; Krishnan et al., 2005; Lizhang et al., 2011). Based on all friction tests performed in the present study, a time dependant response was evident. This is in agreement with previous studies (Armstrong et al., 1984; Forster and Fisher, 1999; Jin et al., 2000;

Lizhang et al., 2011). Such response reflects the biphasic nature of the cartilage, whereby initially the load is supported by the fluid phase, and with an increase in fluid exudation, the load is gradually transferred to the solid matrix (Forster and Fisher, 1996; Krishnan et al., 2004; Katta et al., 2009; Ateshian, 2009). At equilibrium, the applied load is fully supported by the solid matrix.

Typically, in published experimental cartilage friction studies on animal tissue, the stroke length ranges between 4 mm to 8 mm, contact stress between 0.2 to 16 MPa, sliding velocity of 4 mm/s to 8 mm/s with a loading time between 1 to 24 hours (Katta et al., 2008; Lizhang et al., 2011) to replicate conditions representative of an *in-vivo* arrangement. In the present study, for both configurations in the current study, a stroke length of 4 mm, contact stress of 1 MPa, sliding velocity of 4 mm/s were used whereby the test lasted for 1 hour. Due to limited studies on the porcine tissue, such conditions were chosen to closely represent physiological conditions reported in the human ankle (Conti and Wong, 2002). Furthermore, a short stroke length of 4 mm and a low sliding speed of 4 mm/s were suggested to result in significantly lower coefficient of friction compared to a faster velocity of 8 mm/s over a longer stroke length of 8 mm under low contact stress levels over one hour testing (Lizhang et al., 2011). A low sliding speed of 4 mm/s promotes the configurations to remain within mixed or boundary lubrication modes during sliding (Forster and Fisher, 1999), which was assumed to exist within the current study. At a short stroke length of 4 mm, increasing contact stress levels also increases coefficient of friction as the tissue is not able to fully rehydrate itself and cannot maintain a high fluid load support at this sliding distance (Katta et al., 2009).

The coefficient of friction reported in the current study for cartilage on cartilage configuration on porcine ankle cartilage (0.03 ± 0.01 to 0.06 ± 0.02) was within the range reported in other studies for a similar configuration (0.015 to 0.06) (Northwood and Fisher, 2007; Caligaris and Ateshian, 2008; Katta et al., 2009). For cartilage on cartilage configuration, a low coefficient was observed as the biphasic nature of the cartilage has the ability to maintain such low levels with a high fluid-load support (Krishnan et al., 2004; Pawaskar et al., 2011). At high fluid load, the

frictional interaction between the solid phases of interacting cartilage surfaces is kept at a minimum, which is essential to obtain low levels of friction, as well as damage in the joint (Krishnan et al., 2004; Katta et al., 2009; Ateshian, 2009).

In the control study (cartilage on metal configuration), coefficient of friction observed (0.33 ± 0.04 to 0.40 ± 0.05) was within the range reported in previous studies for the cartilage on metal configurations (0.25 to 0.48) (Forster and Fisher, 1996; Pickard et al., 1998; Lizhang et al., 2011). Generally, for articular cartilage, the coefficient of friction has been reported to be in the range of 0.002 to 0.3 depending on the configuration (Forster and Fisher, 1996). Such large range in friction was evident in the current study, whereby friction measured in cartilage on cartilage configuration varied significantly compared to the cartilage on metal configuration. Furthermore, in the control study, a higher level of increase in friction was observed at the initial phase compared to that reported in the cartilage on cartilage configuration. Such response observed in the control study could indicate a higher level of fluid pressurisation loss with a lower level of fluid rehydration compared to cartilage plate articulation.

4.6.2 Surface Roughness Characterisation of Porcine Ankle Cartilage using Contact Profilometry

There was no significant change in the mean surface roughness of the cartilage pins when tested against cartilage plates, whereas using a metal plate showed a significant increase in roughness in most regions in the porcine ankle joint. Previous studies were in agreement with the current study, as no significance was found between pre and post-test for cartilage on cartilage configuration (Russell, 2010; Taylor, 2013; Oungoulian et al., 2015). In this configuration, mixed lubrication was proposed to act between cartilage surfaces (Russell, 2010); therefore it may be expected that pins undergo less damage as fewer asperities are in contact. The surface roughness of the pins that had been tested against the metal counterface were between 0.52 to 1.13 µm, which was slightly lower as reported by Forster and Fisher (1999) using stainless steel plates on bovine knee cartilage (1.6 ± 0.9 µm).

Another study by Northwood and Fisher (2007) showed a significant increase in surface roughness by 70 % between non-tested samples and pins tested against stainless steel using bovine knee cartilage. This is comparable to the current study, in which an average increase of 63 % was noted across the four regions in the porcine ankle joint using metal plate. This may be due poor conformity between the cartilage and metallic counterface, which is considered as impermeable, hard, non-deformable surface (Bronzino and Peterson, 2015). Such interaction does not mimic a natural joint interaction and therefore changes to biochemical environment (i.e. lubrication mechanisms) between the interacting surfaces may be expected which in turn could result in changes in surface texture i.e. higher roughness.

It was assumed that testing cartilage surfaces in the pin on plate set up may change the surface texture and potentially influence the surface roughness of the material. In the present study the surface roughness values of cartilage plates in pre-test condition were significantly higher compared to post-test condition, which has highlighted potential questions regarding the condition of silicon moulds used in pre- and post-conditions. Such finding may be associated with a possible change in viscosity of silicon rubber solution due to varying temperatures as pre- and post-testing were completed on separate instances on different set of pins with new set of cartridges. Higher temperatures were suggested to decrease the working life and cure time of the silicon rubber (Microset Products Ltd, Leicestershire). Furthermore, a standard error of +/- 15% between batches was reported by the manufacturers. A recent study by Goodall et al. (2015) compared seven types of silicon-based media and had suggested that changes in the impression media used can significantly affect the ability to accurately and precisely replicate surfaces. Generally, a low viscosity media replicates surfaces more accurately compared to a high viscosity media. The current study used Microset 101RF, which was suggested to be a high viscosity media by Goodall et al. (2015). When compared to other silicon based medium, Microset 101RF resulted in the lowest accuracy and precision when replicating a rough surface (Goodall et al., 2015). As the findings by Goodall et al. (2015) were published after tests were conducted in the current study, an opportunity was not available to

implement any changes. Therefore, a validation study is required to study the effectiveness of using Microset 101RF to create cartilage impressions.

The surface roughness of CoCr metal plate appeared to increase in the 'wear' region but there was a large variation in measurement, which may be attributed to material being transferred rather randomly during testing as reported previously (section 4.5.2.2). This can occasionally occur, whereby cartilage remains become deposited onto the opposing metal surface during sliding (Owellen, 1997).

All cartilage pins and cartilage plates were visually analysed for any damage pre- and post-testing. After testing, all cartilage plates presented with a small indentation mark on which the pin had been sliding on during one-hour testing period. The surface roughness pre- and post-testing on the cartilage plates had resulted in significant differences in the 'wear' region and the 'non-wear' region, although an overall increase in roughness was expected. Generally, a change in colour was evident in the ankle osteochondral pins from purple/dark pink prior testing to a lighter shade after testing; however, this may be associated with the decrease in fluid pressurisation as water content has exuded out of cartilage over the testing period.

4.6.3 Contact Area and Pressure Characterisation of Porcine Ankle Cartilage using TekScan system on Pin on Plate Friction Rig

Contact areas found in cartilage on cartilage configurations were significantly higher compared to cartilage on metal configuration in medial aspects of talus and tibia. This behaviour may be attributed to the surface curvature and characteristics of pins and plates studied under loading. The tibial pins were extracted from a concave joint surface, and the talar pins were extracted from a concave joint surface. Hence, a concave and convex shaped over one another in the natural joint results in a conforming interaction between the surfaces during motion making the joint very stable.

Bearing geometry in the joint is an important aspect to ensure friction and wear is kept to a minimum. Differences in conformity between contacting surfaces in both

cartilage on cartilage and cartilage on metal configurations, may have resulted in notable differences in contact area in the present study. A non-conforming contact (i.e. cartilage on metal) resulted in smaller contact area in the present study possibly due to fewer contact points (Johnson, 1987), as the metal plate is entirely flat, incompressible and impermeable compared to cartilage plate that was curved, compressible and permeable. A study by Udofia et al. (2009) compared the conformity in the bovine knee joint using 'conforming' and 'flat' tibial plates in a pendulum friction simulator and suggested that an improved conformity between two interacting surfaces can reduce friction and wear as the contact area is increased and stresses are reduced.

Contact pressures were significantly lower for tibial aspects compared to lateral talus as observed in cartilage on metal configurations. Such differences may be attributed to changes in surface curvatures of pins, whereby tibial pins had an increased curvature compared to talar pins (Figure 4-34). An increased surface curvature of pin has less contact with the contacting surface compared to a flat pin suggesting the load is applied onto smaller area resulting in increased pressure. In joint contact studies, a lower contact pressure of 5 to 12 MPa was reported in the natural ankle joint (Kimizuka et al., 1980; Teeple et al., 2008) (cartilage on cartilage contact) compared to polyethylene on metal, 22 MPa (Mak et al., 2011), ceramic on ceramic, 40 to 250 MPa (Al-Hajjar et al., 2011), metal on metal, 200 MPa (Wang et al., 2014) and ceramic on metal, 40 to 112 MPa, (Meng et al., 2013). Therefore, as cartilage on cartilage configuration has an improved interaction between the contacting surfaces compared to other interactions (Mak et al., 2011; Al-Hajjar et al., 2011; Meng et al., 2013; Wang et al., 2014), this may have resulted in lower pressures (Kimizuka et al., 1980; Teeple et al., 2008).
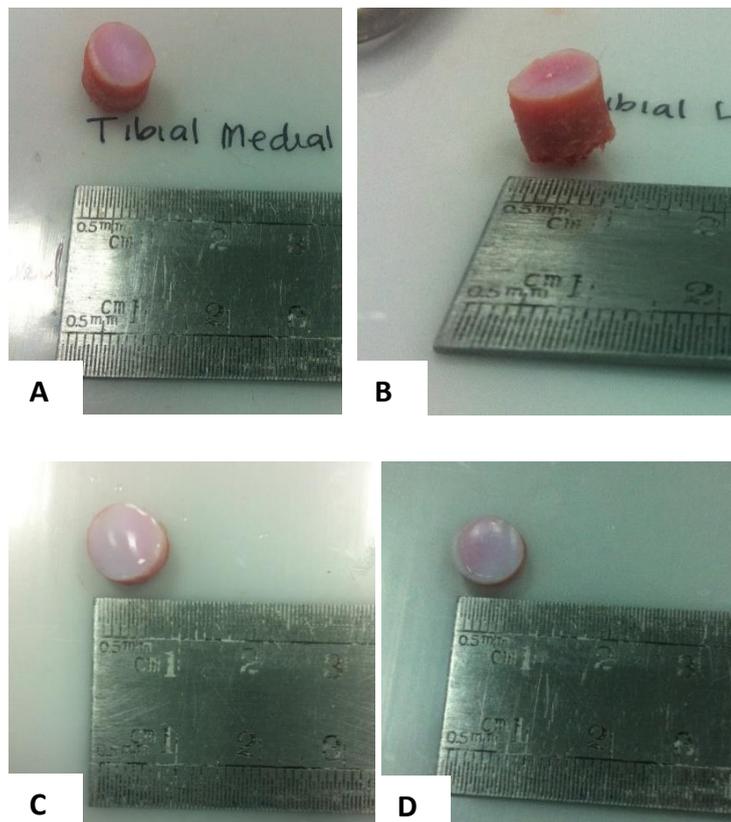
Figure 4-34: An example of surface curvatures of osteochondral pins; A) medial tibia (MED TIB); B) lateral tibia (LAT TIB); C) medial talus (MED TAL); D) lateral talus (LAT TAL).

Although, contact pressures on smaller surfaces (i.e. pins) were lower compared to previously reported studies on the whole cadaveric ankle joint surfaces (Kimizuka et al., 1980; Calhoun et al., 1994), differences in geometry could be one of the reasons for such relationship in contact mechanics. A larger surface area such as the whole joint would have a larger area of contact compared to a flat shaped cylindrical pin. An increased load application of up to 1500 N by previous studies on the whole joint compared to 60 N on the pin in the present study may not provide a direct comparison and fails to suggest whether load applied on a smaller area results in increased pressure due to variables such geometry, applied load and surface/contact area.

To ensure optimal accuracy of measuring contact mechanics using the Tekscan system, the surfaces will ideally need to be flat to avoid risk of uneven load saturation in sensels (Padelecki et al., 2014; Geesli et al., 2015). However, as the natural ankle joint is rather curved, possible inconsistencies will need to be accommodated to

ensure the effect on sensor output is minimised. Therefore, a possible study examining the effect of geometry on the accuracy of contact mechanics using Tekscan system could be useful.

4.7 Conclusion

- Regardless of the type of counterface used (i.e. cartilage or metal plates), the coefficient of friction was comparable between talar and tibial cartilages in the porcine tissue (ANOVA, $p > 0.05$, $p > 0.05$, respectively).

- No change in surface roughness was reported between pre- and post-test conditions for cartilage on cartilage and cartilage on metal configurations (ANOVA, $p > 0.05$, $p > 0.05$, respectively).

- The coefficient of friction and surface roughness of cartilage pins were significantly higher when tested against a metal plate than a cartilage plate (ANOVA, $p > 0.05$, $p > 0.05$, respectively).

- The contact area of cartilage pins against cartilage plates was generally higher compared to metal plates, whereby in two regions (MED TAL and MED TIB), this was significant (ANOVA, $p < 0.05$, $p < 0.05$, respectively).

- The contact pressure of cartilage pins against cartilage plates were generally higher than metal plates (ANOVA, $p > 0.05$).

Chapter 5: Biological Characterisation of Porcine Ankle Cartilage

5.1 Introduction

Biological characterisation of porcine ankle cartilage will enable identification of its constituent components and structure that are essential for load bearing and also for maintaining low friction of the tissue. The key components of articular cartilage that help to absorb and distribute forces in the joint are collagen, proteoglycans, interstitial water, chondrocytes and synovial fluid which aids with lubrication in the joint.

The distribution of collagen fibrils and proteoglycans are comprised of a core protein covalently linked to one or more glycosaminoglycan chains (Chapter 1, section 1.3.1), help to provide optimal mechanical properties for normal joint function. The collagen fibrils, which are tightly packed and tangentially aligned at the superficial surface, are responsible for the tensile strength of the cartilage and therefore allow cartilage to resist large shear stresses experienced in the deep zone (Buckwalter and Mankin, 1998; Berrien, 1999). The compressive strength and ability to resist deformation and distribute loads has been linked to the proteoglycan (PG) content of the cartilage, as PGs are able to expand in solution and their swelling properties create an internal pressure providing great compressive strength (Berrien, 1999). Therefore, cartilage structure and stiffness is maintained by the collagen network and PGs.

Any disruption of collagen fibres has been reported to lead to loss of PGs which accelerates the process of cartilage damage (Poole et al., 2002; Gottardi et al., 2016a). The early changes of an osteoarthritic cartilage in the human knee joint were characterised as increased water content and decreased PG content, which in turn increased tissue permeability (Callaghan, 2003). This further led to poor fluid load support in the knee cartilage due to a diminished fluid pressurisation mechanism (Callaghan, 2003). If the fluid flowed easily out of the cartilage, the collagen-proteoglycan solid matrix would bear the full contact stress. Hence, under such stress

levels, the solid matrix may potentially become damaged. A diminished collagen-proteoglycan solid matrix is considered to be one of the contributing factors which leading to osteoarthritis (OA) (Callaghan, 2003), as loss of PGs are early signs of OA in both hip and knee joints (Gottardi et al., 2016a). In end stage osteoarthritis, gradually increased disruption and loss of collagen fibres is counterbalanced with collagen meshwork remodelling in the hip and knee joints (Gottardi et al., 2016a). However, Aurich et al. (2005) reported an increase in collagen synthesis in ankle lesions, which was not apparent in the knee or hip joints. Hence, the repair and recovery mechanisms within injured ankle, hip and knee joints seem to vary. Such comparison is out of scope in the current study and requires further investigation to understand how these joints vary in the recovery/healing process of the diseased state.

Ageing of cartilage has been related to the development of OA lesions, that have presented changes in biomechanical properties compared to a healthy cartilage (Guerne et al., 1995; Horton et al., 1998; Sandell et al., 2001; Aurich et al., 2002; Long et al., 2008; Loeser, 2009). Gottardi et al. (2016) reported that early signs of ageing in the cartilage were associated with (OA, firstly leading to) the loss of PGs, followed by changes in the supporting collagen meshwork. In the knee and the hip joint, age is related to degeneration and development of OA lesions, whereas in the ankle joint such changes are suggested to be less pronounced (Aurich et al., 2002; Verzijl et al., 2002; Poole et al., 2002; Aurich et al., 2005). Over time in the knee and hip joint an increase in the stiffness of the collagen network has been linked to failure to resist damage (Verzijl et al., 2002), whereas in the ankle cartilage, patients age ranging from 16 up to 75 years have not shown major changes in synthesis or denaturation of collagen or proteoglycans over time (Aurich et al., 2002). However, within the ankle, localised increased fluid flow and pressure in the subchondral bone may lead to osteochondral defects (VanDijk et al., 2010). In normal adult cartilage, chondrocytes that are responsible for development, maintenance and repair of the extracellular matrix (ECM), synthesise matrix components such as glycosaminoglycan (GAGs) (Chapter 1, section 1.3.1). In older adults, an increased cell death (Horton et

al., 1998; Jallali et al., 2005), cytokine production (Aurich et al., 2002; Long et al., 2008) and decreased growth factor production (Guerne et al., 1995) were reported. Such changes to the function of the chondrocytes have been related to the age of the matrix, which in turn contributes to a loss of homeostasis due to changes in biomechanical properties. Previous studies have reported that these characteristics possibly lead to the development of osteoarthritis (Sandell et al., 2001; Loeser, 2009). However, Aurich et al. (2005) stated that OA in the ankle was not age-related rather its postulated that sudden injury or trauma to the cartilage changes the mechanical loading of chondrocytes, caused by the damage to, and loss of matrix molecules and stimulates cartilage degeneration in the ankle joint.

This chapter will focus on biochemical characterisation of the porcine ankle cartilage and its biochemical composition (i.e. chondrocytes, PGs, collagen and water). As the ankle joint is less sensitive to damage and known as a stable joint, comparison of biological properties with other joints such as porcine hip (Taylor, 2012) and porcine knee (Fermor, 2013) can help to understand how such properties in the ankle could aid in the protection of the joint.

5.2 Aims & Objectives

5.2.1 Aims

The overall aim of this part of the study was to identify the biological constituents and their distribution in the porcine ankle cartilage using histological methods and quantitative biochemical assays.

5.2.2 Objectives

- To study the general structure and chondrocyte distribution of talar and tibial cartilage using microscopic images of H&E stained osteochondral tissues

- To study the presence of glycosaminoglycan (GAG) within the lateral talar and lateral tibial cartilage using microscopic images of Alcian Blue stained osteochondral tissues

- To study the presence of collagen and elastin within the lateral talar and lateral tibial cartilage using microscopic images of Sirius Red/Millers' Elastin stained osteochondral tissues

- To determine the chondrocyte cell count within lateral talar and lateral tibial cartilage using H&E stained images of osteochondral tissues

- To determine the thicknesses of the lateral talar and lateral tibial cartilages using H&E and Alcian blue stained images of osteochondral tissues and to compare the staining techniques.

- To determine water content, glycosaminoglycan (GAG) content and hydroxyproline content of porcine ankle cartilage using quantitative biochemical assays.

5.3 Materials

For the histological studies and quantitative assays performed in this Chapter, osteochondral pins of 8.5 mm diameter were extracted from the lateral aspects of the talar and tibial joint surfaces as outlined in Chapter 2, section 2.3.4.1 (n=6 for each aspect, unless otherwise stated).

5.4 Methods

5.4.1 Histological Procedures

5.4.1.1 Preparation of Solutions for Histological Analysis of Porcine Osteochondral Tissues

In the current study for histological analysis of porcine ankle osteochondral tissue, three staining methods were used to characterise the general structure and biological constituents of the ankle cartilage. H&E was used to study the general architecture of cartilage tissue, Alcian Blue was used to stain glycosaminoglycans (GAGs) within cartilage tissue samples; Sirius Red was used to stain for collagen fibres and Miller's stains for elastin fibres.

<u>Histology: Preparation of Solutions for Haematoxylin and Eosin (H&E) Staining</u>

Haematoxylin (Mayer's, Atomic Scientific) and Eosin (VWR International) were used to study the cartilage architecture of the porcine tissue. The pre-prepared Haematoxylin and Eosin solutions were kept at room temperature and poured into separate pots for staining. These solutions were frequently filtered to remove any debris from the glass slides. Scott's tap water (Atomic Scientific) was prepared on the day of staining by adding 100 ml of Scott's tap water to 900 ml of distilled water and used immediately.

<u>Histology: Preparation of Solutions for Alcian Blue Staining</u>

The Alcian Blue staining method was used to visualise glycosaminoglycan (GAG) content within cartilage tissue samples.

The pre-prepared Alcian Blue solution (Atomic Scientific) was stored at room temperature. For the Alcian Blue staining method, other solutions such as aqueous periodic acid solution (0.1 %, v/v) (Sigma), and Schiff's reagent were also purchased as pre-made solutions and stored at 4°C. Haematoxylin (pre-prepared, Gills No 3, Sigma, GH5316) was stored at room temperature.

Histology: Preparation of Solutions for Sirius Red/Millers Elastin Staining

The Sirius Red staining method was used to stain for collagen fibres and Miller's elastin stains for elastin fibres. For the Sirius Red/Miller's Elastin staining method, several solutions were required. All solutions were made in clean autoclaved bottles and stored in appropriately sized bottles for the volume of solution.

Sirius Red/Miller's Elastin Solution

To make Sirius Red (0.1 %, w/v), 0.1 g of Sirius Red (VWR International) was dissolved in 100 ml of aqueous saturated picric acid solution (Sigma Aldrich, pre-made) using a magnetic stirrer. The solution was stored in room temperature and used within six months. The Miller's elastin stain (Raymond A Lamb) was a pre-made solution.

Potassium Permangenante (5% w/v)

A weight of 15 g of Potassium Permanganate (Thermo Fisher Scientific Ltd) was added into 300 ml of distilled water. The solution was placed on magnetic stirrer until fully dissolved. The solution was stored at room temperature and used within six months.

Oxalic Acid (1% w/v)

A weight of 1 g of Oxalic Acid (VWR International) was added to 100 ml of distilled water and the solution was stirred using a magnetic stirrer until dissolved and used immediately.

Weigerts Haematoxylin

Equal volumes of pre-made solution A (RRSP72-D) and pre-made solution B (RRSP73-D) were mixed to make up Weigerts Haematoxylin. The mix was stored at 4˚C in the fridge and used within a month.

Acid Alcohol (1%, v/v)

A volume of 5 ml of concentrated hydrochloric acid (Fisher Scientific, pre-made) was added to 495 ml of 70 % (v/v) ethanol. A volume of 70 ml of ethanol (99.6 %, Thermo

Fisher Scientific Ltd.) was diluted with 30 ml of distilled water to obtain 70 % (v/v) of ethanol.

5.4.1.2 Basic Histological Techniques

Previously in this study (Chapter 3), mechanical testing of all four regions in the porcine ankle joint (lateral talus, LAT TAL; medial talus, MED TAL; lateral tibia, LAT TIB; medial tibia, MED TIB) was carried out and based on these results, only two samples were taken forward for histological evaluation. Mechanical testing revealed that the lateral talus (LAT TAL) was significantly thicker compared to the lateral tibia (LAT TIB) (1.06 mm vs 0.81 mm, respectively, ANOVA, $p < 0.05$), and also deformed more compared to lateral tibia (LAT TIB), which deformed the least out of all four regions (12.23 % vs 8.79 %, respectively) (Chapter 3, section **3.5.5**). Hence, the two porcine osteochondral regions taken forward for histological evaluations were extracted from the lateral aspects of the talus (LAT TAL) and tibia (LAT TIB) (Chapter 2, section **2.3.4.1**), which demonstrated the greatest differences in mechanical characteristics and therefore, differences in their structures and/or biological constituents such as GAGs, chondrocytes and collagen distribution were investigated.

Tissue Fixation and Decalcification

Osteochondral pins were individually fixed by placing each pin in 15 ml of 10 % (v/v) neutral buffered formalin (NBF) for 48 hours at room temperature under static conditions. To decalcify the tissues, each pin was immersed in 12.5 % (w/v) ethylenediaminetetraacetic acid (EDTA, VWR International) for two weeks (or by checking if the bone was soft enough for sectioning by gently cutting through the bone using a scalpel) at 45˚C with agitation. The EDTA solution was replaced with fresh solution every two to three days.

Paraffin Wax Embedding

Osteochondral pins were sectioned longitudinally into two halves from the cartilage through to the bone (Figure 5-1), with a scalpel blade. Each of the halves was placed

cut side down onto a plastic cassette (Histocette®) such that sections were taken at this surface.
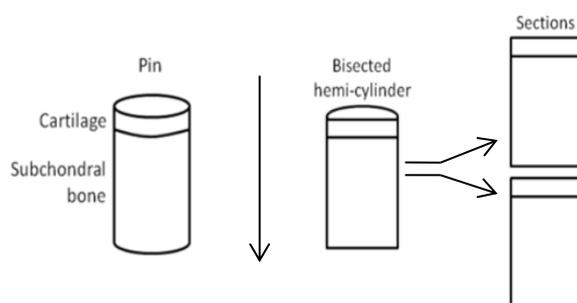
Figure 5-1: Orientation of osteochondral pins prior to tissue processing. Each pin was cut into two halves and each half was placed face down into a histology cassette (Fermor, 2013).

Tissue Processing

An automated tissue processor (Leica Microsystems, TP1020) was set on programme 9, which took a total duration of 22 hours for the cycle to complete (Table 5-1). The processor involved sequential immersion of cartilage samples within cassettes into various solutions (Table 5-1).

Table 5-1: Summary of steps taken to process the porcine osteochondral tissues using Tissue Processor

Steps	Solution	Time
Immersion 1	70 % (v/v) ethanol	1 hour
Immersion 2	90 % (v/v) ethanol	1 hour
Immersion 3	100 % (v/v) ethanol	2 hours 20 mins
Immersion 4	100 % (v/v) ethanol	3 hours 20 mins
Immersion 5	100 % (v/v) ethanol	4 hours 20 mins
Immersion 6	Xylene	1 hour
Immersion 7	Xylene	1 hour 30 mins
Immersion 8	Xylene	2 hours
Immersion 9	Molten Wax	1 hour 30 mins
Immersion 10	Molten Wax	2 hours

<u>Paraffin Wax Embedding</u>

The plastic cassettes containing the tissue samples were removed from the automated tissue processor. Each tissue section was placed on its flat-cut surface, facing down in the mould and then covered in molten wax. The moulds were left overnight to set at room temperature. The following day, any excess wax was trimmed using a spatula. The wax blocks were then removed from the moulds and the tissues were ready to be sectioned.

<u>Sectioning of Osteochondral Tissues</u>

A microtome was used to section wax embedded osteochondral tissues to a thickness of 6 μm. The sections were taken such that a cross section showing both the cartilage and the subchondral bone of the tissue was included in each section. Using forceps and a brush, sections were carefully transferred into a water bath set at 40°C, allowing the sections to float flat on the surface of the water. These sections were then transferred onto Superfrost Plus glass slides (VWR International) and dried using a hotplate set at a temperature between 55 to 60°C for 3 hrs.

<u>Dewaxing and rehydration of paraffin embedded tissues</u>

The initial steps prior to staining of sections included dewaxing and rehydration of the tissues. Slides were placed within a slide holder and immersed into two successive pots of xylene for 10 min each, to remove wax from the sections, followed by three successive immersions into 100 % (v/v) ethanol for 3, 2 and 2 min respectively. Slides were immersed into 70 % (v/v) ethanol for 2 min and then placed in a pot with running tap water for a further 3 min.

<u>Tissue Dehydration and Mounting</u>

The final steps, after staining of the sections was complete, included the dehydration and mounting of the tissue such that the slides were ready to be visualised using a light microscope. Slides were immersed in 70% (v/v) ethanol for 5 sec followed by immersion into three pots of 100 % (v/v) ethanol for 1, 2 and 3 min and two successive immersions into pots of xylene for 10 min each. Inside a fume hood, the

slides were individually mounted using DPX mountant (Bios Europe Ltd) and a coverslip (Bios Europe Ltd). The slides were then left to dry for a minimum of 4 hrs at room temperature, after which slides were ready to be analysed using a light microscope.

5.4.1.3 Histological Staining Methods

<u>Haematoxylin and Eosin Staining</u>

Haematoxylin and Eosin (H&E) staining was used to study the general architecture of cartilage tissue. Slides were dewaxed and rehydrated (as described in section 5.4.1.2) followed by immersion into Mayer's haematoxylin (Thermo Fisher Scientific Ltd) for 1 min. Slides were then rinsed under running tap water until the water ran clear, followed by immersion into eosin for 3 min. As part of the final step, slides were then dehydrated with ethanol and xylene and individually mounted using DPX mountant and a coverslip (section 5.4.1.2).

<u>Alcian Blue Staining</u>

Alcian Blue staining was used to stain glycosaminoglycans (GAGs) within cartilage tissue samples using Alcian Blue solution and a counter stain of periodic acid and Schiff's reagent (PAS). Other tissue structures such as the nuclei were stained using haematoxylin. After slides were dewaxed and rehydrated (as described in section 5.4.1.2) slides were immersed in 1 % (v/v) Alcian Blue solution for 15 min at room temperature. Slides were then immersed under running tap water until the water ran clear, followed by distilled water. Following this, the slides were immersed into periodic acid for 5 min followed by three washes in distilled water, before submerging slides into Schiff's reagent for 15 min at room temperature. Slides were then rinsed in tap water for 5 min followed by immersion into haematoxylin for 90 sec. Slides were then rinsed again in running tap water until the water ran clear, before being dehydrated in ethanol (100 %) and xylene and mounted using DPX (section 5.4.1.2).

<u>Sirius Red/ Miller's Elastin Staining</u>

Sirius Red is used to stain for collagen fibres and Miller's stains for elastic fibres. Once slides were dewaxed and rehydrated (section 5.4.1.2), slides were immersed into 5 % (v/v) potassium permanganate for 5 min before being rinsed in distilled water. Slides were then immersed into 1 % (w/v) oxalic acid for 2 min, rinsed in distilled water for 1 min and for a further 4 min. Slides were immersed into 70 % (v/v) ethanol for 1 min and 95 % (v/v) ethanol for 1 min prior to staining in Miller's solution for 1 hr. Slides were rinsed using 95 % (v/v) ethanol, then immersed in 70 % (v/v) ethanol for 1 min before rinsing in running tap water for 2 min. Slides were stained in Weigerts Haematoxylin for 10 min before being rinsed in running tap water for 1 min and rinsed again using distilled water for further 30 sec. Slides were immersed in Sirius Red for 1 hr, rinsed in distilled water and blotted dry before being dehydrated in ethanol (100 %) and xylene and mounted using DPX (section 5.4.1.2).

5.4.1.4 Cell Count using H&E Stained Osteochondral Tissues

Chondrocyte cell counts were performed according to Fermor (2013). Cell counts were compared between the lateral talus (LAT TAL, n=6) and lateral tibia (LAT TIB, n=6) of the porcine cartilage and 95 % confidence limits (CL) were calculated. Digital images of osteochondral tissues stained with H&E (section 5.4.1.1) were captured using light microscopic analysis and further analysed using ImageJ (version 1.50e, Wayne Rasband, National Institutes of Health, USA). For each sample, two images of different magnifications were analysed for a detailed interpretation of the number of cells in the cartilage layers, and the image showing all cartilage layers was used to calculate the cell count within each zone. For each image of osteochondral tissue, within each of the cartilage zones - superficial, mid and deep, an average cell count from two regions of 50,000 μm^2 (i.e. 500 x 100 μm or 250 x 200 μm) was calculated (Figure 5-2). Once a region of interest was selected, in ImageJ an automated output displayed the number of cells within the chosen area. Prior to calculating the average cell count within each cartilage zone of each image, the automated computed cell count was validated with a manual count three times to ensure the cell counts were

comparable. After calculating the cartilage thickness in each image (section 5.4.1.5), 15 %, 35 % and 50 % of the cartilage thickness were chosen to represent superficial, mid and deep zones, respectively.
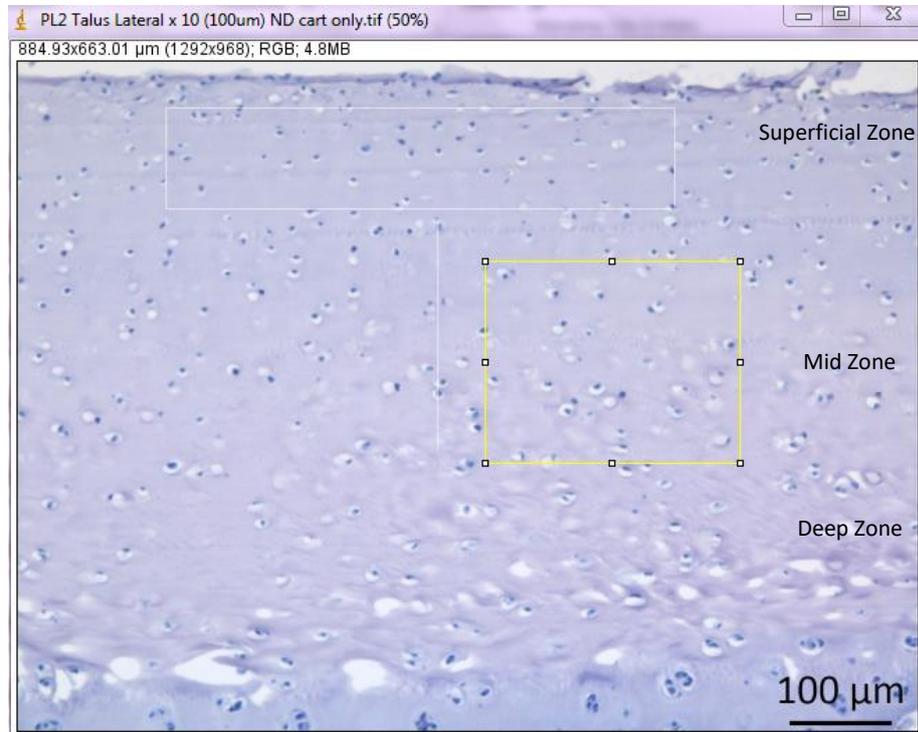
Figure 5-2: An example image showing the total chondrocyte cell count in the superficial zone, mid and deep zone in the lateral talus (LAT TAL) with a scale bar of 100 µm. The yellow box highlighted represents a region of 200 by 250 µm. All regions highlighted have an area of 50,000 µm^2.

The total cell count in lateral talar and tibial cartilage in an area of 500,000 µm^2 was determined on each image (n=6). For each image, the colour threshold (black/white) was modified such that cells were displayed in black for improved visibility (Figure 5-3). As described previously, an automated computed output determined cell count in the given area.
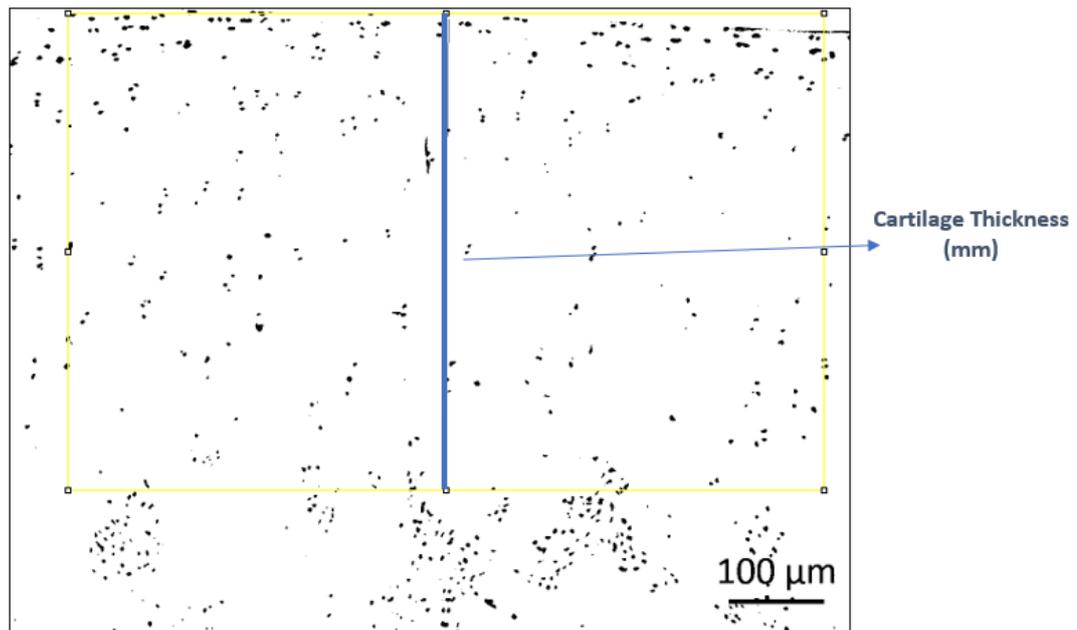
Figure 5-3: An example image showing the total chondrocyte cell count in the ankle cartilage with a scale bar of 100 μm. The yellow box highlighted represents 800 x 625 μm (area of 500,000 μm^2). The black line represents the cartilage thickness for this sample. To ensure the total number of cells were only considered within the cartilage layers (i.e. superficial, mid and deep zones) rather than any deeper layers (i.e. subchondral bone), the thickness of the sample was highlighted.

5.4.1.5 Cartilage Thickness Measurements using Alcian Blue and H&E Stained Osteochondral Tissues

Cartilage thickness measurements using stained osteochondral tissues were performed according to Fermor (2013). Digital images of osteochondral tissues stained with Alcian Blue were further analysed using ImageJ (version 1.50e, Wayne Rasband, National Institutes of Health, USA) to measure the cartilage thickness of the LAT TAL (n=6) and LAT TIB (n=6) regions in the porcine tissue. Five thickness measurements were taken from the superficial zone to the deep zone of the cartilage (Figure 5-4). The point at which the cartilage ended and subchondral bone began was defined as when the alcian blue staining ended and visible light pink eosin staining was evident. To verify the method, cartilage thickness was also determined in H&E stained images (Figure 5-5). For H&E stained images, the region of cartilage was defined as when the light haematoxylin purple staining ended and visible dark eosin

pink staining of the subchondral bone was evident (Figure 5-5). To calculate cartilage thickness within each of the six images obtained (n=6), five thickness measurements were recorded and a mean calculated. The mean cartilage thickness (n=6) in each image was calculated plus 95 % CL for each region - LAT TAL and LAT TIB.
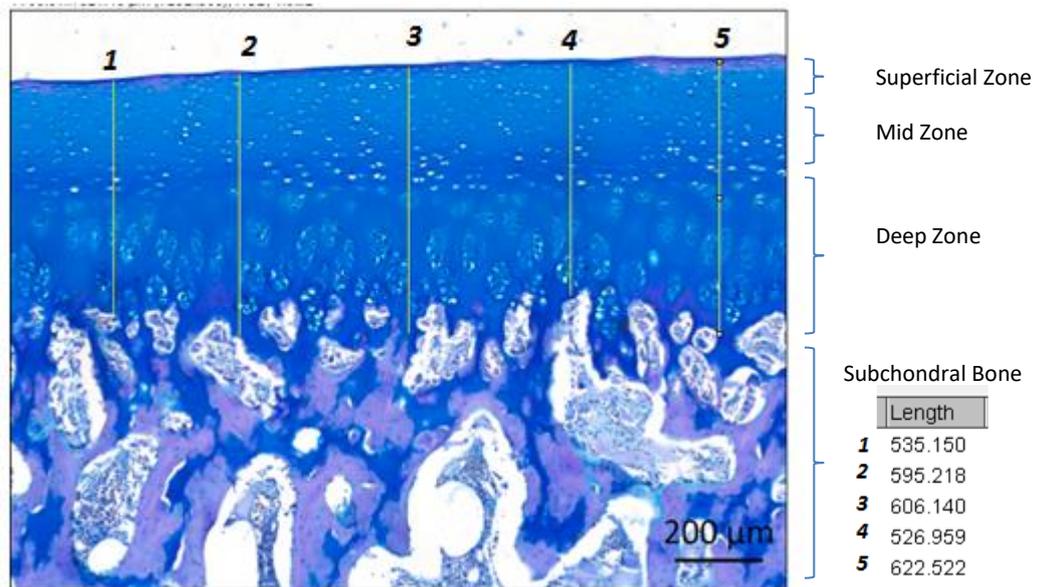
Figure 5-4: An example of cartilage thickness measurements obtained using Alcian Blue stained osteochondral tissue of lateral talus (LAT TAL). Five measurements were taken across the stained section using ImageJ. Each yellow line represents a measurement. The length is given in µm.
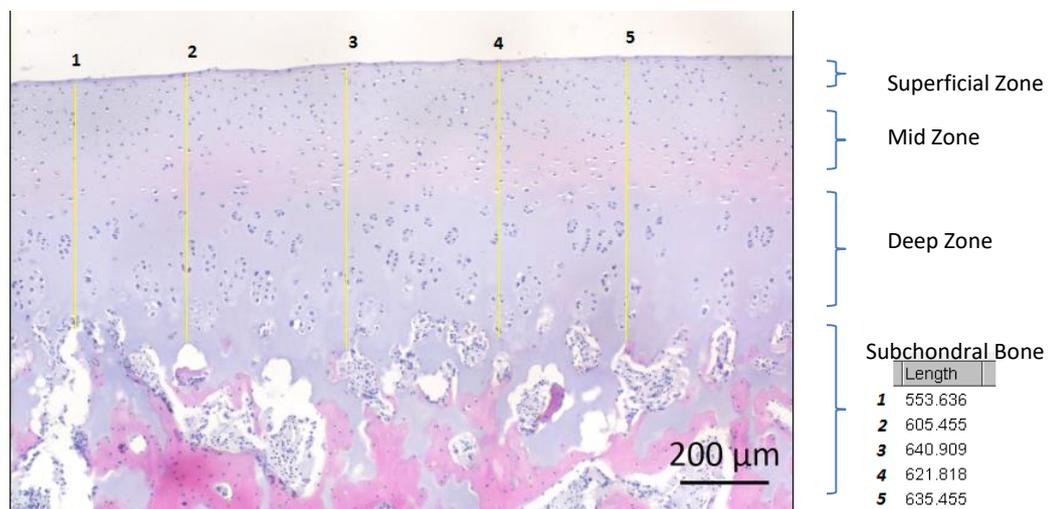
Figure 5-5: An example of cartilage thickness measurements obtained using H&E stained osteochondral tissue of lateral talus (LAT TAL). Five measurements were taken across the stained section using ImageJ. Each yellow line represents a measurement. The length is given in µm.

5.4.2 Determination of Cartilage Water, GAG and Hydroxyproline Content using Quantitative Biochemical Assays

Osteochondral pins of 8.5 mm diameter were extracted from lateral and medial aspects of the porcine talar and tibial surfaces as described in Chapter 2, section **0**. For each region - LAT TAL, MED TAL, LAT TIB and MED TIB, n=6 pins were obtained. All four regions in the porcine ankle joint were tested within this part of the study, such that the biological properties were compared with the mechanical properties (Chapter 3) and friction and wear characteristics (Chapter 4).

5.4.2.1 Sample preparation

<u>Lyophilisation</u>

The cartilage layer was carefully removed from the subchondral bone using a scalpel blade and macerated by cutting into smaller pieces of cartilage. The macerated tissue samples were then weighed three times and a mean wet weight value was obtained. Samples were placed in a freeze dryer (Thermo, Savant ModulyoD) at - 50°C for up to three days.

<u>Determination of Cartilage Water Content</u>

The water content of the cartilage tissue samples was calculated by the change in weight before (tissue wet weight) and after (tissue dry weight) lyophilisation (section 5.4.2.1). The difference in wet and dry weights resulted in the weight of water (in g) which was then converted to a percentage of tissue wet weight.

<u>Determination of GAG Quantification in Cartilage</u>

Sulphated proteoglycans were stained using the cationic dye 1, 9-dimethylemethylene blue (DMB). A colorimetric analysis was used to quantify GAGs in cartilage tissue.

Digestion buffer

Digestion buffer was prepared by adding 0.788 g of L-Cystine hydrochloride (Sigma Aldrich) and 1.8612 g of EDTA to one litre of PBS. The pH was adjusted such that it was 6.0 to 6.1 using 6 M sodium hydroxide or 6 M hydrochloric acid, whilst the buffer was stirred continuously using a magnetic stirrer. Digestion buffer was stored at room temperature for up to six months.

Papain digestion

Papain was prepared by adding 3174.6 mg (31.5 KU/mg) of Papain powder (Sigma Aldrich) to 125 ml digestion buffer before pipetting 5 ml of this mix into each bijou containing lyophilised cartilage. The tissue samples were then incubated in a water bath at 60°C for up to 48 hrs. This solution was used immediately and any remaining solution was discarded

Preparation of Solutions for GAG Assay Buffer

0.1 M di-sodium hydrogen orthophosphate

For the GAG assay buffer, 0.1 M di-sodium hydrogen orthophosphate (VWR International) was required. A weight of 3.55 g of Sodium di-hydrogen orthophosphate was dissolved in 250 ml of distilled water using a magnetic stirrer. The solution was then stored at room temperature for up to three months.

0.1 M sodium-di hydrogen orthophosphate

For the GAG assay buffer, 0.1 M sodium-di hydrogen orthophosphate (VWR International) was required to be made. A weight of 3.45g of Sodium di-hydrogen orthophosphate was dissolved in 250 ml of distilled water using a magnetic stirrer. The solution was stored at room temperature and used within three months.

GAG Assay Buffer

To make up the GAG assay buffer, 63 ml of 0.1 M di-sodium hydrogen orthophosphate was combined with 137 ml of 0.1 M sodium di-hydrogen

orthophosphate, and mixed using a magnetic stirrer. The solution was stored at room temperature for up to three months.

DMB Dye Solution

Firstly, 16 mg of 1, 9- dimethylene blue was dissolved into 5 ml of ethanol and 2 ml of formic acid (Sigma-Aldrich) using a magnetic stirrer. Following this, 2 g of sodium formate (VWR International) was added and the volume increased to 1 litre using distilled water. The pH of the solution was adjusted to 3.0 using formic acid.

Methodology: Determination of GAG Content in Cartilage

The cartilage was removed from the subchondral bone using a scalpel blade. Cartilage tissue samples were weighed, lyophilised (section 5.4.2.1) and digested using papain (section 5.4.2.1) for up to 48 hours. Chondroitin sulphate B was used as a calibration standard and made up in assay buffer at 0, 3.125, 6.25, 12.5, 25, 50 $\mu g.ml^{-1}$ concentrations. Samples were diluted 1 in 50 in GAG assay buffer (section 5.4.2.1). Each standard and digested tissue sample (40 µl) was added to a clear flat-bottomed 96 well plate. To each well, 250 µl of DMB solution (section 5.4.2.1) was added. The plate was then placed on a shaker for 2 mins at 60 rpm at room temperature before placing it on a microplate spectrophotometer, to measure the absorbance within each well at 525 nm. A standard curve was plotted and linear regression analysis of the standard curve was used to interpolate unknown values (Figure 5-6).
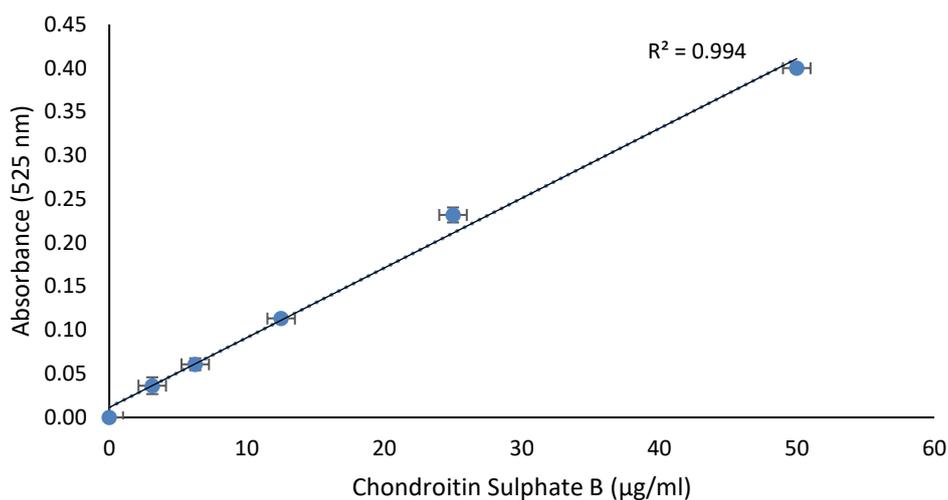
Figure 5-6: A standard curve showing the absorbance (525 nm) against standard (chondroitin sulphate B) concentration for determination of GAG content. A strong correlation is reported with R^2 value of 0.99.

5.4.2.2 Determination of Hydroxyproline Content in Cartilage

<u>Hydroxyproline Assay Buffer</u>

Citric acid (13.3 g) (VWR International) was added to 3.2 ml glacial acetic acid, 32 g sodium acetate (trihydrate) (Thermo Fisher Scientific Ltd), 9.1 g sodium hydroxide (VWR International) and 80 ml of propan-1-ol (n-propanol) (VWR International). A volume of 300 ml of distilled water was added to the resulting solution. The pH was adjusted such that it was 6.0 to 6.5 using 6 M sodium hydroxide or 6 M hydrochloric acid (VWR International), whilst the buffer was stirred continuously on a magnetic stirrer. The final volume of the solution was increased to 400 ml using distilled water. The assay buffer was stored in a dark bottle at 4˚C for up to two months.

<u>Chloramine T- solution</u>

Chloramine T solution was prepared by adding 1.41 g of chloramine T (Sigma Aldrich) to 100 ml distilled water and stirring until dissolved on magnetic stirrer. This solution was used immediately.

<u>Ehrlich's reagent</u>

To 7.5 g p-dimethylbenzaldehyde (Sigma Aldrich), 30 ml propan-1-ol, 13.4 ml 60% (v/v) perchloric acid (BDH) and 6.6 ml distilled water was added. The resulting solution was stirred using magnetic stirrer. This solution was used within an hour of preparation.

<u>Acid hydrolysis</u>

The cartilage was removed from osteochondral pins and macerated using a scalpel blade. The macerated tissue was transferred into a sterile universal and 5 ml of hydrochloric acid was added to each sample. Using a block heater within a fume hood, the samples were incubated at 120˚C for up to 16 hrs.

5.4.2.3 Methodology: Determination of Hydroxyproline Content in Cartilage

Wet cartilage tissue samples were weighed, lyophilised (section 5.4.2.1) and acid hydrolysed (section 5.4.2.3). After acid hydrolysis, the samples were neutralised to pH 7 using 1 M and 6 M sodium hydroxide and hydrochloric acid, respectively. Standards of trans-4-hydroxy-L-proline were made up in hydroxyproline assay buffer (section 5.4.2.2) at concentrations between 1 and 30 μg.ml^{-1}. Samples were diluted 1 in 10 in assay buffer. Each standard and tissue sample was added to a clear flat-bottomed 96 well plate at a volume of 50 μl. To each well, 100 μl of chloramine T was added (section 5.4.2.2) and the plate was placed on a shaker for 5 min at 60 rpm at room temperature. To each well, 100 μl of Ehrlich's reagent (section 5.4.2.2) was added before placing the plate at 60˚C for 45 min. The absorbance of each well was measured at 570 nm on a microplate spectrophotometer. A standard curve was plotted and linear regression analysis of the standard curve was used to interpolate unknown values (Figure 5-7).
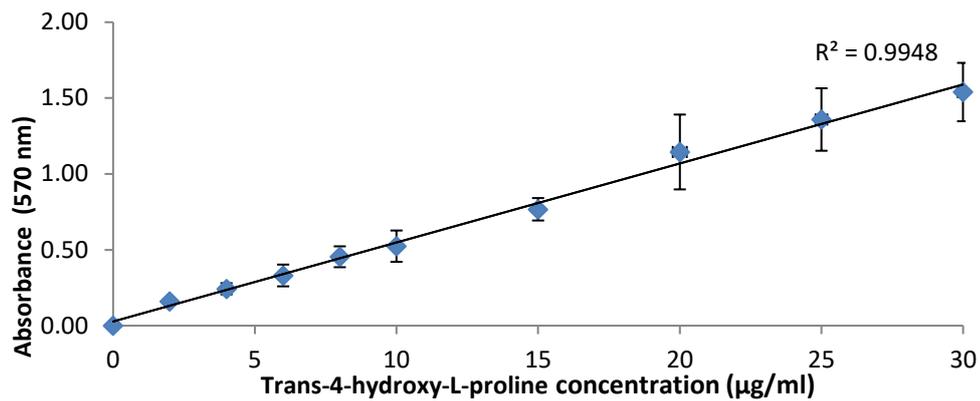
Figure 5-7: A standard curve showing the absorbance (570 nm) against standard (trans-4-hydroxy-L-proline) concentration for determination of hydroxyproline content a strong correlation was reported with R^2 value of 0.99.

5.4.3 Statistical Analysis

For statistical analysis, ANOVA (one-way analysis of variance) was used to find the overall p-value to determine significance across the means. Further analysis was required in case significant differences were reported across the means; in such instances, the tukey-method was used to determine individual significant differences across the means (Chapter 2, section **2.4**).

All percentage data (i.e. cartilage water content) were arcsine transformed as required and compared by analysis of variance (ANOVA), to fulfil a normal distribution. Mean percentage cartilage deformation values obtained for porcine osteochondral tissue (n=6) and intact talus surfaces (n=6) were arcsine transformed prior calculation of the 95 % confidence limits and back transformed for graphical presentation (Chapter 2, section **2.4.1**).

A linear regression analysis was performed on standard curves to interpolate the results for GAG (glycosaminoglycan) and hydroxyproline assays (Chapter 2, section **2.4.2**) such that a relationship between absorbance and standard concentrations were plotted.

5.5 Results

5.5.1 Histological Analysis of Porcine Ankle Osteochondral Tissues

5.5.1.1 General Architecture of Porcine Talar and Tibial Cartilage using H&E

H&E staining of osteochondral sections from the lateral aspects of the talar (n=6) and tibial cartilage (n=6) surfaces are shown in Figure 5-8. The general cell orientation is shown in Figure 5-8. The superficial zone contained visibly higher numbers of flattened chondrocytes that became rounder and more randomly distributed towards the mid zone and in the deep zone, formed linear columns perpendicular to the cartilage bone interface. Overall, the talar and tibial cartilage presented comparable cell characteristics and surfaces were convex and concave, respectively.
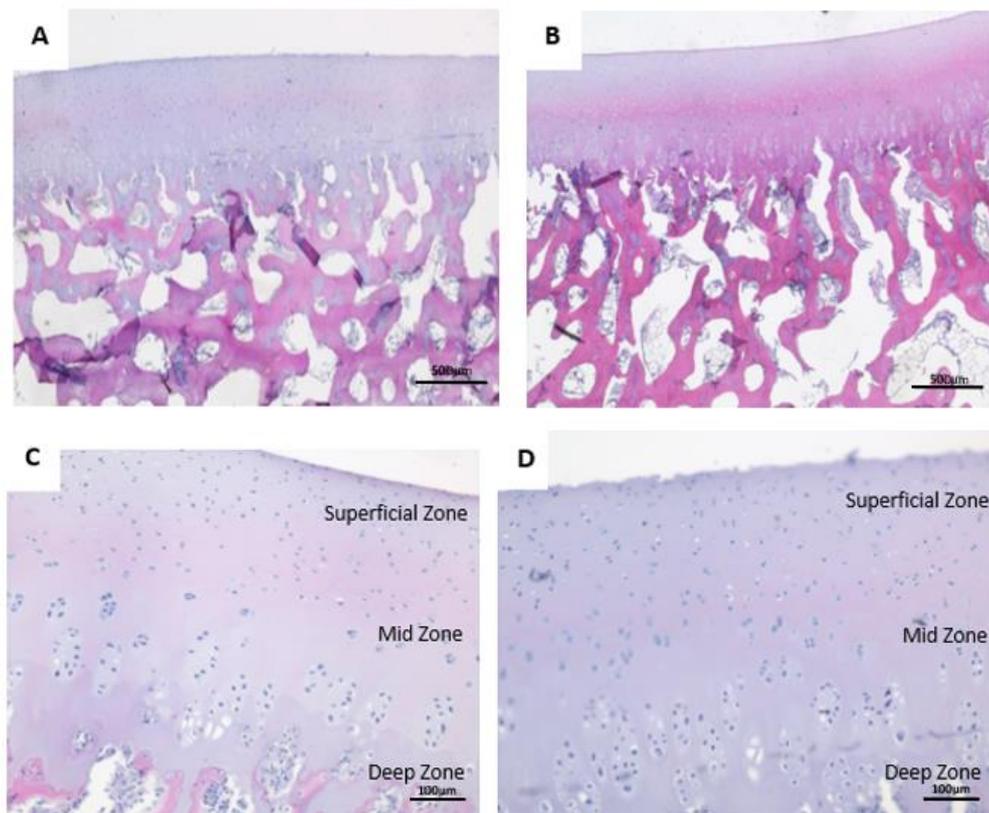
Figure 5-8: Porcine osteochondral tissues of lateral talus (LAT TAL) and lateral tibia (LAT TIB) stained using Haematoxylin and Eosin (H&E) shown at two different magnifications (100 μm and 500 μm) (A) LAT TAL (scale bar 500 μm); (B) LAT TIB (scale bar 500 μm); (C) LAT TAL (scale bar 100 μm); (D) LAT TIB (scale bar 100 μm).

5.5.1.2 Presence of GAGs in Porcine Talar and Tibial Cartilage using Alcian Blue

A qualitative observation was made of Alcian Blue stained osteochondral tissues. The lateral aspects of the talar (n=6) and tibial cartilage (n=6) of porcine tissue (Figure 5-9) were stained to study the presence of GAG. Based on the images, there seems to be slightly darker patches of blue present in the superficial and mid zone of both the talar and tibial cartilages, whereas a slight reduction in intensity was visible in the deep zone (Figure 5-9). Overall, some variation in blue intensity was highlighted for both talar and tibial stained tissues (Figure 5-9). In areas of cartilage not stained by Alcian Blue, PAS staining showed mild pink staining of the subchondral bone in the deep and calcified cartilage of the talus (Figure 5-9A). Within the superficial zone of the tibial cartilage, mild pink staining was also notable (Figure 5-9B). Both talar and tibial cartilage showed mild pink staining in the subchondral bone with patches of Alcian Blue staining.
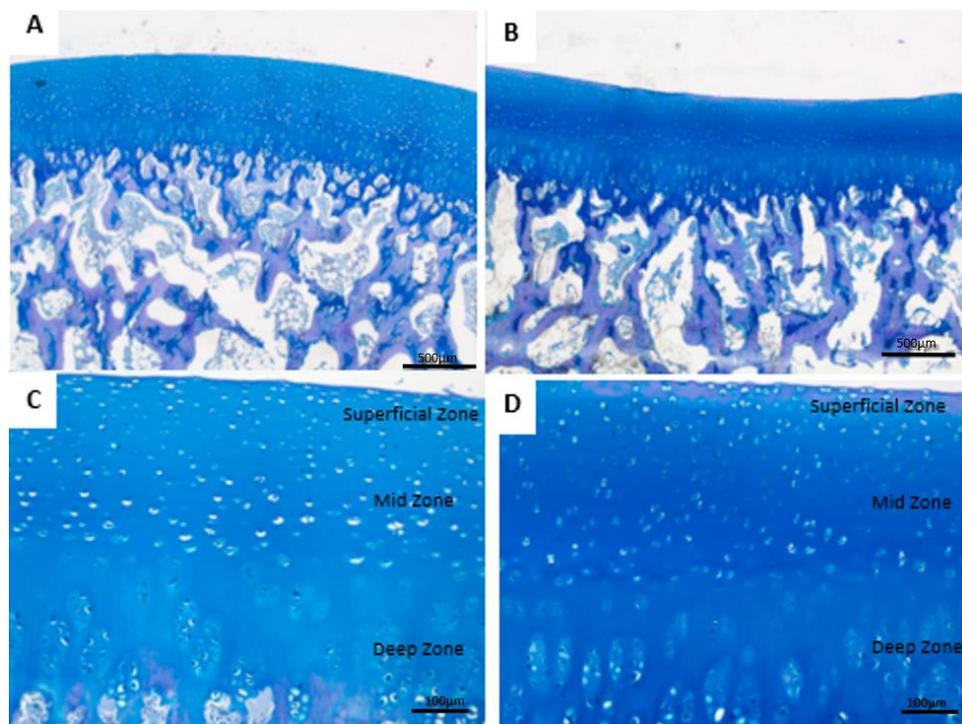
Figure 5-9: Porcine osteochondral tissues from the lateral talus (LAT TAL) and lateral tibia (LAT TIB) stained using Alcian Blue and PAS shown at two different magnifications at 500 μm and 100 μm; (A) LAT TAL (scale bar 500 μm); (B) LAT TIB (scale bar 500 μm); (C) LAT TAL (scale bar 100 μm); (D) LAT TIB (scale bar 100 μm).

5.5.1.3 Presence of Collagen and Elastin Fibres in Porcine Talar and Tibial Cartilage using Sirius Red

Sirius Red was used to study collagen fibres under polarised light (Figure 5-10) and Miller's stain was used to study the elastin fibres under brightfield settings (Figure 5-11) in the lateral aspects of the talar (n=6) and tibial cartilage (n=6) surfaces from porcine tissue. Collagen and elastin fibres in the lateral aspects of the talar (n=6) and tibial cartilage (n=6) of the porcine tissue were compared. The polarised light setting was used to view collagen distribution within cartilage. Under polarised light, the cartilage superficial layer was stained intense orange/red indicating densely packed collagen fibers, which were arranged parallel to the cartilage surface. Both tissue types, lateral talus (LAT TAL) and lateral tibia (LAT TIB) exhibited green staining of collagen fibres within the deep zone (Figure 5-10), which indicates a change in fibre thickness.
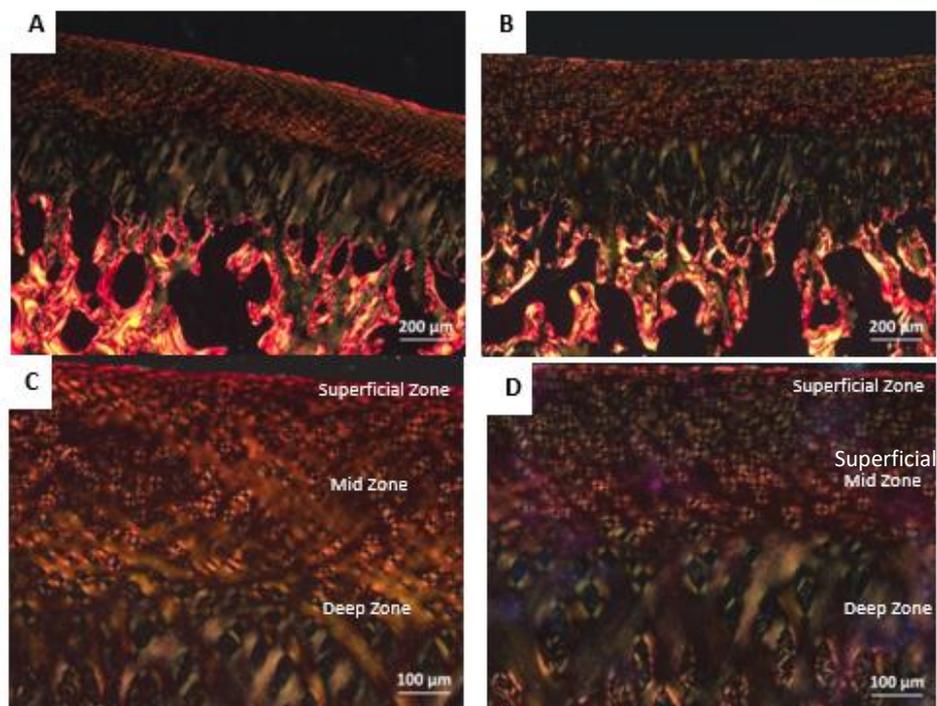
Figure 5-10: Porcine osteochondral tissues of lateral talus (LAT TAL) and lateral tibia (LAT TIB) stained using Sirius Red/Miller's Elastin in polarised light shown at two different magnifications (100 µm and 200 µm; (A) LAT TAL (scale bar 200 µm); (B) LAT TIB (scale bar 200 µm); (C) LAT TAL (scale bar 100 µm); (D) LAT TIB (scale bar 100 µm).

The 'brightfield' setting was used to study elastin distribution within porcine lateral talar and lateral tibial cartilages in sections stained with Miller's Elastin (Figure 5-11), and the cell distribution was also studied. Neither tissue showed positive staining for elastin under brightfield microscopy. The cell distribution from the superficial to deep zones of the cartilage showed visibly higher numbers of cells at the surface, that became rounder and more randomly distributed towards the mid zone and in the deep zone, forming linear columns perpendicular to the cartilage bone interface. Cell distribution in the porcine osteochondral tissues using the brightfield setting with Miller's stained tissues was in agreement with H&E (section 5.5.1.1) and Alcian Blue (section 5.5.1.2) stained tissues.
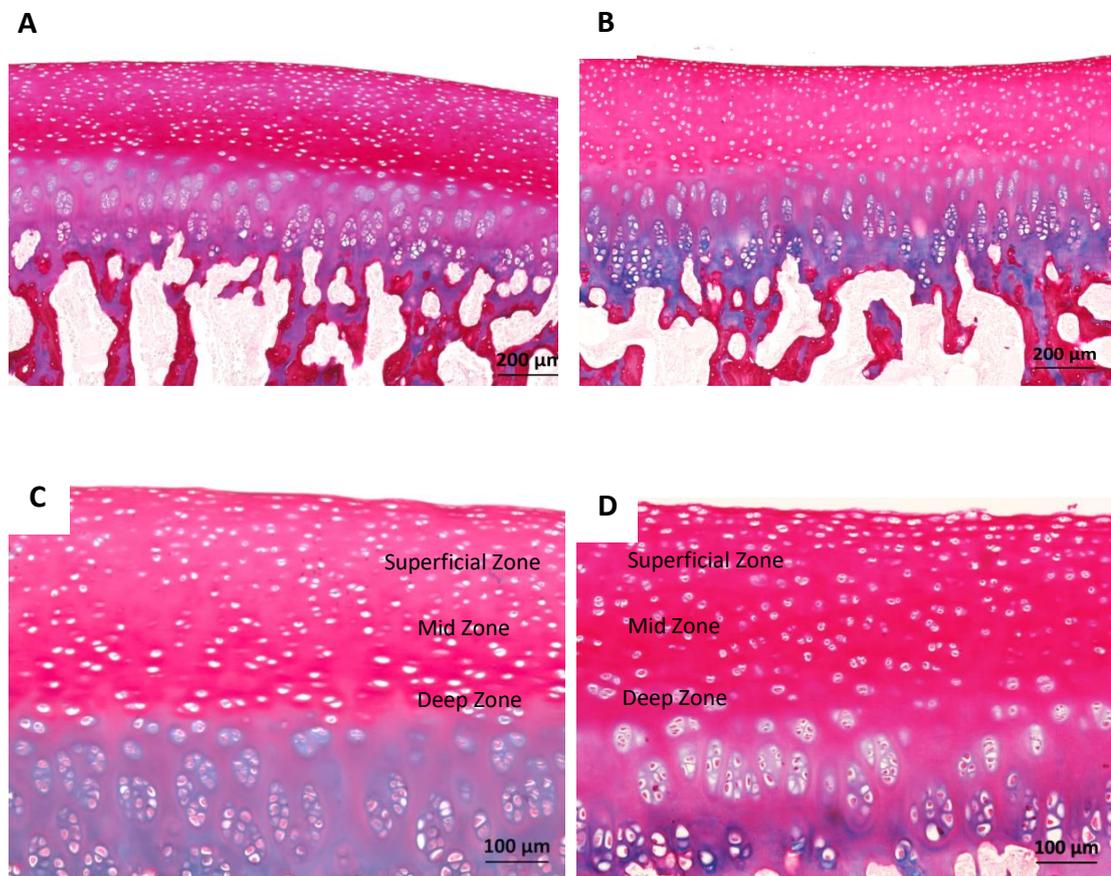
Figure 5-11: Porcine osteochondral tissues of lateral talus (LAT TAL) and lateral tibia (LAT TIB) stained using Sirius Red/Miller's Elastin in brightfield setting shown at two different magnifications (100 μm and 200 μm); (A) LAT TAL (scale bar 200 μm); (B) LAT TIB (scale bar 200 μm); (C) LAT TAL (scale bar 100 μm); (D) LAT TIB (scale bar 100 μm).

5.5.2 Cell Counts in Porcine Ankle Osteochondral Tissues

H&E stained images of lateral talus (LAT TAL) and lateral tibia (LAT TIB) osteochondral tissues from porcine ankle joints were analysed with ImageJ to determine the total number of cells within the superficial, mid and deep zones per 50,000 μm^2 and the average total number of cells for each image per 500, 000 μm^2.

Within the LAT TAL and LAT TIB, the superficial zone had the highest concentration of cells (79.92 ± 9.58 and 81.42 ± 22.20, respectively). The lowest cell concentrations were found in the mid zone for LAT TAL (47.92 ± 8.68) and in the deep zone for LAT TIB (41.58 ± 8.15) (Figure 5-12). Within both tissue types (LAT TAL and LAT TIB), the superficial zone had a significantly higher cell count compared to the mid zone (ANOVA, $p<0.05$) and deep zone (ANOVA, $p<0.05$). However, no significant differences were observed between the mid and deep zones of the same tissue type (ANOVA, $p>0.05$).
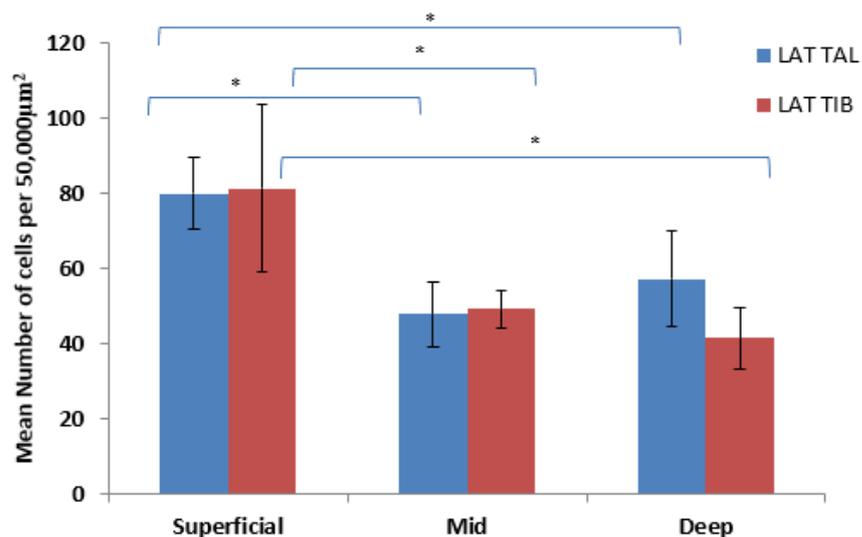
Figure 5-12: Mean cartilage cellularity per 50,000 μm^2 within superficial, mid and deep zones in lateral talus (LAT TAL) and lateral tibia (LAT TIB) of porcine ankle joint. Data is expressed as the mean (n=6) ± 95 % confidence limits.* indicates a significant difference reported (ANOVA, $p<0.05$).

The total average cell count for each image (n=6) within an area of 500,000 μm^2 was determined for the LAT TAL and LAT TIB tissues (Figure 5-13). A significant difference was found between the LAT TAL (621 ± 109) and LAT TIB (412 ± 56) cell

concentrations (Figure 5-13), where talar cartilage had a significantly higher cellularity compared to tibial cartilage (ANOVA, p<0.05).
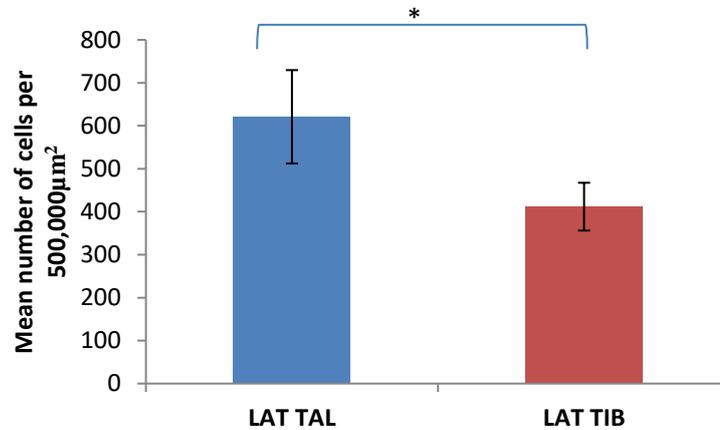
Figure 5-13: Mean cartilage cellularity per 500,000 μm^2 in each of lateral talus (LAT TAL) and lateral tibia (LAT TIB) of porcine ankle joint. Data is expressed as the mean (n=6) ± 95 % confidence limits and a significant difference was reported between both cartilage tissues (ANOVA, p<0.05).

5.5.3 Comparison of Cartilage Thickness between Porcine Talar and Tibial Regions

Alcian Blue and H&E stained images of porcine LAT TAL and LAT TIB were analysed further using ImageJ to measure cartilage thicknesses (Figure 5-14). No significant differences in cartilage thickness were observed between the two staining methods in their respective tissue types (e.g. H&E - LAT TAL vs Alcian Blue - LAT TAL). Although the talar cartilage was generally found to be thicker than the tibial cartilage using both staining methods, no significant difference was reported when comparing between different tissue types (i.e. LAT TAL vs LAT TIB, ANOVA, p>0.05, Figure 5-14). The talar cartilage thickness was measured to be 0.63 ± 0.05 mm and 0.59 ± 0.06 mm using H&E and Alcian Blue staining methods, respectively. The tibial cartilage thickness was determined to be 0.57 ± 0.05 mm and 0.51 ± 0.06 mm using H&E and Alcian Blue staining methods, respectively.
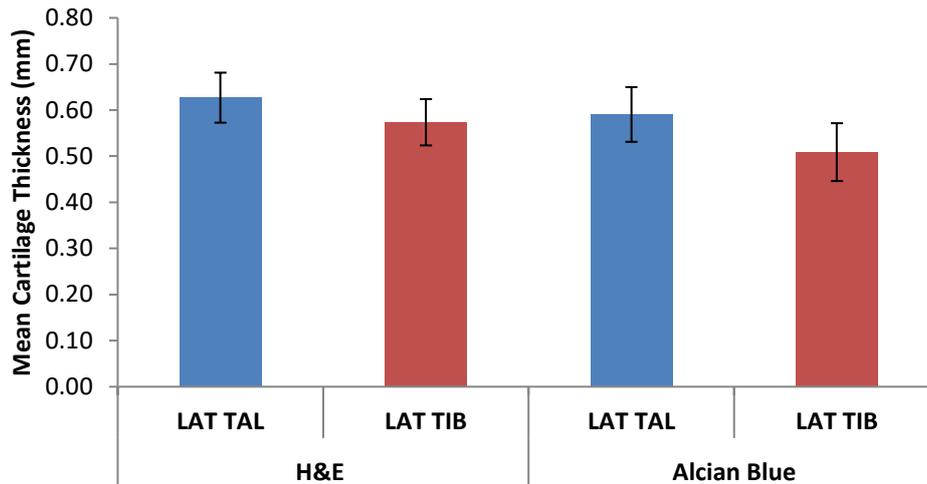
Figure 5-14: Cartilage thicknesses (mm) were obtained by viewing H&E and Alcian Blue stained images of porcine lateral talus (LAT TAL) and lateral tibia (LAT TIB) tissues on ImageJ. No significant differences were reported between both staining methods (ANOVA, p>0.05). Data is expressed as the mean (n=6) ± 95 % confidence limits.

5.5.4 Determination of Water Content in Porcine Talar and Tibial Cartilage

The water content was determined by calculating the change in weight before and after lyophilisation (section 5.4.2.1). The cartilage water content in the four regions of the porcine ankle joint (LAT TAL, MED TAL, LAT TIB and MED TIB) were not significantly different (ANOVA, p>0.05, Figure 5-15). All cartilage regions had a water content between 77.28 ± 1.95 % and 83.86 ± 5.69 %. Generally, the lateral aspects were more permeable (i.e. had a higher water content) compared to the medial aspects of their respective cartilage surfaces of the talus and tibia.
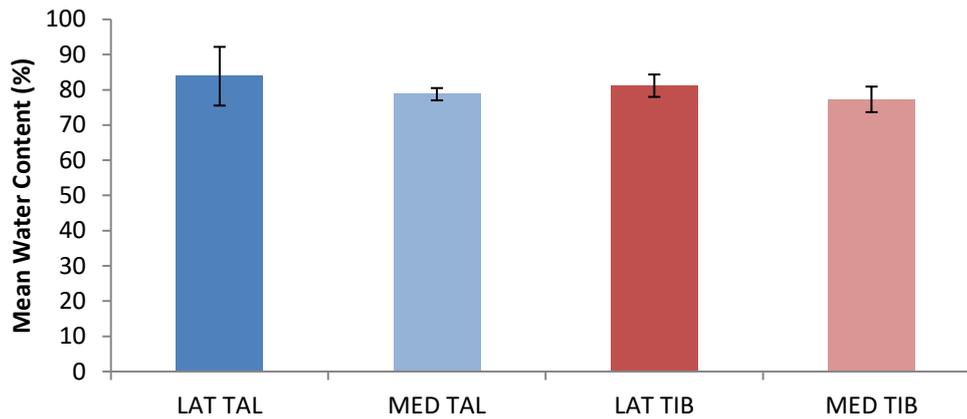
Figure 5-15: Cartilage water content (%) in four regions of the porcine ankle – lateral talus (LAT TAL), medial talus (MED TAL), lateral tibia (LAT TIB) and medial tibia (MED TIB). No significant differences were reported in the four regions (ANOVA, p>0.05). Data was subject to arcsin transformation prior to calculation of the 95 % confidence limits. Data is expressed as back transformed mean (n=6) ± 95% confidence limits.

5.5.5 Determination of GAG Content in Porcine Talar and Tibial Cartilage

The GAG content of the porcine ankle cartilage was found to be consistent in the four regions (LAT TAL, MED TAL, LAT TIB and MED TIB). The highest GAG content was measured in the LAT TIB (216.81 ± 45.08 µg.mg^{-1}) and the lowest was measured in MED TIB (144.31 ± 60.47 µg.mg^{-1}) (Figure 5-16). However, no significant differences were found between the four regions of the porcine ankle joint (ANOVA, p>0.05).
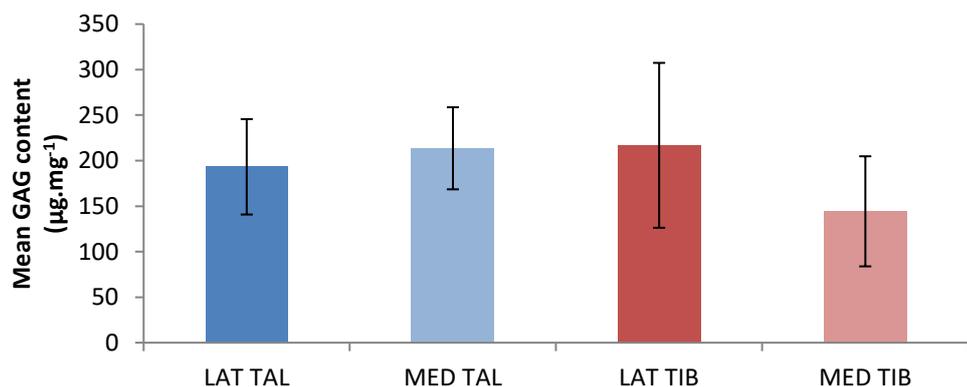
Figure 5-16: GAG content (µg.mg^{-1}) in four regions of the porcine ankle – lateral talus (LAT TAL), medial talus (MED TAL), lateral tibia (LAT TIB) and medial tibia (MED TIB). No significant differences were reported in the four regions (ANOVA, p>0.05). Data is expressed as the mean (n=6) ± 95 % confidence limits.

5.5.6 Determination of Hydroxyproline Content in Porcine Talar and Tibial Cartilage

No significant differences were reported in the hydroxyproline content in the four regions of the porcine ankle cartilage (LAT TAL, MED TAL, LAT TIB and MED TIB) (ANOVA, $p>0.05$, Figure 5-17). The highest hydroxyproline content was found in the LAT TAL tissue (53.92 ± 16.33 µg.mg^{-1}) and the lowest was found in the MED TIB tissue (37.50 ± 13.43 µg.mg^{-1}). Generally, the medial aspects of talar and tibial cartilages were lower in hydroxyproline content than their respective lateral aspects.
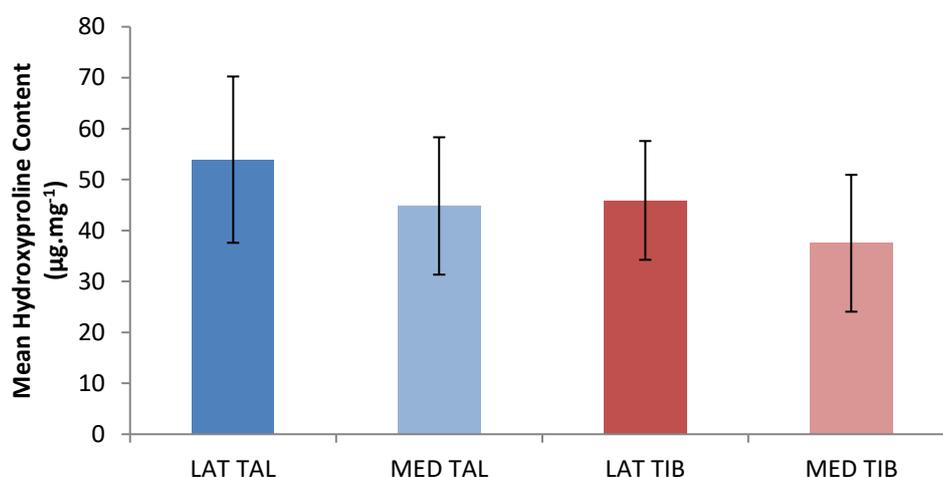
Figure 5-17: Hydroxyproline content (µg.mg^{-1}) in four regions of the porcine ankle – lateral talus (LAT TAL), medial talus (MED TAL), lateral tibia (LAT TIB) and medial tibia (MED TIB). No significant differences were reported in the four regions (ANOVA, $p>0.05$). Data is expressed as the mean (n=6) $\pm$ 95 % confidence limits.

5.6 Discussion

The overall aim of this chapter was to characterise the composition of cartilage biological constituents in the porcine ankle joint using histological staining methods and quantitative biochemical assays. The staining methods were used to qualitatively characterise the porcine ankle cartilage from osteochondral stained images to establish a potential difference between the lateral aspects of tibial and talar joint surfaces, as these samples presented with the greatest differences in mechanical characteristics (Chapter 3, section 3.5.1 and 3.5.5). Based on stained osteochondral tissues, using H&E, the general structure and chondrocyte distribution appeared comparable between talar and tibial cartilages, using Alcian Blue, some variation in blue colour intensity was observed through the depth in both talar and tibial cartilages, and using Sirius Red, thicker collagen fibrils were found in the superficial zones compared to the deep zones in talar and tibial cartilages. Chondrocyte cell population is used as an indicator to predict overall function and state of cartilage, as reduced cellularity was associated with degenerative changes in the cartilage (Rolauffs et al., 2002). In the current study, a decrease in cell count with increasing in depth was reported in the porcine ankle joint. To analyse the accuracy of thickness measurements in the current study, cartilage thickness methods were compared using biological staining methods and mechanical thickness method (needle probe, Chapter 3). The staining method resulted in lower thickness measurements compared to needle probe method. The accuracy of such results will be discussed later in this section. As water retention within the matrix is paramount in the maintenance of unique mechanical properties of the cartilage as fluid pressurisation in matrix derives the ability of the tissue to withstand high loading (Fox et al., 2009), water content was compared for both joint surfaces in the porcine ankle joint. Additionally, studying GAG and hydroxyproline content of the porcine ankle cartilage could help to predict the state of the tissue, as a loss of proteoglycans and collagen fibres were associated with an osteoarthritic cartilage (Callaghan, 2003; Gottardi et al., 2016b). Overall, using biochemical assays, the water content, GAG and hydroxyproline contents between the porcine tibial and talar joint surfaces were

comparable. Each of these outcomes in this Chapter will be discussed in greater detail.

5.6.1 Histological Analysis of Porcine Ankle Osteochondral Tissues

The variation in the orientation and number of chondrocyte cells with depth have been reported across many studies in both human and animal joints such as hip and knee cartilage (Poole, 1997; Kuettner and Cole, 2005; Jadin et al., 2005; Hunziker et al., 2002; Fermor, 2013). The present study on histological analysis of H&E stained osteochondral porcine ankle tissues agrees with previous studies reported in literature, whereby a decrease in the number of chondrocyte cells was visible with increasing depth of the cartilage and a change in chondrocyte cell orientation from flat to the formation of linear columns perpendicular to the bone interface was observed in the superficial and deep zones, respectively. In the current study on immature porcine tissue (3 to 6 months), the orientation of chondrocytes was rather homogenous, as also reported in other immature tissues (Hunziker et al., 2002; Jadin et al., 2005). Other studies have suggested that during tissue growth and maturation, changes in chondrocyte differentiation have resulted in a decrease in cell count and orientation (Hunziker et al., 2002; Jadin et al., 2005). To confirm these findings by previous studies that aging has an influence on the chondrocyte cell count and orientation in the cartilage, mature porcine ankle tissue could be compared with the current study on immature porcine tissue.

Based on Alcian blue stained osteochondral tissues of both the talar and tibial cartilage surfaces, some variation in blue intensity was evident through the depth of the cartilage. A possible explanation for a slight variation in the intensity of the Alcian Blue staining could be due to staining on different days. A recent study by Bejnordi (2016) had mentioned how slides stained on different days in the week resulted in colour variations in histology images due to possible differences in absorption characteristics of different stains. Furthermore, such variation could be associated with the skill required to optimise the microscopy imaging; whereby poor contrast and resolution could impact on the visibility of an image analysed (McGavin, 2014).

Therefore, to ensure such variations are minimised, slides should be stained on the same day for accurate comparison and accurate optimisation of histology images should be sought to ensure optimal contrast is achieved. Although qualitatively, a change in the Alcian Blue intensity observed from superficial to deep zones may indicate changes in GAG distributions, in the present study, no quantitative assessment of GAGs within the different zones was performed. Therefore, this will need to be investigated and confirmed quantitatively within each zone.

In the present study, based on Sirius Red stained images of osteochondral talar and tibial cartilage surfaces, the collagen fibres were arranged parallel to the cartilage surface in the superficial zone. A previous study by Julkunen et al. (2009) found collagen fibres to be aligned in a parallel manner in young rabbit knees (4 to 6 weeks), and as the tissue matured (3 to 18 months), the collagen fibres were aligned perpendicularly to the surface. Therefore, the findings in the present study are in agreement with other studies of immature cartilage in other species and joints. This age range in the porcine tissue would be considered as immature as the life expectancy of pigs is reported to be between 10 to 15 years (Swindle and Adams, 1988). A comparison of collagen fibre orientation with mature porcine ankle tissue will confirm whether the collagen fibres are aligned perpendicularly to the surface as reported in previous studies in animal and human cartilages (Julkunen et al., 2009; Rieppo et al., 2009).

Previous studies have reported collagen fibres to vary in thickness from the superficial zone through to the deep zone by presenting a change in colour in Sirius Red stained cartilage samples (Junqueira et al., 1982; Gough, 2013; Yassin et al., 2014). In the current study, in the immature tissue, thicker collagen fibrils were found near the surface compared to the deep zone. This is in contrast to mature human tissue, where the opposite trend has been reported (Fox et al., 2009). Such differences in collagen fibre thickness through cartilage depth may be associated with tissue maturity, as ageing tissue has been related to a reduced collagen expression (Li et al., 2013). Therefore, further investigation is necessary to investigate whether aging has an influence in collagen fibre thickness in the porcine ankle tissue.

5.6.2 Cell Counts in Porcine Ankle Osteochondral Tissues

In the current study, the porcine ankle cartilage had a significantly higher number of cells in the superficial zone compared to the mid and deep zones (ANOVA, $p<0.05$). Such variation with depth of cartilage is in agreement with previous studies on human and bovine knee cartilages (Stockwell, 1979; Hunziker et al., 2002; Williamson et al., 2003; Jadin et al., 2005), suggesting cellularity decreases from near the cartilage surface through the depth of the cartilage. A study by Hunziker et al. (2002) in the human knee reported a 3.5-fold drop in the number of cells in the deep zone (6,866 cells per mm^3) when compared to superficial zone (24,018 cells per mm^3), which is in agreement with the current study on porcine ankle. Higher numbers of chondrocytes near the cartilage surface could be associated with cells being responsible for the overall integrity of the layer, which is imperative to the protection and maintenance of the deeper layers (Fox et al., 2009). As the superficial cartilage layer is in contact with the synovial fluid, this top layer needs to be able to resist sheer, tensile and compressive forces imposed by articulation. As chondrocytes play a key part in the maintenance of tissue homeostasis by regulating the extracellular-matrix, imbalance in their function (i.e. lower cellularity) could lead to degenerative diseases such as OA (Akkiraju and Nohe, 2015). Quantitative differences in the number of chondrocytes with increasing depth of the cartilage could provide useful information for understanding state of the tissue (healthy versus diseased).

The tibial cartilage had a significantly lower number of cells compared to the talar cartilage in the porcine tissue. As a low chondrocyte count is associated with reduced matrix metabolic activities and low cell density (Jadin et al., 2005), tibial and talar cartilages may have potential differences in ECM regulation. Overall, an increased cell count in the talar cartilage could present favourable biological properties, such as the ability to protect and maintain tissue homeostasis, improved healing and better maintenance of a wear-resistant, frictionless and load-bearing surface for joint articulation (Jadin et al., 2005). Although, a high cellurarity in the talus may aid in protecting the joint from high impact forces, such finding does not appear to support the clinical problem as osteochondral defects are found more commonly in talar

surfaces rather than tibial surfaces (Hangody et al., 2001; Grady and Sanchez, 2017). This may be a result of testing porcine cartilage rather than human tissue. Therefore, cellularity through the depth of the ankle cartilage in the human tissue will need to be investigated to comment on the clinical issue.

5.6.3 Cartilage Thickness in Porcine Ankle Osteochondral Tissues

Porcine ankle cartilage thickness was compared using a needle probe method (Chapter 3, section 3.4.1.1), and histological staining methods – H&E and Alcian Blue (Chapter 5). Based on histological analysis (i.e. Alcian Blue staining and H&E staining), cartilage thicknesses in porcine talar and tibial cartilages were comparable in both the lateral talus (Figure 5-18A) and lateral tibia (Figure 5-18B). However, compared to the Instron needle probe technique (Chapter 3, section 3.4.1.1), thicknesses derived using histological analysis in the porcine ankle in lateral talus (Figure 5-18A) and lateral tibia (Figure 5-18B) were significantly lower. Generally, during fixation and dehydration processes, it is hypothesised that the tissues may shrink as chemical fixation of biological tissue samples followed by dehydration in organic solvents has been shown to cause shrinkage (Kääb et al., 1998). A recent study has also reported substantial tissue shrinkage of up to 50 % (Richardson and Lichtman, 2015) during dehydration. In addition, ethanol, often used as a dehydration agent, causes the tissue to shrink (Boyde and MacOnnachie, 1979; Kääb et al., 1998). Possible reasons for shrinkage could be osmotic effects, with the extraction of water and lipids (Glauert and Lewis, 2014). Therefore, tissue shrinkage may have affected the thickness results obtained for porcine ankle cartilage using histological methods in comparison to the needle probe method. However, as previously discussed in Chapter 3, there are also limitations with the needle probe method such as over-measuring, whereby needle could penetrate into the subchondral bone resulting in an overestimation of the cartilage thickness.
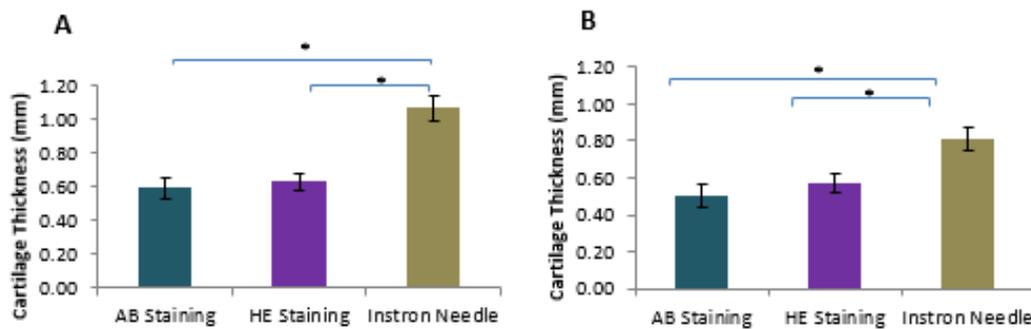
Figure 5-18: Comparison of cartilage thickness (mm) measurement by viewing H&E and Alcian Blue stained images using ImageJ and the Instron needle technique (Chapter 3) of porcine A) lateral talus (LAT TAL) and B) lateral tibia (LAT TIB) tissues. No significant differences were reported between the staining methods (ANOVA, $p>0.05$). Data is expressed as the mean (n=6) ± 95 % confidence limits; * indicates a significant difference reported (ANOVA, $p<0.05$).

5.6.4 Biological Properties in Porcine Joints

In the current study, the porcine ankle cartilage was thinner with a higher GAG content compared to porcine knee cartilage (Fermor, 2013). Porcine hip cartilage was the thickest tissue and the highest GAG content (Taylor, 2012) compared to the ankle (current study) and knee cartilage (Fermor, 2013). In the current study, the average cell count was lower in porcine ankle cartilage when compared to a study by Fermor (2013) in porcine knee cartilage. The lower number of chondrocytes in porcine ankle cartilage may be associated with thinner cartilage compared to the porcine knee (Fermor, 2013). This is not in agreement with other studies that have suggested a significantly thicker cartilage to have resulted in significantly lower numbers of cells (Fermor, 2013) and a lower cell density (Stockwell, 1971) than a thin cartilage. When comparing between joints and/or species, other factors such as mechanical loading could potentially vary due to differences in gait patterns and/or joint congruency and will need to be considered.

Table 5-2: Summary of biological properties of porcine tissue – ankle, knee and hip joints.

Studies	Cell count (per 50,000 μm^2)	Thickness (mm)	GAG Content ($\mu g.mg^{-1}$)	Water content (%)	Hydroxyproline content ($\mu g.mg^{-1}$)
Current study Porcine Ankle	49 to 80	0.51 ± 0.06 to 0.63 ± 0.05	144.31 ± 60.47 to 216.81 ± 90.58	77.28 ± 1.95 and 83.86 ± 5.69	37.50 ± 13.43 To 53.92 ± 16.33
Porcine Knee (Fermor, 2013)	150 to 200	0.82 ± 0.08 to 2.23 ± 0.20	78 ± 30	73 to 82	38 to 80
Porcine Hip (Taylor 2012)	n/a	1.22	500 to 600	70 to 80	n/a

5.7 Conclusion

- Based on H&E staining of the tissues, the number of chondrocytes (high to low, respectively) and orientation (flat to formation of linear columns, respectively) varied with increasing depth. This was comparable between talar and tibial cartilages.

- For both talar and tibial cartilages, a variation in Alcian blue intensity with increasing depth may indicate possible differences in the presence of GAGs; however quantitative assays for each zone would be needed to confirm this proposal.

- Based on Sirius Red staining of the tissues, thicker fibrils were found in the superficial zone compared to the deep zone in the immature porcine ankle cartilage.

- The cell count in the superficial zone was significantly higher compared to the other zones in the talar and tibial cartilages, suggesting a possible decrease in cellularity with increasing depth.

- Processes such as fixation and dehydration may have caused tissue shrinkage, resulting in significantly thinner cartilage measurements using histological methods (such as H&E and Alcian Blue) compared to the needle probe method (ANOVA, $p < 0.05$).

- Biological characterisation using biochemical assays did not reveal any significant differences in water content, GAG content and hydroxyproline content between porcine talar and tibial tissues.

Chapter 6: Mechanical and Surface Roughness Characterisation of Human Ankle Cartilage

6.1 Introduction

Following on from Chapter 3 and 4, investigation of the mechanical properties and surface roughness characterisation of human ankle cartilage is detailed in this chapter, applying methods refined in Chapters 3 and 4.

There are several methods used to determine the cartilage thickness in the ankle joint, which can be categorised as 'non-destructive' and 'destructive. Cartilage thickness measurements using *in-vitro* imaging techniques (MRI) ('non-destructive') and needle probe techniques ('destructive') in the human ankle joint have been studied to a certain extent (Shepherd and Seedhom, 1999; Millington et al., 2007c). Millington et al. (2007c) studied thickness in eight cadaveric ankle joints using MRI methods with a semi-automated directional gradient vector flow (dGVF) snake segmentation algorithm that allowed manual editing of segmentation lines in each image, whilst enhancing noise reduction. This method was able to longitudinally measure changes in thickness using surface reconstruction methods (Millington et al., 2007c). However, measuring cartilage thickness using MRI methods in thin cartilage and congruent joints such as the ankle, has been reported to be inaccurate, due to sharp surface curvatures whereas a greater measurement reliability in cartilage layers thicker than 2 mm, such as in the knee was reported in previous studies (Kladny et al., 1996; Koo et al., 2005; Millington et al., 2007c). Furthermore, when imaging techniques (i.e MRI and CT) were compared to detemine an accurate method to measure thickness, MRI techniques has been considered to be less reliable as a greater scatter of readings were seen in the images compared to those reported using the CT-imaging based method (El-Khoury et al., 2004). Although the needle probe thickness method has been used in the human (Shepherd and Seedhom, 1999) and animal models (McLure et al., 2012; Taylor, 2012; Fermor et al., 2015), this method causes damage to the cartilage surface and limits further tests being carried

out on the same sample. For the purposes of human tissue study, CT and needle probe methods were compared using porcine tissue (Chapter 3, section 3.5.4) and resulted in no correlation. Based on this outcome, a non-destructive CT method was considered in the current study on human ankle cartilage, as tissue hydration was ensured and tissue samples remained intact throughout testing period unlike needle method.

Joint lubrication is key in understanding fluid flow behaviour in the tissue. During deformation, the fluid flow in the tissue is enhanced to maintain healthy joint function and can help to understand how permeable the tissue is (i.e. rate of fluid flow). The lubrication mode in which the tissue operates within can help to determine the permeability of the tissue. The lubrication mode within healthy human ankle joints has been suggested to operate within elastohydrodynamic mode (EHD) (Medley, 1981) (Chapter 1, section 1.5.2.6). This lubrication regime occurs, when a considerable increase in fluid-film pressure is able to deform the asperities of the articulating surfaces. However, once the cartilage zones are damaged within the ankle joint, through degenerative changes such as arthritis, boundary lubrication (BL) mode is proposed to operate under steady sliding motion during walking (Hlavácek, 1999). As a continuous boundary lubrication, this regime can further damage the joint as broken asperities cause an increase in friction and wear between articulating surfaces (Hou et al., 1992). In summary, in a healthy cartilage, fluid does not flow out of cartilage as easily as observed in damaged cartilage (Mansour, 2009). A diminished fluid phase in the cartilage can result in changes to the mechanical properties (i.e. high permeability) of the tissue, compared to a healthy cartilage which assumes a low permeability (Athanasiou et al., 1991; Mansour, 2009).

This chapter will determine cartilage deformation of the human ankle joint using methods described in Chapter 3 (section 3.4.2) on the porcine tissue. Cartilage thickness in the ankle joint will be determined using a non-destructive CT-imaging based method to make use of available human tissue. Surface roughness measurements were taken on intact cartilage samples and compared with results obtained on porcine ankle tissue (Chapter 4).

6.1 Aims and Objectives

6.1.1 Aims

The aim of the study was to determine cartilage deformation, thickness and the surface roughness of human ankle cartilage. Such investigation will identify how the human ankle cartilage responds to loading in relation to thickness. Furthermore, the roughness of the cartilage can help to determine the quality of the tissue in its natural state. Such comparisons will help to build an understanding of the healthy model and comment on its sensitivity to damage.

6.1.2 Objectives

- To determine cartilage thickness of human ankle osteochondral tissues from tibial and talar joint surfaces using CT- based imaging method

- To characterise percentage deformation of the human ankle osteochondral tissues from tibial and talar joint surfaces using indentation methods

- To determine surface roughness of untested human cartilage tissue using Talysurf (contact stylus profilometry)

6.2 Materials

The human tissue specimen preparation is detailed in Chapter 2, section 2.3.3. Osteochondral pins of 8.5 mm diameter were dissected from talar and tibial joint surfaces. In total 8 pins were extracted from each joint surfaces (talus and tibia); four from the talar joint surface (TalCL, TalAL, TalCM, TalPM) and four from the tibial joint surface (TibPL, TibAL, TibM, TibC) (Figure 6-1, as outlined in Chapter 2, section 2.3.4.2).

6.3 Methods

Indentation tests (Chapter 3, section 3.4.2) were performed to derive cartilage deformation in the human ankle joint. The deformation rate at the initial phase of testing and at equilibrium state was determined as studied on porcine tissue (Chapter 3, section 3.5.5). Such analysis will provide details on fluid flow behaviour for each sample and its response to loading can be understood at the initial phase of testing. The initial rate of deformation is an indicator on how quickly flow flows out of tissue for deformation to occur. The final steady state can indicate the properties of solid phase and therefore it can provide relative properties of the tissue as the fluid phase has entirely diminished and load is supported by solid phase. Although such analysis is not a specific measure of mechanical properties, it can help to predict mechanical properties such as permeability and stiffness in the human tissue.

In Chapter 3, mechanical characterisation of porcine tissue using pins and whole joints highlighted that both tissue samples presented comparable biomechanical properties (Chapter 3, section 3.5.3 and 3.5.6). Hence, pins were selected for analysis in the human tissue study, in order to conduct experimental studies that could be compared with previous literature.

On the talar joint surface, as defects were commonly found in the anterior-lateral (AL) and posterior-medial (PM) aspect of the joint, these regions were studied in the human tissue in the current study (Figure 6-1). On the tibial joint surface, four pins were extracted to maximise the use of the tissue. The rationale for choosing these locations has been discussed in Chapter 2 (section 2.3.4).
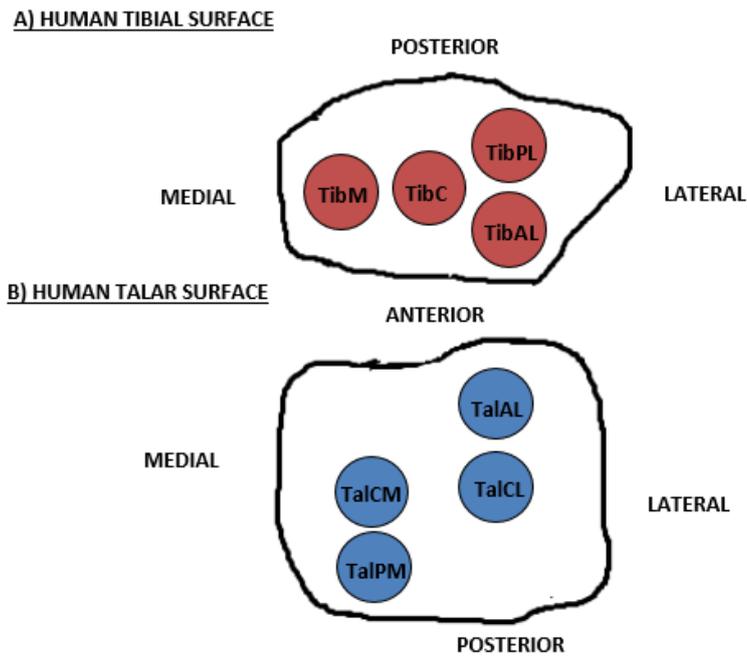
Figure 6-1: Schematic drawing showing human ankle joint labelled according to pin extraction from specific regions of the joint surfaces; A) osteochondral regions of the human tibial joint surface; B) osteochondral regions of the human talus joint surface; TalCM – talus central-medial; TalPM – talus posterior-medial; TalAL – talus anterior-lateral; TalCL – talus central-lateral; TiblPL – tibia posterior-lateral; TiblAL – tibia anterior-lateral; TibM– tibia medial; TibC– tibia central.

6.3.1 MicroCT Imaging Technique for Human Osteochondral Tissue

For the human tissue, CT100 scanner (µCT, Scanco Medical AG, Basserdorf, Switzerland) was used to determine cartilage thickness, as described in Chapter 3 (section 3.4.1.5). Pins were fully submerged in PBS within the specimen holders (14 mm by 92 mm) ensuring the tissue remained hydrated during testing. Using the scanner, the settings for this study matched those used for porcine tissue (Chapter 3, section 3.4.1.5) including the voltage (70 kV), current (114 mA), and integration time (300 ms) as recommended by the CT manufacturer (µCT, Scanco Medical AG, Basserdorf, Switzerland) and resolution of each image (5µm per slice). Greyscale thresholding was conducted and the best fit was obtained considering the entire stack rather than a single slice. To ensure the whole cartilage layer was considered, layers above and below the cartilage were selected as highlighted in Chapter 3, section 3.4.1.5. The cross-sectional images (i.e. slices) of the pin in which cartilage first appeared (above) and the image in which the bone first appeared (below) were

identified and the number of slices between was mulitiplied by the resolution to determine cartilage thickness (Chapter 3, section 3.4.1.5).

6.3.2 Creep Indentation of Human Osteochondral Tissue

A 'creep' confined indentation testing method (described previously in section 3.4.2) was utilised with human ankle cartilage under a constant load of 0.24 N over a period of one-hour using a flat-ended indenter (Figure 6-2), whereby the displacement was measured as a function of time as the fluid flows out of the tissue. As detailed in Chapter 3 (section **3.4.2.1**), an indentation apparatus was used to perform mechanical tests on human cartilage surfaces to derive cartilage properties and deformation outputs. The displacement of the shaft was measured by LVDT and the force was measured by a piezoelectric force transducer.
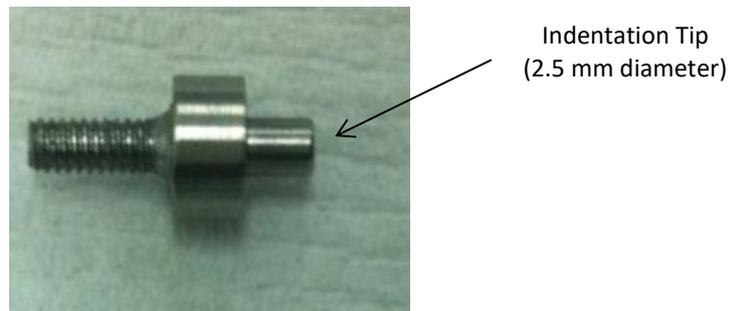
Figure 6-2: Flat-ended indenter of 2.5 mm diameter

6.3.3 Surface Roughness Characterisation of Human Osteochondral Tissue

The surface structure of human ankle cartilage specimens were replicated using Silicon mould kit as described using porcine tissue in Chapter 4 (section 4.4.2.1). Once the liquid poured over the specimen hardened within 10-15 mins, moulds were carefully removed from the cartilage surface and stored in plastic pots in room temperature. Surface profilometry (as described in Chapter 4, section 4.4.2.2) was used to measure the surface roughness for each specimen using silicon moulds.

6.4 Results

6.4.1 Visual Analysis of Cartilage Surface Prior Testing

The quality of the human ankle joint surfaces was visually examined (Figure 6-3). The talar and tibial cartilage surfaces may have become dehydrated as the tissues were exposed to room temperature over 15 mins prior to pin extraction. The colour appearance for both joint surfaces was varied, in which the talus was light orange/pink and the tibia was dark pink/purple. Both surfaces had visible marks (Figure 6-3), and it was ensured osteochondral pins were extracted away from these regions.
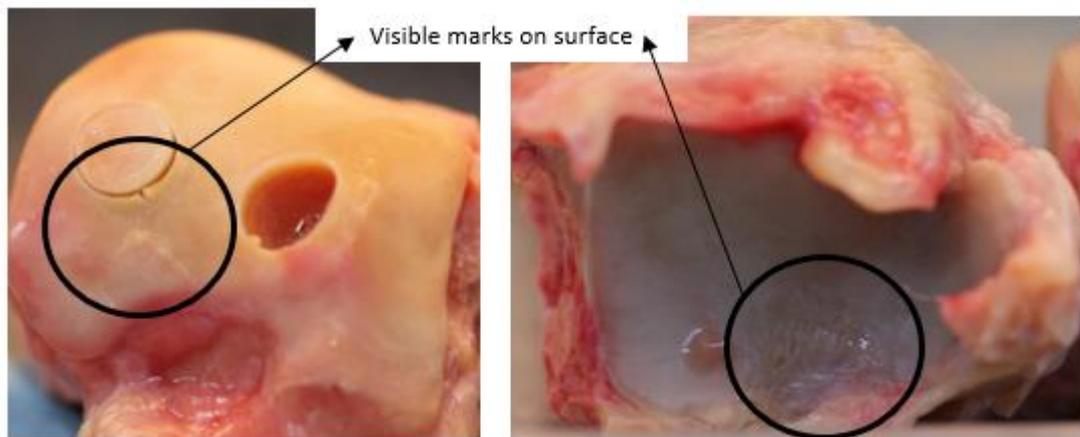
Figure 6-3: Visual analysis of human ankle joint specimen 1 with talar (left) and tibial (right) cartilage surfaces with visible marks on both joint surfaces within black circled region, specimen 1 (Appendix B).

6.4.2 Cartilage Thickness in the Human Ankle Joint

The cartilage thickness of the human ankle joint using osteochondral tissues was determined, through MicroCT measurements and comparisons were made between talar and tibial pins (Figure 6-4). In each specimen, for the mean thickness measurements in the talar cartilage, measurements across four regions were combined, and for mean tibial thickness measurements, measurements across four regions were combined, as highlighted in Figure 6-4.
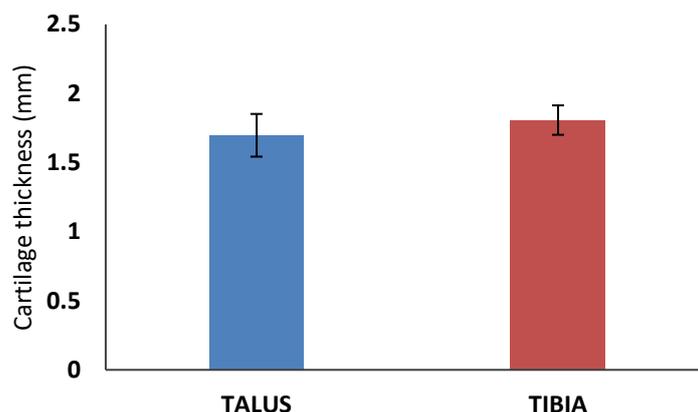
Figure 6-4: Comparison of cartilage thicknesses (mm) in talar (n=3) and tibial cartilage surfaces (n=3) of osteochondral tissues extracted from the human ankle joint using CT imaging technique. Data is expressed as mean (n) ± 95 % confidence limits.

No significant difference in cartilage thickness was reported between human talus and tibial cartilage surfaces. The average cartilage thicknesses for the talus was 1.70 ± 0.15 mm and for the tibia, the thickness was 1.81 ± 0.11 mm. A thickness map showed the distribution of thicknesses across both tibial and talar cartilages (Figure 6-5). Although all cartilage thickness measurements were comparable (ANOVA, $p > 0.05$) within each joint surface, the central regions for both joint surfaces were generally higher (Figure 6-5).
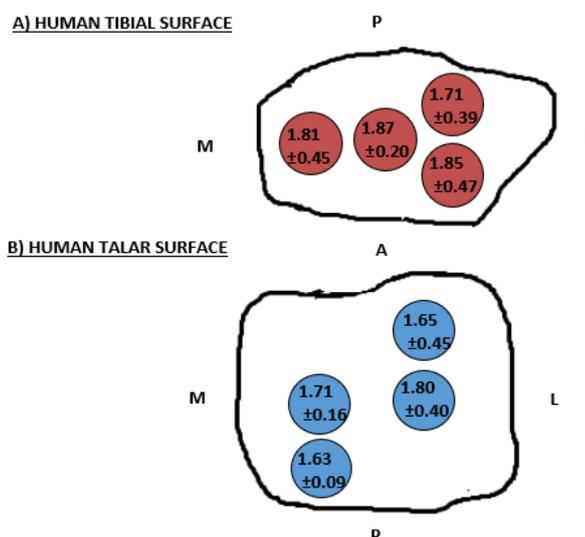
Figure 6-5: Cartilage thickness map of human ankle joint; all measurements in mm, each measurement represents three repeats (n=3); A) Thickness within human tibial cartilage; B) Thicknesses within human talar cartilage; L-Lateral, M-Medial, P-Posterior, A-Anterior.

The cartilage measurements reported in this chapter were compared against the porcine cartilage thickness previously discussed (Chapter 3; Figure 6-6). To make comparisons across lateral and medial aspects in the porcine tissue, thickness of the TalCM and TalPM of the human osteochondral tissue were combined to represent data under medial talus (MED TAL); TalAL and TalCL were combined to represent data under lateral talus (LAT TAL); TibPL and TibAL were combined to give represent under lateral tibia (LAT TIB) and TibM was compared against medial tibia (MED TIB) (n=3) porcine pins.
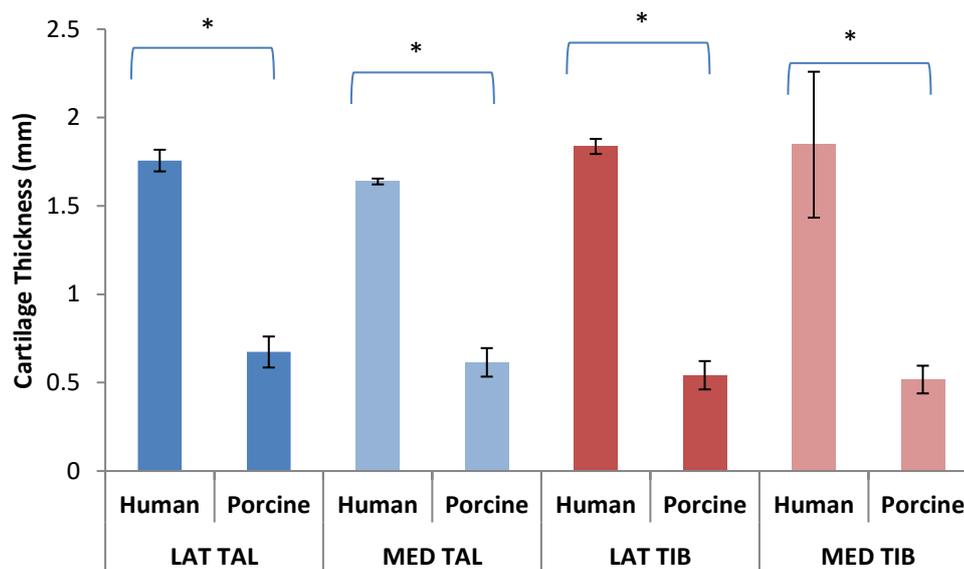
Figure 6-6: Comparison of ankle cartilage thicknesses between human and porcine osteochondral tissues using CT methods in four regions on the joint- medial talus (MED TAL) and lateral talus (LAT TAL), medial tibia (MED TIB) and lateral tibia (LAT TIB). Each data represents n=3 (for porcine and human tissue). Data is expressed as mean (n) ± 95% confidence limits.

Cartilage thickness for human ankle cartilage was significantly thicker compared to porcine ankle cartilage in all four regions in the ankle joint (ANOVA, $p < 0.05$). Overall, human ankle cartilage was approximately 3-fold thicker compared to porcine ankle cartilage.

6.4.3 Indentation Testing of Human Ankle Cartilage

6.4.3.1 Mechanical Behaviour of Human Ankle Cartilage

In total, 8 pin regions per ankle specimen were studied – four talar pins (two medial, two lateral) and four tibial pins (two lateral, one medial, one central) (Chapter 2, section **2.3.4.2**; Chapter 6, section 6.1). To determine the rate of deformation across all regions in the human ankle joint, the gradient for each curve at the beginning prior to tissue sample reaching steady state (by less than 500 seconds) was compared as highlighted in Chapter 3, section 3.5.5. All samples in the human ankle joint reached an equilibrium state of deformation by 3600 seconds. Cartilage deformation was highest in TibC and lowest in TalCL at 3600th second of testing (Figure 6-7). Based on the gradients, the slowest rate of deformation in the initial phase of testing was found in TalCM and TibPL for talar and tibial cartilages (both $m = 2 \times 10^{-5}$), respectively, and the highest rate of deformation was found in TalPM ($m = 5 \times 10^{-5}$) and TibC ($m = 6 \times 10^{-5}$) for talar cartilage and tibial cartilage, respectively (Table 6-1). The strain rates were highest in TibC with $3.21 \times 10^{-5} \, s^{-1}$ and lowest in TibPL with $1.17 \times 10^{-5} \, s^{-1}$. Overall, deformations in the human ankle were between 0.02 mm to 0.12 mm.
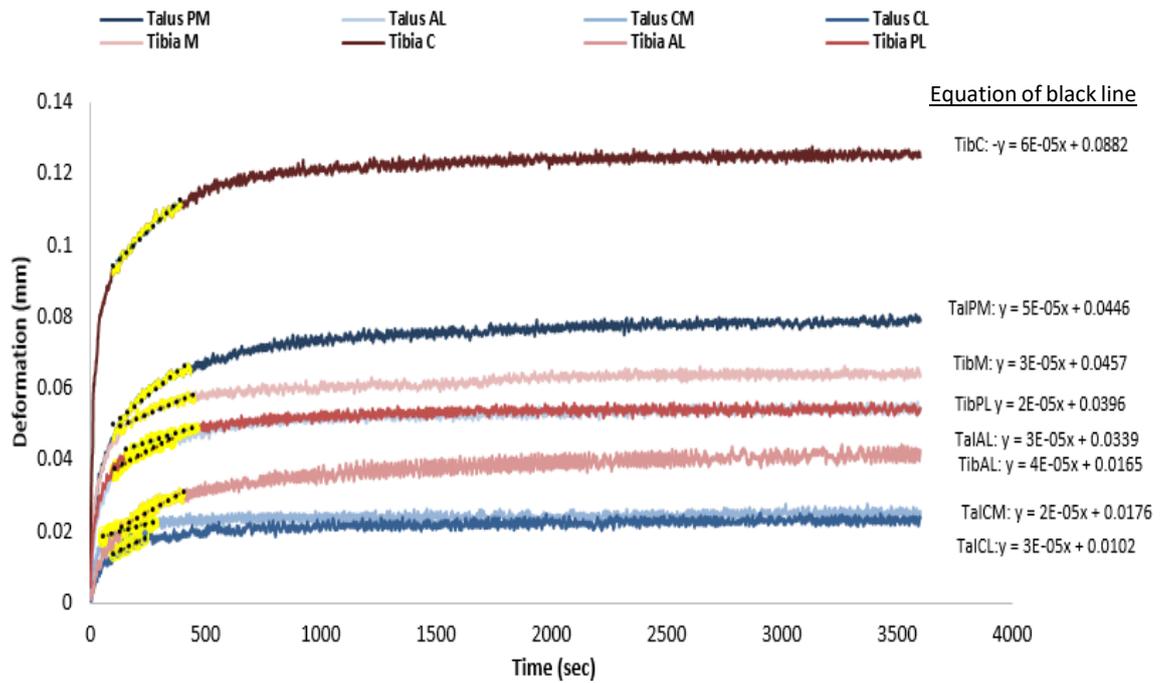
Figure 6-7: Human ankle cartilage deformation (mm) over 3600 seconds of testing on the indentation rig using 8.5 mm diameter pins. The yellow region with black dotted line represents the determination of the initial rate of deformation by finding the equation of the line, the gradient of this region for each curve is determined. The equation of the straight line is presented on the right. TalPM – talus posterior-medial; TalAL – talus anterior-lateral; TalCM – talus central-medial; TalCL – talus central-lateral; TibM– tibia medial; TibC– tibia central; TiblAL – tibia anterior-lateral; TiblPL – tibia posterior-lateral.

The equilibrium rates across the 8 regions were comparable (ANOVA, p>0.05, Figure 6-8, Figure 6-9). Although no significant difference was reported across all regions in the human ankle joint (ANOVA, p>0.05), the greatest deformed tissue, TibC (11.32 ± 9.96 %), which also had the highest rate of deformation in the initial phase of testing (m=6 x 10^{-5} mm/s), (Figure 6-7) compared to the rest of the samples (i.e. fluid escaped quicker out of the matrix), had a wider range of data resulting in larger error bars. The sample that deformed the second highest, TalPM (6.47 ± 6.41 %), also had the highest rate of deformation at the initial phase (m=5 x 10^{-5} mm/s) for talar cartilage and resulted in a wider range of data. The strain rates were highest in TibC (3.21 x 10^{-5} s^{-1}) and lowest in both TalCM and TalPL (both 1.17 x 10^{-5} s^{-1}) (Table 6-1). No samples had a 'shallow' gradient that continued beyond the equilibrium stage; therefore, the initial gradient seems to be a good predictor of deformation.

Table 6-1: Summary of all gradients determined for human ankle cartilage based on curves presented in Figure 6-7.

Location	Talus				Tibia			
	PM	AL	CM	CL	M	C	AL	PL
Equation of line	y = 5E-05x + 0.0446	y = 3E-05x + 0.0339	y = 2E-05x + 0.0176	y = 3E-05x + 0.0102	y = 3E-05x + 0.0457	y = 6E-05x + 0.0882	y = 4E-05x + 0.0165	y = 2E-05x + 0.0396
Rate of deformation mm/s (x 10⁻⁵)	5	3	2	3	3	6	4	2
Strain rates (per second) (x 10⁻⁵)	3.07	1.82	1.17	1.67	1.66	3.21	2.16	1.17
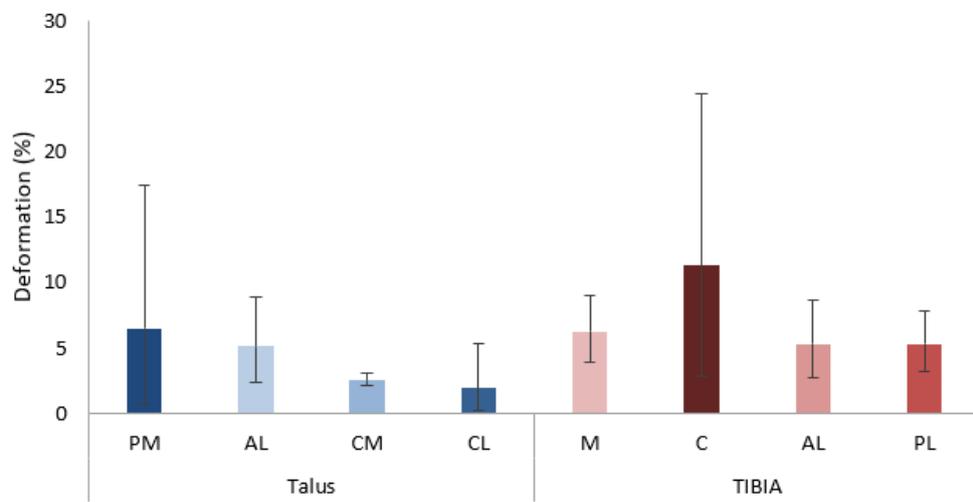
Figure 6-8: Human mean ankle cartilage deformation (%) at 3600th second during indentation testing on 8.5 mm diameter talar (n=3) and tibial (n=3) pins. Data was subject to arcsine transformation prior to calculation of the 95 % confidence limits. TalPM – talus posterior-medial; TalAL – talus anterior-lateral; TalCM – talus central-medial; TalCL – talus central-lateral; TibM– tibia medial; TibC– tibia central; TiblAL – tibia anterior-lateral; TiblPL – tibia posterior-lateral. Error bars represent mean ± 95 % confidence limits.

A) HUMAN TIBIAL SURFACE

P

5.29
±2.34

6.24
±2.54

11.33
±9.96

5.32
±2.93

M

L

B) HUMAN TALAR SURFACE

A

5.15
±3.26

2.54
±0.48

1.95
±1.72

6.47
±6.41

M

L

P
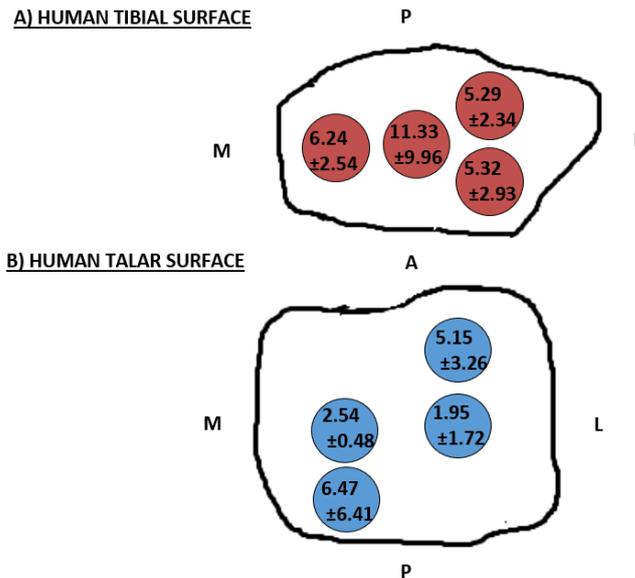
Figure 6-9: Cartilage deformation map of human ankle joint; all measurements in %; A) deformation within human tibial cartilage (n=3); B) deformation within human talar cartilage (n=3); Error bars represent mean ± 95 % confidence limits. L-Lateral, M-Medial, P-Posterior, A-Anterior.

6.4.3.2 Comparison of Mechanical Behaviour of Human and Porcine Osteochondral Tissues

Cartilage deformation values for the porcine (Chapter 3, section **3.5.5**) and human tissues were compared and are highlighted in Figure 6-10. To make comparisons across lateral and medial aspects in the porcine tissue, percentage deformation of the TalCM and TalPM of the human osteochondral tissue were combined to represent data under medial talus (MED TAL); TalAL and TalCL were combined to represent data under lateral talus (LAT TAL); TibPL and TibAL were combined to give represent under lateral tibia (LAT TIB) and TibM was compared against medial tibia (MED TIB) (n=3) porcine pins.

In the porcine tissue, cartilage deformation values were significantly higher compared to human ankle tissue in all regions (Figure 6-10). The mean deformation in lateral talus (LAT TAL) showed the greatest difference (8.68 %) for porcine and human ankle cartilage, respectively), whereas the lateral tibia (LAT TIB) showed the smallest difference (3.48 %), for porcine and human ankle cartilage, respectively (Figure 6-10).
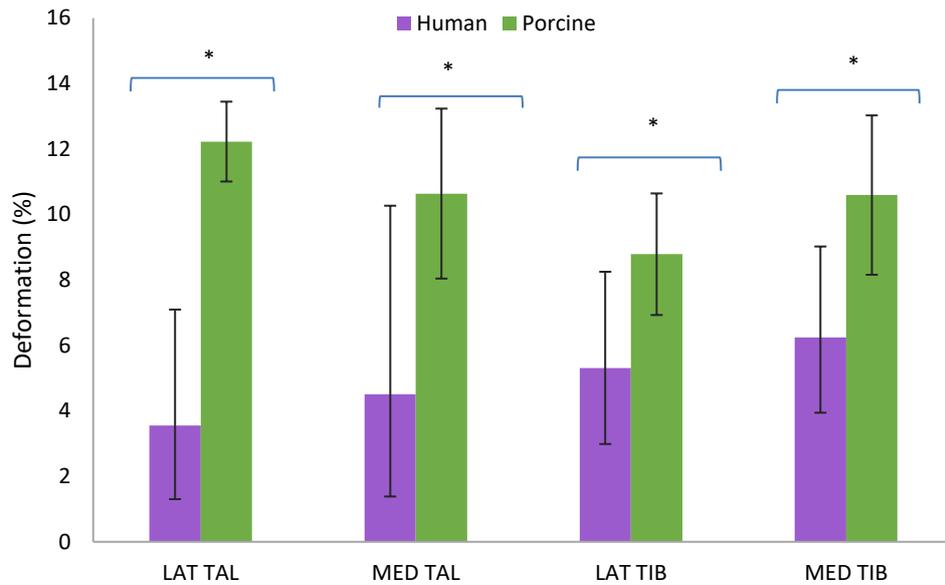
Figure 6-10: Comparison of cartilage deformation of human (n=3) and porcine ankle cartilage (n=6); Significant difference was reported between human and porcine tissue for each region (ANOVA, p<0.05); Error bars represent mean ± 95 % confidence limits.

6.4.4 Surface Roughness Characterisation of Human Ankle Cartilage

6.4.4.1 Surface Roughness of Human Ankle Osteochondral Pins

For the human tissue, the surface roughness of eight regions of osteochondral tissue extracted from tibial and talar surfaces was measured for each specimen (n=3) in the untested state only (control study) using surface profilometry. All regions in the human ankle joint had a comparable surface roughness ranging from 1.19 ± 0.76 µm to 1.96 ± 1.68 µm (TalCM and TalCL, respectively) (ANOVA, p>0.05) as shown in Figure 6-11.
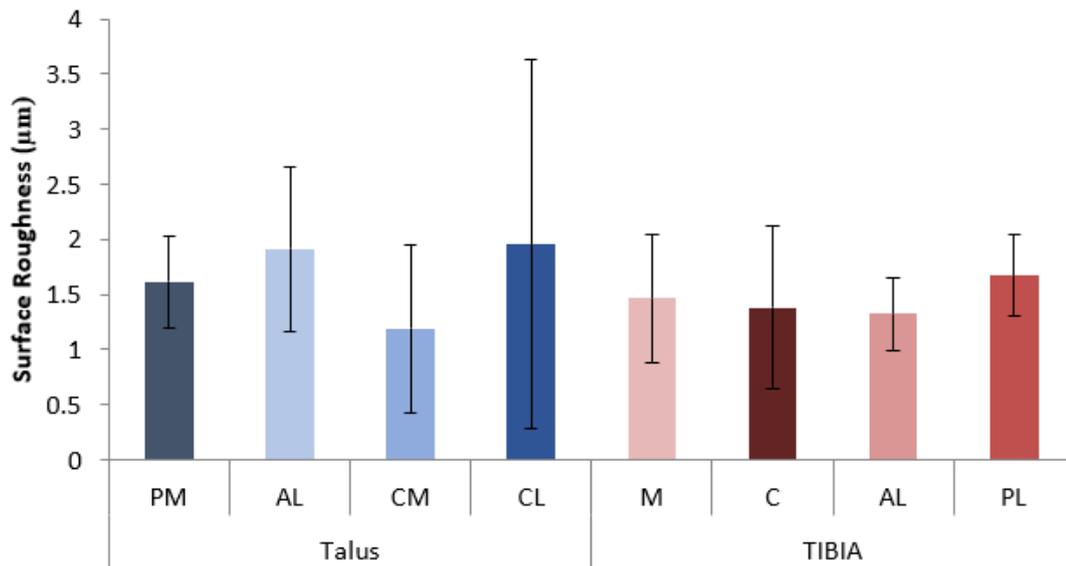
Figure 6-11: Surface roughness values (μm) in untested condition (control study) in total of eight regions of osteochondral tissues extracted from talar (4 regions) and tibial surfaces (4 regions) of the human ankle joint using contact profilometry; TalPM – talus posterior-medial; TalAL – talus anterior-lateral; TalCM – talus central-medial; TalCL – talus central-lateral; TibM– tibia medial; TibC– tibia central; TiblAL – tibia anterior-lateral; TiblPL – tibia posterior-lateral. No significant difference was reported across the regions; Error bars represent mean ± 95 % confidence limits.

6.4.4.2 Comparison of Surface Roughness of Human and Porcine Ankle Osteochondral Pins in Untested Condition

Comparing porcine ankle and human ankle cartilage in the untested condition, the human ankle cartilage pins were significantly rougher in all four regions (ANOVA, $p<0.05$) (Figure 6-12). The mean roughness in lateral talus (LAT TAL) showed the greatest difference (1.40 μm) for porcine and human ankle cartilage, respectively, whereas the medial tibia (MED TIB) showed the smallest difference (0.75 μm), for porcine and human ankle cartilage, respectively (Figure 6-12).
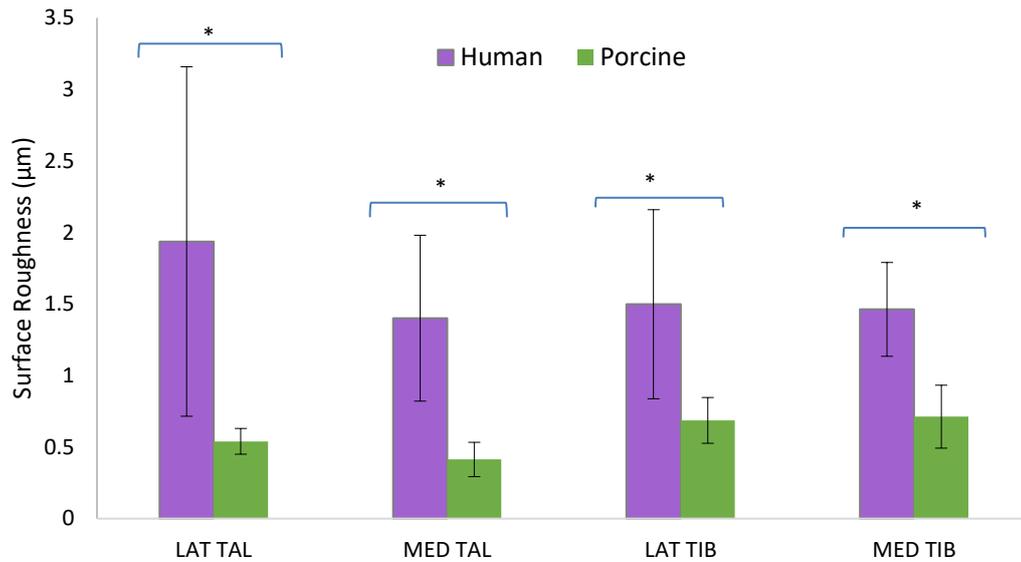
Figure 6-12: Comparison of surface roughness values (μm) in untested condition (control study) across four regions of human and porcine ankle joint using contact profilometry; Significant difference was reported between human and porcine tissue for each region (ANOVA, $p<0.05$); TalPM – talus posterior-medial; TalAL – talus anterior-lateral; TalCM – talus central-medial; TalCL – talus central-lateral; TibM– tibia medial; TibC– tibia central; TiblAL – tibia anterior-lateral; TiblPL – tibia posterior-lateral. No significant difference was reported across the regions; Error bars represent mean ± 95 % confidence limits.

6.5 Discussion

All data presented in this section on the human ankle tissue is based on previous methods such as needle thickness method, indentation testing and surface profilometry that were optimised using porcine ankle tissue (Chapter 3 and Chapter 4). This chapter aims to address overall function of the cartilage in three 'healthy' human ankle joints (n=3) by using non-damaging CT technique to characterise the cartilage thickness, and an indentation method to determine mechanical behaviour under a given load. Such characterisation assists the understanding of how thickness and/or deformation in the human ankle joint could contribute to the overall function of the joint. In the current study, a low roughness was expected as the ankle joint is known to be highly stable and least affected by cartilage degeneration (Kuettner and Cole, 2005).

6.5.1 Cartilage Thickness in the Human Ankle Joint

In the current study, cartilage thickness in the human ankle joint was comparable between the talar and tibial surfaces. This was in agreement with a study on the human ankle joint by Millington (2007a) which used another imaging method (stereophotography, Chapter 1 section 1.5.1.1). However, a previous study that used the needle probe method (Shepherd and Seedhom, 1999) had shown tibial cartilage to be significantly thicker than talar cartilage in 7 out of 11 samples. Furthermore, the human ankle cartilage thickness reported in the current study was in a higher range of 1.63 - 1.87 mm (n=3), when compared to Shepherd and Seedhom (1999) and Millington et al. (2007), with 0.94 - 1.63 mm (n=11) and 1.10 - 1.16 mm (n=12), respectively. The difference in thickness measured could be due to the method used, as highlighted in the previous comparative study on porcine ankle cartilage in Chapter 3 (section 3.6.3), whereby the MicroCT method resulted in significantly lower cartilage thickness measurements compared to a needle probe method. Notably, however, the comparison demonstrated the needle probe method to yield higher cartilage thickness measurements than the imaging methods. This demonstrates the need to note the method of measurement when comparing

between studies. Any differences in thickness measurements within the current study and literature may be due to differences in the number of samples tested, whereby the current study tested three specimens, and previous studies tested up to 12 specimens (Shepherd and Seedhom, 1999, Millington, 2007a). Potential differences between the current study and those reported by Shepherd and Seedhom (1999) could be related to possible differences in patient data, i.e. age, height, mass (BMI), as heavier and larger donors were suggested to have thicker cartilage in lower limbs based on moderate correlations (R=0.67) between thickness and BMI in the human ankle joints (Shepherd and Seedhom, 1999). To confirm findings in literature, the changes in thickness and its impact on the overall joint congruency and any joint diseases such as defects in the ankle joint requires further research, which was out of scope for the current study. There are, however, other possible explanations such as changes in the quality of the specimens (section 6.4.1) tested, which may impact on the overall thickness. In damaged tissue, a decrease in thickness due to cartilage loss in human knee cartilage was reported using MRI imaging techniques (Eckstein et al. 2011). Any differences in the quality of specimens and its effect on the thickness is currently unknown and will require further research to establish a possible link.

In the current study, human ankle cartilage thickness (1.63 ± 0.09 mm to 1.87 ± 0.20 mm, n=3) seems to be in a similar range to those reported in other human joints, such as hip (1.35 - 2.00 mm, Shepherd and Seedhom, 1999; 1.82 ± 0.18 mm, Taylor et al. 2012) and knee joints (1.69 - 2.55 mm, Shepherd and Seedhom, 1999; 1.57 - 2.43 mm, Eckstein et al. 2000). However, a study by Shepherd and Seedhom (1999) reported human ankle cartilage to be significantly thinner than other joints. As highlighted earlier, differences in cartilage thickness across joints could potentially be due to the use of different methods to characterise the thickness. A study by Wyler et al. (2007) used the CT imaging technique and reported thicknesses in the human hip joint to be in the wider range of 0.32 - 3.13 mm, whereas using the needle probe other studies reported a range of 1.20 – 2.25 mm. A comparison across

different studies is limited due to differences in methods used across other joint cartilage studies.

In the present study, the central regions in both talar and tibial joint surfaces were generally thicker than all other regions, but no significant difference was reported. Other studies have identifed the thickest cartilage to be over the anterior-lateral (AL) and posterior medial (PM) talar shoulders (O'Farrell and Costello, 1982; Millington, Grabner, et al., 2007). These regions in the ankle are also commonly affected by osteochondral lesions (van Dijk et al., 2010). This could be due to a lower joint congruency in regions with thicker cartilage (Braune and Fischer, 1891). Earlier studies have reported the thickness of the cartilage to be related to the congruency of the joint (Braune and Fischer, 1891; Simon et al., 1973), whereby thin cartilage is found in the congruent ankle joint, whereas thick cartilage is found in the incongruent knee joint (Shepherd and Seedhom, 1999). In the congruent ankle joint with thin cartilage, the compressive loads are spread over a wide area, whilst decreasing the local stresses and removing the need for large deformation of the cartilage. Thicker regions in the ankle could result in lower joint congruency and malalignment may increase the contact pressure per area due changes in the distribution of stress across the joint surface. Furthermore, this could result in inadaquate containment for the fluid to support the load when the joint is exposed to high-impact forces. This may cause water to enter the microfractured areas of the subchondral bone and with continous high fluid pressure, may lead to osteolysis and large osteochondral defects (Ramsey and Hamilton, 1976; Yamamoto and Bullough, 2000; Dürr et al., 2004). Overall, cartilage thickness and its role in osteochondral defects requires further investigation to support findings by van Dijk et al. (2010) (i.e. higher thickness more likley to result in cartilage lesions).

6.5.2 Percentage Deformation of Human Ankle Cartilage

In the current study, the initial phase of testing (i.e. rate of deformation) and the equilibrium deformation were studied in the human talar and tibial cartilages. The

cumulative deformation was in agreement with previously reported deformation curves for the human ankle tissue (Mow et al., 1989), whereby a rapid rate of fluid exudation was evident at the initial phase of testing that decreased over time resulting in the load being fully supported by the solid content as equilibrium deformation was reached. Within each joint surface in the ankle joint, the highest rate of deformation (and strain rate) in the initial phase and the equilibrium deformation were found to be in the central aspect of the tibia, TibC, and posterior-medial aspect of the talus, TalPM. This suggests that both of these regions could deform more under the same load compared to the other regions in the ankle. In both regions, a faster loss of the fluid content in the initial phase of testing suggest a higher tissue permeability and the equilibrium deformation suggests a lower stiffness compared to other regions in the ankle joint. A combination of higher permeability and lower stiffness are considered as unfavourable mechanical properties as poor ability to withstand high stresses are associated with cartilage deteriorating over time (Mansour, 2009). Previous studies have suggested osteochondral defects to be commonly found in the posterior-medial aspect of the talar joint (VanDijk et al., 2010) due to the mechanisms of torsional impaction and axial loading (Berndt and Harty, 1959; Canale and Belding, 1980). As the current study identified higher deformation in TalPM and based on literature, this region in the ankle could be more vulnerable to deterioration over time.

Although no significant difference was reported across the specimens, generally, the human tibial cartilage has deformed more (7.05 %) compared to human talar cartilage (4.03 %). A higher cartilage deformation does not necessarily indicate cartilage damage, since cartilage generally tends to deform during loading (Millington et al. 2007). A higher deformation in tibial cartilage may be associated with greater load transfer under a given load. However, maintained cartilage deformation and dehydration of tissue after loading could increase the vulnerability of cartilage to accelerated degeneration with repetitive high impact forces (Song et al., 2008; Van Ginckel et al., 2013).

In the current study, a large variation in deformation output was observed across the specimens. This could be due to potential differences in the quality of the tissue studied across the three specimens, as mentioned earlier (section 6.5.1). The quality of the tissue may have become compromised during transportation from abroad and/or due to unknown freeze/thaw cycles prior to arriving to the laboratory, as noted in Figure 6-3. Such procedures may have impacted the overall state of the tissue.

The shape of the indenter needs to be carefully chosen based on the surface curvature of the cartilage for indentation testing, as otherwise a non-linear load-displacement response may be the result, as contact area could increase during loading (i.e. hemispherical indenter on a flat surface Figure 6-13B, as reported by Delaine-Smith et al. (2016). For the human ankle tissue, a flat-ended indenter was considered instead of a hemispherical indenter as the osteochondral pins extracted were rather flat (Figure 6-13C) such that a uniform contact area was assumed throughout the period of loading. Previous studies have also considered a flat ended indenter to be ideal to test osteochondral tissues (Athanasiou et al., 1995; Hons, 2009; Katta et al., 2008; Athanasiou et al., 1994). An earlier study by Medley et al. (1983) measured surface curvatures in eight cadaveric human ankle joints using a Talycontor instrument (Rank Taylor Hobson) which uses a similar technique to Talysurf (Chapter 4, section 4.4.2.2) in which a stylus pin takes measurements across the surface profile. To accurately determine curvatures in the pin or joint surface, Talysurf could be used and a comparison method between human and porcine tissues could be studied as part of future work to understand how changes in surface curvatures affect deformation output.
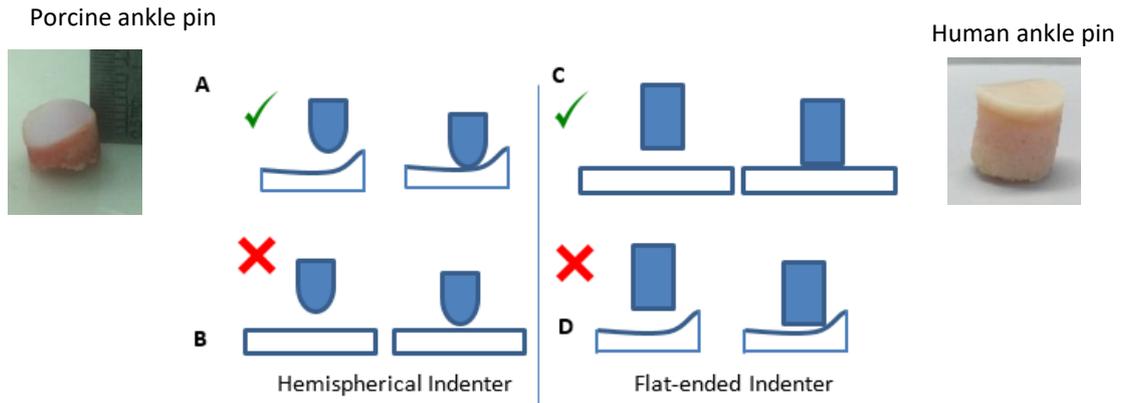
Figure 6-13: Illustration showing a comparison of flat-ended and hemispherical indenters on a curved and flat surface. A) Hemispherical indenter against a curved surface (example of porcine ankle pin of 8.5 mm in diameter); B) Hemispherical indenter against a flat surface; C) Flat-ended indenter against a flat surface (example of a human ankle pin of 8.5 mm in diameter); D) Flat-ended indenter against a curved surface.

6.5.3 Surface Roughness of Human Ankle Cartilage

In the current study, the average roughness in the talus and tibia was found to be 1.67 µm and 1.45 µm, respectively, and were comparable across both joint surfaces. Surface roughness of human ankle cartilage has not been previously reported though general roughness in human articular cartilage has been reported to range between 2 to 6 µm (Clarke et al., 1975; Sayles et al., 1979; Thomas et al., 1980; P A Smyth et al., 2012). The human ankle cartilage roughness values appear to be at the lower end of the range reported in literature. A low roughness may be a favourable factor in protecting the cartilage from damage as the joint operates within a lubricated environment whilst reducing friction. Furthermore, as the ankle joint is considered to be less sensitive to cartilage damage compared to other joints such as the knee and hip joints (Kuettner and Cole, 2005), the roughness observed in the current study may reflect that the ankle joint is less likely to be arthritic. In the current study, the average age of the three specimens tested was 59 ± 1 years and no degenerative characteristics were noted on the joint surfaces, and therefore considered as 'healthy' models. Despite an increase in roughness has been associated with an increase in age (Lotz and Loeser, 2012) and roughness in the 'damaged' model would

be generally higher than the 'healthy' model, as the cartilage surface texture would be worn out, cartilage roughening in the ankle relating to age and degeneration may be less pronounced than in other joints. A comparison of roughness between the 'healthy' model and 'damaged' model and different age groups (young versus old tissue) in the human ankle joint could be conducted to understand the changes in roughness in relation to age and state of tissue, if possible.

6.5.4 Comparison of Cartilage Thickness, Percentage Deformation and Surface Roughness in Human and Porcine Ankle Cartilage

A summary of mechanical and roughness characterisation of the human ankle and porcine ankle joints are shown in Table 6-2.

Table 6-2: Summary of thickness, deformation and surface roughness measurements in the human (n=3) and porcine tissues (n=6)

	Thickness (mm)	Deformation (%)	Surface roughness (µm)
Human (n=3)	1.76 – 1.85	3.55 – 6.24	1.46 – 1.94
Porcine (n=6)	0.52 – 0.67	8.77 – 12.22	0.41 – 0.71

In the human ankle joint, the tibial cartilage was generally thicker and underwent higher deformation than talar cartilage. This was contrary to the porcine ankle tissue (Chapter 3, section 3.5.1 and 3.5.5), whereby tibial cartilage was significantly thinner and deformed less than talar cartilage. The porcine ankle was significantly thinner, deformed significantly higher and were significantly smoother compared to the human ankle (ANOVA, $p<0.05$, $p<0.05$, $p<0.05$, respectively (Table 6-2). Such variation in results may be attributed to several factors including the differences in surface curvature, biomechanical function, age and inter-species variation. The present study investigated porcine ankle pins with a considerably higher curvature compared to human ankle pins (Figure 6-13), which may influence the joint congruity (Nickel and McLachlan, 1994; Hamrick, 1996; Hohe et al., 2002). Surface curvature may limit accurate cartilage thickness assessment as inaccurate measurements were reported with sharp curvatures using MRI imaging techniques in the human ankle

(Millington et al., 2007c). Furthermore, differences in gait patterns between porcine and human ankle joint could influence the loading pattern during walking, as the pigs are known to trot. However, due to unknown physiological load transmissions in the porcine ankle joint, any comparisons with the human ankle joint is rather limited. Furthermore, any significant differences between human and porcine tissues could be further explained by the differences in skeletal maturity. The porcine ankle joints used were immature (3 to 6 months) compared to the human ankle joints (Appendix B). This could influence the relative roughness in two ways. Firstly, the younger tissue samples may not have been at a fully developed stage, and therefore a change in roughness may be observed as the cartilage matures. Secondly, it is well known cartilage surface roughness may increase with age in humans (Loeser, 2004), relating to natural wear and tear of the joint. The relative skeletal maturity of the species (i.e. porcine and human tissue) was not studied as this study focused on readily available tissue. For accurate comparisons relative tissue maturity will need to be comparable between species.

Both species, human and porcine ankle cartilage had varied significantly in thickness, deformation and surface roughness. Due to these significant differences between both species, the immature porcine tissue was considered to be a poor representative model for tribological studies. In the future, older porcine tissues could be explored for accurate comparisons between both species. This may be challenging to identify, as the relative age group between porcine and human tissue may not be accurate due to their differences in life expectancy.

6.6 Conclusion

- Cartilage thickness, deformation and surface roughness measurements were in a comparable range between human talar and tibial cartilages (ANOVA, $p>0.05$, $p>0.05$, $p>0.05$, respectively).

- A comparison between human and porcine ankle cartilage revealed significant differences in thickness, deformation and roughness measurements (ANOVA, $p>0.05$, $p>0.05$, $p>0.05$), whereby porcine ankle cartilage was significantly thinner, deformed significantly more and was significantly lower in roughness compared to human tissue.

- Based on these current findings, immature porcine tissue was not considered as an ideal representative model for tribological studies.

Chapter 7: Overall Discussion

This thesis focused on investigating the fundamental biomechanical characteristics of ankle cartilage by adapting and developing experimental methods such as indentation and cartilage thickness methods. These investigations will improve the understanding of how ankle cartilage responds to mechanical loading and how the biological characteristics of the tissue contribute towards the biomechanical response. Determining the biomechanical properties of a 'healthy' human ankle cartilage (intact cartilage), will provide an understanding of the natural ankle joint, giving a basis for future assessment of ankle degeneration and potentially supporting future development of early interventions.

In this study, mechanical characterisation of the ankle cartilage has helped to determine several cartilage properties. This includes the determination of mechanical behaviour (e.g. cartilage deformation) using indentation methods and thickness measurements using needle probe techniques and CT methods in the porcine tissue (Chapter 3) and human tissue (Chapter 6), respectively. Such characterisation has enhanced understanding of the response of ankle cartilage to loading. Tribological properties (Chapter 4) such as the coefficient of friction and surface roughness of both porcine and human ankle cartilages were determined to address how susceptible the natural ankle joint is to damage. Biological characterisation of porcine ankle cartilage (Chapter 5) using histological analysis identified the composition and structure of the 'healthy' model, and quantitative assays were used to determine water, GAG and hydroxyproline content in the cartilage to comment on the distribution of these biological constituents in the natural cartilage.

7.1　Mechanical Characterisation of Ankle Cartilage

Cartilage thickness is an important consideration for early interventions used for treating osteochondral defects such as microfracture and grafting procedures

(Chapter, 1, section 1.4.2.2). Although there are a range of treatment options for osteochondral defects of the ankle, in some cases osteochondral grafts from the human knee joint have been used (Whittaker et al., 2005), which could result in a mismatch of cartilage thickness and affect the overall joint congruency as different joints vary in thickness, i.e. human ankle – 0.94 to 1.63 mm (Athanasiou et al., 1995; Shepherd and Seedhom, 1999), human hip – 0.32 to 3.13 mm (Shepherd and Seedhom, 1999; Wyler et al., 2009; Taylor et al., 2011) and human knee - 1.54 to 2.98 mm (Shepherd and Seedhom, 1999; Eckstein, 2004). Such procedures will need to consider whether grafts taken from other joints/species have comparable cartilage thicknesses to the joint undergoing treatment, as there may be implications for differing thicknesses that could potentially affect the overall joint congruency (Simon, 1970; Hangody et al., 2001). The current study found human ankle cartilage thicknesses to be in a similar range (1.63 ± 0.09 mm to 1.87 ± 0.20 mm, n=3) to previously reported studies in the knee as stated earlier (Shepherd and Seedhom, 1999; McLure et al., 2012; Eckstein et al., 2015); however previous studies have suggested ankle cartilage to be thinner (0.94 to 1.63 mm) than knee cartilage (1.54 to 2.98 mm) (Athanasiou et al., 1995; Shepherd and Seedhom, 1999). In the same species, i.e. human, replacing the ankle cartilage with cartilage from another joint such as the knee, could potentially affect the overall joint function due to differences in thickness. An option could be to investigate an animal tissue to replace the cartilage with comparable thickness characteristics. Although in the current study, the immature porcine ankle (3 to 6 months of age) and mature human ankle (mean 59 ± 1, Appendix B) resulted in significantly different thicknesses (mean thickness 0.59 ± 0.06 mm versus 1.75 ± 0.33 mm, human and porcine respectively), with the age/skeletal maturity matched, there is a potential to compare such features of the cartilage in the 'older' porcine ankle with the mature human ankle. With recent advancing tissue engineering techniques, xenotransplantation of using porcine chondrocytes for the treatment of human cartilage defects has been considered as autologous and allogenic chondrocytes have resulted in moderate clinical success (Sommaggio et al., 2016). The potential of such concept is yet to be further developed to determine its suitability for treating cartilage defects in the human

tissue. However, research is currently advancing in finding solutions using xenotransplantation approaches with promising techniques such as decellularised porcine ECM which was suggested to have a great potential for tissue engineering approaches for the use in human tissue (Wainwright et al., 2010; Choi et al., 2012). Therefore, a potential treatment option for early interventions to treat defects in the human tissue could be to use porcine cartilage as a repair strategy as also suggested in a recent study by Sommaggio et al. (2016). Hence, in the human ankle joint, mature porcine could be explored as this may present with comparable features (i.e. thickness) for replacing cartilage. It is important to understand any potential risks such as transfer of infectious organisms; therefore further work is required to reveal any such risks and any implications this may have on the treatment for using different cartilage thicknesses for such treatment options, which is currently unknown.

Indentation tests have been widely used to study mechanical behaviour and properties such as permeability and elastic modulus (Kempson et al., 1971; Mak et al., 1987; Mow et al., 1989; Taylor, 2012; Fermor, 2013). These compressive properties are useful for determining fluid flow behaviour in the cartilage and to understand how the cartilage responds to loading. In the current study, the human talar cartilage underwent a lower average rate of deformation in the initial phase (3.25×10^{-5} mm/s) (i.e. gradual loss of fluid content out of the tissue matrix, lower permeability) and an average lower equilibrium deformation (4.02 ± 1.34 %) (i.e. higher stiffness as tissue is less likely to deform) than the equivalent tibial cartilage (3.75×10^{-5} mm/s; 7.05 ± 3.19 %). In the human knee joint, cartilage deformation was suggested to range between 22 to 30 % (Bingham et al., 2008), which appears to be considerably higher compared to the human ankle deformation reported in the current study (2 to 11 %). With a lower deformation output observed in the current study in the human ankle joint in addition to previous studies suggesting 'favourable' biomechanical properties such as higher stiffness and lower permeability, these could all contribute towards the protection of the human ankle joint from high impact forces compared to human knee joint (Treppo et al., 2000; Kuettner and Cole,

2005). Such properties may be reasons for less primary OA cases found in the ankle joint compared with the knee joint (Huch, 2001; Kuettner and Cole, 2005).

In the current study on the porcine tissues, the opposite relationship was observed, whereby talar cartilage deformed more than tibial cartilage. Although the overall deformation trend was similar in both species to those reported in literature (Mow et al., 1989) as all samples reached an equilibrium deformation by 3600 seconds, the deformation values varied significantly between both species, whereby the human ankle cartilage deformed significantly more than the porcine ankle cartilage (ANOVA, $p<0.05$). Significant differences in deformation output across species may be attributed to a number of factors, including differences in gait patterns. Differences in gait mechanics can influence the cartilage loading pattern during walking as well as cartilage thickness due to variation in joint congruity (Von Eisenhart et al., 1999). In the human hip joint, varying joint congruity was reported to 'considerably' influence cartilage thickness throughout the joint surfaces with greatest difference of 3 mm in joint space width during gait cycle (Von Eisenhart et al., 1999). During the gait cycle, changes in cartilage thickness, could also be associated with physiological load transmission in the joint and may influence deformation output. Currently, due to unknown physiological load transmissions in the porcine ankle joint, any comparisons with the human ankle joint is rather limited. Furthermore, the typical mass of a 4-legged pig is 75 kg and a 2-legged human is 65 kg with human joints being relatively large in size compared to porcine joints. Such features could influence the weightbearing regions of the joints, their overall stability/congruity and/or deformational behaviour. Variation in joint congruity could be studied by comparing the gait patterns across species (i.e. porcine and human), which could potentially identify reasons for significant differences in the deformation output across both species in the current study.

In the current study, cartilage thickness and deformation outputs in an immature porcine model (3 to 6 months) was compared with mature human tissue (59 ± 1 year). For a given species, the age at which stage tissue maturation is reached, (whereby the growth plate is fused into the bone) depends on its lifespan. In the

porcine tissue, an age of 4 months corresponds to an age of 6 to 8 years in humans and an age of 21 months in the animal tissue corresponds to an age of 20 to 25 years in the humans (Swindle and Adams, 1988). As the expected lifespan of a pig is between 10 to 15 years, the animal tissue is expected to reach maturity at a lower age compared to human tissue (Swindle and Adams, 1988, Rieppo et al., 2009). During skeletal maturation, a gradual replacement of the original collagen network into a new framework of collagen takes place (Hunziker et al., 2007). As the animal matures skeletally, changes in the growth plates have been commonly described (Wardale and Duance, 1994; Horton et al., 1998; van der Kraan and van den Berg, 2008). Growth plates, also known as epiphyseal plates, are hyaline cartilage plates that promote bone growth and mainly consists of water, collagen and proteoglycans as with other hyaline cartilages. In most species, growth plates are present in young tissue and these close over time as maturity is reached. In young tissues, growth plates are commonly known to be vulnerable to fractures as the bone hardens over time. It can be assumed that in the immature tissue, the presence of growth plate may affect cartilage behaviour such that stiffness may change as more load is transmitted to the bone rather than cartilage. The process of skeletal growth is highly complex and is poorly understood and needs to be studied in greater detail. As various species reach skeletal maturity at different ages with human reaching maturity between 13 to 17 years, (Karimian et al., 2011) and porcine beyond 21 months (Rieppo et al., 2003), the skeletal maturity of tissues of different species (i.e. porcine versus human) will need to be comparable for understanding ankle cartilage biomechanics. Further investigation into biomechanical properties of immature and mature ankle cartilages for a given species may reveal how aging affects the tissue quality and its biomechanical properties.

7.2   Friction Characterisation of Ankle Cartilage

In the porcine ankle joint, the coefficient of friction was determined using cartilage on cartilage and cartilage on metal configurations to mimic natural conditions in the

joint and a control study, respectively. Studying the effects of friction output using metal plates could also mimic metallic implants such as HemiCAP, that are used as early interventions for treating osteochondral defects (Anderson et al., 2010; van Bergen et al., 2014). In the current study, coefficient of friction values were significantly higher using a metal plate configuration, compared to the cartilage plate configuration. Such differences were attributed to the change in fluid flow behaviour during loading. Cartilage biphasic properties (fluid phase and solid phase) play a significant role in reducing the frictional output, whilst enhancing lubrication in the joint as seen in cartilage on cartilage configurations (Forster and Fisher, 1999). Cartilage against a metal counterface resulted in a loss of fluid load support due to load transfer between the solid and fluid phases was associated with an increase in friction (Krishnan et al., 2004). Such configuration was suggested to allow depressurisation of the cartilage interstitial fluid, which flows away from the loaded region (Oungoulian et al., 2015). The metal plate in the pin on plate study was entirely flat, whereas in clinical applications the joint conformity will need to be taken into consideration for improved surface interaction. In clinical applications, the artificial material chosen for joint replacement will need to ensure friction and wear is kept to a minimum and replicate the natural properties of the cartilage as closely as possible.

The determination of contact area and pressures using pin on plate studies are important to understand how the surfaces conform during interaction and to identify stress distribution across the joint surface in natural bearings as well as in implants with metal-cartilage contacts. Investigation into contact mechanics is useful to identify how articulating surfaces respond to load transfer and predict their capabilities to transfer high loads. As implants aim to mimic natural bearings, the changes to frictional output compared to cartilage-cartilage contacts, and the effect on contact stress levels with metallic surfaces should be considered. For a localised defect repair, materials such as hydrogels (3D scaffolds) could be a better alternative to metallic counterfaces to substitute for cartilage. A recent study bu Yu et al. (2017) used a modified sodium hyaluronic acid (HA) to repair cartilage defects as HA has many unique properties such as good biocompatibility, viscoelasticity and lack of

immunogenicity. As hyaluronic acid (HA) is one of the major ingredients of ECM and involved in processes from cell proliferation to wound repair, the use of this material in treating cartilage defects has been strongly supported by other studies (Shi et al., 2016). However, such research is still emerging and further investigation is required to support these findings. A suitable material and/or treatment method to replace cartilage to restore its natural cartilage function is still ongoing research.

7.3 Biological Characterisation of Ankle Cartilage

In the human tissue, talar lesions have been reported to be more common than tibial lesions (Barnes et al., 2003). Based on this, it was hypothesised that the cellularity of the talar cartilage would be lower than the tibial cartilage, as a lower number of chondrocytes lead to poor turnover of the extracellular-matrix impacting on joint protection, as chondrocytes are responsible for the development, maintenance and repair of the matrix. Furthermore, with limited potential for chondrocyte replication, a low chondrocyte cell count could impact on its overall cartilage function. In the current study, the porcine talar cartilage had a significantly higher cellularity compared to porcine tibial cartilage. Although chondrocyte cell count has not been investigated in the human ankle tissue, the clinical problem involving the human talus may not support the current findings on the porcine talus. This suggests that the porcine talus may provide a better protective surface under high loads compared to the human talus. Such differences between species may be attributed to differences in relative maturity, as porcine cartilage was immature in the current study. Additionally, a reduction in cartilage cellularity with aging was reported to lead to abnormal cell activation and differentiation which provide a basis upon which the cartilage remodelling and destruction process could trigger the onset of OA (Lotz and Loeser, 2012).

In the porcine ankle cartilage, the overall water content, GAG and hydroxyproline content did not vary with joint region (i.e. talus and tibia). Despite a comparable water content between the porcine ankle cartilage (current study), the porcine knee cartilage (Fermor, 2013), and the human knee cartilage (Mow and Huiskes, 2005),

each joint may respond differently in supporting high loads and operate in varying mechanical environment to provide protection to the joint. The GAG content is responsible for the compressive stiffness of the cartilage (Poole et al., 2001), as immobilisation of proteoglycans as aggregates in the collagen network provides stability and rigidity in the extracellular matrix (Muir, 1995). When porcine ankle cartilage was compared to porcine knee cartilage (Fermor, 2013), differences were observed, namely the GAG content was lower in the ankle. As a decreased GAG content was suggested to act as a strong factor in the early stage development of OA in the knee and hip joints (Ericsson et al., 2009), the porcine ankle cartilage could potentially be more sensitive to damage compared to porcine knee cartilage. This was in contrast to the human tissue, as reported by Treppo et al. 2000, that highlighted a higher GAG content (3.8 % per wet weight) for the ankle tissue compared to knee cartilage (2.2 % per wet weight). Generally, the human ankle is considered to be less susceptible to cartilage disorders compared to human knee joints, which may be attributed to differences in how the joint responds to damage (i.e. repair mechanisms) (Kuettner and Cole, 2005), whereby a higher GAG content was found in ankle lesions (47.12 ± 22.24 µg/mg) compared to knee lesions (40.31 ± 14.31 µg/mg) (Aurich et al., 2005). A higher GAG content reported in the damaged ankle cartilage by Aurich et al. (2005) indicates how this may help to protect the joint in the early stages of OA compared to the knee joint. Investigation into the biological processes of ankle cartilage such as the rate of proteoglycan synthesis and cartilage repair mechanisms was beyond scope in the current study. Further work is required to understand how these biological processes in the human ankle cartilage compare to other joints, such that cartilage degeneration can be better understood.

7.4 Summary of Biomechanical Properties of Ankle Cartilage

In the current study, the biomechanical properties of the 'healthy' models of porcine and human ankle cartilages were investigated, whereby the cartilage was in its intact state with no visible damage to its surface. Generally, porcine talar cartilage was rougher and thicker and had higher cellularity; water content; hydroxyproline content and a lower GAG content compared to porcine tibial cartilage, corresponding

with a higher contact pressure, and lower contact area and co-efficient of friction. Based on these outcomes, the talar cartilage in the immature porcine tissue could be more susceptible to deterioration over time with these biomechanical properties, as greater cartilage thickness may affect the overall joint congruency (Shepherd and Seedhom, 1999), increased surface roughness could influence the tissue quality (Poon and Bhushan, 1995; Oungoulian et al., 2015) and higher water content results in greater fluid escape causing imbalance to the biphasic nature of the cartilage (Treppo et al., 2000; Kuettner and Cole, 2005), as observed in osteoarthritic cartilage (Mankin and Thrasher, 1975; Guilak et al., 1994). Biomechanical differences between talar and tibial cartilages in the porcine tissue may go some way towards explaining how these surfaces may respond differently to injury/trauma to the joint.

In the 'healthy' model (intact cartilage) of human ankle cartilage, thickness, deformation and surface roughness measurements were all comparable across talar and tibial joint surfaces. This was not in agreement with literature reporting significant topographical changes in material properties between the talus and tibia, whereby tibial cartilage was stiffer than talar cartilage (Athanasiou et al., 1995). In the current study, the tibal cartilage was generally thicker and deformed more than the talar cartilage, which are considered as unfavourable properties in protecting the joint from deterioration as greater deformation has been suggested to cause deformations of the chondrocytes and their nuclei that could potentially influence cell signalling and corresponding anabolic and catabolic responses (Guilak, 1995; Abusara et al., 2011); however to gain a better understanding of the natural properties of the human ankle cartilage, mechanical characterisation combined with biological properties such as chondrocyte distribution and cellularity could provide useful insights into its susceptibility to damage. Due to limited comparisons of biomechanical characteristics between the talus and tibia, further investigation is required to establish a link with clinical problems in the human ankle joint.

Currently, interventions for ankle cartilage repair such as grafting or metallic HemiCAP are lacking strong long-term clinical performance. In the present study, the use of metallic surfaces led to increased frictional output and surface roughness

values compared to cartilage surfaces. The biomechanical performance of metallic HemiCAP may be a cause for concern, though tribological conditions (i.e. sliding speed, conformity etc) used in the pin on plate study and those found in the metal implant were assumed to vary. As an alternative material to using metallic surfaces for cartilage repair, as previously discussed (section 7.2), hydrogels containing HA could be another approach for the replacement of ankle cartilage, however whether this material will be able to support the loads experienced in the ankle is still to be investigated. Furthermore, as an improved joint conformity between the interacting surfaces was expected to reduce friction and/or wear, for a given implant material, the conformity will need to be comparable to that observed in the natural joint between talus and tibia.

This thesis provided an insight into the fundamental cartilage properties of the ankle joint using mechanical, biological and tribological approaches. Furthermore, in preparation for the human ankle study, indentation and thickness methods were modified using porcine ankle cartilage. For the human ankle cartilage, osteochondral pins were studied as specimen preparation had no influence on the deformation outputs when whole joint study and pin study were compared (i.e. no significance reported, $p<0.05$). For the human ankle cartilage, CT method was the chosen method as this ensured tissue hydration during testing without compromising on the quality of the cartilage, whereas needle probe is a damaging technique and set-up failed to incorporate tissue hydration during testing. Using the porcine tissue in the pin on plate studies, the friction and roughness measurements were significantly higher when tested against a metal plate than a cartilage plate (ANOVA, $p>0.05$, $p>0.05$, respectively). This indicates that the material for the counterface plays a key part during joint articulation in ensuring friction and wear is kept to a minimum. Although the water content, GAG content and hydroxyproline content were comparable across talar and tibial cartilages in the porcine tissue, a significantly higher cellurarity was found in the talar cartilage. This could indicate potential differences in how the talus responds to high impact forces compared to tibial cartilage. Overall, the immature porcine cartilage was a poor representative model of the human ankle cartilage as

significant differences were reported in cartilage deformation, cartilage thickness and surface roughness measurements (ANOVA, p>0.05, p>0.05, p>0.05, respectively). Future work, outlined within the next section, is required to establish a better understanding of the human ankle cartilage by investigating biomechanical and tribological properties to support clinical findings, whereby talar lesions are more common than tibial lesions.

Chapter 8: Future Work and Conclusion

8.1 Future Work

The aim of this thesis was to develop a better understanding of key biomechanical characteristics of the natural ankle joint. Such investigation on the natural state of the cartilage i.e. 'healthy' model, helped to understand the function of the joint and comment on its sensitivity to damage. For the human ankle study, methods were developed and refined using immature porcine ankle tissues. Such investigation using immature porcine tissue provided a strong foundational ground for testing human tissue as mechanical testing such as indentation and thickness tests developed for animal tissue was translated directly into studying human tissue.

As the porcine tissues studied were immature (3 to 6 months) and the human tissues were older (mean 59 ± 1 year), in the future a comparable age group across species will need to be studied for valid comparisons. A possible option would be to study an 'older' porcine model and establish a comparison with the human tissue to study its relevance for suitability in tribological studies as mentioned earlier in Chapter 7, section 7.1.

Although this work highlighted that the pin study and whole joint study were comparable in thickness and deformation output, in future, a whole joint simulation could be helpful in understanding the tribological performance of the ankle joint. A recent study by Liu et al. (2015) investigated the biomechanical properties and tribological behaviour of a porcine knee model using a whole natural knee joint simulator. The whole joint simulation in the knee had six degrees of freedom, applied a peak load of 4500 N and had five axes of motion (flexion-extension, anterior-posterior, tibial rotation, medial-lateral and abduction-adduction) that were controlled by displacement and/or force inputs (Liu et al., 2015). For a whole joint simulation in the ankle, adapting the knee simulator with translations in directions of inversion-eversion (instead of abduction-adduction in the knee), plantar-dorsiflexion (instead of flexion-extension in the knee), medial-lateral, anterior-posterior and

internal-external rotations is proposed. A selection of other conditions that will need to be adapted to reflect the whole joint function include, the interaction and complexities of geometries (i.e. talar and tibial joint surfaces), loads, motions, biomechanics and tribological function of the ankle joint. There is great potential for investigating the tribological performance using a porcine ankle model that can be adopted for human tissue in the future to assess ankle cartilage tribology. Such *in-vitro* investigation could be used to pre-clinically assess cartilage repair interventions prior to *in-vivo* studies in the ankle joint.

In the friction study on porcine ankle cartilage, bovine knee cartilage plates were used in cartilage on cartilage configuration due to difficulties in obtaining plates from porcine ankle joint as the surface area was small and the surfaces were largely curved compared to bovine knee cartilage. The porcine ankle joint was small in size (40 mm x 30 mm x 20 mm, length, width, depth, respectively), and cartilage plates of 45 mm by 17 mm x 7 mm (length, width, depth, respectively) were required to be secured into the stainless steel bath to act as a counterface. Therefore, this was not possible, as the porcine ankle joint was too small. For a given species, as part of future work, an adjustable stainless steel bath in the pin on plate rig could be designed such that cartilage plates of different dimensions can also be tested. Depending on the plate dimensions, the sliding distance needed may vary accordingly. For human tissue, talar pins reciprocating against tibial plates and tibial pins against talar cartilage plates could be tested to determine the coefficient of friction of the tibia and talar cartilages. As the total available articular area was reported to be 1408 mm^2 of which 922 mm^2 is the central zone, 178 mm^2 is the medial zone and 308 mm^2 is the lateral zone (Kura et al., 1998), appropriate dimensions will need to be chosen for cartilage plates extracted from the human ankle joint. Furthermore, for testing the human tissue on the pin on plate rig, animal models cannot be used as its counterface (i.e. human tissue versus animal tissue), due to ethical restrictions. Therefore, for friction study, both interacting surfaces will need to be obtained from the same species (i.e. human tissue).

For indentation and friction studies, a short-term study was performed (i.e. 1-hour tests). In the future, for both methods, a long-term study of up to 24 hours testing could be explored with increased applied loads. These test conditions of long-term study could potentially mimic joint conditions in prolonged sitting/standing, especially in those with limited mobility. A long-term study with increased loads can potentially alter the biomechanics of the ankle cartilage as the tissue may experience underlying changes in the cartilage that may result in collagen disruption (i.e. change in orientation) and/or loss of GAGs in the superficial zones are this layer provides a protective layer from high loads. Any changes to the cartilage biomechanics could potentially result in cartilage breakdown.

In the future, indentation and friction studies with increased applied loads on ankle cartilage surfaces can be further analysed using histological methods to determine whether tests under such conditions indicate damage to the deeper cartilage layers. Investigation of human tissues would identify any differences in biological properties such as GAG content, chondrocyte distribution and overall structure as the quality may be affected with elevated stress levels and potential links to mechanical degradation can also be made.

In the current study, static loading was applied on the cartilage samples instead of dynamic motions to identify general contact areas and pressure distribution between pin and plate samples. However, in future studies within a whole joint model, dynamic motions should be applied to identify how the contact area and pressure is distributed under a given load over the talar and tibial joint surfaces. Such information may reveal stress distribution across the joint surface and potentially identify any mechanisms of joint failure.

Building on the current work, each of these future studies may provide a pre-clinical assessment method for evaluation of novel interventions for cartilage repair, as well as providing fundamental characteristics of the natural ankle.

8.2 Conclusion

This thesis aimed to develop a better understanding of biomechanical characteristics of the natural ankle joint. As porcine ankle joints closely represent the human ankle joints, mechanical, tribological and biological properties of the cartilage was investigated in preparation for the human ankle study. Therefore, for the human study, the porcine model was used to refine testing approaches to directly translate these into testing the human tissue to obtain cartilage deformation, thickness and surface roughness measurements. A comparison of such outcomes between both species was reported.

In the porcine and human ankle joints, a comparison between their respective talar and tibial joint surfaces were made, as talar joint was reported to be most commonly affected by lesions (van Bergen et al., 2014; Georgiannos et al., 2016) and therefore assumed to be more sensitive to deterioration. In the porcine ankle joint, the talar cartilage resulted in a higher number of cells compared to tibial cartilage, but also resulted in a higher roughness, increased water content, increased contact pressures and a lower glycosaminoglycan (GAG) content. This may indicate that the talar cartilage in the young porcine tissue to be more sensitive to deterioration over time than tibial cartilage; however lesions in this animal tissue has not been previously reported and requires further investigation. In the human ankle joint, both joint surfaces resulted in comparable cartilage thicknesses, deformation and roughness measurements suggesting that both joint surfaces may not respond any differently under a high impact load. Furthermore, as porcine and human ankle joints resulted in significant differences in mechanical characteristics such as thickness, deformation and roughness values (ANOVA, $p < 0.05$, for all comparators), the immature porcine tissue was considered to be a poor representative model for tribological studies.

The investigation of fundamental biomechanical properties of porcine and human ankle cartilage has provided an interesting insight into a relatively new area of research on the ankle cartilage. Such investigation through biomechanical and biotribological characterisation can be carried forward into the human ankle joint to

study cartilage breakdown and cartilage damage, which may be helpful in a clinical setting to potentially reveal the development of ankle osteoarthritis (OA) and to find potential treatment options for diseased ankle cartilage.

Appendix A Materials

Table 1: List of Equipment

Equipment	Model	Supplier
Automatic Pipettes	Gilson P2-P1000	Anachem Ltd
Class II safety cabinet	Heraeus 85	Kendro
Coverslip	-	Bios Europe Ltd
DPX mountant	-	Bios Europe Ltd
Freeze dryer	Modulyod-230	Thermo Savant
Histology Cassettes (Histocette)	CMB-160-030R	Thermo Fisher Scientific Ltd
Hot Plate	E18.1 hotplate	Raymond A Lamb
Hot Wax Dispenser	E66 was dispenser	Raymond A Lamb
Instron material testing machine	3365	Instron, Bucks, UK
Linear variable differential transducer (LVDT)	RDP D5-200H	Electrosence, PA, USA
Magnetic stirrer	Stuart SB161	Scientific Laboratory Systems Ltd
MicroCT Scanner	μCT100	Scano Medial AG, Basserdorf, Switzerland
Microplate spectrophotometer	Multiscan Spectrum 1500	Thermo Scientific
Microscope	Olympus BX51	Microscopes, Medical Diagnostics Systems and Olympus Patient Systems Ltd Leica
Microset Silicon Rubber Compound	Silicon mould kit, 50 ml system, 101RF	Microset
Microtome	RM2125 RTR	Leica Microsystems
Orbital Shaker	IKA KS130 basic	
piezoelectric force transducer	Part No. 060-1896-02	Electrosence, PA, USA
Plate Shaker	IKA KS130 basic	Jencons PLC
Slide holder	E102	Raymond A Lamb
Superfrost Plus Glass Slides	-	VWR International
Talysurf	Utra PGI800 Profilometer	Taylor & Hobson Ltd, Leicester, UK
Tekscan I-Scan pressure measurement system	'6900' sensors	Tekscan
Tissue Processor	TP1020	Leica Microsystems

Universal three-way angle machine vice	-	Mitchell, Fox & Co. Ltd, UK
Water Bath	Grant	Jencons PLC
Wax Oven	Windsor E18/31	Scientific Laboratory Supplies

Table 2: Chemical/reagents used throughout this study

Chemicals/Reagent	Supplier
1, 9- dimethylene blue	Sigma-Aldrich
Acetic acid	Thermo Fisher Scientific Ltd
Alcian blue solution	Atomic Scientific
Chloramine T	Sigma Aldrich
Citric Acid	VWR International
di-sodium hydrogen orthophosphate	VWR International
Eosin	VWR International
Ethanol	Thermo Fisher Scientific Ltd
Ethylenediaminetetraacetic acid (EDTA)	VWR International
Formic Acid	Sigma-Aldrich
Haematoxylin (Gills No 3)	Sigma Aldrich
Haematoxylin (Mayer's)	Thermo Fisher Scientific Ltd
Haematoxylin (Weigert's)	Atomic Scientific
Hydrochloric acid	Thermo Fisher Scientific
L-Cystine hydrochloride	Sigma Aldrich
Miller's Stain	Raymond A Lamb
Neutral buffered formalin (NBF)	Genta Medical
Oxalic Acid	VWR International
Papain powder	Sigma Aldrich
Paraffin Wax	Thermo Fisher Scientific Ltd
P-dimethylbenzaldehyde	Sigma Aldrich
Perchloric acid (BDH)	BDH
Periodic acid solution (0.1%)	Sigma Aldrich
Phosphate Buffered Saline (PBS)	MP Biomedicals (OH, United States)
Picric acid solution	Sigma Aldrich
Potassium Permanganate	Thermo Fisher Scientific Ltd
Propan-1-ol	VWR International
Schiff's reagent	Sigma Aldrich
Scott's tap water	Atomic Scientific
Sirius red	VWR International
Sodium acetate (trihydrate)	Thermo Fisher Scientific Ltd

Sodium di-hydrogen orthophosphate	VWR International
Sodium Formate	VWR International
Sodium hydroxide	VWR International
Trigene	Scientific Laboratory Supplies Ltd
Virkon	Scientific Laboratory Supplies Ltd
Xyelene	Genta Medical

Appendix B Human Cadaveric Tissue

Table 4: Human Ankle Tissue Details

Specimen number	Age	Left or Right Leg	Cause of Death	Height Unit: Feet, inches	Weight Unit: pounds	Gender	Race	Source
SPEC 1	60	Right-sided	Hepatic Cirrhosis	6' 0''	184	M	Caucasian	MedCure USA
SPEC 2	60	Right-sided	Cardiac arrest	5' 8''	134	M	Caucasian	MedCure USA
SPEC 3	58	Right-sided	Hemorrhage	5' 4''	162	F	Caucasian	MedCure USA

References

Abusara, Z., Seerattan, R., Leumann, A., Thompson, R. and Herzog, W. 2011. A novel method for determining articular cartilage chondrocyte mechanics in vivo. Journal of Biomechanics. 44(5),pp.930–934.

Abusara, Z., Von Kossel, M., Herzog, W., Gill, T., Grodzinsky, A. and Rubash, H. 2016. In Vivo Dynamic Deformation of Articular Cartilage in Intact Joints Loaded by Controlled Muscular Contractions H. A. Awad, ed. PLOS ONE. 11(1), pp. 1-12

Affatato, S., Spinelli, M., Zavalloni, M., Leardini, W. and Viceconti, M. 2008. Predictive role of the Λ ratio in the evaluation of metal-on-metal total hip replacement. Proceedings of the Institution of Mechanical Engineers, Part H: Journal of Engineering in Medicine. 222(5),pp.617–628.

Ahlberg, A., Moussa, M. and Al-Nahdi, M. 1988. On geographical variations in the normal range of joint motion. Clinical orthopaedics and related research. (234),pp.229–231.

Akkiraju, H. and Nohe, A. 2015. Role of Chondrocytes in Cartilage Formation, Progression of Osteoarthritis and Cartilage Regeneration. Journal of Developmental Biology. 3(4),pp.177–192.

Al-Hajjar, M., Jennings, L.M., Leslie, I.J. and Fisher, J. 2011. Ceramic-on-ceramic total hip replacement: influence of cup inclination angle and head position. Orthopaedic Proceedings. 93–B(SUPP I).

Alexander, A.H. and Lichtman, D.M. 1980. Surgical treatment of transchondral talar-dome fractures (osteochondritis dissecans). Long-term follow-up. The Journal of bone and joint surgery. American volume. 62(4),pp.646–52.

Anderson, D.D., Tochigi, Y., Rudert, M.J., Vaseenon, T., Brown, T.D. and Amendola, A. 2010. Effect of Implantation Accuracy on Ankle Contact Mechanics with a Metallic Focal Resurfacing Implant. J Bone Joint Surg Am. 2010 Jun; 92(6),pp.1490-500

Ando, K., Mimura, T., Matsusue, Y. and Mori, K. 2010. Opinion Statement of the Effect of Mechanical Stress on Cartilage Tissue Engineering. The Open Bone Journal. 2,pp.32–37. [Accessed 30 April 2017]. Armstrong, C.G., Lai, W.M. and Mow, V.C. 1984. An Analysis of the

Unconfined Compression of Articular Cartilage. Journal of Biomechanical Engineering. 106(2),p.165.

Arnell, R.D., Davies, P.B., Halling, J. and Whomes, T. 1991. Principles and Design Applications. London. ISBN 978-1-4684-8976-7

Ateshian, G.A. 2009. The role of interstitial fluid pressurization in articular cartilage lubrication. Journal of Biomechanics. 42(9),pp.1163–1176.

Athanasiou, Agarwal, A., Muffoletto, A., Dzida, F.J., Constantinides, G. and Clem, M. 1996. Biomechanical properties of hip cartilage in experimental animal models. Clinical orthopaedics and related research. (316),pp.254–266.

Athanasiou, K.A., Agarwal, A. and Dzida, F.J. 1994. Comparative study of the intrinsic mechanical properties of the human acetabular and femoral head cartilage. Journal of Orthopaedic Research. 12(3),pp.340–349.

Athanasiou, K.A., Rosenwasser, M.P., Buckwalter, J.A., Malinin, T.I. and Mow, V.C. 1991. Interspecies comparisons of in situ intrinsic mechanical properties of distal femoral cartilage. Journal of Orthopaedic Research. 9,pp.330–340.

Athanasiou, Niederauer, G.G. and Schenck, R.C. 1995. Biomechanical topography of human ankle cartilage. Annals of biomedical engineering. 23(5),pp.697–704.

Aurich, M., Poole, A.R., Reiner, A., Mollenhauer, C., Margulis, A., Kuettner, K.E. and Cole, A.A. 2002. Matrix homeostasis in aging normal human ankle cartilage. Arthritis and Rheumatism. 46(11),pp.2903–2910.

Aurich, M., Squires, G.R., Reiner, A., Mollenhauer, J.A., Kuettner, K.E., Poole, A.R. and Cole, A.A. 2005. Differential matrix degradation and turnover in early cartilage lesions of human knee and ankle joints. Arthritis and Rheumatism. 52,pp.112–119.

Bachus, K.N., DeMarco, A.L., Judd, K.T., Horwitz, D.S. and Brodke, D.S. 2006. Measuring contact area, force, and pressure for bioengineering applications: Using Fuji Film and TekScan systems. Medical Engineering and Physics. 28(5),pp.483–488.

Badekas, T., Takvorian, M. and Souras, N. 2013. Treatment principles for osteochondral lesions in foot and ankle. International Orthopaedics. 37(9),pp.1697–1706.

Barnes, C.J. and Ferkel, R.D. 2003. Arthroscopic debridement and drilling of osteochondral lesions of the talus. Foot and Ankle Clinics. 8(2),pp.243–257.

Barnett, C.H. and Napier, J.R. 1952. The axis of rotation at the ankle joint in man. Its influence upon the form of the talus and the mobility of the fibula. Journal of anatomy. 86,pp.1–9.

Baums, M.H., Heidrich, G., Schultz, W., Steckel, H., Kahl, E. and Klinger, H.M. 2006. Autologous chondrocyte transplantation for treating cartilage defects of the talus. The Journal of Bone and Joint Surgery. 88(2),pp.303–308.

Van Den Bekerom, M.P.J., Oostra, R.J., Alvarez, P.G. and Van Dijk, C.N. 2008. The anatomy in relation to injury of the lateral collateral ligaments of the ankle: A current concepts review. Clinical Anatomy. 21(7),pp.619–626.

Bentley, G. 2009. European instructional lectures. Vol. 9, 2009 10th EFORT Congress, Vienna, Austria. Springer. ISBN 978-3-642-00966-2.

van Bergen, C.J.A., van Eekeren, I.C.M., Reilingh, M.L., Gerards, R.M. and Dijk, C.N. van 2014. The Use of HemiCAP for the Treatment of Osteochondral Lesions. Operative Techniques in Orthopaedics. 24(3),pp.190–194.

Berndt, A.L. and Harty, M. 1959. Transchondral fractures (osteochondritis dissecans) of the talus. The Journal of bone and joint surgery. American volume. . 41–A,pp.988–1020.

Berrien, L.S.J. 1999. Biotribology : Studies of the Effects of Biochemical Environments on the Wear and Damage of Articular Cartilage Biotribology : Studies of the Effects of Biochemical Environments on the Wear and Damage of Articular Cartilage.

Berthier, Y., Vincent, L. and Godet, M. 1989. Fretting fatigue and fretting wear. Tribology International. 22(4),pp.235–242.

Bingham, J.T., Papannagari, R., Van de velde, S.K., Gross, C., Gill, T.J., Felson, D.T., Rubash, H.E. and Li, G. 2008. In vivo cartilage contact deformation in the healthy human tibiofemoral joint. Rheumatology. 47(11),pp.1622–1627.

Bonasia, D.E., Dettoni, F., Femino, J.E., Phisitkul, P., Germano, M. and Amendola, A. 2010. Total ankle replacement: why, when and how? The Iowa orthopaedic journal. 30,pp.119–30.

Boschetti, F., Pennati, G., Gervaso, F., Peretti, G.M. and Dubini, G. 2004. Biomechanical properties of human articular cartilage under compressive loads. Biorheology. 41,pp.159–166.

Boschetti, F. and Peretti, G.M. 2008. Tensile and compressive properties of healthy and osteoarthritic human articular cartilage In: Biorheology., pp. 337–344.

Bouysset, M., Tourné, Y. and Tillmann, K. 2006. Foot and Ankle in Rheumatoid Arthritis. France: Springer-Verlag.

Bowden, F.P. and Tabor, D. 2001. The Friction and Lubrication of Solids. New York: Oxford University Press.

Boyde, A. and MacOnnachie, E. 1979. Volume changes during preparation of mouse embryonic tissue for scanning electron microscopy. Scanning. 2(3),pp.149–163.

Braune, W. and Fischer, O. 1891. Die bewegungen des Kneigelenkes nach einer neuen Methode am lebendon menschen Gemessen. Des XVII, Bandes der Abhand lungen der Mathematisch. Physicchen Classe der Konigl. 11,p.1.

Brimacombe, J.M., Wilson, D.R., Hodgson, A.J., Ho, K.C.T. and Anglin, C. 2009. Effect of Calibration Method on Tekscan Sensor Accuracy. J Biomech Eng. 131:034503

Brittberg, M., Lindahl, A., Nilsson, A., Ohlsson, C., Isaksson, O. and Peterson, L. 1994. Treatment of deep cartilage defects in the knee with autologous chondrocyte transplantation. The New England journal of medicine. 331(14),pp.889–95..

Bronzino, J.D. and Schneck, D.J. 2003. Biomechanics : principles and applications. CRC Press. ISBN 9781420040029

Bruns, J. and Rosenbach, B. 1990. Pressure distribution at the ankle joint. Biomechanical factors such as trauma or overweight are discussed in relation to the aetiology of osteochondral lesions. As a consequence of the possible influence of these factors on joint loading patterns the pressure distribution on the load-bearing ank. 5,pp.153–161.

Buckwalter, J., Mankin, H.J. and Grodzinsky, A.J. 2005. Articular cartilage and osteoarthritis. Instructional course lectures. 54,pp.465–480.

Buckwalter, J., Mow, V. and Ratcliffe, A. 1994. Restoration of Injured or Degenerated Articular Cartilage. The Journal of the American Academy of Orthopaedic Surgeons. 2(August 1994),pp.192–201.

Buckwalter, J.A. and Mankin, H.J. 1998. Articular cartilage: tissue design and chondrocyte-matrix interactions. Instructional course lectures. 47,pp.477–486.

Buckwalter, J.A. and Mankin, H.J. 1997. Instructional Course Lectures, The American Academy of Orthopaedic Surgeons - Articular Cartilage. Part I: Tissue Design and Chondrocyte-Matrix Interactions. J Bone Joint Surg Am. 79(4),pp.600–11.

Buckwalter, J.A., Saltzman, C. and Brown, T. 2004. The impact of osteoarthritis: implications for research. Clinical orthopaedics and related research. (427 Suppl), pp.S6-15.

Bulstrode, C., Wilson-MacDonald, J; Eastwood, D.M., McMaster, J., Fairbank, J., Singh, P.J., Bawa, S., Gikas, P.D., Bunker, T., Giddins, G. and Blyth, M. 2011. Oxford Textbook of Trauma and Orthopaedics. New York: Oxford University Press. ISBN: 9780198569589

Burks, R.T. and Morgan, J. 1994. Anatomy of the Lateral Ankle Ligaments. The American Journal of Sports Medicine. 22(1),pp.72–77.

Calhoun, J.H., Li, F., Ledbetter, B.R. and Viegas, S.F. 1994. A comprehensive study of pressure distribution in the ankle joint with inversion and eversion. Foot & ankle international / American Orthopaedic Foot and Ankle Society [and] Swiss Foot and Ankle Society. 15,pp.125–133.

Caligaris, M. and Ateshian, G.A. 2008. Effects of sustained interstitial fluid pressurization under migrating contact area, and boundary lubrication by synovial fluid, on cartilage friction. Osteoarthritis and Cartilage. 16(10),pp.1220–1227.

Callaghan, J.J. 2003. Biomechanics of the articular cartilage and menisci of the adult knee, in The Adult Knee, Volume 1. Lippincott Williams & Wilkins. ISBN: 0-7817-3247-6.

Canale, S.T. and Belding, R.H. 1980. Osteochondral lesions of the talus. J Bone Joint Surg Am. 62(1),pp.97–102.

Caron, M., Kron, E. and Saltrick, K.R. 1999. Tibiotalar joint arthrodesis for the treatment of severe ankle joint degeneration secondary to rheumatoid arthritis. Clinics in podiatric medicine and surgery. 16(2),pp.337–61.

Chai, H.M. 2004. Joint Structure of the Ankle Complex. [Accessed 28 April 2017]. Available from: http://www.pt.ntu.edu.tw/hmchai/Kines04/KINlower/Ankle.htm.

Chew, K.T.L., Tay, E. and Yue, S.W. 2008. Osteochondral lesions of the talus. Annals of the Academy of Medicine Singapore. 37,pp.63–68.

Choo, R.J., Firminger, C., Müller, R. and Stok, K.S. 2013. Prevention of cartilage dehydration in imaging studies with a customized humidity chamber. Review of Scientific Instruments. 84(9),p.093703.

Chow, Y. 2001. Advanced arthroscopy. New York: Spring-Verlag. ISBN 0-387-98808-4

Clarke, I.C., Contini, R. and Kenedi, R.M. 1975. Friction and Wear Studies of Articular Cartilage: A Scanning Electron Microscope Study. Journal of Lubrication Technology. 97(3),pp.358–366.

Conti, S.F. and Wong, Y.S. 2002. Complications of total ankle replacement. Foot and ankle clinics. 7(4),p.791–807, vii.

Cooke, A., Dowson, D. and Wright, V. 1978. The rheology of synovial fluid and some potential synthetic lubricants for degenerate synovial joints. Engineering in Medicine. 7(66),pp.66–72.

Cooper, G. 2007. The Arthritis Handbook: The Essential Guide to a Pain-Free, Drug-Free Life. New York: DiaMedica Publications.

Cuyer, É. 2011. The Project Gutenberg eBook of The Artistic Anatomy of Animals, by Édouard Cuyer.

Daniels, T. and Thomas, R. 2008. Etiology and Biomechanics of Ankle Arthritis. Foot and Ankle Clinics. 13,pp.341–352.

Delaine-Smith, R.M., Burney, S., Balkwill, F.R. and Knight, M.M. 2016. Experimental validation of a flat punch indentation methodology calibrated against unconfined compression tests for determination of soft tissue biomechanics. Journal of mechanical behaviour of biomedical materials. 60,pp.401–415.

Demarco, A.L., Rust, D.A. and Bachus, K.N. 2000. Measuring contact pressure and contact area in orthopedic applications: fuji film vs. Tekscan. Orthopaedic Bioengineering Research Laboratory, University of Utah. Salt Lake City, Poster Session, Orthopaedic Research Society, Orlando, Florida

DiDomenico, L.A. and Anania, M.C. 2011. Total Ankle Replacements: An Overview. Clinics in Podiatric Medicine and Surgery. 28(4),pp.727–744.

DiGiovanni, C.W. and Greisberg, J. 2007. Foot and Ankle: Core Knowledge in Orthopaedics. Philadelphia, USA: Elsevier, 1st edition, ISBN 9780323076302

van Dijk, C.N., Reilingh, M.L., Zengerink, M. and van Bergen, C.J.A. 2010. Osteochondral defects in the ankle: why painful? Knee surgery, sports traumatology, arthroscopy: official journal of the ESSKA. 18(5),pp.570–80.

Doets, H.C., Brand, R. and Nelissen, R.G.H.H. 2006. Total ankle arthroplasty in inflammatory joint disease with use of two mobile-bearing designs. The Journal of bone and joint surgery. American volume. 88(6),pp.1272–84.

Dowson, D. and Wright, V. 1973. Bio-tribology. Proceedings of the Conference on The Rheology of Lubrication. The Institution of Mechanical Engineers and the British Society of Rheology, Barking, pp. 81–88.

Dumbleton, J. 1981. Tribology of Natural and Artificial Joints. Volume 1. Amsterdam: Elsevier. ISBN 9780080875675

Dürr, H.D., Martin, H., Pellengahr, C., Schlemmer, M., Maier, M. and Jansson, V. 2004. The cause of subchondral bone cysts in osteoarthrosis: a finite element analysis. Acta orthopaedica Scandinavica. 75(5),pp.554–8..

Eckstein, F. 2004. Correlation and sex differences between ankle and knee cartilage morphology determined by quantitative magnetic resonance imaging. Annals of the Rheumatic Diseases. 63(11),pp.1490–1495.

Eckstein, F., Collins, J.E., Nevitt, M.C., Lynch, J.A., Kraus, V.B., Katz, J.N., Losina, E., Wirth, W., Guermazi, A., Roemer, F.W. and Hunter, D.J. 2015. Cartilage Thickness Change as an Imaging Biomarker of Knee Osteoarthritis Progression: Data From the Foundation for the National

Institutes of Health Osteoarthritis Biomarkers Consortium. Arthritis & rheumatology. 67(12),pp.3184–3189.

El-Husseini, T.F. 2005. Viscoelastic Supplementation. Ain Shams University. [Accessed 30 April 2017]. Available from: http://www.egydoc.com/sites/Arthroclub/AC_Files/Articles/article34.htm.

El-Khoury, G.Y., Alliman, K.J., Lundberg, H.J., Rudert, M.J., Brown, T.D. and Saltzman, C.L. 2004. Cartilage Thickness in Cadaveric Ankles: Measurement with Double-Contrast Multi–Detector Row CT Arthrography versus MR Imaging. Radiology. . 233(3),pp.768–773.

Ericsson, Y.B., Tjörnstrand, J., Tiderius, C.J. and Dahlberg, L.E. 2009. Relationship between cartilage glycosaminoglycan content (assessed with dGEMRIC) and OA risk factors in meniscectomized patients. Osteoarthritis and Cartilage. 17(5),pp.565–570.

Ferkel, R.D., Zanotti, R.M., Komenda, G.A., Sgaglione, N.A., Cheng, M.S., Applegate, G.R. and Dopirak, R.M. 2008. Arthroscopic treatment of chronic osteochondral lesions of the talus: long-term results. The American journal of sports medicine. 36(9),pp.1750–1762.

Fermor, H.L. 2013. Engineering of Natural Cartilage Substitution Biomaterials. Faculty of Biological Sciences, PhD Thesis, University of Leeds, UK.

Fermor, H.L., Russell, S.L., Williams, S., Fisher, J. and Ingham, E. 2015. Development and characterisation of a decellularised bovine osteochondral biomaterial for cartilage repair. Journal of Materials Science: Materials in Medicine. 26(5).

Ferrario, V.F., Turci, M., Lovecchio, N., Shirai, Y.F. and Sforza, C. 2007. Asymmetry of the active nonweightbearing foot and ankle range of motion for dorsiflexion-plantar flexion and its coupled movements in adults. Clinical Anatomy. 20(7),pp.834–842.

Flavin, R., Coleman, S.C., Tenenbaum, S. and Brodsky, J.W. 2013. Comparison of gait after total ankle arthroplasty and ankle arthrodesis. Foot & ankle international. / American Orthopaedic Foot and Ankle Society [and] Swiss Foot and Ankle Society. 34(10),pp.1340–1348.

Forster, H. and Fisher, J. 1999. The influence of continuous sliding and subsequent surface wear on the friction of articular cartilage. Proceedings of the Institution of Mechanical Engineers, Part H: Journal of Engineering in Medicine. 213(4),pp.329–345.

Forster, H. and Fisher, J. 1996. The influence of loading time and lubricant on the friction of articular cartilage. Proceedings of the Institution of Mechanical Engineers. Part H, Journal of engineering in medicine. 210,pp.109–119.

Fox, A.J.S., Bedi, A. and Rodeo, S.A. 2009. The basic science of articular cartilage: structure, composition, and function. Sports health. 1(6),pp.461–8.

Freeman, M.E., Furey, M.J., Love, B.J. and Hampton, J.M. 2000. Friction, wear, and lubrication of hydrogels as synthetic articular cartilage In: Wear., pp. 129–135.

Freeman, P. 1962. Lubrication and Friction. Isaac Pitman & Sons, London

Furey, M. 1995. Joint Lubrication Biomedical In: J. Bronzino, ed. Biomedical Engineering Handbook. Boca Raton: CRC Press, pp. 333–351.

Furey, M.J. and Burkhardt, B.M. 1997. Biotribology: Friction, wear, and lubrication of natural synovial joints. Lubrication Science. 9(3),pp.255–271.

Georgiannos, D., Bisbinas, I. and Badekas, A. 2016. Osteochondral transplantation of autologous graft for the treatment of osteochondral lesions of talus: 5-to 7-year follow-up. Knee Surg Sports Traumatol Arthroscopy. 24(12), pp. 3722-3729.

Giannini, S., Buda, R., Ruffilli, A., Cavallo, M., Pagliazzi, G., Bulzamini, M.C., Desando, G., Luciani, D. and Vannini, F. 2014. Arthroscopic autologous chondrocyte implantation in the ankle joint. Knee Surgery, Sports Traumatology, Arthroscopy. 22(6),pp.1311–1319.

Van Ginckel, A., Verdonk, P., Victor, J. and Witvrouw, E. 2013. Cartilage Status in Relation to Return to Sports After Anterior Cruciate Ligament Reconstruction. The American Journal of Sports Medicine. 41(3),pp.550–559.

Glauert, A.M. and Lewis, P.R. 2014. Biological Specimen Preparation for Transmission Electron Microscopy. Princeton University Press. ISBN 0691007497

Glazebrook, M., Daniels, T., Younger, A., Foote, C.J., Penner, M., Wing, K., Lau, J., Leighton, R. and Dunbar, M. 2008. Comparison of health-related quality of life between patients with end-stage ankle and hip arthrosis. The Journal of bone and joint surgery. American volume. 90(3),pp.499–505.

Gleghorn, J.P. and Bonassar, L.J. 2008. Lubrication mode analysis of articular cartilage using Stribeck surfaces. Journal of Biomechanics. 41(9),pp.1910–1918.

Golanó, P., Vega, J., de Leeuw, P.A.J., Malagelada, F., Manzanares, M.C., Götzens, V. and van Dijk, C.N. 2016. Anatomy of the ankle ligaments: a pictorial essay. Knee Surgery, Sports Traumatology, Arthroscopy. 24(4),pp.944–956.

Goodall, R.H., Darras, L.P. and Purnell, M.A. 2015. Accuracy and precision of silicon-based impression media for quantitative areal texture analysis. Scientific reports. . 5,p.10800.

Gottardi, R., Hansen, U., Raiteri, R., Loparic, M., Düggelin, M., Mathys, D., Friederich, N.F., Bruckner, P. and Stolz, M. 2016a. Supramolecular Organization of Collagen Fibrils in Healthy and Osteoarthritic Human Knee and Hip Joint Cartilage J. P. R. O. Orgel, ed. PLOS ONE. 11(10),p.e0163552.

Gottardi, R., Hansen, U., Raiteri, R., Loparic, M., Düggelin, M., Mathys, D., Friederich, N.F., Bruckner, P. and Stolz, M. 2016b. Supramolecular Organization of Collagen Fibrils in Healthy and Osteoarthritic Human Knee and Hip Joint Cartilage J. P. R. O. Orgel, ed. PLOS ONE. 11(10),p.e0163552.

Gough, C.S. 2013. The Biology of the Ovine Functional Spinal Unit : Facet Cartilage and Intervertebral Disc. PhD Thesis, University of Leeds, UK.

Gougoulias, N.E., Khanna, A. and Maffulli, N. 2009. History and evolution in total ankle arthroplasty. British Medical Bulletin. 89(1),pp.111–151.

Grady, J. and Sanchez, P. 2017. Addressing Osteochondral Lesions Of The Talus | Podiatry Today. Podiatry Today. 30(4).

Graindorge, S.L. and Stachowiak, G.W. 2000. Changes occurring in the surface morphology of articular cartilage during wear In: Wear., pp. 143–150.

Gray, H. 1918. Anatomy of the human body, 20th ed. Philadelphia: Lea & Febiger. ISBN 139781782124269

Guerne, P., Blanco, F., Kaelin A., Desgeorges A. and Lotz, M. 1995. Growth factor responsiveness of human articular chondrocytes in aging and development. Arthritis and rheumatism. 38(7),pp.960–968.

Guilak, F. 1995. Compression-induced changes in the shape and volume of the chondrocyte nucleus. Journal of Biomechanics. 28(12),pp.1529–1541.

Guilak, F., Ratcliffe, A., Lane, N., Rosenwasser, M.P. and Mow, V.C. 1994. Mechanical and Biochemical Changes in the Superficial Zone of Articular Cartilage in Canine Experimental Osteoarthritis. Journal of Orthopaedic Research, The Journal of Bone and Joint Surgery. 12(4),pp.474-84.

Hamrick, M.W. 1996. Articular size and curvature as determinants of carpal joint mobility and stability in strepsirhine primates. Journal of Morphology. 230(2),pp.113–127.

Hamrock, B.H.J., Schmid, S.R. and Jacobson, B. 1994. Lubrication Regimes In: Fundamentals of Fluid Film Lubrication. USA: Marcel Dekker, Inc. ISBN 9780824753719

Hangody, L., Kish, G., Kárpáti, Z., Szerb, I. and Udvarhelyi, I. 1997. Arthroscopic autogenous osteochondral mosaicplasty for the treatment of femoral condylar articular defects. A preliminary report. Knee surgery, sports traumatology, arthroscopy : official journal of the ESSKA. 5(4),pp.262–267.

Hangody, L., Kish, G., Kárpáti, Z., Udvarhelyi, I., Szigeti, I. and Bély, M. 1998. Mosaicplasty for the treatment of articular cartilage defects: application in clinical practice. Orthopedics. 21(7),pp.751–756.

Hangody, L., Kish, G., Módis, L., Szerb, I., Gáspár, L., Diószegi, Z. and Kendik, Z. 2001. Mosaicplasty for the Treatment of Osteochondritis Dissecans of the Talus: Two to Seven Year Results in 36 Patients. Foot & Ankle International. 22(7),pp.552–558

Hangody, L., Ráthonyi, G.K., Duska, Z., Vásárhelyi, G., Füles, P. and Módis, L. 2004. Autologous Osteochondral Mosaicplasty. Journal of Bone and Joint Surgery. 86–A, Supp

Hannon, C.P., Smyth, N.A., Murawski, C.D., Savage-Elliott, I., Deyer, T.W., Calder, J.D.F. and Kennedy, J.G. 2014. Osteochondral lesions of the talus. Bone & Joint Journal. 96–B(2).

Hashimoto, T. and Inokuchi, S. 1997. A kinematic study of ankle joint instability due to rupture of the lateral ligaments. Foot and Ankle International. 18(11),pp.729–734.

Hattori, K., Takakura, Y., Ohgushi, H., Habata, T., Uematsu, K., Takenaka, M. and Ikeuchi, K. 2004. Which cartilage is regenerated, hyaline cartilage or fibrocartilage? Non-invasive ultrasonic evaluation of tissue-engineered cartilage. Rheumatology. 43(9),pp.1106–1108.

Hayes, A., Tochigi, Y. and Saltzman, C.L. 2006. Ankle morphometry on 3D-CT images. The Iowa orthopaedic journal. 26,pp.1–4.

Hendrickx, R.P.M., Stufkens, S. a. S., de Bruijn, E.E., Sierevelt, I.N., van Dijk, C.N. and Kerkhoffs, G.M.M.J. 2011. Medium- to Long-Term Outcome of Ankle Arthrodesis. Foot & Ankle International. 32(10),pp.940–947.

Hermans, J.J., Beumer, A., de Jong, T.A.W. and Kleinrensink, G.-J. 2010. Anatomy of the distal tibiofibular syndesmosis in adults: a pictorial essay with a multimodality approach. Journal of anatomy. 217(6),pp.633–45.

Herregodts, S., De Baets, P., Victor, J. and Verstraete, M.A. 2015. Use of Tekscan pressure sensors for measuring contact pressures in the human knee joint. Belgium. Sustain. Constr. Des. 6(2):8–10, 2005.

Hertel, J. 2002. Functional Anatomy, Pathomechanics, and Pathophysiology of Lateral Ankle Instability. Journal of athletic training. 37(4),pp.364–375.

Hicks, J.H. 1953. The mechanics of the foot. I. The joints. Journal of anatomy. 87(4),pp.345–57.

Hintermann, B. 1999. Short- and mid-term results with the STAR total ankle prosthesis. Der Orthopäde. 28(9),pp.792–803.

Hirose, K., Murakami, G., Minowa, T., Kura, H. and Yamashita, T. 2004. Lateral ligament injury of the ankle and associated articular cartilage degeneration in the talocrural joint: Anatomic study using elderly cadavers. Journal of Orthopaedic Science. 9(1),pp.37–43.

Hlavácek, M. 1999. Lubrication of the human ankle joint in walking with the synovial fluid filtrated by the cartilage with the surface zone worn out: steady pure sliding motion. Journal of biomechanics. 32(10),pp.1059–69.

Hlaváček, M. 2000. Squeeze-film lubrication of the human ankle joint with synovial fluid filtrated by articular cartilage with the superficial zone worn out. Journal of Biomechanics. 33,pp.1415–1422.

Hohe, J., Ateshian, G., Reiser, M., Englmeier, K.H. and Eckstein, F. 2002. Surface size, curvature analysis, and assessment of knee joint incongruity with MRI in vivo. Magnetic Resonance in Medicine. 47(3),pp.554–561.

Hons, L.M. 2009. Tribological Investigation of Articular Cartilage Substitution in the Medial Compartmental Knee. PhD Thesis, University of Leeds, UK.

Horisberger, M., Hintermann, B. and Valderrabano, V. 2009. Alterations of plantar pressure distribution in posttraumatic end-stage ankle osteoarthritis. Clinical Biomechanics. 24,pp.303–307.

Horisberger, M., Valderrabano, V. and Hintermann, B. 2009. Posttraumatic ankle osteoarthritis after ankle-related fractures. Journal of orthopaedic trauma. 23,pp.60–67.

Horton, W.E., Bennion, P. and Yang, L. 2006. Cellular, molecular, and matrix changes in cartilage during aging and osteoarthritis. Journal of musculoskeletal & neuronal interactions. 6(4),pp.379–81.

Horton, W.E., Feng, L. and Adams, C. 1998. Chondrocyte apoptosis in development, aging and disease. Matrix Biology. 17(2),pp.107–115.

Hou, J.S., Mow, V.C., Lai, W.M. and Holmes, M.H. 1992. An analysis of the squeeze-film lubrication mechanism for articular cartilage. Journal of Biomechanics. 25(3),pp.247–259.

Huch, K. 2001. Knee and ankle: Human joints with different susceptibility to osteoarthritis reveal different cartilage cellularity and matrix synthesis in vitro. Archives of Orthopaedic and Trauma Surgery. 121(6),pp.301–306.

Hunt, S.A. and Sherman, O. 2003. Arthroscopic treatment of osteochondral lesions of the talus with correlation of outcome scoring systems. Arthroscopy - Journal of Arthroscopic and Related Surgery. 19(4),pp.360–367.

Hunziker, E.B., Kapfinger, E. and Geiss, J. 2007. The structural architecture of adult mammalian articular cartilage evolves by a synchronized process of tissue resorption and neoformation during postnatal development. Osteoarthritis and cartilage. 15(4),pp.403–13.

Hunziker, E.B., Quinn, T.M. and Häuselmann, H.J. 2002. Quantitative structural organization of normal adult human articular cartilage. Osteoarthritis and Cartilage. 10(7),pp.564–572.

Huson, A. 1987. Joints and movements of the foot: terminology and concepts. Acta Morphol Neerl Scand. 25,pp.117–130.

Imhof, H., Sulzbacher, I., Grampp, S., Czerny, C., Youssefzadeh, S. and Kainberger, F. 2000. Subchondral bone and cartilage disease: a rediscovered functional unit. Investigative radiology. 35(10),pp.581–8.

International Organisation for Standardisation 2015. Specification of Parameters.

Ivins, D. 2006. Acute ankle sprain: an update. American family physician. . 74(10),pp.1714–20.

Jadin, K.D., Wong, B.L., Bae, W.C., Li, K.W., Williamson, A.K., Schumacher, B.L., Price, J.H. and Sah, R.L. 2005. Depth-varying density and organization of chondrocytes in immature and mature bovine articular cartilage assessed by 3d imaging and analysis. The journal of histochemistry and cytochemistry : official journal of the Histochemistry Society. 53(9),pp.1109–19.

Jallali, N., Ridha, H., Thrasivoulou, C., Underwood, C., Butler, P.E.M. and Cowen, T. 2005. Vulnerability to ROS-induced cell death in ageing articular cartilage: The role of antioxidant enzyme activity. Osteoarthritis and Cartilage. 13(7),pp.614–622.

Jin, Z.M., Pickard, J.E., Forster, H., Ingham, E. and Fisher, J. 2000. Frictional behaviour of bovine articular cartilage. Biorheology. 37,pp.57–63.

Johnson, K.L. and Kenneth L. 1987. Contact mechanics. Cambridge University Press. ISBN 978 0521347969

Julkunen, P., Harjula, T., Iivarinen, J., Marjanen, J., Seppänen, K., Närhi, T., Arokoski, J., Lammi, M.J., Brama, P.A., Jurvelin, J.S. and Helminen, H.J. 2009. Biomechanical, biochemical and structural correlations in immature and mature rabbit articular cartilage. Osteoarthritis and Cartilage. 17(12),pp.1628–1638.

Junqueira, L.C., Montes, G.S. and Sanchez, E.M. 1982. The influence of tissue section thickness on the study of collagen by the Picrosirius-polarization method. Histochemistry. 74(1),pp.153–6.

Kääb, M.J., Nötzli, H.P., Clark, J., Ap Gwynn, I. and Kääb, M.J. 1998. Dimensional changes of articular cartilage during immersion-freezing and freeze-substitution for scanning electron microscopy. 12(3),pp.465–474.

Karimian, E., Chagin, A.S. and Sävendahl, L. 2011. Genetic regulation of the growth plate. Frontiers in endocrinology. 2,p.113.

Katta, J. 2007. Self-assembling Peptide Networks for Treatment of Cartilage Degenerative Diseases PhD Thesis, University of Leeds, UK.

Katta, J., Jin, Z., Ingham, E. and Fisher, J. 2009. Effect of nominal stress on the long-term friction, deformation and wear of native and glycosaminoglycan deficient articular cartilage. Osteoarthritis and Cartilage. 17,pp.662–668.

Katta, J., Stapleton, T., Ingham, E., Jin, Z.M. and Fisher, J. 2008. The effect of glycosaminoglycan depletion on the friction and deformation of articular cartilage. Proceedings of the Institution of Mechanical Engineers. Part H, Journal of engineering in medicine. 222,pp.1–11.

Kelikian, A.S., Sarrafian, S.K. and Sarrafian, S.K. 2011. Sarrafian's anatomy of the foot and ankle: descriptive, topographical, functional. Third edition, LWW. ISBN 978-0781797504

Kempson, G.E. 1991. Age-related changes in the tensile properties of human articular cartilage: a comparative study between the femoral head of the hip joint and the talus of the ankle joint. Biochimica et Biophysica Acta (BBA) - General Subjects. 1075(3),pp.223–230.

Kempson, G.E., Spivey, C.J., Swanson, S.A. V. and Freeman, M.A.R. 1971. Patterns of cartilage stiffness on normal and degenerate human femoral heads. Journal of Biomechanics. 4(6).

Kimizuka, M., Kurosawa, H. and Fukubayashi, T. 1980. Load-bearing pattern of the ankle joint - Contact Area and Pressure Distribution. Archives of Orthopaedic and Traumatic Surgery. 96,pp.45–49.

Kladny, B., Bail, H., Swoboda, B., Schiwy-Bochat, H., Beyer, W.F. and Weseloh, G. 1996. Cartilage thickness measurement in magnetic resonance imaging. Osteoarthritis and cartilage. 4(3),pp.181–6.

Kleipool, R.P. and Blankevoort, L. 2010. The relation between geometry and function of the ankle joint complex: A biomechanical review. Knee Surgery, Sports Traumatology, Arthroscopy. 18,pp.618–627.

Kobayashi, S., Yonekubo, S. and Kurogouchi, Y. 1996. Cryoscanning electron microscopy of loaded articular cartilage with special reference to the surface amorphous layer. Journal of anatomy. 188 (Pt 2),pp.311–322.

Kobayashiv, S. and Kurogouchf, Y. 1995. Cryoscanning electron microscopic study of the surface amorphous layer of articular cartilage. J. Anat. 187,pp.429–444.

Kono, M., Takao, M., Naito, K., Uchio, Y. and Ochi, M. 2006. Retrograde drilling for osteochondral lesions of the talar dome. The American journal of sports medicine. 34(9),pp.1450–6.

Koo, S., Gold, G.E., Andriacchi, T.P., Nakanishi, K., Sugano, N., Kubota, T. and al., et 2005. Considerations in measuring cartilage thickness using MRI: factors influencing reproducibility and accuracy. Osteoarthritis and cartilage. 13(9),pp.782–9.

Kozanek, M., Rubash, H.E., Li, G. and de Asla, R.J. 2009. Effect of post-traumatic tibiotalar osteoarthritis on kinematics of the ankle joint complex. Foot & ankle international / American Orthopaedic Foot and Ankle Society [and] Swiss Foot and Ankle Society. 30,pp.734–740.

van der Kraan, P.M. and van den Berg, W.B. 2008. Osteoarthritis in the context of ageing and evolution. Loss of chondrocyte differentiation block during ageing. Ageing Research Reviews. 7(2),pp.106–113.

Krishnan, R., Kopacz, M. and Ateshian, G. A. 2004. Experimental verification of the role of interstitial fluid pressurization in cartilage lubrication. Journal of orthopaedic research : official publication of the Orthopaedic Research Society. 22(3),pp.565–570.

Krishnan, R., Mariner, E.N. and Ateshian, G.A. 2005. Effect of dynamic loading on the frictional response of bovine articular cartilage. Journal of Biomechanics. 38(8),pp.1665–1673.

Kuettner, K.E. and Cole, A.A. 2005. Cartilage degeneration in different human joints. Osteoarthritis and cartilage / OARS, Osteoarthritis Research Society. 13(2),pp.93–103.

Kugan, R., Aslam, N., Bose, D. and McNally, M.A. 2013. Outcome of arthrodesis of the hindfoot as a salvage procedure for complex ankle pathology using the ilizarov technique. Bone and Joint Journal. 95B(3),pp.371–377.

Kura, H., Kitaoka, H.B., Luo, Z.-P. and An, K.-N. 1998. Measurement of surface contact area of the ankle joint. Clinical biomechanics (Bristol, Avon). 13,pp.365–370..

Kutzner, I., Heinlein, B., Graichen, F., Bender, A., Rohlmann, A., Halder, A., Beier, A. and Bergmann, G. 2010a. Loading of the knee joint during activities of daily living measured in vivo in five subjects. Journal of Biomechanics. 43(11),pp.2164–2173.

Kutzner, I., Heinlein, B., Graichen, F., Bender, A., Rohlmann, A., Halder, A., Beier, A. and Bergmann, G. 2010b. Loading of the knee joint during activities of daily living measured in vivo in five subjects. Journal of Biomechanics. 43(11),pp.2164–2173.

Latif, M.J. 2011. Characterisation and Modelling of Spinal Facet Joints. Phd Thesis.

Lee, T.K. and Maleski, R. 2002. Physical examination of the ankle for ankle pathology. Clinics in podiatric medicine and surgery. 19(2),p.251–69, vi.

Lees, D. and Partington, P. 2016. Articular cartilage. Orthopaedics and Trauma. 30(3),pp.265–272.

Li, L.P., Buschmann, M.D. and Shirazi-Adl, A. 2003. Strain-rate Dependent Stiffness of Articular Cartilage in Unconfined Compression. Journal of Biomechanical Engineering. 125(2),pp161.

Li, Y., Wei, X., Zhou, J. and Wei, L. 2013. The age-related changes in cartilage and osteoarthritis. BioMed Research International. 2013, ID: 916530, pp.12

Lindsjö, U. 1985. Operative treatment of ankle fracture-dislocations. A follow-up study of 306/321 consecutive cases. Clinical orthopaedics and related research. (199),pp.28–38.

Linn, F.C. and Sokoloff, L. 1965. Movement and composition of interstitial fluid of cartilage. Arthritis and rheumatism. 8(4),pp.481–494.

Lipshitz, H., Etheredge, R. and Glimcher, M.J. 1975. In vitro wear of articular cartilage. The Journal of bone and joint surgery. American volume. 57(4),pp.527–34.

Lipshitz, H. and Glimcher, M.J. 1974. A technique for the preparation of plugs of articular cartilage and subchondral bone. Journal of Biomechanics. 7(3),pp.293-IN18

Lipshitz, H. and Glimcher, M.J. 1979. In vitro studies of the wear of articular cartilage II. Characteristics of the wear of articular cartilage when worn against stainless steel plates having characterized surfaces. Wear. 52(2),pp.297–339.

Liu, A., Jennings, L.M., Ingham, E. and Fisher, J. 2015. Tribology studies of the natural knee using an animal model in a new whole joint natural knee simulator. Journal of Biomechanics. 48(12), pp.3004–3011.

Lizhang, J., Fisher, J., Jin, Z., Burton, A. and Williams, S. 2011. The effect of contact stress on cartilage friction, deformation and wear. Proceedings of the Institution of Mechanical Engineers, Part H: Journal of Engineering in Medicine. 225(5),pp.461–475.

Loeser, R.F. 2009. Aging and osteoarthritis: the role of chondrocyte senescence and aging changes in the cartilage matrix. Osteoarthritis and cartilage / OARS, Osteoarthritis Research Society. 17(8),pp.971–9.

Loeser, R.F. 2004. Aging Cartilage and Osteoarthritis--What's the Link? Science of Aging Knowledge Environment. (29),pp.pe31-pe31.

Long, D., Blake, S., Song, X.-Y., Lark, M. and Loeser, R.F. 2008. Human articular chondrocytes produce IL-7 and respond to IL-7 with increased production of matrix metalloproteinase-13. Arthritis research & therapy. 10(1),p.R23.

Lord, G. and Marotte, J.H. 1973. [Total ankle prosthesis. Technic and 1st results. Apropos of 12 cases]. Revue de chirurgie orthopedique et reparatrice de l'appareil moteur. 59(2),pp.139–51.

Lotz, M. and Loeser, R.F. 2012. Effects of aging on articular cartilage homeostasis. Bone. 51(2),pp.241–8.

Lu, X.L. and Mow, V.C. 2008. Biomechanics of articular cartilage and determination of material properties. Medicine and Science in Sports and Exercise. 40,pp.193–199.

Lundberg, A., Svensson, O.K., Nemeth, G. and Selvik, G. 1989. The axis of rotation of the ankle joint. Journal of Bone & Joint Surgery, British Volume. 71–B,pp.94–99.

Mak, A.F., Lai, W.M. and Mow, V.C. 1987. Biphasic indentation of articular cartilage-I. Theoretical analysis. Journal of Biomechanics. 20(7),pp.703–714.

Mak, M., Jin, Z., Fisher, J. and Stewart, T.D. 2011. Influence of Acetabular Cup Rim Design on the Contact Stress During Edge Loading in Ceramic-on-Ceramic Hip Prostheses. Journal of Arthroplasty. 26(1),pp.131–136.

Mankin, H.J. and Thrasher, A.Z. 1975. Water content and binding in normal and osteoarthritic human cartilage. The Journal of bone and joint surgery. American volume. 57(1),pp.76–80.

Mansour, J.M. 2009. Biomechanics of Cartilage In: Kinesiology: the mechanics and pathomechanics of human movement.,pp. 66–79.

Maroudas, A. and Bullough, P. 1968. Permeability of articular cartilage. Nature. 219(5160),pp.1260–1261.

Martino, L.J. 2013. Gross Anatomy. [Accessed 28 April 2017]. Available from: https://academic.amc.edu/martino/grossanatomy/site/Medical/CASES/Lower limb/POP_UPS/eversion injuryanspop_up6.htm.

McCann, L., Ingham, E., Jin, Z., Fisher, J., Maschek, H., Erhardt, W. 2009. Influence of the meniscus on friction and degradation of cartilage in the natural knee joint. Osteoarthritis and cartilage. 17(8),pp.995–1000.

McCutchen, C.W. 1983. Joint lubrication. Bulletin of the Hospital for Joint Diseases Orthopaedic Institute. 43,pp.118–129.

McCutchen, C.W. 1962. The frictional properties of animal joints. Wear. 5,pp.1–17.

McGann, M.E., Vahdati, A. and Wagner, D.R. 2012. Methods to assess in vitro wear of articular cartilage. Proceedings of the Institution of Mechanical Engineers. Part H, Journal of engineering in medicine. 226(8),pp.612–22.

McGavin, M.D. 2014. Factors Affecting Visibility of a Target Tissue in Histologic Sections. Veterinary Pathology. 51(1),pp.9–27.

McLure, S. 2012. Improving Models for Translational Research in Osteoarthritis. PhD Thesis, University of Leeds, UK.

McLure, S.W.D., Fisher, J., Conaghan, P.G. and Williams, S. 2012. Regional cartilage properties of three quadruped tibiofemoral joints used in musculoskeletal research studies.

Proceedings of the Institution of Mechanical Engineers, Part H: Journal of Engineering in Medicine. 226(8),pp.652–656.

McNary, S.M., Athanasiou, K.A. and Reddi, A.H. 2012. Engineering lubrication in articular cartilage. Tissue engineering. Part B, Reviews. 18(2),pp.88–100.

Medley, J.B. 1981. The Lubrication of Normal Human Ankle Joints. PhD Thesis, University of Leeds, UK.

Meng, Q., Liu, F., Fisher, J. and Jin, Z. 2013. Contact mechanics and lubrication analyses of ceramic-on-metal total hip replacements In: Tribology International., pp. 51–60.

Michael, J.M., Golshani, A., Gargac, S. and Goswami, T. 2008. Biomechanics of the ankle joint and clinical outcomes of total ankle replacement. Journal of the Mechanical Behavior of Biomedical Materials. 1,pp.276–294.

Miller, M.D. 2012. Review of orthopaedics. Sixth edition, Elsevier/Saunders. ISBN 9781455737383

Millington, S. 2008. Quantitative Stereophotogrammetric and MRI Evaluation of Ankle Articular Cartilage and Ankle Joint Contact Characteristics. PhD Thesis, School of Medical and Surgical Sciences, University of Nottingham

Millington, S., Grabner, M., Wozelka, R., Anderson, D.D., Hurwitz, S.R. and Crandall, J.R. 2007a. Quantification of ankle articular cartilage topography and thickness using a high resolution stereophotography system. Osteoarthritis and Cartilage. 15(2), pp.205–211.

Millington, S., Grabner, M., Wozelka, R., Hurwitz, S. and Crandall, J. 2007b A stereophotographic study of ankle joint contact area. Journal of Orthopaedic Research. 25(11), pp.1465–1473.

Millington, S., Li, B., Tang, J., Trattnig, S., Crandall, J.R., Hurwitz, S.R. and Acton, S.T. 2007c. Quantitative and topographical evaluation of ankle articular cartilage using high resolution MRI. Journal of Orthopaedic Research. 25(2), pp.143–151.

Milner, P.E., Parkes, M., Puetzer, J.L., Chapman, R., Stevens, M.M., Cann, P. and Jeffers, J.R.T. 2018. A low friction, biphasic and boundary lubricating hydrogel for cartilage replacement. Acta Biomaterialia. 65,pp.102–111.

Mirzayan, R. 2006. Basic Science In: L. Peterson, ed. Cartilage Injury in the Athlete. New York, USA: Thieme Medical Publishers, Inc., pp. 1–31.

Mow, C. Van and Hung, T.C. 2001. Biomechanics of Articular Cartilage In: Basic Biomechanics of the Musculoskeletal System., pp. 61–69.

Mow, V. and Hung, C. 2001. Biomechanics of Articular Cartilage In: M. Nordin and V. Frankel, eds. Basic Biomechanics of the Musculoskeletal System. Philadelphia: Lippincott Williams & Wilkins, pp. 60–93.

Mow, V.C. and Ateshian, G. 1997. Lubrication and Wear of Diarthrodial Joints In: V. C. Mow and W. C. Hayes, eds. Basic Orthopaedic Biomechanics. Philadelphia: Lippincott-Raven Publishers.

Mow, V.C., Gibbs, M.C., Lai, W.M., Zhu, W.B. and Athanasiou, K.A. 1989. Biphasic indentation of articular cartilage--II. A numerical algorithm and an experimental study. Journal of biomechanics. 22,pp.853–861.

Mow, V.C., Holmes, M.H. and Michael Lai, W. 1984. Fluid transport and mechanical properties of articular cartilage: A review. Journal of Biomechanics. 17(5),pp.377–394.

Mow, V.C. and Huiskes, R. 2005. Basic orthopaedic biomechanics; mechano-biology, Lippincott Williams & Wilkins. ISBN 9780781739337

Mundt, L.A. and Shanahan, K. 2010. Textbook of Routine Urinalysis and Body Fluids. Philadelphia: Lippincott Williams & Wilkins.

Myant, C. 2013. In contact observation of model synovial fluid lubricating mechanisms. Tribology International. 63,pp.97–104.

Nam, S.J. and Kehtarnavaz, N. 2012. Flash shadow detection and removal in stereo photography. IEEE Transactions on Consumer Electronics. 58(2),pp.205–211.

National Joint Registry 2013. National Joint Registry for England, Wales and Northern Ireland: 10th Annual Report 2013. UK.

Neu, C.P., Komvopoulos, K. and Reddi, H. 2008. The interface of functional biotribology and regenerative medicine in synovial joints. Tissue engineering. Part B, Reviews. 14(3),pp.235–47.

Nickel, J.C. and McLachlan, K.R. 1994. An analysis of surface congruity in the growing human temporomandibular joint. Archives of Oral Biology. 39(4),pp.315–321.

Nigg, B.M., Fisher, V., Allinger, T.L., Ronsky, J.R. and Engsberg, J.R. 1992. Range of motion of the foot as a function of age. Foot & ankle. 13(6),pp.336–343.

Nordin, M. and Frankle, V. 2001. Biomechanical behaviour of articular cartilage In: J. Butler, ed. Basic Biomechanics of the Musculoskeletal System. Pennsylvania, USA: Lippincott Williams & Wilkins, pp. 70–78.

Norkus, S.A. and Floyd, R.T. 2001. The anatomy and mechanisms of syndesmotic ankle sprains. Journal of athletic training. 36(1),pp.68–73.

Northwood, E. and Fisher, J. 2007. A multi-directional in vitro investigation into friction, damage and wear of innovative chondroplasty materials against articular cartilage. Clinical Biomechanics. 22,pp.834–842.

Nyska, M. and Mann, G. 2002. The Unstable Ankle. Champaign, USA.

O'Farrell, T.A. and Costello, B.G. 1982. Osteochondritis dissecans of the talus. The late results of surgical treatment. The Journal of bone and joint surgery. British volume. 64(4),pp.494–497.

Oberg, T., Karsznia, A. and Oberg, K. 1993. Basic gait parameters: reference data for normal subjects, 10-79 years of age. Journal of rehabilitation research and development. 30(2),pp.210–23.

Olsen, S. and Oloyede, A. 2002. A finite element analysis methodology for representing the articular cartilage functional structure. Computer methods in biomechanics and biomedical engineering. 5(6),pp.377–386.

Olson, T.R. and Pawlina, W. 2008. A.D.A.M. Student Atlas of Anatomy, 2nd Edition, Cambridge University Press. ISBN 978-0-521-71005-3

Oster, J. 2009. The CT Band, CT Band Biomechanics and CT Band Syndrome. The Foot and Ankle Journal. 2(5),p.2.

Oungoulian, S.R., Durney, K.M., Jones, B.K., Ahmad, C.S., Hung, C.T. and Ateshian, G. 2015. Wear and damage of articular cartilage with friction against orthopedic implant materials. Journal of Biomechanics. 48(10),pp.1957–1964.

Owellen, M.C. 1997. Biotribology: The Effect of Lubricant and Load on Articular Cartilage Wear and Friction. MS Thesis, Mechanical Engineering, Virginia Polytechnic Institute and State University, Blacksburg, VA

Padalecki, J.R., Jansson, K.S., Smith, S.D., Dornan, G.J., Pierce, C.M., Wijdicks, C.A. and Laprade, R.F. 2014. Biomechanical consequences of a complete radial tear adjacent to the medial meniscus posterior root attachment site: in situ pull-out repair restores derangement of joint mechanics. Am J Sports Med. 42(3),pp.699–707.

Park, S., Hung, C. and Ateshian, G.. 2004. Mechanical response of bovine articular cartilage under dynamic unconfined compression loading at physiological stress levels. Osteoarthritis and Cartilage. 12(1),pp.65–73.

Patterson, R., Pogue, D. and Viegas, S. 1997. The effects of time and light exposure on contact and pressure measurements using Fuji prescale film. The Iowa orthopaedic journal. 17,pp.64–9.

Pawaskar, S.S. 2006. Contact Mechanics Modelling of Articular Cartilage and Applications. Master of Science (Eng) by Research, School of Mechanical Engineering, University of Leeds, UK.

Pawaskar, S.S. 2010. Joint Contact Modelling of Articular Cartilage in Synovial Joints, PhD Thesis, School of Mechanical Engineering, University of Leeds, UK.

Pawaskar, S.S., Ingham, E., Fisher, J. and Jin, Z. 2011. Fluid load support and contact mechanics of hemiarthroplasty in the natural hip joint. Medical Engineering and Physics. 33(1), pp.96–105.

Pearle, A.D., Warren, R.F. and Rodeo, S.A. 2005. Basic science of articular cartilage and osteoarthritis. Clinics in Sports Medicine. 24(1),pp.1–12.

Pereira, D.S., Koval, K.J., Resnick, R.B., Sheskier, S.C., Kummer, F. and Zuckerman, J.D. 1996. Tibiotalar contact area and pressure distribution: the effect of mortise widening and

syndesmosis fixation. Foot & ankle international / American Orthopaedic Foot and Ankle Society [and] Swiss Foot and Ankle Society. 17,pp.269–274.

Peterson, L., Minas, T., Brittberg, M., Lindahl, A. and Surgery, J. 2003. Treatment of osteochondritis dissecans of the knee with autologous chondrocyte transplantation: results at two to ten years. The Journal of bone and joint surgery. American volume. 85–A Suppl,pp.17–24.

Pham, A. and Hull, M.L. 2007. Dehydration rates of meniscus and articular cartilage in vitro using a fast and accurate laser-based coordinate digitizing system. Journal of biomechanics. 40(14),pp.3223–9.

Pickard, J., Ingham, E., Egan, J. and Fisher, J. 1998. Investigation into the effect of proteoglycan molecules on the tribological properties of cartilage joint tissues. Proceedings of the Institution of Mechanical Engineers. Part H, Journal of engineering in medicine. 212(3),pp.177–82.

Pollard, H., Sim, P. and McHardy, A. 2002. Lateral ankle injury. Literature review and report of two cases. Australasian chiropractic & osteopathy: journal of the Chiropractic & Osteopathic College of Australasia. 10(1),pp.21–30.

Poole, A.R., Kobayashi, M., Yasuda, T., Laverty, S., Mwale, F., Kojima, T., Sakai, T., Wahl, C., El-Maadawy, S., Webb, G., Tchetina, E. and Wu, W. 2002. Type II collagen degradation and its regulation in articular cartilage in osteoarthritis. Annals of the rheumatic diseases. 61 Suppl 2(suppl 2),pp.ii78-81.

Poole, C.A. 1997. Articular cartilage chondrons: form, function and failure. Journal of anatomy,191,Pt, 1,pp.1–13.

Poon, C.Y. and Bhushan, B. 1995. Comparison of surface roughness measurements by stylus profiler, AFM and non-contact optical profiler. Wear. 190(1),pp.76–88.

Procter, P. and Paul, J.P. 1982. Ankle joint biomechanics. Journal of biomechanics. 15(9),pp.627–34.

Quinn, G.P. and Keough, M.J. 2002. Experimental Design and Data Analysis for Biologists, Cambridge University Press, ISBN 0521009766

Quiroga, J.M.P., Wilson, W., Ito, K. and van Donkelaar, C.C. 2017. The effect of loading rate on the development of early damage in articular cartilage. Biomechanics and Modeling in Mechanobiology. 16(1),pp.263–273.

Radin, E.L., Swann, D.A., Paul, I.L. and Mcgrath, P.J. 1982. Factors influencing articular cartilage wear in vitro. Arthritis & Rheumatism. 25(8),pp.974–980.

Ramsey, P. and Hamilton, W. 1976. Changes in tibiotalar area of contact caused by lateral talar shift. The Journal of Bone & Joint Surgery. 58(3),pp.356–357.

Rana, F. 2011. Structure of Dinosaur Collagen Unravels the Case for a Young Earth. [Accessed 30 April 2017]. Available from: https://www.twr360.org/blog/details/453/structure-of-dinosaur-collagen-unravels-the-case-for-a-young-earth.

Reddy, S., Pedowitz, D.I., Parekh, S.G., Sennett, B.J. and Okereke, E. 2007. The morbidity associated with osteochondral harvest from asymptomatic knees for the treatment of osteochondral lesions of the talus. The American Journal of Sports Medicine. 35(1),pp.80–85.

Richardson, D.S. and Lichtman, J.W. 2015. Clarifying Tissue Clearing. Cell. 162(2),pp.246–257.

Rieppo, J., Halmesmäki, E.P., Siitonen, U., Laasanen, M.S., Töyras, J., Kiviranta, I., Hyttinen, M.M., Jurvelin, J.S. and Helminen, H.J. 2003. Histological differences of human, bovine and porcine cartilage. Trans Orthop Res Soc. 28.

Rieppo, J., Hyttinen, M.M., Halmesmaki, E., Ruotsalainen, H., Vasara, A., Kiviranta, I., Jurvelin, J.S. and Helminen, H.J. 2009. Changes in spatial collagen content and collagen network architecture in porcine articular cartilage during growth and maturation. Osteoarthritis and Cartilage. 17(4),pp.448–455.

Robinson, D.E., Winson, I.G., Harries, W.J. and Kelly, A.J. 2003. Arthroscopic treatment of osteochondral lesions of the talus. J Bone Joint Surg Br. 85(7),pp.989–993.

Rolauffs, B., Margulis, Kuettner, K. and Cole 2002. The cell density of the superficial layer of adult human articular cartilage is joint-specific and is altered by age and degenerative changes. 48th annual meeting of the orthopaedic research society. Department of Biochemistry, Rush Medical College, 1653 W. Congress Parkway, Chicago

Rosenberg, L., Margolis, R., Wolfenstein-Todel, C., Pal, S. and Strider, W. 1975. Organisation of Extracellular Matrix in bovine articular cartilage In: H. Slavkin and R Greulick, eds. Extracellular Matrix Influence on Gene Expression. New York, USA: Academic Press, Inc, p. 417.

Roth, V. and Mow, V.C. 1980. The intrinsic tensile behavior of the matrix of bovine articular cartilage and its variation with age. The Journal of bone and joint surgery. American volume. 62(7),pp.1102–17.

Russell, S.L. 2010. Friction, Wear, Wear Debris and Functional Biocompatibility of Cartilage Substitution Biomaterials, PhD Thesis, The University of Leeds School of Mechanical Engineering School of Biological Sciences, UK.

Saltzman, C.L. 1999. Total ankle arthroplasty: state of the art. Instr Course Lect. 48,pp.263–268.

Sanford, B.A., Williams, J.L., Zucker-Levin, A.R. and Mihalko, W.M. 2014a. Hip, Knee, and Ankle Joint Forces in Healthy Weight, Overweight, and Obese Individuals During Walking In: Computational Biomechanics for Medicine. New York, NY: Springer New York, pp. 101–111.

Sanford, B.A., Williams, J.L., Zucker-Levin, A.R. and Mihalko, W.M. 2014b. Hip, Knee, and Ankle Joint Forces in Healthy Weight, Overweight, and Obese Individuals During Walking In: Computational Biomechanics for Medicine. New York, NY: Springer New York, pp. 101–111.

Sayles, R.S., Thomas, T.R., Anderson, J., Haslock, I. and Unsworth, A. 1979. Measurement of the surface microgeometry of articular cartilage. Journal of biomechanics. 12(4),pp.257–67.

Schumacher, B.L., Su, J.L., Lindley, K.M., Kuettner, K.E. and Cole, A.A. 2002. Horizontally oriented clusters of multiple chondrons in the superficial zone of ankle, but not knee articular cartilage. Anatomical Record. 266(4),pp.241–248.

Seireg, A. and Gerath, M. 1975. An in vivo investigation of wear in animal joints. Journal of Biomechanics. 8(3–4).

Sekiya, J.K. and Kuhn, J.E. 2003. Instability of the proximal tibiofibular joint. The Journal of the American Academy of Orthopaedic Surgeons. 11(2),pp.120–8.

Setton, L.A., Zhu, W. and Mow, V.C. 1993. The biphasic poroviscoelastic behaviour of articular cartilage: role of the surface zone in governing the compressive behaviour. Journal of biomechanics. 26(4–5),pp.581–92.

Sharma, A.R., Jagga, S., Lee, S.S. and Nam, J.S. 2013. Interplay between cartilage and subchondral bone contributing to pathogenesis of osteoarthritis. International Journal of Molecular Sciences. 14(10),pp.19805–19830.

Shepherd, D.E. and Seedhom, B.B. 1999. Thickness of human articular cartilage in joints of the lower limb. Annals of the rheumatic diseases. 58(1),pp.27–34.

Shi, D., Xu, X., Ye, Y., Song, K., Cheng, Y., Di, J., Hu, Q., Li, J., Ju, H., Jiang, Q. and Gu, Z. 2016. Photo-Cross-Linked Scaffold with Kartogenin-Encapsulated Nanoparticles for Cartilage Regeneration. ACS Nano. 10(1),pp.1292–1299.

Siebelt, M., Waarsing, J.H., Kops, N., Piscaer, T.M., Verhaar, J.A.N., Oei, E.H.G. and Weinans, H. 2011. Quantifying osteoarthritic cartilage changes accurately using in vivo microCT arthrography in three etiologically distinct rat models. Journal of Orthopaedic Research. 29(11),pp.1788–1794.

Simon, W.H. 1970. Scale effects in animal joints. I. articular cartilage thickness and compressive stress. Arthritis & Rheumatism. 13(3),pp.244–255.

Simon, W.H., Friedenberg, S. and Richardson, S. 1973. Joint congruence. A correlation of joint congruence and thickness of articular cartilage in dogs. The Journal of bone and joint surgery. American volume. 55(8),pp.1614–20.

Smyth, P.A., Rifkin, R., Jackson, R.L. and Hanson, A.R.R. 2012. The Average Roughness and Fractal Dimension of Articular Cartilage During Drying. (36),pp.368–375.

Smyth, P.A., Rifkin, R.E., Jackson, R.L. and Hanson, R.R. 2012. A Surface Roughness Comparison of Cartilage in Different Types of Synovial Joints. Journal of Biomechanical Engineering. 134(2),p.021006.

Sokal, R.R. and Rohlf, F.J. 1995. Biometry: The Principles and Practices of Statistics in Biological Research, third edition, ISBN 978-0716724117

Sommaggio, R., Uribe-Herranz, M., Marquina, M. and Costa, C. 2016. Xenotransplantation of pig chondrocytes: therapeutic potential and barriers for cartilage repair. European cells & materials. 32,pp.24–39.

Song, Y., Greve, J.M., Carter, D.R. and Giori, N.J. 2008. Meniscectomy alters the dynamic deformational behavior and cumulative strain of tibial articular cartilage in knee joints subjected to cyclic loads. Osteoarthritis and Cartilage. 16(12),pp.1545–1554.

Southern California Orthopedic 2012. Anatomy of the Ankle | Southern California Orthopedic Institute. Available from: https://www.scoi.com/specialties/anatomy-ankle.

Stachowiak, G. and Batchelor, A.. 2011. Engineering Tribology. US: Butterworth-Heinemann.

Stachowiak, G.W. and Batchelor, A.W. 2014. Fatigue Wear In: Engineering Tribology., pp. 657–681.

Stauffer, R.N., Chao, E.Y. and Brewster, R.C. 1977. Force and motion analysis of the normal, diseased, and prosthetic ankle joint. Clinical orthopaedics and related research.,pp.189–196.

Stauffer, R.N. and Segal, N.M. 1981. Total ankle arthroplasty: four years' experience. Clinical orthopaedics and related research. (160),pp.217–221.

Stockwell, R.A. 1979. Biology of cartilage cells, Cambridge University Press. ISBN 9780521224109

Stockwell, R.A. 1971. The interrelationship of cell density and cartilage thickness in mammalian articular cartilage. Journal of anatomy. 109(Pt 3),pp.411–21.

Stufkens, S.A., Knupp, M., Horisberger, M., Lampert, C. and Hintermann, B. 2010. Cartilage lesions and the development of osteoarthritis after internal fixation of ankle fractures: a prospective study. The Journal of bone and joint surgery. American volume. 92,pp.279–286.

Tan, T.C.F., Wilcox, D.M., Frank, L., Shih, C., Trudell, D.J., Sartoris, D.J. and Resnick, D. 1996. MR imaging of articular cartilage in the ankle: Comparison of available imaging sequences and methods of measurement in cadavers. Skeletal Radiology. 25(8),pp.749–755.

Taylor, C. 2013. Development and characterisation of mechanical and enzymatic models of cartilage degeneration. PhD Thesis, University of Leeds, UK.

Taylor, S. 2012. An In-vitro Medium Term Simulation of Hip Hemiarthroplasty. PhD Thesis, University of Leeds, UK.

Taylor, S.D., Tsiridis, E., Ingham, E., Jin, Z., Fisher, J. and Williams, S. 2011. Comparison of human and animal femoral head chondral properties and geometries. Proceedings of the Institution of Mechanical Engineers, Part H: Journal of Engineering in Medicine. 226(1),pp.55–62.

Teeple, E., Elsaid, K.A., Fleming, B.C., Jay, G.D., Aslani, K., Crisco, J.J. and Mechrefe, A.P. 2008. Coefficients of friction, lubricin, and cartilage damage in the anterior cruciate ligament-deficient guinea pig knee. Journal of orthopaedic research: official publication of the Orthopaedic Research Society. 26(2),pp.231–7.

Tekscan 2013. I-Scan User Manual. South Boston, United States.

Tekscan Inc. 2015. Pressure Mapping Sensor 5315. ,p.1.

Thakker, V., Whyte, M., Eisman, J. and Igarashi, T. 2013. Overview of Joint Anatomy and Cartilage Biology In: R. Lories and F. Luyten, eds. Genetics of Bone Biology and Skeletal Disease. Elsevier Inc., pp. 1–621.

Thomas, B.H., Craig Fryman, J., Liu, K. and Mason, J. 2009. Hydrophilic-hydrophobic hydrogels for cartilage replacement. Journal of the Mechanical Behavior of Biomedical Materials. 2(6),pp.588–595.

Thomas, R., Daniels, T.R. and Parker, K. 2006. Gait analysis and functional outcomes following ankle arthrodesis for isolated ankle arthritis. The Journal of bone and joint surgery. American volume. 88(3),pp.526–35.

Thomas, T.R., Sayles, R.S. and Haslock, I. 1980. Human Joint Performance and the Roughness of Articular Cartilage. Journal of Biomechanical Engineering. 102(1),p.50.

Thordarson, D. 2004. Foot and Ankle: Orthopaedic Surgery Essentials. Philadelphia, USA: Lippincott Williams & Wilkins. ISBN 978-1451115963

Treppo, S., Koepp, H., Quan, E.C., Cole, A.A., Kuettner, K.E. and Grodzinsky, A.J. 2000. Comparison of biomechanical and biochemical properties of cartilage from human knee and ankle pairs. Journal of orthopaedic research: official publication of the Orthopaedic Research Society. 18,pp.739–748.

Udofia, I., McCann, L., Graindorge, S., Jin, Z. and Fisher, J. 2009. Friction and wear testing of articular cartilage in the medial compartment of the knee using an anatomic simulator: part 2-the effect of tibial plate conformity. Orthopaedic Proceedings. 91–B(SUPP II).

Unsworth, A., Dowson, D. and Wright, V. 1975. The Frictional Behavior of Human Synovial Joints—Part I: Natural Joints. Journal of Lubrication Technology. . 97(3),p.369.

Valderrabano, V., Hintermann, B., Horisberger, M. and Fung, T.S. 2006. Ligamentous posttraumatic ankle osteoarthritis. The American journal of sports medicine. 34,pp.612–620.

Valderrabano, V., Hintermann, B., Nigg, B.M., Stefanyshyn, D. and Stergiou, P. 2003. Kinematic changes after fusion and total replacement of the ankle: part 3: Talar movement. Foot & ankle international / American Orthopaedic Foot and Ankle Society [and] Swiss Foot and Ankle Society. 24,pp.897–900.

Valderrabano, V., Horisberger, M., Russell, I., Dougall, H. and Hintermann, B. 2009. Etiology of ankle osteoarthritis. Clinical orthopaedics and related research. . 467(7),pp.1800–6.

Valderrabano, V., Nigg, B.M., von Tscharner, V., Stefanyshyn, D.J., Goepfert, B. and Hintermann, B. 2007. Gait analysis in ankle osteoarthritis and total ankle replacement. Clinical Biomechanics. 22,pp.894–904.

VanDijk, N.C., Reilingh, M.L., Zengerink, M. and VanBergen, C.J.A. 2010. Osteochondral defects in the ankle: Why painful? Knee Surgery, Sports Traumatology, Arthroscopy. 18,pp.570–580.

Verzijl, N., DeGroot, J., Ben, Z.C., Brau-Benjamin, O., Maroudas, A., Bank, R.A., Mizrahi, J., Schalkwijk, C.G., Thorpe, S.R., Baynes, J.W., Bijlsma, J.W.J., Lafeber, F.P.J.G. and TeKoppele, J.M. 2002. Crosslinking by advanced glycation end products increases the stiffness of the collagen network in human articular cartilage: a possible mechanism through which age is a risk factor for osteoarthritis. Arthritis and rheumatism. 46(1),pp.114–23.

Wainwright, J.M., Czajka, C.A., Patel, U.B., Freytes, D.O., Tobita, K., Gilbert, T.W. and Badylak, S.F. 2010. Preparation of Cardiac Extracellular Matrix from an Intact Porcine Heart. Tissue Engineering Part C: Methods. 16(3),pp.525–532.

Wan, L., de Asla, R.J., Rubash, H.E. and Li, G. 2006. Determination of in-vivo articular cartilage contact areas of human talocrural joint under weightbearing conditions. Osteoarthritis and cartilage / OARS, Osteoarthritis Research Society. . 14(12),pp.1294–301.

Wang, C.L., Cheng, C.K., Chen, C.W., Lu, C.M., Hang, Y.S. and Liu, T.K. 1995. Contact areas and pressure distributions in the subtalar joint. Journal of Biomechanics. 28(3).

Wang, L., Liu, X., Li, D., Liu, F. and Jin, Z. 2014. Contact mechanics studies of an ellipsoidal contact bearing surface of metal-on-metal hip prostheses under micro-lateralization. Medical Engineering and Physics. 36(4),pp.419–424.

Wardale, R.J. and Duance, V.C. 1994. Characterisation of articular and growth plate cartilage collagens in porcine osteochondrosis. Journal of cell science. 107,pp.47–59.

Weightman, B. 1976. Tensile fatigue of human articular cartilage. Journal of Biomechanics. 9(4),pp.193–200.

Whitehouse, D.J. 2000. Surface characterization and roughness measurement in engineering In: Photo-Mechanics., pp. 413–461.

Whittaker, J.P., Smith, G., Makwana, N., Roberts, S., Harrison, P.E., Laing, P. and Richardson, J.B. 2005. Early results of autologous chondrocyte implantation in the talus. J Bone Joint Surg Br. 87(2),pp.179–183.

Williamson, A.K., Chen, A.C., Masuda, K., Thonar, E.J.M.A. and Sah, R.L. 2003. Tensile mechanical properties of bovine articular cartilage: Variations with growth and relationships to collagen network components. Journal of Orthopaedic Research. 21(5),pp.872–880.

Wilson, D.R., Apreleva, M. V, Eichler, M.J. and Harrold, F.R. 2003. Accuracy and repeatability of a pressure measurement system in the patellofemoral joint. Journal of biomechanics. 36(12),pp.1909–15.

Woo, S.L.Y., Akeson, W.H. and Jemmott, G.F. 1976. Measurements of nonhomogeneous, directional mechanical properties of articular cartilage in tension. Journal of Biomechanics. 9(12),pp.785–791.

Wyler, A., Bousson, V., Bergot, C., Polivka, M., Leveque, E., Vicaut, E. and Laredo, J.D. 2009. Comparison of MR-arthrography and CT-arthrography in hyaline cartilage-thickness

measurement in radiographically normal cadaver hips with anatomy as gold standard. Osteoarthritis and Cartilage. 17(1),pp.19–25.

Yamagata, M., Chao, E.Y., Ilstrup, D.M., Melton, L.J., Coventry, M.B. and Stauffer, R.N. 1987. Fixed-head and bipolar hip endoprostheses. A retrospective clinical and roentgenographic study. The Journal of arthroplasty. 2(4),pp.327–41.

Yamamoto, T. and Bullough, P.G. 2000. Spontaneous osteonecrosis of the knee: The result of subchondral insufficiency fracture. Journal of Bone and Joint Surgery - Series A. 82(6),pp.858–866.

Yassin, F.E.-Z.E.-D., El-Dawela, R. and Kerim, M. 2014. Picrosirius red staining assessment of collagen after dermal roller application: A minimally invasive percutaneous collagen induction therapy. Indian Journal of Dermatopathology and Diagnostic Dermatology. 1(2),p.68.

Zengerink, M., Struijs, P. a a, Tol, J.L. and van Dijk, C.N. 2010. Treatment of osteochondral lesions of the talus: a systematic review. Knee surgery, sports traumatology, arthroscopy: official journal of the ESSKA. 18(2),pp.238–46.

Zhang, L.Z., Zheng, H.A., Jiang, Y., Tu, Y.H., Jiang, P.H. and Yang, A.L. 2012. Mechanical and biologic link between cartilage and subchondral bone in osteoarthritis. Arthritis Care and Research. 64(7),pp.960–967.